Investigation of Buckling Distortion of Ship Structure due to Welding Assembly Using Inherent Deformation Theory

固有変形法を用いた溶接組立時における船体構造の座屈変形に関する研究

Jiangchao Wang
王　江超

2012 年 12 月

Osaka University
大阪　大学

Doctoral Dissertation (博士学位論文)

Investigation of Buckling Distortion of Ship Structure due to Welding Assembly Using Inherent Deformation Theory
(固有変形法を用いた溶接組立時における船体構造の座屈変形に関する研究)

Jiangchao Wang

2012.12

Department of Naval Architecture and Ocean Engineering
Division of Global Architecture
Graduate School of Engineering
Osaka University

Doctoral Dissertation (博士学位論文)

Investigation of Buckling Distortion of Ship Structure due to Welding Assembly Using Inherent Deformation Theory
(固有変形法を用いた溶接組立時における船体構造の座屈変形に関する研究)

Submitted to Department of Naval Architecture and Ocean Engineering, Division of Global Architecture, Graduate School of Engineering, Osaka University, in partial fulfillment of requirements for the degree of Doctor of Philosophy in Engineering

By
Jiangchao Wang
Osaka University

2012

Supervisor(指導教官): Professor Hidekazu Murakawa
Dissertation Committee:
Professor Hidekazu Murakawa
Professor Masahiko Fujikubo
Professor Naoki Osawa
Associate Professor Keiji Nakacho
Associate Professor Hisashi Serizawa

With Infinite Respect and Greatest Thanks To

Professor **Hidekazu Murakawa**
Professor **Sherif Rashed**
Professor **Ninshu Ma**
Professor **Yu Luo**
Professor **Dean Deng**

Abstract

With the development of lightweight technology to improve the fuel economy and enhance the carrying capacity of modern vehicles such as ships, thin plates are widely used to assemble large-scale and complex welded structure. However, beside the unavoidable welding distortion, welding induced buckling may occur in such thin plate welded structures. Welding distortion, and in particular buckling, will influence the dimensional accuracy and structural performance, and may delay the whole production process.

In this research, welding distortion of ship panel structures is selected as a research subject. Welding induced buckling is investigated, and buckling mechanism is clarified using the computational approach and the inherent deformation theory. Further, straightening using line heating to correct welding distortion is considered.

The in-house code JWRIAN(Joining and Welding Research Institute ANalysis), which is developed by the research group of mathematic modeling and computational analysis at Osaka University, headed by Prof. Hidekazu Murakawa, is employed to carry out analysis of welding distortion through out this thesis. Relevant theories and methods are introduced.

Three methods are presented to accurately evaluate the longitudinal inherent shrinkage, namely (1) empirical and theoretical formulae, (2) calculation from computed longitudinal displacement and (3) integration of computed longitudinal plastic strain/residual stress. The influence of plate size and heat input on longitudinal inherent shrinkage is investigated and the average temperature is proposed to clarify the difference between computed results and results obtained using simple theoretical analysis.

When a thin plate made of high tensile strength steel is used, not only residual buckling after cooling but also transient buckling during welding may occur. Because of the high yield stress of high tensile strength steel, larger compressive thermal stress is produced near the welding line compared with that in the case of carbon steel. Therefore the plate may buckle due to thermal expansion, before the material near the heat source yields. During cooling, the compressive thermal stress close to the welding line disappears and tensile residual stress is produced due to contraction. Meanwhile, compressive residual stress occurs far from the welding line to balance the tensile stress close to the welding line. This distribution of residual stress would change the deformed shape into a saddle buckling type when the stress exceeds the critical buckling condition.

Bead on plate, as a representative of butt welded joints of thin plates is investigated. Out-of-plane welding distortion measured by digital photometry shows that saddle type buckling is produced after cooling. Thermal elastic plastic FE analysis also predicts a saddle type deformed shape in the case of bead on plate. Eigenvalue analysis considering the same welding condition shows the ideal buckling mode of bead on plate. The computed lowest buckling mode is the saddle type and

the corresponding eigenvalue is less than 1. Using elastic FE analysis based on the inherent deformation theory, out-of-plane welding distortion considering initial deflection is predicted with high accuracy. It was shown that, the longitudinal inherent shrinkage is the dominant reason of buckling, and it determines the buckling mode. Initial deflection and inherent bending are considered to be disturbances which trigger buckling. They may not influence the buckling mode but may change the magnitude of welding distortion.

Stiffeners are usually employed to increase the strength and stiffness of thin plate structures. A stiffened thin plate welded structure with fillet welded joints is examined to investigate welding induced buckling. When bending stiffness is increased due to stiffeners, welding may not induce buckling of plate fields in bending modes. However, the whole stiffened structure may buckle in a twisting mode, while plate panels remain unbuckled. In this case, experimental result, thermal elastic plastic analysis and elastic FE analysis show similar out-of-plane welding distortion. The influence of initial deflection can be neglected in this case due to its relatively small magnitude compared with out-of-plane welding distortion. Eigenvalue analysis gives the twisting buckling mode as the lowest buckling mode. However, it was found that, in stiffened welded structures, not only longitudinal inherent shrinkage but also transverse inherent shrinkage are responsible for buckling. As an application to predict welding induced buckling using the inherent deformation theory, a ship stiffened panel is considered. The inherent deformations of different types of welded joints included in the panel are evaluated beforehand using thermal elastic plastic FE analysis. Applying idealized boundary condition to focus on the local deformation, elastic FE analysis and eigenvalue analysis show that the considered ship panel will buckle near the edge and only bending distortion is dominant in the internal region. In order to correct welding distortion, straightening using line heating is employed. In the internal region, only inherent bending with the same magnitude as welding induced inherent bending is applied on the opposite side of welded joints, (fast moving torch). On the other hand, only in-plane inherent strain produced by line heating is introduced to the edge region to correct buckling distortion (slow moving torch). The magnitude of out-of-plane welding distortion in this ship panel can be minimized to an accepted level.

Table of Contents

Chapter 1 Introduction

1.1 Background

Welding is a high productive and practical joining method that is widely used in constructing and manufacturing industries such as shipbuilding, automobiles, passenger trains, bridges and pressure vessels industries [1]. Welding is the non-detachable joining or coating of components or base materials under the (mostly local) application of heat and/or pressure, with or without the use of filler materials [2]. Welding is widely employed to join parts and blocks to assemble welded structures because of its advantages in comparison with other joining and manufacturing methods such as bolting, riveting, casting, forging etc. Advantages of welding are simple structural design; weight and cost saving; high practicability and joining efficiency; flexibility and feasibility of joining; reliability and excellent performance of joints. However, it is well-known that there are some difficulties with welding and welded structures, such as (a) cracking and fracture of welded joints; (b) possibility of weld defects; (c) influence to material properties; (d) lack of reliable non-destructive testing techniques; (e) residual stress and welding distortion.

Welding distortion is one of the most complex difficulties in the fabrication of welded structures. It is the result of the non-uniform expansion/contraction, and the associated plastic strain produced in the weld and surrounding base material, caused by the heating and cooling cycle in the welding process. Because the expansion and subsequent contraction of the hot material is restrained by the surrounding colder material, plastic strain and tensile stresses build-up in and around the weld, combined with simultaneously generated compressive stresses in locations of the parts off the welding region [3]. These plastic strains, tensile and compressive stresses are inherent to the welding process and are the primary cause of welding distortion. Basically there are two major causes of geometrical error in welded structures as shown in **Fig. 1.1** [4]. The first is the inherent strain/deformation due to expansion and contraction and the other is the gap and misalignment which are produced in the joint before and/or during fitting and welding. Welding distortion not only degrades the performance of a welded structure, but also, when mitigated, it delays the production schedule and increases fabrication cost.

Generally speaking, the welding induced distortion of thin plate structures can be divided into in-plane and out-of-plane distortion. Welding shrinkage is the typical in-plane type. Out-of-plane welding distortion may be divided in two different kinds: bending distortion and buckling distortion. **Figure 1.2** shows all typical welding distortions of a thin plate butt welded joint. In particular, buckling distortion can take various modes.

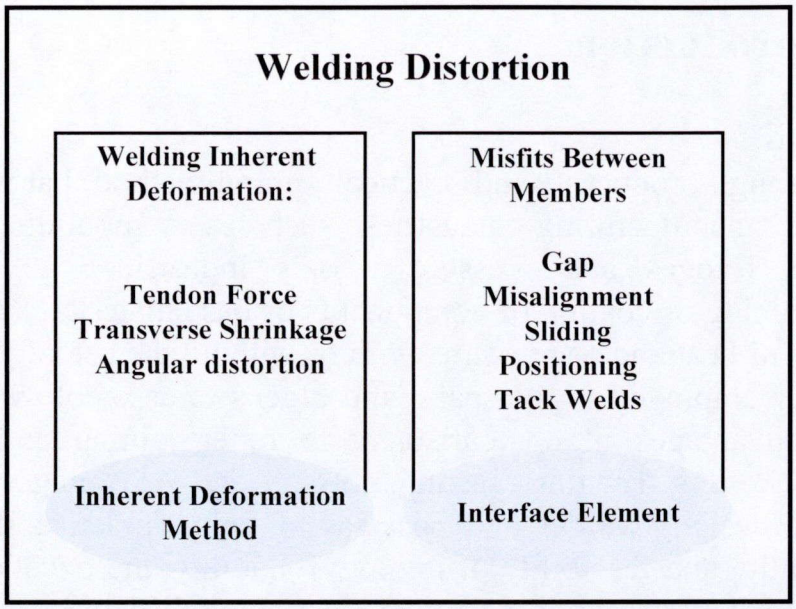

Fig. 1.1 Basic causes of geometrical error in the welded structures.

At present, it is impossible to completely eliminate or correct welding distortion because of the difficulty due to the non-linear irreversible nature of the welding and the straightening processes. There are many factors within the welding procedure contributing to welding distortion such as joint dimensions, material property, stiffener spacing, welding method, welding condition, welding sequence, degree of restraint, joint details, preheating [5]. However, welding distortion should and can be minimized to an acceptable magnitude to control dimensional tolerances during assembly. Therefore, prediction and control of welding distortion are of critical importance in modern construction and manufacturing industries.

In actual manufacturing, shrinkage and bending distortion of a welded structure can be controlled with techniques such as shrinkage allowance, prebending, prestressing, mechanical restraint, heat sinking, rolling, flame heating, vibratory stress relieving and electromagnetic hammer [6-11], which significantly improve product quality and reduce the influence of welding distortion on production schedule. However, it is difficult to correct welding induced buckling due to its instability, and, therefore, buckling should be avoided whenever possible.

To control welding distortion, it is necessary to be able to predict the distortion of a weldment before a single bead is laid. Prediction of welding distortion should be considered as a part of the design cycle rather than as a part of the manufacturing cycle [12]. In this research, experimental, theoretical and computational approaches are employed to predict welding distortion beforehand in production of thin plate welded structures.

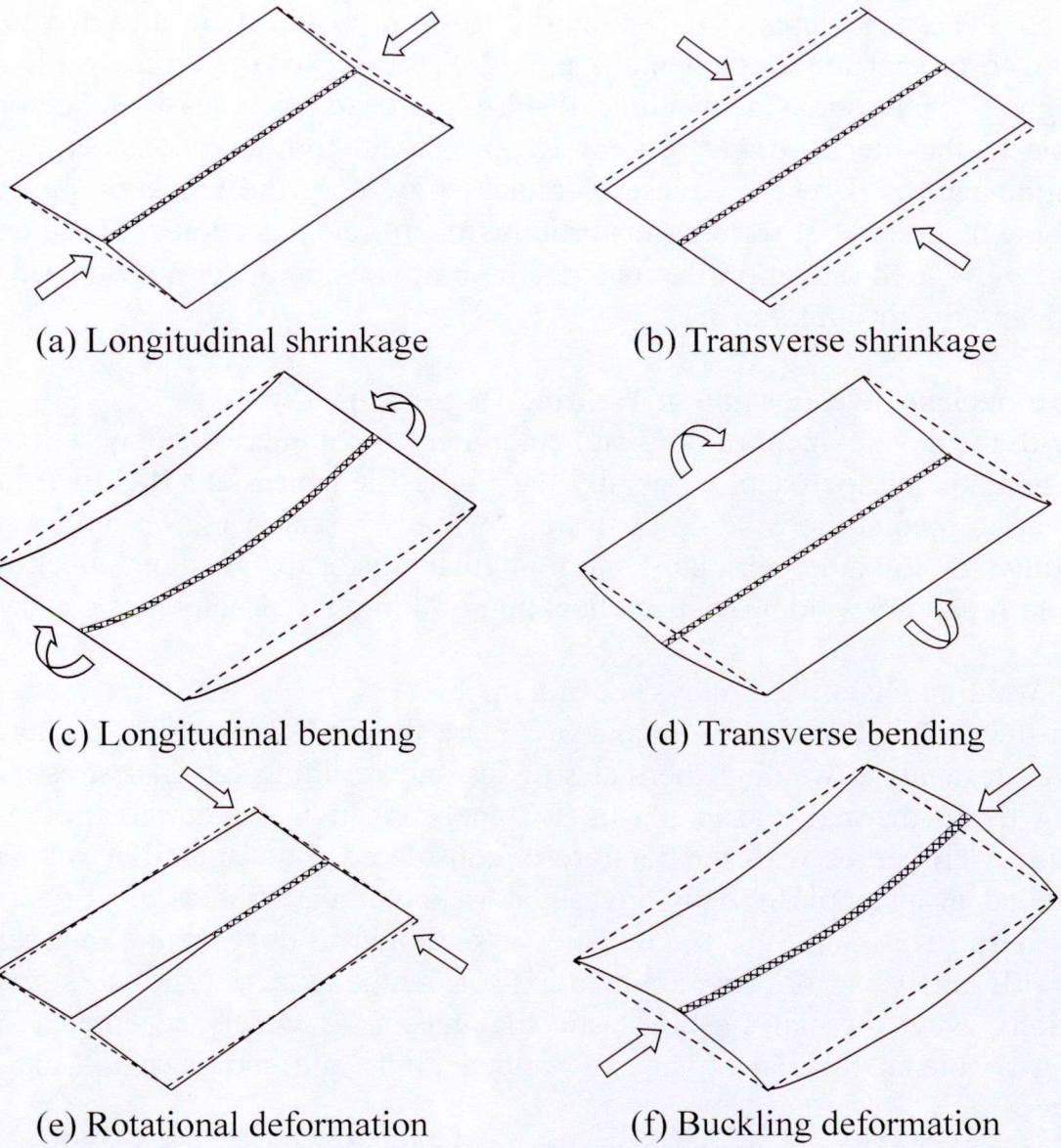

(a) Longitudinal shrinkage (b) Transverse shrinkage

(c) Longitudinal bending (d) Transverse bending

(e) Rotational deformation (f) Buckling deformation

Fig. 1.2 Basic types of welding distortion in thin plate butt welded joint.

1.2 Literature Review

Variety of methods are presented in the literature and employed to predict welding distortion of welded structures. In the following sections, these methods are briefly reviewed

1.2.1 Experimental and Empirical Investigation of Welding Distortion

Over the years, many studies of welding distortion were conducted by experimental measurement and empirical formulas for basic welding distortion such as longitudinal shrinkage, transverse shrinkage and angular distortion were presented. Satoh and Terasaki [13] investigated the effect of welding conditions, such as welding heat input, physical and mechanical properties of materials, and size of welded structure on welding deformations in bead on plate and multi-pass butt welded joint. Masubuchi [14] proposed systematical methodologies for analyzing the welding

distortion. The mechanism of welding distortion is clarified and formulas are proposed to predict the fundamental welding distortion for the typical welded joint. Verhaeghe [3] investigated welding distortion based on measured deformation available in the literature and reviewed approximate formulae considering various production factors. However, these formulae show only the tendency, but can not predict the magnitude of welding distortion with sufficient accuracy. These empirical formulae are based on simplifications and assumptions, and can not be used outside the domain of their limitations.

1.2.2 Numerical Investigation of Welding Distortion

With the development of powerful computers and numerical analysis technology, the computational approach, especially the Finite Element Method (FEM) has been employed to predict the welding distortion by many researchers. Welding distortions consisting of in-plane shrinkage and angular distortion without buckling, are reviewed first, then welding induced buckling of thin plate structures is discussed.

1.2.2.1 Welding Distortion Analysis Using the FEM

In the 1970s, Ueda and Yamakawa [15] are the first to present a computational approach to analyze welding thermal stresses and resulting residual stresses during welding using thermal elastic plastic FE analysis. In this method, the change of mechanical properties with temperature is considered. Butt and fillet welded joints are studied as examples. Many investigators including Hibbitt [16], Friedman [17], Lindgren and Karlsson [18] and Goldak [19] continued to develop the thermal elastic plastic FE analysis for the computation of temperatures, residual stresses and distortions. Now thermal elastic plastic FE analysis is widely accepted to analyze welding problems for many types of welded joints and simple small size welded structures.

Goldak [20] proposed a more accurate mathematical model for weld heat sources based on a Gaussian distribution of power density, so called double ellipsoid heat source. Using this heat source model, the size and shape of the heat source can be easily changed to model both the shallow penetration arc welding process and the deeper penetration laser and electron beam welding processes. Ueda and Murakawa [21] discussed the advances in computer technology and utilization of computers in welding research. They have shown that the progress in computer technology and numerical analysis has made it possible to simulate complex phenomena and to discuss welding problems from the quantitative aspect. They also pointed out that there are still some problems to be overcome before truly meaningful research can be achieved. Gu et al [22] used a three-dimensional model to investigate the out-of-plane deformation due to butt welding, in which they account for gravity and different restraint. Ueda et al [23] reviewed the history of computational welding mechanics. They also summarized their current research activities such as analysis of residual stress and distortion in welding and cutting, measurement of three dimensional distributions of residual stresses and computation of weldability lobes for spot

welding.

To realize automation and mechanization in the shipbuilding industry, Ueda et al [24-26] investigated in-plane and out-of-plane deformation caused by one-side automatic submerged arc welding. For in-plane deformation, the effect of factors involved in the process, such as local heating, welding sequence, initial stress, type of tabs, pitch of tack welds and root gap are investigated using numerical simulation. Further, practical methods to correct groove gaps are studied and the influence of the corrections is computed. The effects of various factors on out-of-plane deformation are also investigated. These factors include gravity, the method of support, magnetic constraint and force from the opposite side of the weld near the welding line.

Although finite element analysis has accomplished remarkable achievements for investigation of the short single pass welds, welding is perhaps the most nonlinear problem encountered in structural mechanics [27]. Therefore, Lindgren [27-29] in 2001 published a review which presented the development of welding simulation from different aspects of finite element modeling and analysis, consisting of three parts: (1) increased complexity, (2) improved material modeling and (3) efficiency and integration. This review also has shown the possibilities in modeling and simulation of welding to encourage the increase of the use of the FEM in the field of welding mechanics. Meanwhile, the computational approach is clearly elaborated to be appropriate for those who are entering this field of research and useful as a reference for those already familiar with this subject. Then Lindgren [30] described the application of the finite element method as a tool of computational welding mechanics to predict thermal, material and mechanical effects of welding and focused on modeling aspects.

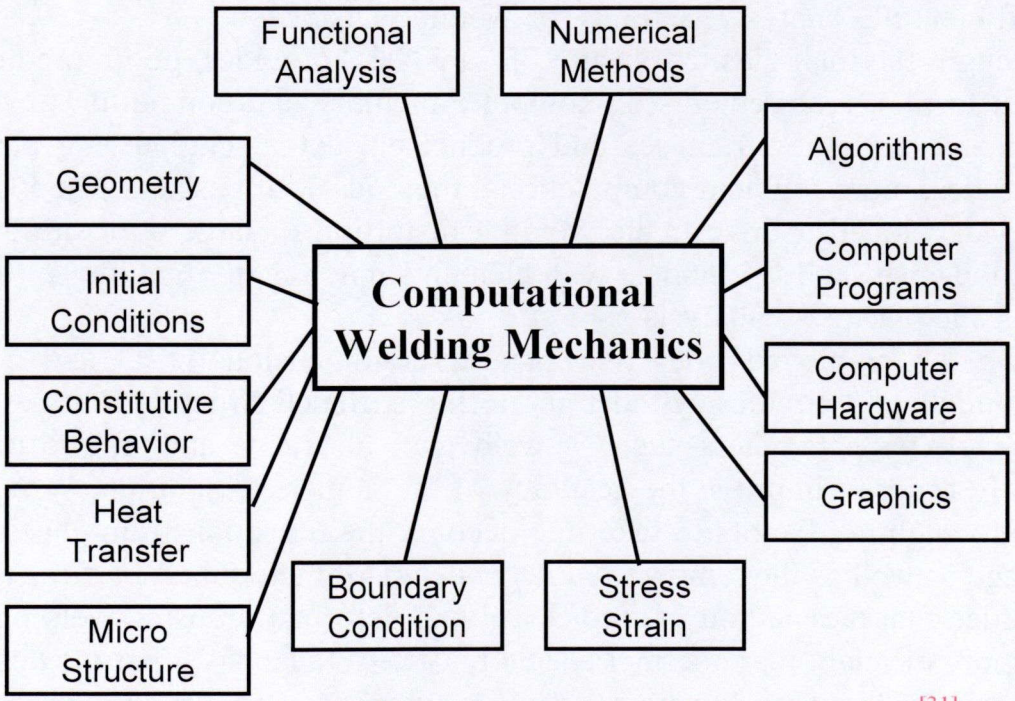

Fig. 1.3 Disciplines of computational welding mechanics [31].

As pioneers in the field of computational welding mechanics and the investigation of welding mechanical problems, such as temperature effects, strain, residual stress, and welding distortion, using the computational approach, Professor Ueda (Osaka University, Japan), Professor Goldak (Carleton University, Canada) and Professor Lindgren (Luleå University of Technology, Sweden) established the research disciplines of Computational Welding Mechanics (CWM) as shown in **Fig. 1.3** [31].

A paper collection[32], titled "Computational Welding Mechanics", has been published in commemoration of the retirement of Professor Yukio Ueda from Osaka University in 1996, in which professor Ueda with his colleagues developed the basic theories and their applications in analysis, measurement and prediction of welding residual stresses and deformation. Goldak and Akhlaghi [31] emphasized the exposition of computational principles and the application of computational welding mechanics to problems in the industry. The primary aim of this work is to transfer technology from the research specialists who are developing it to the engineering society to apply it in design and production of welded structures. Goldak and Akhlaghi also pointed out that the computational welding mechanics will be widely used in welding industry to give designers the capability to predict residual stress and welding distortion in welds and welded structures. Lindgren [33] in his monograph concluded that the aim of the computational welding mechanics is to establish methods and model that are usable for control and design of welding processes to obtain appropriate mechanical performance of welded component or structure. This monograph is of benefit to anyone that wants to master CWM or simulation of manufacturing process in general.

1.2.2.2 Efficient FE Analysis Methods for Welding Distortion

Although thermal elastic plastic FE analysis provides good predictions of welding distortion, requirements on computer memory and computing time make it less applicable to large structures and products in actual engineering practice. In recent decades, more efficient computational methods, still based on the FE method, have been developed to investigate welding distortion of large structures. Many of these methods use shell FE models with elements much larger than those required in thermal elastic plastic FE analysis.

Brown [34] employed both two- and three-dimensional (2D and 3D) finite element models of a circular cylinder and a ring stiffened structure to investigate the effect of welding parameters such as weld gap, clearance and fixture on a large structure. In order to improve the accuracy of the numerical solution, Wang et al [35] introduced weighting factors to take into account the transition from elastic stage to plastic stage as well as the temperature dependency of material properties. Wang et al [36] concluded that the method to predict welding deformation using welding inherent strain is more efficient than thermal elastic plastic FE analysis. First they established the relationships between inherent strain components and welding parameters of typical joints in the considered structure based on experimental results and 3D

thermal elastic plastic FE analysis. Then, inherent strains are introduced as initial strains to compute welding deformation of the whole structure. The effectiveness of the proposed method is demonstrated through the deformation analysis of a large welded cylinder with multipass welding.

Elastic FE analysis using shell element models and inherent strain and/or inherent deformation is proposed by a research group of Joining and Welding Research Institute at Osaka University, Japan lead by Prof Hidekazu Murakawa. This is a practical and efficient computational approach to investigate the welding distortion of large-scale and complex welded structures. Luo et al. [37] examined bead on plate as an ideal case of a butt welded joint. In this work, inherent strain produced during the welding process is primarily determined by the highest temperature reached in the thermal cycles and the constraint at each point. Then an elastic FE analysis is carried out to predict the welding residual stress and distortion using the inherent strain as an initial strain. Murakawa et al [38] proposed that the total distortion is determined as the elastic response of the structure to accumulated inelastic strains, such as plastic strain, creep strain and that produced by phase transformation. The inelastic strains are defined as the inherent strains, which depend on local conditions and can therefore be computed using a limited number of typical joints and then used in different application. They showed that inherent deformation can be evaluated by integrating the inherent strain distributed on each transverse cross section and is easier to store in databases for prediction of welding distortion in future. Luo et al [39] first analyzed welding deformation of plates with longitudinal curvature using thermal elastic plastic FE analysis. Luo suggested that since both welding distortion and residual stress are produced by the inherent strain, then, integration of the inherent strain gives not only the inherent deformations but also the tendon force. A method to predict the welding deformation by elastic FE analysis using the inherent deformations and the tendon force is proposed and its validity is demonstrated through numerical examples [39]. Luo at al [40], through a series of thermal elastic plastic FE analysis, established a database of inherent deformation for an aluminum alloy butt welded joint. An elastic FE analysis base on this database was developed to predict the welding deformation for large welded structures such as a large aluminum alloy coping. Deng and Murakawa [41] developed a large deformation elastic FE analysis to accurately predict welding distortion. In this work, a thermal elastic plastic FE analysis is first used to evaluate the inherent deformations of various types of welded joints and an elastic FE analysis is performed to predict welding distortion based on the obtained inherent deformation. In this paper, the influence of initial gap on welding distortion is also investigated. Wang et al. [42] studied welding distortion of thin plates due to bead on plate welding with varying plate thickness using elastic analysis based on the inherent deformation method. They showed that this kind of elastic analysis using the inherent deformation not only saves a large amount of computing time but also preserves the computation accuracy as was verified by experimental results. Wang et al. [43] studied a spherical structure assembled from thin plates, in which the overall welding distortion due to each welding line is

experimentally measured; then thermal elastic plastic FE analysis of the butt welded joint is carried out to evaluate the inherent deformation. Then an elastic analysis utilizing shell element model of this spherical structure and the evaluated inherent deformation is carried out to predict the welding distortion. Numerical predictions show good agreement with experimental measurements.

Michaleris and Debiccari [44] presented a numerical analysis technique combining 2D welding simulation with 3D structural analyses, which is effective when the computer resources are limited. Bachorski et al [45] presented a linear elastic finite element modeling technique called Shrinkage Volume Method which can significantly reduce the solution time. Jung [46] employed plasticity-based distortion analysis to investigate the relationship between cumulative plastic strains and welding distortion. In this analysis Jung mapped each cumulative plastic strain component evaluated by a 3D thermal elastic plastic analysis incorporating the effects of moving heat and non-linear material properties into elastic models using equivalent thermal strains. Camilleri et al [47] examined the applicability of finite element analysis to the out-of-plane welding distortion. Transient thermal analysis was done on a 2D cross section of the welded joint, and then the transverse angular deformation and the longitudinal contraction force are predicted. These results were then applied into a non-linear elastic finite element model to provide predictions of the final overall deformations of butt welded plates. Cheng [48] examined the in-plane shrinkage plastic strains through welding simulation of three types of simple welded joints. He found that these plastic strains are determined by the peak welding temperature and material's softening temperature range. Then an engineering approach was developed to introduce the obtained plastic strain into the FE model by means of applying equivalent thermal load.

Zhang et al [49] developed a 3D "Applied Plastic Strain Method" to predict the welding distortion of structures. In this Applied Plastic Strain Method, six components of the plastic strain of each welding line are calculated by performing a thermal elastic plastic FE analysis assuming moving heat source on a small 3D model with a shorter length, and then the plastic strain components of the small models are mapped on a large 3D structural model to obtain the final distortion. Jung [50] carried out a shell-element-based elastic analysis for prediction of the distortion induced in ship panels. Only longitudinal and transverse plastic strains are employed to compute the welding distortion, without significant loss of accuracy compared with results of thermal elastic plastic FE analysis. Yang et al [51] developed a stepwise computational method for prediction of welding distortion of large welded structures to reduce the computational time. This method consists of lump-pass modeling and mapping of plastic strain. The lump-pass modeling of local small models includes a thermal and a mechanical analysis to obtain the plastic strain. The mapping plastic strain method is carried out to predict the welding distortion by mapping plastic strains evaluated from local small models into the global model.

Focusing on the improvement of computational speed, Nishikawa et al [52-53] developed the Iterative Substructure Method (ISM) to reduce the computational time

in three dimensional welding analyses. In this method, the computational domain is divided into a large quasi-linear region and a small but moving strong non-linear region. Ikushima et al [54] developed a parallelized idealized explicit FEM using Graphic Processing Unit (GPU) to examine the mechanical behavior of large-scale welded structures, in which dynamic explicit FEM is employed using shorter computing time and less memory. Runnemalm and Hyun [55] applied an adaptive strategy for coupled thermo-mechanical analysis of welding in order to reduce the computer time. Parallel computation technique is also shown to be an effective method to improve the computational speed. Kim et al [56] developed a parallel multi-frontal solver for finite element analysis of arc-welding process, in which phase evolution, heat transfer and deformation of structures are considered. Tian et al [57] performed a parallel calculation by establishing a computer cluster system composed of four PCs to predict the final distortion of a large complicated Al alloy structure during Electron Beam Welding (EBW).

1.2.2.3 Buckling Distortion due to Welding

In modern manufacturing, design of transport vehicles such as ships, automobiles, trains and aircrafts emphasizes minimizing weight to improve fuel economy and/or enhance the carrying capacity. Therefore the demand for lightweight structures assembled using thin plates densely stiffened has significantly increased. For thin plate ship structures, buckling type distortion may be produced by the welding process. Buckling is considered to be the most critical type of welding distortion because of its instability and difficulty of straightening [58].

Experimental investigation of welding induced buckling can be found in the literature. Masubuchi [59] conducted experiments of buckling type deformation of thin plates due to welding, and presented the critical buckling wave length as influenced by the size of plate and welding conditions. Watanabe and Satoh [60] observed welding induced buckling distortion, the so-called concave-convex or convex-concave type, in a series of experiments of bead on plate welding on thin plates. The critical buckling force and the moment when buckling occurs in welded plates with different aspect ratio is measured and studied [61]. Frank [62] indicated that thin plates can buckle during and after welding due to thermal and residual welding stresses. Critical residual buckling stresses are calculated for a number of different boundary conditions and a test program is conducted to partially verify the predictions. Terasaki et al. [63-64] also investigated plate buckling behavior caused by welding, utilizing experiments and numerical analyses. They have shown that welding induced buckling is affected by the welding conditions, size of plate and material properties.

Taking advantage of numerical analysis and high performance computers, investigation of welding induced buckling distortion using the computational approach is developed. Zhong et al [65] proposed an elastic FE method, based on the elastic large deflection theory of plates, utilizing the inherent strain as an equivalent load determined by the process conditions. Zaeem et al [66] investigated the local and global welding induced buckling distortion of a thin wall aluminum T joint during

and after welding. Computations using thermal viscoelastic plastic models consist of two uncoupled analyses to determine temperature history and longitudinal residual stresses. Mollicone et al [67] studied buckling in the fabrication of large, thin plate welded structures and found that minor variations in fabrication procedures has significant effects on out-of-plane welding distortion. Buckling instability behavior is investigated considering the initial out-of-plane distortion due to tack welding, clamping conditions during welding and cooling.

Tsai et al [5] studied the distortion mechanism and the effect of welding sequence on panel distortion. Using the finite element method, local plate bending and buckling were investigated. They concluded that, in their models, buckling does not occur in structures with a skin plate thickness of more than 1.6mm unless the stiffening girder bends excessively. Tsai et al [68] pointed out that the bifurcation phenomenon of buckling starts during the cooling cycle and this may continue to grow until the completion of the cooling process. An integrated experimental and numerical approach was applied to investigate the mechanism of welding induced buckling evolution process. Meanwhile, eigenvalue analysis using welding longitudinal inherent strain distribution and 3D thermal elastic plastic FE analysis considering large deformation were performed on welded structural models to understand the buckling distortion process observed in the experiments.

P Michaleris [69-70] pointed out that the compressive residual stress parallel to welding line contributes a loading that eventually results in buckling if the stress exceeds the critical buckling stress of the welded structure. He called this stress the Applied Weld Load (AWL), which is determined by performing local 3D thermal elastic plastic FE analysis of the welding process. A 2D shell model depicting the actual ship panel using a relatively coarse mesh is then used to perform an eigenvalue analysis that determines the various buckling modes caused by welding residual stress. The minimum eigenvalue obtained from the analysis is used to evaluate the resistance to buckling. This resistance to buckling has been called the Critical Buckling Load (CBL). A comparison of the AWL and the CBL indicates whether the welded structure is expected to buckle and what mode of buckling is likely to occur. Vanli and Michaleris [71] considered fillet welded joints with a particular emphasis on welding induced buckling instabilities. The effects of stiffener geometry, welding sequence, welding heat input and mechanical fixtures on the occurrence of buckling and the distortion pattern are investigated. Deo et al [72] examined welding induced buckling distortion by means of decoupled 2D and 3D approaches, where the investigation process is divided into two steps, first determination of welding residual stress based on a 2D thermal mechanical welding simulation, then, obtaining the critical buckling stress and the buckling mode using a 3D eigenvalue analysis. Michaleris et al [73] suggested that the magnitude of longitudinal residual stress is critical in the prediction of buckling distortion. An evaluation of modeling procedures to predict welding induced buckling distortion incorporating a moving heat source, 2D and 3D small deformation analysis, 3D large deformation analysis and 2D-3D applied plastic strain analyses is carried out by comparing computed residual stress

and distortion with experimental measurements. Bhide et al [74] compared submerged arc welding, gas metal arc welding and friction stir welding in terms of their buckling propensity by measuring the longitudinal residual stress using the blind hole drilling method, and welding distortion using digital gauges at points on the welded plates.

Huang et al [75-76] carried out a comprehensive assessment of fabrication technology of lightweight structures produced using relatively thin plates with a major initiative fund by the U.S Navy Office of Naval Research. The assessment includes a comprehensive investigation of the fabrication and assembly processes of thin steel plate structures and their contributions to the final dimensional accuracy and distortion. An optical measurement system and advanced computational tools are employed to understand the underling mechanism of buckling distortion and critical process parameters for ship panels. They noted that dimensional accuracy due to thermal cutting can have a significant impact on buckling distortion. They also noted that effective mitigation techniques for minimizing buckling distortion should either reduce the buckling driving force (fabrication induced stresses) and/or increase the buckling resistant (panel geometric parameters). Yang and Dong [77] considered welding induced buckling distortion as an unstable type of welding distortion and proposed a buckling analysis procedure incorporating welding induced residual stress state.

Tajima et al [78] pointed out that welding longitudinal shrinkage (tendon force) produces compressive stress in the surrounding plate fields that sometimes cause these plate fields to buckle. In order to avoid buckling, a series of thermal elastic plastic finite element analyses is carried out to predict welding tendon forces and transverse shrinkage/bending when utilizing continuous and intermittent welding with different welding specifications. A cross stiffened panel of a car deck of a car carrier is investigated. Bi-directional residual stresses are then evaluated for different welding patterns. The effectiveness of welding pattern (continuous, parallel and zigzag intermittent welding) in reducing welding residual stress and preventing buckling is quantified. Deng and Murakawa [79] developed a prediction method of welding distortion, which combines thermal elastic plastic finite element method and large deformation elastic FE method base on inherent strain/deformation method and the interface element. The inherent deformations of two typical welded joints used in a large thin plate structure were evaluated using thermal elastic plastic FE method. Then an elastic analysis using these inherent deformations is employed to investigate the influence of heat input, welding procedure, welding sequence, plate thickness and spacing between the stiffeners on buckling propensity of this structure. Wang et al [80] investigated welding induced buckling with an elastic analysis based on the inherent deformation method. They considered a thin plate welded structure, for which the inherent deformation is evaluated for a typical welded joint by means of 3D thermal elastic plastic FE analysis. Straightening using line heating on the plate side opposite to the stiffener side to reduce buckling distortion is also investigated utilizing the same approach.

From the above, it may be seen that welding induced buckling is experimentally

and numerically investigated. Computed results are in good agreement with experimental measurement. Although these achievements are essential to recognize welding induced buckling, the generation mechanism of this kind of welding distortion is still not well understood. It is still difficult to clearly understand and predict buckling distortion of large scale and complex welded structures such as ship structures.

1.3 Objectives of Dissertation

Despite the large body of research on welding induced buckling, it is a complex phenomenon that is still not well understood. It is the objectives of this research to;

1. Clarify the mechanism by which welding induced buckling occurs;
2. Investigate the applicability of the computational approach and the inherent deformation method to predict buckling in welded joints and large welded structures;
3. Utilize the computational approach to accurately predict and explain welding distortion, including buckling;
4. Propose methods to minimize or ultimately avoid welding induced buckling in assembly and welding of ship panel structures;

1.4 Framework of Dissertation

In this research, welding induced buckling of ship structures is investigated using the computational approach utilizing the inherent deformation theory and the mechanism of buckling is clarified. Further, straightening to correct welding distortion is considered also using the same computational approach. The dissertation is organized as follows:

Background and objective of this research are presented together with the literature survey in the filed of computational welding mechanics and welding distortion in this chapter. In **Chapter 2**, fundamental theories and methods used in this research and incorporated in the JWRIAN (in-house code developed by Joining and Welding Research Institute of Osaka University) are introduced from the physical and mathematical aspects. These include, Thermal Elastic Plastic FE Analysis, Inherent Strain Method, Inherent Deformation Method, Concept of Tendon Force, Interface Element, Large Deformation Elastic Analysis and Eigenvalue Analysis. Theoretical analysis is also performed to get simple formulae of inherent strain and tendon force.

Due to importance of the longitudinal inherent shrinkage in welding induced buckling, **Chapter 3** focused on evaluation methods of the longitudinal inherent shrinkage namely;

(1) Empirical and theoretical formula;

(2) Calculation from longitudinal displacements;

(3) Integration of computed plastic strain/residual stress.

The influence of the size of a welded structure and the heat input used in welding on the magnitude of inherent deformation is examined. Cases with extreme

conditions (narrow width and large heat input) are analyzed using thermal elastic plastic FE analysis, and the results are discussed and explained using the concept of the average temperature.

Chapter 4 focuses on buckling behavior during the whole welding process consists of the heating and the cooling processes. For thin plate structures made of high tensile steel, not only residual buckling during or after cooling but also transient buckling during heating may occur. The thermal elastic plastic FE analysis to investigate buckling during the whole welding process is presented.

In **Chapter 5**, the buckling phenomenon in bead on plate of a rectangular plate is studied by experiment and computations to understand the fundamental feature of the problem. Out-of-plane distortion measured by digital photography is presented showing that the saddle type buckling occurred after cooling. Thermal elastic plastic FE analysis is conducted to predict the welding distortion and the results show a saddle type buckling mode. Also, eigenvalue analyses considering the same welding conditions are conducted to clarify the critical condition for buckling and the deformation mode. Then the elastic analysis based on the inherent deformation theory is presented. Out-of-plane welding distortion is predicted considering initial deflection. It is shown that the longitudinal inherent shrinkage is the dominant reason of buckling and the magnitude of the longitudinal inherent shrinkage determines the buckling mode. The initial deflection and the inherent bending are considered as disturbance to trigger buckling and they may not influence the buckling mode but would change the magnitude of welding distortion.

In **Chapter 6**, a thin plate stiffened welded structure is examined to investigate welding induced buckling. Experiment and analysis show that, because bending stiffness of the plate is increased by the stiffeners, welding does not cause the buckling of plate in local bending mode. The whole stiffened structure buckled in a twisting mode, while the plate stays almost straight. Good agreement of out-of-plane welding distortion is observed among experimental results, thermal elastic plastic analysis results and elastic FE analysis results. Eigenvalue analysis is also presented illustrating that the twisting buckling mode is the lowest buckling mode for the considered stiffened welded structure. Through the comparison between experiment and computation, effectiveness of the inherent deformation theory is demonstrated.

Chapter 7 presents an application of the inherent deformation theory for the prediction of welding induced buckling of a large scale thin plate structure. A stiffened panel structure in Pure Car Carrier is selected as a practical example. The inherent deformations of all the welded joints contained in the structure are evaluated using thermal elastic plastic FE analysis. The elastic FE analysis and the eigenvalue analysis show that the stiffened ship panel buckles at the edges and only hungry horse type bending distortion is produced in the internal region. After clarifying the mechanism of welding distortion, straightening process by line heating is investigated numerically in this chapter. In the internal region, inherent bending with the same magnitude as that induced by welding is applied on the plate side opposite to the welded stiffeners side. In this process, it is assumed that the torch moves fast to

reduce the in-plane inherent shrinkage. At the edge region only the in-plane inherent strain produced by line heating with slow moving torch is introduced to correct buckling. It is shown that distortion of the considered ship panel can be reduced to an acceptable level after the welding and then straightening processes.

Finally, **Chapter 8** concludes this thesis with summarizing its contributions and presents suggestions for the future research.

Chapter 2 Theory and Method of Investigation

Computational analysis is an advanced and effective research tool. To investigate welding induced buckling, computational analysis is employed in this research. In this chapter, theories and methods employed in this research are presented.

Due to the importance of buckling behavior in distortion of thin structures during welding assembly, the large deformation theory is discussed first. Computational analysis to predict out-of-plane welding distortion is carried out using the in-house code JWRIAN. This code incorporates algorithms that carry out a range of analyses to predict welding distortion and residual stresses in welded joints, as well as in large welded structures.

1. Thermal elastic plastic FE analysis using solid element models;
2. Elastic FE analysis using shell element models. Beside conventional loading, welding inherent strain and/or welding inherent deformation may be applied as a load;
3. Eigenvalue analysis using shell element models and loading as in 2 above.

In the following, the framework of these analyses and the underlying concepts and theories are introduced. The interface element, used to model the connection between the parts to be welded, is presented. Finally the concept of the tendon force (longitudinal inherent shrinkage) is also presented.

2.1 Strain-Displacement Relationship in Large Deformation Theory

The equation relating the strain and the displacement is an essential equation to describe buckling behavior. If small deformation is assumed, the strains are given as a linear function of displacements. When large deformation is considered, Green-Lagrange strain as shown in **Eq. (2-1)** is employed. The strains have a nonlinear relationship to the displacements.

$$
\begin{aligned}
\varepsilon_x &= \frac{\partial u}{\partial x} + \frac{1}{2}\left\{\left(\frac{\partial u}{\partial x}\right)^2 + \left(\frac{\partial v}{\partial x}\right)^2 + \left(\frac{\partial w}{\partial x}\right)^2\right\} \\
\varepsilon_y &= \frac{\partial v}{\partial y} + \frac{1}{2}\left\{\left(\frac{\partial u}{\partial y}\right)^2 + \left(\frac{\partial v}{\partial y}\right)^2 + \left(\frac{\partial w}{\partial y}\right)^2\right\} \\
\varepsilon_z &= \frac{\partial w}{\partial z} + \frac{1}{2}\left\{\left(\frac{\partial u}{\partial z}\right)^2 + \left(\frac{\partial v}{\partial z}\right)^2 + \left(\frac{\partial w}{\partial z}\right)^2\right\} \\
\gamma_{xy} &= \frac{\partial u}{\partial y} + \frac{\partial v}{\partial x} + \left\{\left(\frac{\partial u}{\partial x}\right)\left(\frac{\partial u}{\partial y}\right) + \left(\frac{\partial v}{\partial x}\right)\left(\frac{\partial v}{\partial y}\right) + \left(\frac{\partial w}{\partial x}\right)\left(\frac{\partial w}{\partial y}\right)\right\} \\
\gamma_{yz} &= \frac{\partial v}{\partial z} + \frac{\partial w}{\partial y} + \left\{\left(\frac{\partial u}{\partial y}\right)\left(\frac{\partial u}{\partial z}\right) + \left(\frac{\partial v}{\partial y}\right)\left(\frac{\partial v}{\partial z}\right) + \left(\frac{\partial w}{\partial y}\right)\left(\frac{\partial w}{\partial z}\right)\right\} \\
\gamma_{zx} &= \frac{\partial w}{\partial x} + \frac{\partial u}{\partial z} + \left\{\left(\frac{\partial u}{\partial z}\right)\left(\frac{\partial u}{\partial x}\right) + \left(\frac{\partial v}{\partial z}\right)\left(\frac{\partial v}{\partial x}\right) + \left(\frac{\partial w}{\partial z}\right)\left(\frac{\partial w}{\partial x}\right)\right\}
\end{aligned}
\tag{2-1}
$$

Where, ε_x , ε_y and ε_z are Green-Lagrange strain in x , y and z directions; γ_{xy}, γ_{yz} and γ_{zx} are the shear strain on the x-y , y-z and z-x planes. u, v and w are the displacement in x, y and z directions, respectively.

In **Eq. (2-1)**, the first order terms express linear response, and the second order terms are essential to express non-linear behavior such as buckling.

2.2 Thermal Elastic Plastic FE Analysis

In thermal elastic plastic FE analysis, two processes are considered, the thermal process and the mechanical process. The thermal process has a decisive effect on the mechanical process. However, since the mechanical process has only a very small influence on the thermal process, as shown in **Fig. 2.1**, a coupled thermal mechanical analysis is not necessary. Therefore, a thermal/mechanical uncoupled formulation is used in this study to analyze the thermal-mechanical behavior during the welding process. This kind of uncoupled formulation considers the contribution of the transient temperature field to stresses through thermal expansion, as well as temperature dependent thermal-physical properties and mechanical properties. **Figure 2.2** shows the temperature-dependent material properties of carbon steel that are used through out this thesis except for high tensile strength steel.

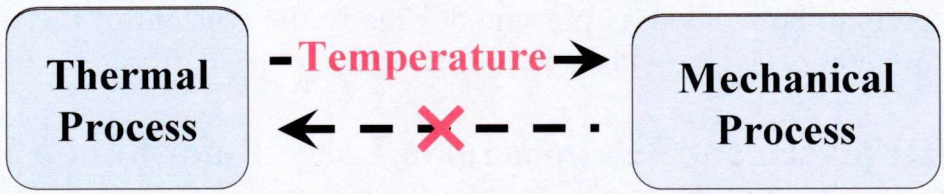

Fig. 2.1 Relationship between thermal process and mechanical process in thermal elastic plastic FE analysis.

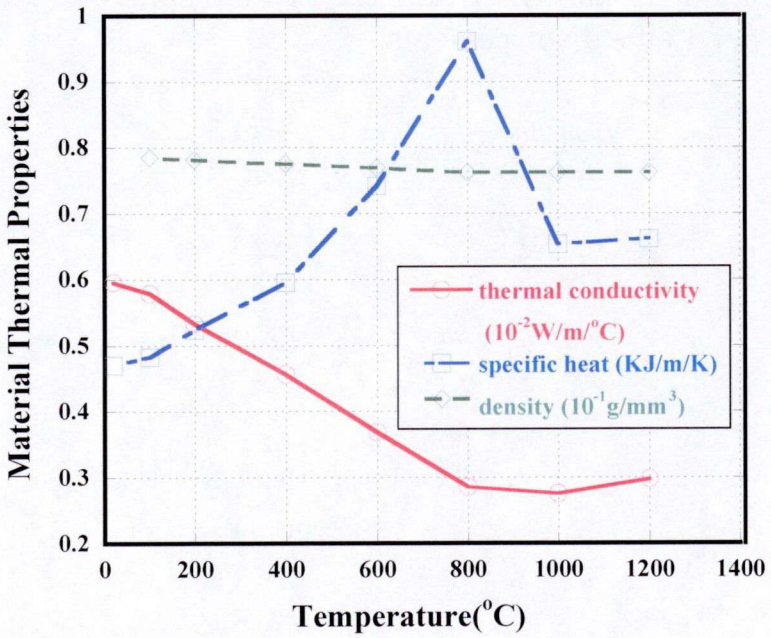

(a) Thermal-physical properties of carbon steel

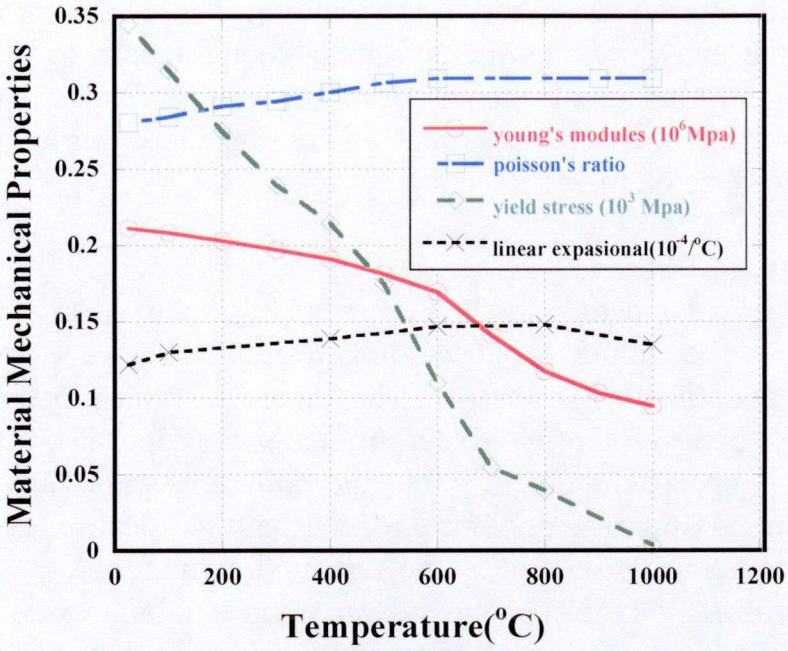

(b) Mechanical properties of carbon steel

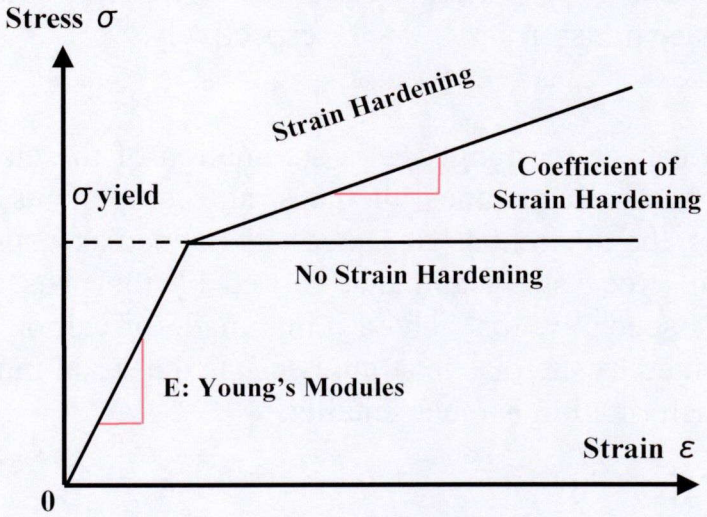

(c) Strain hardening diagram (coefficient of strain hardening is assumed as 0.4% of Young's modules)

Fig. 2.2 Temperature dependent material properties used in this research.

The solution procedure consists of two steps. First, temperature distribution history is computed using transient heat transfer (conduction, convection and radiation) analysis. Then the transient temperature distribution obtained from the heat transfer analysis is introduced as a thermal load in a subsequent mechanical analysis, in which the residual stresses, plastic strains and displacements are computed.

2.3 Elastic FE Analysis

If the inherent strain or the inherent deformation is evaluated using a computational or an experimental approach, an elastic FE analysis can be employed to predict welding distortion of welded structures. In this elastic FE analysis, the

inherent strain/deformation is applied to the welding lines in shell element models of welded structures. Meanwhile, the interaction between the parts to be welded together is represented by the Interface Element. Bonding strength, gaps, and misalignments that arise during different assembly processes are considered through controlling the stiffness of the interface element.

2.3.1 Inherent Strain Theory

Based on thermal elastic plastic FE analysis and experimental observations, Ueda et al [22, 36, 37, 80] concluded that welding residual stress and welding distortion are produced by the inherent strain ε^*. The inherent strain mostly depends on the joint parameters, such as type of welded joint, material properties, plate thickness and heat input. For a specific welded joint, the inherent strain at each location is determined by the maximum temperature reached at this location during the welding process, and the constraint provided by the surrounding material.

The total strain ε^{total} during the heating and cooling cycle of the welding process can be divided into the strain components given by **Eq. (2-2)**, namely, elastic strain $\varepsilon^{elastic}$, plastic strain $\varepsilon^{plastic}$, thermal strain $\varepsilon^{thermal}$, creep strain ε^{creep} and that produced through phase transformation ε^{phase}, respectively.

$$\varepsilon^{total} = \varepsilon^{elastic} + \varepsilon^{thermal} + \varepsilon^{plastic} + \varepsilon^{phase} + \varepsilon^{creep} \tag{2-2}$$

The total strain can be rearranged as a summation of the elastic strain and the inherent strain $\varepsilon^{inherent}$ which includes all the strain components except the elastic strain. In other words, the inherent strain $\varepsilon^{inherent}$ is defined as a summation of plastic strain, thermal strain, creep strain and that caused by the phase transformation as given by **Eq. (2-3)**. Especially, for welded joints made of carbon steel, the inherent strain can be represented by the plastic strain because the strain induced by creep and solid-state phase transformation is much smaller.

$$\varepsilon - \varepsilon^{elastic} = \varepsilon^{thermal} + \varepsilon^{plastic} + \varepsilon^{phase} + \varepsilon^{creep} = \varepsilon^{inherent} = \varepsilon^* \tag{2-3}$$

The distributions of inherent strain which remains in a narrow area near the welding line are schematically illustrated in **Fig. 2.3.** It may be seen that the longitudinal strain ε_x^* exists throughout the length of the welded joint and is constant in the middle part where the effect of free ends may disappear; however, the transverse strain ε_y^* exists in relatively narrower region with much larger magnitude throughout the length of welded joint [81]. **Figure 2.4** shows typical distributions of longitudinal and transverse plastic strain (inherent strain) on one cross section normal to the welding line.

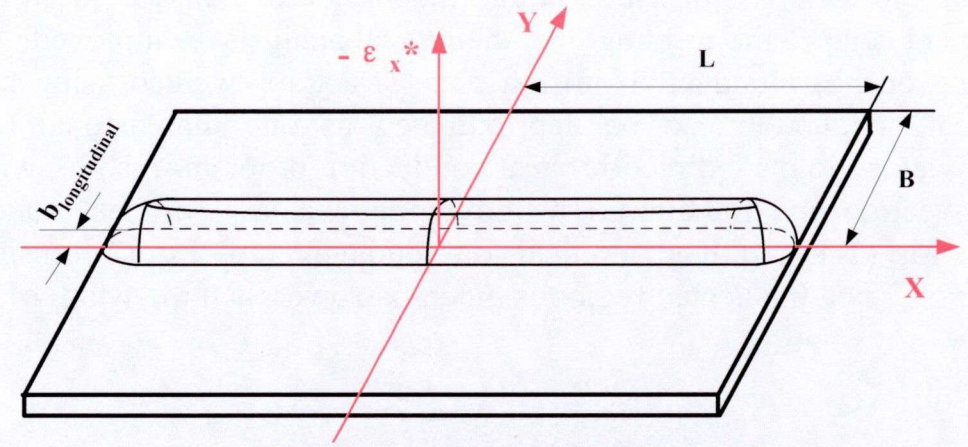

(a) Longitudinal plastic strain (inherent strain)

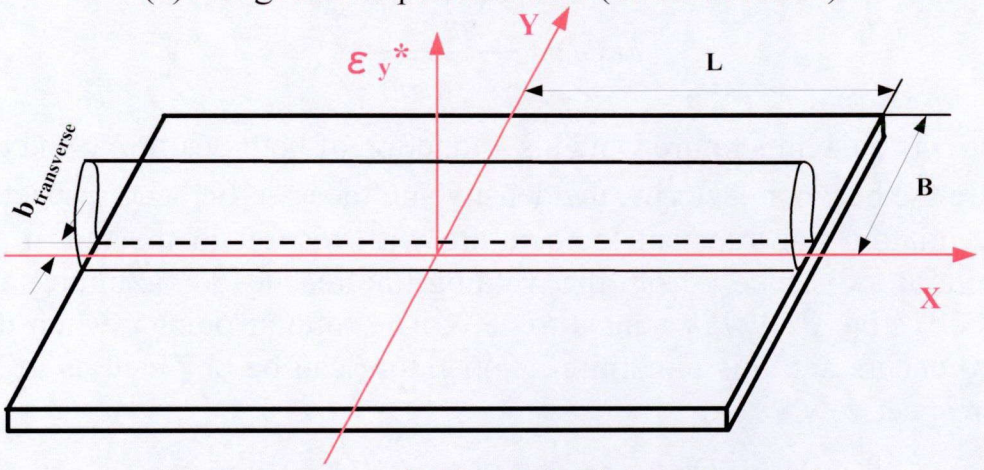

(b) Transverse plastic strain (inherent strain)

Fig. 2.3 Schematic representations of inherent strain distribution in butt welding.

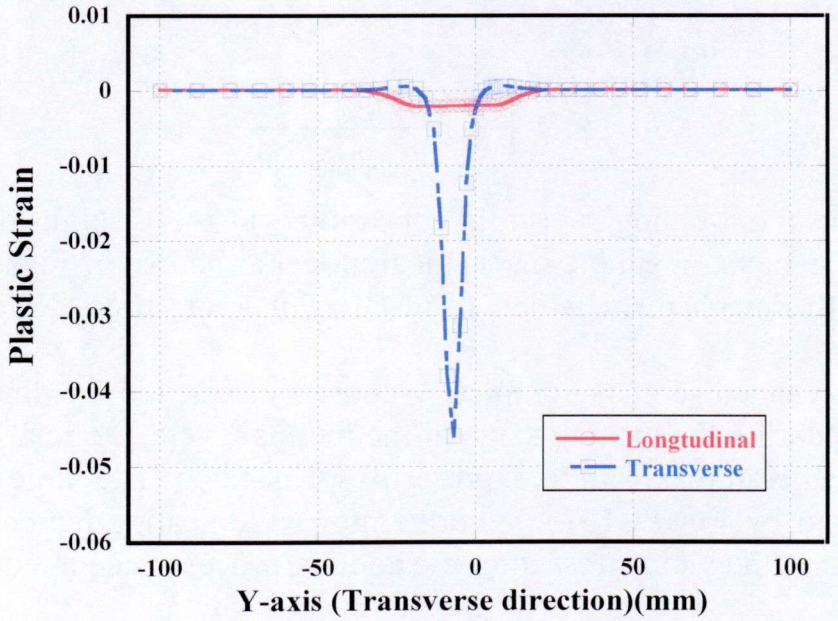

Fig. 2.4 Distribution of plastic strain at the neutral axis of the middle transverse cross section.

To obtain an idealized distribution and magnitude of inherent strain on a cross section perpendicular to the welding line, theoretical analysis is employed.

Focusing on heat conduction in thin plate structures welded using high speed welding, heat conduction can be approximated as one dimensional (transverse direction of welded joint: y direction) heat conduction problem in solid, without heat loss by convection and radiation. The governing equation of heat conduction is expressed as **Eq. (2-4)** and the theoretical solution is given by **Eq. (2-5)** using Fourier Transformation when the heated region is much narrower than the width of the whole plate.

$$a\frac{\partial^2 T(y,t)}{\partial y^2}=\frac{\partial T(y,t)}{\partial t}\quad (a=\frac{\lambda}{\rho c}) \tag{2-4}$$

$$T(y,t)=\frac{\eta Q}{\rho c\sqrt{4\pi at}}e^{-\frac{y^2}{4at}} \tag{2-5}$$

Where, $T(y, t)$ is the temperature which is a function of both position y and time t. λ, ρ and c are the heat conductivity, the density and the specific heat, respectively.

Differentiating the transient temperature with respect to the time t, as in **Eq. (2-6),** a point at a distance y from the welding line reaches a maximum temperature when the derivative $\partial T(y,t)/\partial t$ equals to zero. The time at point y when the highest temperature occurs and this maximum temperature can be obtained as in **Eqs. (2-7)** and **(2-8)**, respectively.

$$\frac{\partial T(y,t)}{\partial t}=\frac{Q_{net}}{\rho c\sqrt{4\pi a}}\frac{\partial}{\partial t}(\frac{1}{\sqrt{t}}e^{-\frac{y^2}{4at}})=\frac{Q_{net}}{\rho c\sqrt{4\pi at}}e^{-\frac{y^2}{4at}}(\frac{y^2}{4at^2}-\frac{1}{2t}) \tag{2-6}$$

$$\frac{y^2}{4at^2}-\frac{1}{2t}=0\qquad when\ ,t=\frac{y^2}{2a} \tag{2-7}$$

$$T_{\max}(y)\Big|_{t=\frac{y^2}{2a}}=\frac{Q_{net}}{\rho c\sqrt{2\pi e}}\frac{1}{y} \tag{2-8}$$

Noting that the welding region is constrained in the welding direction by the surrounding base metal, a simple mechanical model as shown in **Fig. 2.5** is proposed to investigate the mechanism which forms the inherent strain during the welding process.

When the welded joint is completely constrained in the welding direction and remains elastic during the heating stage of the thermal cycle, the relation between the stress σ and temperature T can be expressed by **Eq. (2-9)**. The yield temperature T_Y can be expressed by **Eq. (2-10)** [36]. Furthermore, the heating temperature which is necessary to attain the yield stress after the cooling process is denoted T_2 and is given by **Eq. (2-11)**.

$$\sigma=-\alpha TE \tag{2-9}$$

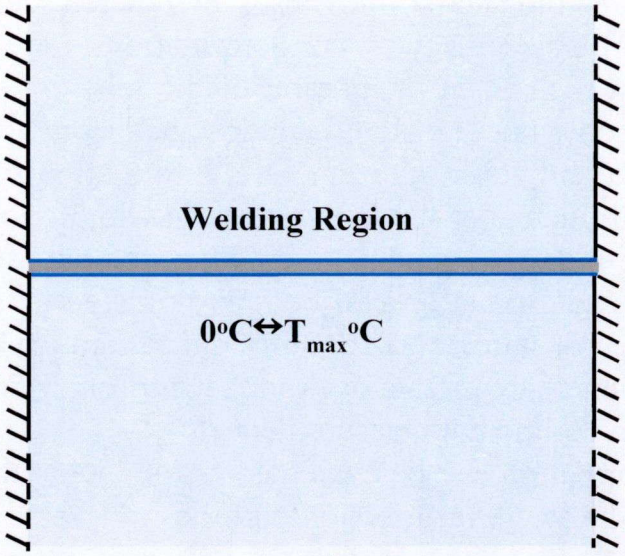

Fig. 2.5 Mechanical constraint along the welding line.

$$T_Y = \frac{\sigma_Y}{\alpha E} = T_1 \tag{2-10}$$

$$T_2 = 2T_Y \tag{2-11}$$

Where, α is the coefficient of linear expansion and E and σ_Y are Young's modules and the yield stress.

Considering these equations, the inherent strain in the welding direction can be derived for the three regions according to the maximum temperature $T_{\max}$ as given by **Eq. (2-12)**, and corresponding longitudinal inherent strains ε_x^* are also obtained.

$$\begin{aligned} T_{\max} \le T_Y \qquad & \varepsilon_x^* = 0 \\ T_Y > T_{\max} < 2T_Y \qquad & \varepsilon_x^* = -\alpha(T_{\max} - T_Y) \\ 2T_Y \le T_{\max} \qquad & \varepsilon_x^* = -\alpha T_Y \end{aligned} \tag{2-12}$$

This model assumes fully restrained edges normal to the weld line. Also it does not take account of the temperature dependency of material properties. However, it is very useful to obtain a quick idealized solution. To take account of actual conditions, the inherent strain can be experimentally measured, or evaluated using thermal elastic plastic FE analysis.

If the inherent strain is known, deformation and residual stress after the end of the welding process can be predicted by an elastic FE analysis using the inherent strain as an initial strain.

2.3.2 Inherent Deformation Theory

As just mentioned above, the residual stress and the distortion after welding can be predicted using elastic FE analysis if the distribution of the inherent strain is known. To do this, a fine enough FE mesh, which is not desirable from practical point

of view, is required. To avoid such a fine mesh, the inherent deformation is proposed [37, 38]. Noting that the displacement or the deformation is the integration of strain, inherent deformation, which is an integration of the inherent strain, can be used to predict welding distortion without a significant loss of accuracy.

Similar to the inherent strain, the inherent deformation mostly depends on the joint parameters. The influence of the length and the width of a welded joint is small if the size of the plate is large enough [82, 83]. When the edges effect is ignored, the components of inherent deformation can be approximated as constant values along the welding line. These constant values are introduced into the elastic model as loads (forces and displacements) to predict welding distortion. Computed results are in good agreement with experimental measurements [84, 85].

The inherent deformation can be evaluated as the integration of the longitudinal inherent strain ε_x^* in the welding direction and the transverse inherent strain ε_y^* in the transverse direction distributed on the cross section normal to the welding line according to the following equations.

$$\begin{aligned}
\delta_x^* &= \frac{1}{h}\iint \varepsilon_x^* dydz \\
\delta_y^* &= \frac{1}{h}\iint \varepsilon_y^* dydz \\
\theta_x^* &= \frac{12}{h^3}\iint (z-\frac{h}{2})\varepsilon_x^* dydz \\
\theta_y^* &= \frac{12}{h^3}\iint (z-\frac{h}{2})\varepsilon_y^* dydz
\end{aligned} \tag{2-13}$$

Where, δ_x^* and δ_y^* are the inherent deformation in the longitudinal and the transverse directions, θ_x^* and θ_y^* are the inherent bending deformation in the longitudinal and the transverse directions; h is the thickness of the welded joint, and x, y, z are the welding direction, transverse direction and thickness direction, respectively.

The longitudinal inherent shrinkage has a different nature from the other inherent deformation components. This is caused by the constraint provided by the surrounding material that prevents free shrinkage along the weld line. Therefore, the longitudinal inherent deformation appears as a tensile force acting in the weld line that is referred to as the Tendon Force. Other components are subjected to only a small constraint and appear as deformation.

2.3.3 Interface Element

If all parts to be assembled by welding have no geometrical errors and they are fully fitted by tack welding with sufficient stiffness and welded simultaneously, the final distortion of the structure after welding assembly is solely determined by welding inherent deformation.

However in actual assembly processes of large scale welded structures, the parts are assembled sequentially by repeated fitting, tack welding and welding. In this situation, due to welding distortion, the already assembled members no longer have the designed geometry or dimensions. This leads to gaps and the misalignments in the fitting stage. Gaps and misalignments can also be produced by geometrical errors due to cutting and forming. If the gap or the misalignment between two parts to be welded exceeds the tolerable limit, they are corrected during the fitting process before welding. In this case, the final distortion of the whole structure is influenced by gaps and misalignments and their correction during fitting. Therefore, gaps and misalignments should be considered to predict and control the distortion of a large structure during the assembly process. The evolution of the mechanical interaction between parts to be assembled from free to fitting, tack welding and fully welded states can be conveniently described by the interface element [87, 88].

Essentially, the interface element is a nonlinear spring arranged between the parts to be welded as shown in **Fig. 2.6**. Its mechanical properties can be defined through the opening displacement-bonding force curve (δ-F curve) shown in **Fig. 2.7**, which are defined by the maximum force F_{max} and the stiffness $K = F_{\max} / r_0$ which is the slope of the straight line marked with K, K_o or K_c. **Fig. 2.7 (a)** illustrates the relations between the displacement and force in the normal direction for the opening and closing mode of deformation. Stiffness K_c, that is the resistance against the deformation in the closing direction, is set large enough to prevent the penetration between the parts. The mechanical property for the deformation in the opening direction is defined by the stiffness K_o and the maximum joining force F_{max}. The stiffness of the joint K_o is set small when the parts are free. In the fitting process, the value of stiffness K_o is set to an appropriate value according the type of tack welding. A large enough value is given to K_o after the parts are fully welded together. The value of the maximum joining force F_{max} can be selected depending on the maximum capacity of the tools used to control the gaps. For the sliding, misalignment and rotational deformation, the δ-F curve is given as an odd function as shown in **Fig. 2.7(b)**. **Table 2.1** shows the recommended values of the parameters used in the interface element for different processes.

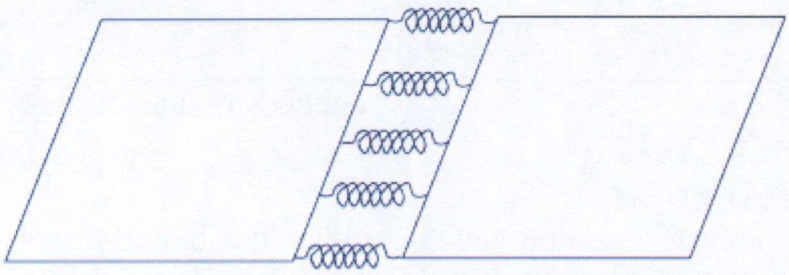

Fig. 2.6 Interface element between parts to be welded.

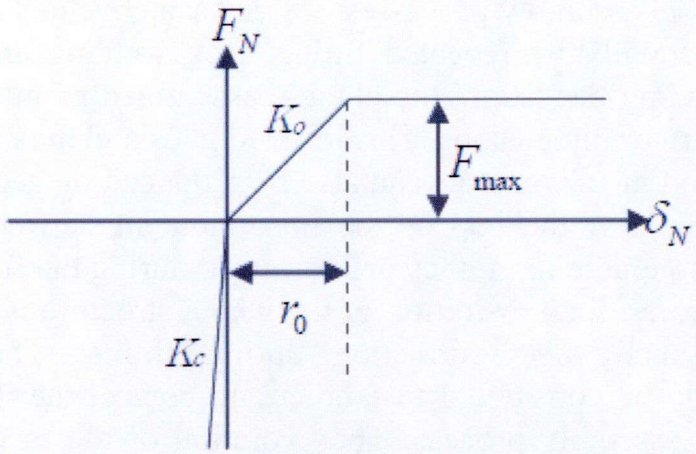

(a) Relations between bonding force and relative displacement in the normal direction

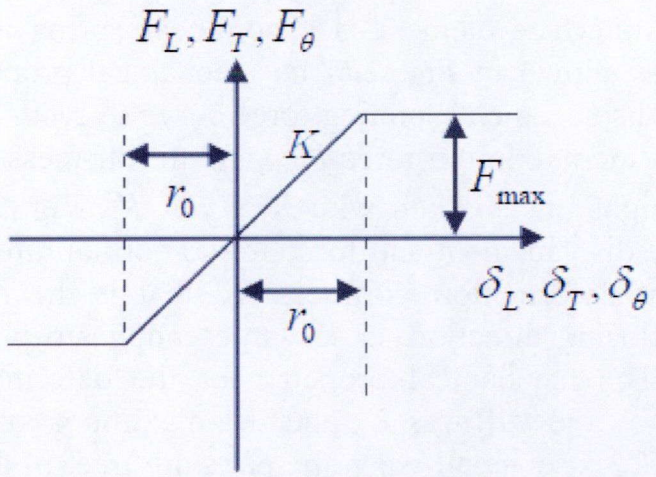

(b) Relations between bonding force and relative displacement in the shear and rotational directions

Fig. 2.7 Mechanical properties of the interface element.

Table 2.1 Value of parameters used in interface element.

	F_{max}	r_0	K
Free	$0.0(10^{-5})$	1000	$K = F_{max} / r_0 = 0$
Tack Welded	10^n	1000	$K = F_{max} / r_0 = 10^{n-3}$
Welded	10^{10}	1000	$K = F_{max} / r_0 = 10^7$

("n" depends on the stiffness of tack welding)

2.4 Eigenvalue Analysis

Eigenvalue analysis is employed to predict the buckling force of a structure assumed as an ideal linear elastic body. In the classical eigenvalue analysis, eigenvalues are computed with regard to the applied compressive force and constraints of a given system. For a basic structural configuration, each applied combination of forces has a minimum critical buckling value at which the structure

buckles, and a corresponding buckling mode. Eigenvalue analysis also gives higher buckling values and the associated buckling modes. Theoretically, there are values and modes equal in number to the number of degrees of freedom in the considered system. Eigenvalue analysis is useful to solve the following problems:

(1) Buckling of structures under external load;

(2) Buckling of structures under thermal load;

(3) Buckling of welded structures.

The difference among these three problems is the physical value to be determined by eigenvalue analysis. The values to be determined in cases (1) and (2) are the applied forces or the temperatures, respectively. In case (3), the inherent deformation at which the structure buckles is obtained. Though the physical values obtained are different, the framework of the theory is the same as reviewed in the following.

The basic variables, such as the displacement $u_{t+\Delta t}$, the strain $\varepsilon_{t+\Delta t}$, and the stress $\sigma_{t+\Delta t}$ at time $t+\Delta t$ can be decomposed into the sum of their values at time t and their increments, i.e.

$$\begin{aligned} u_{t+\Delta t} &= u_t + \Delta u \\ \varepsilon_{t+\Delta t} &= \varepsilon_t + \Delta\varepsilon = \varepsilon_t + \Delta^1\varepsilon + \Delta^2\varepsilon \\ \sigma_{t+\Delta t} &= D\varepsilon_{t+\Delta t} = \sigma_t + D\Delta\varepsilon = \sigma_t + D\Delta^1\varepsilon + D\Delta^2\varepsilon \end{aligned} \tag{2-14}$$

Where, D is the elastic matrix (stress-strain matrix), $\Delta^1\varepsilon$ and $\Delta^2\varepsilon$ are the first order (linear) and the second order (non-linear) terms of strain increment.

When **Eq. (2-1)** is used and taking ε_x for an example, it is shown that

$$\begin{aligned} \varepsilon_x(t+\Delta t) &= \frac{\partial u_{t+\Delta t}}{\partial x} + \frac{1}{2}\left(\frac{\partial u_{t+\Delta t}}{\partial x}\right)^2 + \frac{1}{2}\left(\frac{\partial v_{t+\Delta t}}{\partial x}\right)^2 + \frac{1}{2}\left(\frac{\partial w_{t+\Delta t}}{\partial x}\right)^2 \\ &= \varepsilon_x(t) + \Delta^1\varepsilon_x + \Delta^2\varepsilon_x \end{aligned} \tag{2-15}$$

Where

$$\begin{aligned} \varepsilon_x(t) &= \frac{\partial u_t}{\partial x} + \frac{1}{2}\left(\frac{\partial u_t}{\partial x}\right)^2 + \frac{1}{2}\left(\frac{\partial v_t}{\partial x}\right)^2 + \frac{1}{2}\left(\frac{\partial w_t}{\partial x}\right)^2 \\ \Delta^1\varepsilon_x &= \frac{\partial \Delta u}{\partial x} + \frac{\partial u_t}{\partial x}\frac{\partial \Delta u}{\partial x} + \frac{\partial v_t}{\partial x}\frac{\partial \Delta v}{\partial x} + \frac{\partial w_t}{\partial x}\frac{\partial \Delta w}{\partial x} \\ \Delta^2\varepsilon_x &= \frac{1}{2}\left(\frac{\partial \Delta u}{\partial x}\right)^2 + \frac{1}{2}\left(\frac{\partial \Delta v}{\partial x}\right)^2 + \frac{1}{2}\left(\frac{\partial \Delta w}{\partial x}\right)^2 \end{aligned} \tag{2-16}$$

To derive the governing equation for eigenvalue analysis, the minimum potential energy theorem is employed. The total energy of the system at times t and $t+\Delta t$ are given by **Eq. (2-17)** and **(2-18)**, respectively.

$$\pi(u_t) = \int \frac{1}{2}\varepsilon_t^T D\varepsilon_t dv - \int f_t u_t ds \tag{2-17}$$

$$\pi(u_t + \Delta u) = \int \frac{1}{2}(\varepsilon_t + \Delta^1\varepsilon + \Delta^2\varepsilon)^T D(\varepsilon_t + \Delta^1\varepsilon + \Delta^2\varepsilon)dv - \int (f_t + \Delta f)(u_t + \Delta u)ds$$
$$= \pi(u_t) + \Delta\pi(\Delta u) \tag{2-18}$$

Because the potential energy at time t is already known and fixed, the condition for the potential energy $\pi(u_t + \Delta t)$ to be a minimum is equivalent to that condition for its increment $\Delta\pi(\Delta u)$, given by **Eq. (2-19)** in which the higher order terms are neglected. **Eq. (2-19)** can be rewritten in matrix form as shown in **Eq. (2-20)**.

$$\Delta\pi(\Delta u) = \pi(u_t + \Delta t) - \pi(u_t)$$
$$= \int \frac{1}{2}\{(\Delta^1\varepsilon)^T D(\Delta^1\varepsilon) + 2D\varepsilon_t\Delta^1\varepsilon + 2D\varepsilon_t\Delta^2\varepsilon\}dv - \int (f_t\Delta u + \Delta f u_t)ds$$
$$= \int \frac{1}{2}\{(\Delta^1\varepsilon)^T D(\Delta^1\varepsilon) + 2\sigma_t\Delta^2\varepsilon\}dv - \int \Delta f u_t ds + \int \sigma_t\Delta^1\varepsilon dv - \int f_t\Delta u ds \tag{2-19}$$

Eq. (2-19) can be rewritten in the following matrix form,

$$\Delta\pi(\Delta u) = \frac{1}{2}\{\Delta u\}^T\left[K_1(u_t)\right]\{\Delta u\} + \frac{1}{2}\{\Delta u\}^T\left[K_2(\sigma_t)\right]\{\Delta u\}$$
$$-\{\Delta f\}^T\{\Delta u\} + \{F\}^T\{\Delta u\} - \{f_t\}^T\{\Delta u\} \tag{2-20}$$

Where

$$\frac{1}{2}\{\Delta u\}^T\left[K_1(u_t)\right]\{\Delta u\} = \int \frac{1}{2}(\Delta^1\varepsilon)^T D(\Delta^1\varepsilon)dv$$
$$\frac{1}{2}\{\Delta u\}^T\left[K_2(\sigma_t)\right]\{\Delta u\} = \int D\varepsilon_t\Delta^2\varepsilon dv = \int \sigma_t\Delta^2\varepsilon dv$$
$$\{F\}^T\{\Delta u\} = \int D\varepsilon_t\Delta^1\varepsilon dv$$
$$\{\Delta f\}^T\{\Delta u\} = \int \Delta f\Delta u_t dv$$
$$\{f_t\}^T\{\Delta u\} = \int f_t\Delta u dv$$

From the condition for the minimum value of $\Delta\pi(\Delta u)$, the following equation is derived.

$$\frac{\partial\Delta\pi(\Delta u)}{\partial\Delta u} = \left[K_1(u_t)\right]\{\Delta u\} + \left[K_2(\sigma_t)\right]\{\Delta u\} + \{F\} - \{f_t\} - \{\Delta f\} = 0 \tag{2-21}$$

Due to the equilibrium of the system at time *t*

$$\{F\} - \{f_t\} = 0 \tag{2-22}$$

Because of the fact that the buckling occurs without increase of external forces, **Eq. (2-23)** is satisfied.

$$\{\Delta f\} = 0 \tag{2-23}$$

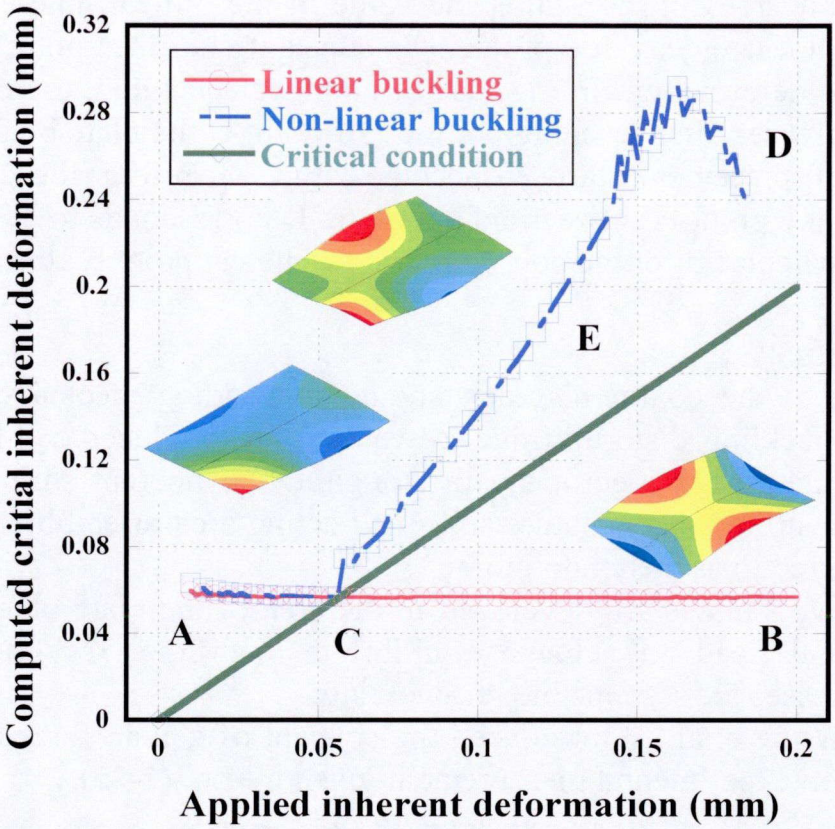

Fig. 2.8 Comparison between critical inherent deformations in linear and non-linear buckling.

If the system buckles under an internal force $\lambda\{\sigma_t\}$, **Eq. (2-21)** is reduced to an eigenvalue problem given by **Eq. (2-24)**.

$$[K_1(u_t)]\{\Delta u\} + \lambda[K_2(\sigma_t)]\{\Delta u\} = 0 \tag{2-24}$$

From **Eq. (2-24)**, it is clear that buckling is an eigenvalue problem. In case of welding, the stress σ_t is the stress produced by the inherent deformation associated with the welding and the parameter λ is the eigenvalue to be determined. When the stress becomes equal to $\lambda\sigma_t$, the structure buckles. This means that the structure has already buckled when λ is less than 1.0.

At this point, it should be noted that the current deformation u_t and stress σ_t are included in the stiffness matrices $[K_1]$ and $[K_2]$. This implies that the value of $\lambda\sigma_t$ is not unique, but changes with the deformation u_t. On the other hand, in the standard buckling problem, the effect of the current deformation u_t is either negligible (as in buckling of a flat plate under in-plane load) or ignored and the value of $\lambda\sigma_t$ can be uniquely determined. For convenience, the former is referred to as nonlinear buckling problem and the latter is referred to as linear buckling problem.

Figure 2.8 shows the critical inherent deformation for a rectangular welded plate computed as a linear and as a nonlinear buckling problem. In these computations, the eigenvalue is computed while increasing the applied inherent deformation. As may be

seen from the line A-B in the figure, the value of the critical inherent deformation computed as a linear eigenvalue problem is constant and does not change with the applied inherent deformation. In the case of nonlinear buckling, the critical inherent deformation increases after reaching point C. At point C the plate buckles in the first mode and the displacement starts to become large. Therefore, the critical inherent deformation at any point E between points C and D corresponds to a higher buckling mode which is calculated for the configuration reached at point E after first buckling.

2.5 Tendon Force

According to the common understanding in welding mechanics, longitudinal shrinkage and buckling distortion due to welding are produced by the longitudinal inherent shrinkage, more specifically the longitudinal inherent shrinkage force [89]. This force has a strong tensile nature and small acting area resembling a tendon. This is why it is referred to as the tendon force.

Compressive stresses are developed in the area of the plate other than the area around the weld bead to achieve equilibrium with the Tendon Force. These compressive stresses are responsible for buckling.

In 1980, White et al [90] introduced the concept of tendon force and proposed a formula based on experimental measurement given by **Eq. (2-25)**.

$$F_{tendon} = 0.2Q_{net} \quad (Q_{net} = \eta Q) \tag{2-25}$$

Where, F_{tendon} is in KN, Q_{net} (J/mm) is the net heat input per unit length.

Meanwhile, Sato et al [1] proposed the relation between tendon force and heat input as shown in **Eq. (2-26)**. Terasaki et al [91] concluded that the relation between tendon force and heat input is influenced by the thickness of the welded plate. For thin plates, **Eq. (2-27-1)** can be used to evaluate the tendon force. The relation expressed by **Eq. (2-27-2)** is suitable for thick plates. Luo et al [92] presented the relation shown in **Eq. (2-28)** utilizing thermal elastic plastic FE analysis and pointed out that the tendon force is not produced until the heat input exceeds a critical value.

$$F_{tendon} = 0.107Q_{net} \tag{2-26}$$

$$F_{tendon} = 0.215Q_{net} \quad \textit{Thin Plate Structure} \tag{2-27-1}$$

$$F_{tendon} = 0.159Q_{net} \quad \textit{Thick Plate Structure} \tag{2-27-2}$$

$$F_{tendon} = 0.172(Q_{net} - 28.56) \tag{2-28}$$

To theoretically evaluate the tendon force in a welded joint, the inherent strain is employed. When the welding speed is fast enough, the heat by welding can be idealized as an instantaneous heat source distributed uniformly along the welding line. In this case, the problem can be reduced to one dimensional heat conduction problem in a solid, and the distribution and the magnitude of inherent strain can be evaluated [36]. As shown by **Eq. (2-12)**, the longitudinal inherent strain can be evaluated for three temperature regions separately.

The relation between the tendon force F_{tendon} and the longitudinal inherent strain ε_L^* in an infinitesimal area dA is given by **Eq. (2-29)**. **Eq. (2-30)** is employed to evaluate the tendon force as an integration of longitudinal inherent strain over the cross-section normal to the welding direction.

$$dF_{tendon} = E\varepsilon_L^* \times dA \tag{2-29}$$

$$F_{tendon} = E \times \iint_{-\infty}^{\infty} \varepsilon_L^* dydz = 2Eh \times \int_0^{\infty} \varepsilon_L^* dy \tag{2-30}$$

Meanwhile, substituting **Eq. (2-10)** and **(2-11)** into **Eq. (2-8)**, the positions y_1 and y_2 which reach the maximum temperature T_Y (T_1) and $2T_Y$ (T_2) respectively can be calculated as given by **Eq. (2-31)**.

$$y_1 = \frac{Q_{net}}{\rho ch\sqrt{2\pi e}} \frac{\alpha E}{\sigma_Y} \qquad y_2 = \frac{Q_{net}}{2\rho ch\sqrt{2\pi e}} \frac{\alpha E}{\sigma_Y} \tag{2-31}$$

Integrating the inherent strain on the whole cross section, **Eq. (2-31),** the tendon force (longitudinal inherent shrinkage force) produced by welding can be evaluated as follows:

$$\begin{aligned} F_{tendon} &= 2h(\int_0^{y2} E \times (-\alpha T_Y)dy + \int_{y2}^{y1} -\alpha(T_{\max} - T_Y) \times Edy + \int_{y1}^{+\infty} E \times 0dy) \\ &= 2h(\int_0^{y2} E \times (-\alpha T_Y)dy + \int_{y2}^{y1} \alpha T_Y \times Edy + \int_{y2}^{y1} -\alpha T_{\max} \times Edy) \\ &= 2h(-\alpha T_Y E(y_2 - 0) + \alpha T_Y E(y_1 - y_2) + (-\alpha E)\frac{Q_{net}}{\rho ch\sqrt{2\pi e}} \ln(\frac{y_1}{y_2})) \\ &= (-\alpha E)\frac{2Q_{net}}{\rho c\sqrt{2\pi e}} \ln(2) = -0.335 \times \frac{\alpha E}{\rho c} \times Q_{net} \end{aligned} \tag{2-32}$$

When the material properties of carbon steel at room temperature are used, the tendon force can be expressed as given by **Eq. (2-33)**. This equation has an approximately similar coefficient as that in the empirical formula given by **Eq. (2-25)**.

$$F_{tendon} = -0.335\frac{E\alpha}{\rho c}\eta Q = -0.235\eta Q = -0.235Q_{net} \tag{2-33}$$

Where, η is the welding heat efficiency

E is Young's modules, $E = 2.1 \times 10^6\ MPa$

α is the coefficient of line expansion, $\alpha = 1.2 \times 10^{-5}\ /\ °C$

ρ is the density, $\rho = 7800 kg / m^3$

and c is the specific heat of material, $c = 4.6 \times 10^2 J / kg \cdot °C$

Furthermore, the relation between the longitudinal inherent deformation δ_L^* and the tendon force F_{tendon} (longitudinal inherent shrinkage force) [93], can be derived from their definitions given by **Eq. (2-34)**.

$$F_{tendon} = \int E \times \varepsilon_L^* dA = E \times h \times \frac{1}{h} \int \varepsilon_L^* dA = Eh\delta_L^* \tag{2-34}$$

Where, ε_L^* and $\delta_L^* = \frac{1}{h}\int \varepsilon_L^* dA$ are the inherent strain and inherent deformation in the longitudinal direction, h is the thickness of the welded joint.

2.6 Conclusions

Since welding induced buckling is a nonlinear problem involving geometrical and material nonlinearities, the nonlinear strain displacement relationship for large deformation problems and temperature dependent material properties used in this research are presented. Then the framework of three methods employed for the analysis of buckling distortion of thin plate structures during welding assembly is presented. The first method is a thermal elastic plastic FE method which can trace the transient behavior of the structure. The second method is an elastic FE method for large deformation analysis using the inherent deformation theory. This method can predict the welding deformation of a large structure following the actual assembly sequence, consuming a very short computing time. Eigenvalue analysis can be used to predict the critical condition of buckling and the possible buckling modes. In the latter two methods, the inherent deformation and the interface element are used to represent the local shrinkage due to welding and to represent the bonding strength between welded parts which changes with the progress of assembly stages. Since longitudinal inherent strain/deformation mostly transforms into stress because of the strong constraint in the welding direction, the tendon force is introduced and its relationship with the longitudinal inherent deformation is presented.

As for the eigenvalue analysis, its theoretical formulation is presented based on the minimum potential energy theorem in the incremental form and the difference between the linear and the nonlinear eigenvalue analyses is discussed using bead on plate welding as an example.

Chapter 3 Inherent Deformation in Welding

To predict welding distortion using elastic analysis, the inherent deformation should be evaluated beforehand. Due to its importance in welding induced buckling, three practical methods to evaluate the longitudinal inherent shrinkage, namely empirical or theoretical formulae, estimation using longitudinal displacement, and integration of inherent strain or residual stress are presented in this chapter. Also the influences of factors, such as plate size and heat input, on the accuracy of the predicted longitudinal inherent shrinkage are examined using thermal elastic plastic FE analysis.

3.1 Brief Review of Inherent Deformation

As mentioned in **section 2.3**, the inherent strain or the inherent deformation is considered to be the cause of residual stress and welding distortion. Also, plastic strain is the major part of welding inherent strain in carbon steel.

In order to avoid the inconvenience of applying the inherent strain directly, the concept of inherent deformation is introduced. The inherent deformation is defined as the integration of inherent strain on each cross section normal to the welding line. There are four components of inherent strain as shown in **Chapter 2** by **Eq. (2-13)**, restated below.

$$\begin{aligned}
\delta_L^* &= \frac{1}{h}\iint \varepsilon_L^* dydz \\
\delta_T^* &= \frac{1}{h}\iint \varepsilon_T^* dydz \\
\theta_L^* &= \frac{12}{h^3}\iint (z-\frac{h}{2})\varepsilon_L^* dydz \\
\theta_T^* &= \frac{12}{h^3}\iint (z-\frac{h}{2})\varepsilon_T^* dydz
\end{aligned} \tag{2-13}$$

Where, ε_L^* is the longitudinal inherent strain in the welding direction (parallel to welding line) and ε_T^* is the transverse inherent strain in the transverse direction (normal to welding line). δ_L^* and δ_T^* are the inherent deformation in the longitudinal and the transverse directions. θ_L^* and θ_T^* are the inherent bending deformation in the longitudinal and the transverse directions. h is the thickness of the welded joint, and x, y, z are the coordinates in welding direction, transverse direction and thickness direction, respectively.

Taking the longitudinal inherent shrinkage as an example, **Fig. 3.1(a)** shows the middle cross section of a simple butt welded joint with uniform thickness. The longitudinal inherent shrinkage can be evaluated by integrating the whole longitudinal inherent strain on this cross section. Then it is equally divided into two parts, and applied to the two plates to be welded in the elastic analysis. For a butt welded joint with different plate thicknesses as shown in **Fig. 3.1 (b)**, the longitudinal

inherent shrinkages of the two parts can be evaluated separately, and then applied in the elastic analysis. Similarly, the longitudinal inherent shrinkage of a fillet welded joint as shown in **Fig. 3.1 (c)** can be divided into three parts and applied to the three plates forming the fillet joint. This method can also be applied to other typical welded joints such as a lap welded joint.

3.2 Evaluation of Longitudinal Inherent Shrinkage

When the inherent deformation is known, an elastic FE analysis can be carried out to predict welding distortion of large complex structures by applying the known inherent deformation as nodal forces (tendon force) or nodal moment (longitudinal bending) along the welding line, and discontinuity of displacement across the welding line (transverse shrinkage and bending). Therefore, the magnitude of inherent deformation should be evaluated before an elastic FE welding analysis can be carried out.

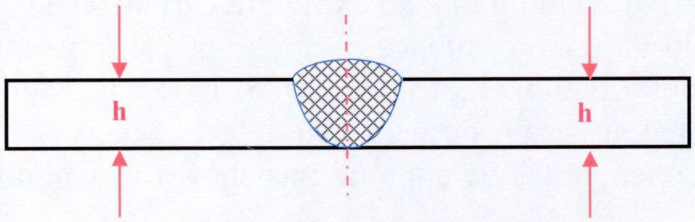

(a) Standard butt welded joint

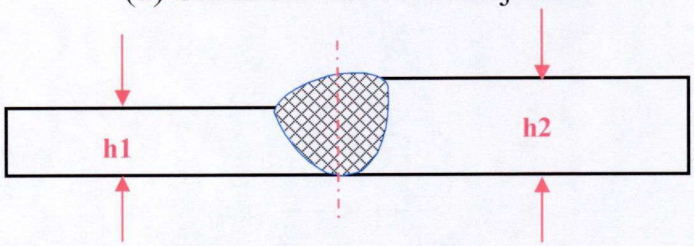

(b) Butt welded joint of two plates with different thicknesses

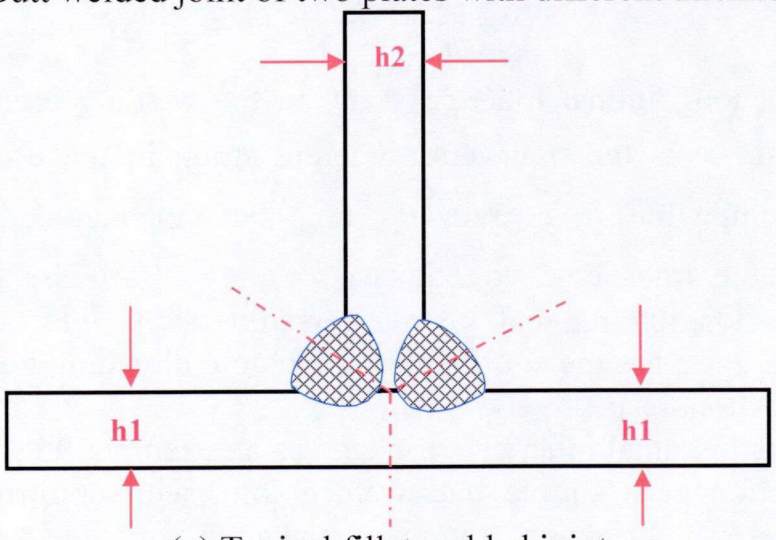

(c) Typical fillet welded joint

Fig. 3.1 Welded joints considered.

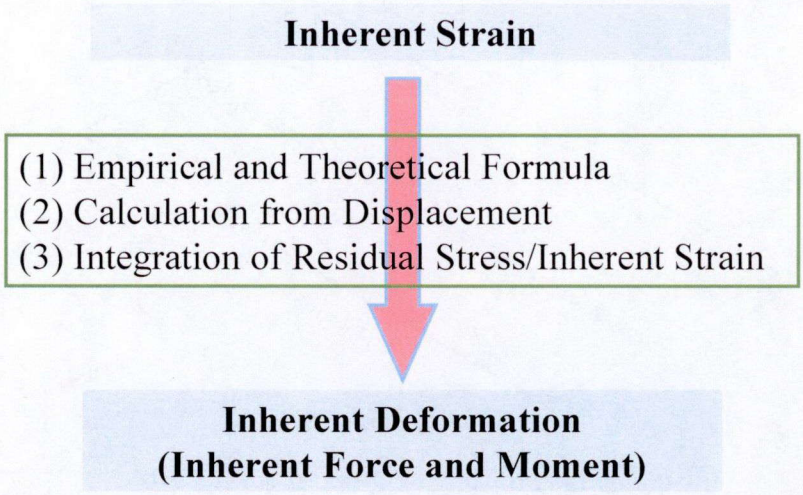

Fig. 3.2 Understanding longitudinal inherent deformation.

Inherent deformation can be evaluated using inverse analysis [84, 85, 95]. However, due to the importance of longitudinal inherent shrinkage for welding induced buckling and to deeply understand the longitudinal inherent deformation as shown in **Fig. 3.2**, the following discussion is presented.

Since longitudinal inherent shrinkage is considered to be the dominant reason of welding induced buckling, focus in this section is placed on the inherent longitudinal shrinkage. As mentioned in **Chapter 2**, inherent longitudinal shrinkage (tendon force) can be evaluated using the empirical formula given in **Eq. (2-25)** or the simple theoretical formula given in **Eq. (2-33)**. The relationship between the inherent longitudinal shrinkage δ_L^* and the tendon force F_{tendon} may be expressed in terms of welding net heat input as follows:

$$\delta_L^* = \frac{F_{tendon}}{Eh} = \frac{0.2Q_{net}}{Eh} \quad (empirical \quad formula) \tag{3-1}$$

$$\delta_L^* = \frac{F_{tendon}}{Eh} = \frac{0.235Q_{net}}{Eh} \quad (analytical \quad formula) \tag{3-2}$$

In addition to these equations, two approaches to evaluate the longitudinal inherent shrinkage are proposed. One is a direct method based on displacement. The other is the integration method: integration of the longitudinal plastic strain according to the definition of inherent deformation, and integration of longitudinal residual stress which is corresponding to the tendon force.

3.2.1 Evaluation of Longitudinal Inherent Shrinkage from Longitudinal Displacement

For the purpose of discussion, the 600×300×2.28 mm rectangular plate shown in **Fig. 3.3** is taken as an example. The plate is butt welded in x direction with heat input of 230 J/mm.

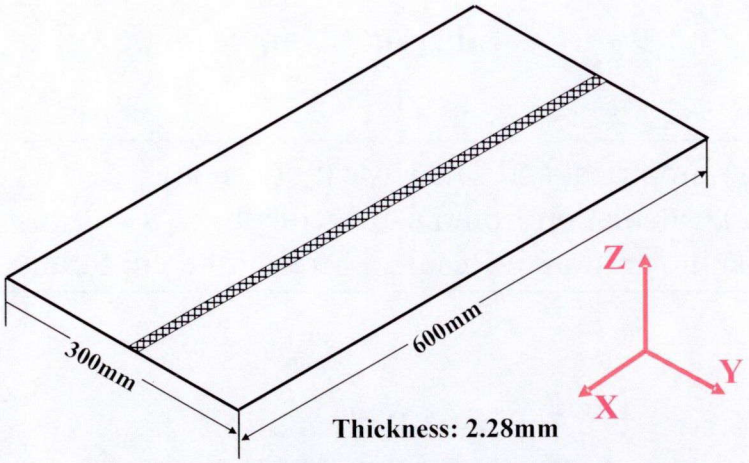

Fig. 3.3 Considered butt welded plate.

Figure 3.4 is a result of a thermal elastic plastic FE analysis and shows the distribution of longitudinal displacement along the welding line. The curve can be divided into a middle part and two ends. In the middle part, the curve is almost linear with almost a constant slope. From this slope, the longitudinal inherent deformation can be evaluated as follows.

Since the slope of the longitudinal displacement in **Fig. 3.4** is the longitudinal strain ε_L in welding direction ($\varepsilon_L = \partial u/\partial x$), it can be related to the tendon force F_{tendon} and the longitudinal inherent shrinkage δ_L^* through the following equation.

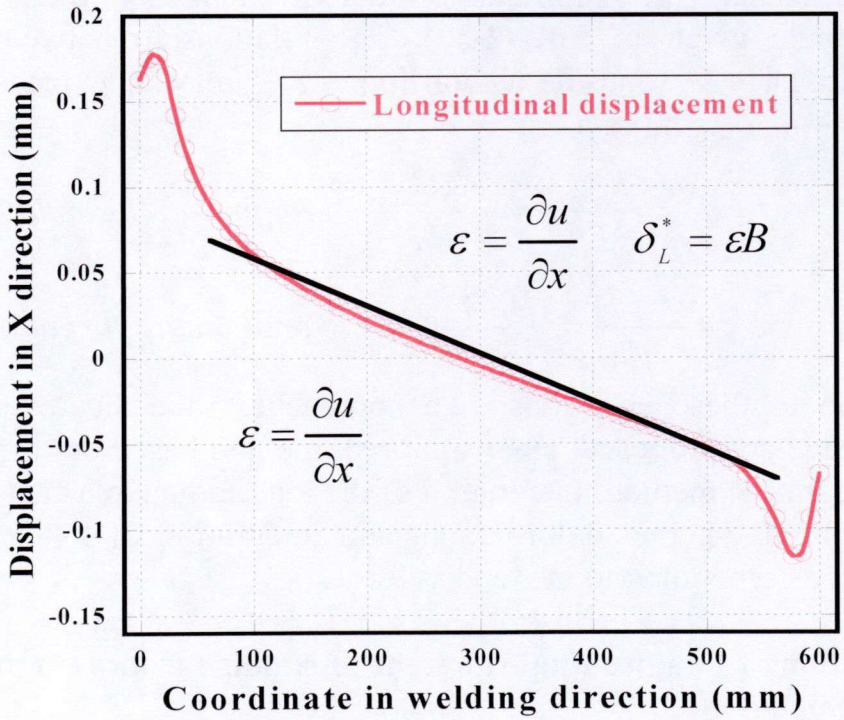

Fig. 3.4 Distribution of longitudinal displacement along welding line.

$$\varepsilon_L = \frac{F_{tendon}}{AE} = \frac{Eh\delta_L^*}{BhE} = \frac{\delta_L^*}{B} \tag{3-3}$$

or

$$\delta_L^* = B\varepsilon_L \tag{3-4}$$

That is δ^*_L = Shrinkage in X direction of a length equal to B.

The above equation means that, the longitudinal inherent shrinkage δ_L^* can be evaluated as the longitudinal displacement between two points separated in X direction by a length equal to the plate width B. If the specimen or the model is long enough, this equation can be used to evaluate the longitudinal inherent deformation both in experiments and in thermal elastic plastic FE analysis.

Applying this to the considered plate, the longitudinal inherent shrinkage can be calculated using the measured longitudinal displacement as follows,

$$\delta_L^* = B\varepsilon_L = 300 \times \frac{0.1638}{480} = 0.10238mm \tag{3-5}$$

3.2.2 Evaluation of Longitudinal Inherent Shrinkage by Integration

According to the definition of inherent deformation given by **Eq. (2-23)**, the longitudinal inherent shrinkage can be evaluated by integrating the longitudinal inherent strain. Also, utilizing the relationship between the tendon force and longitudinal inherent shrinkage, the later can be evaluated by integration of the longitudinal component of residual stress.

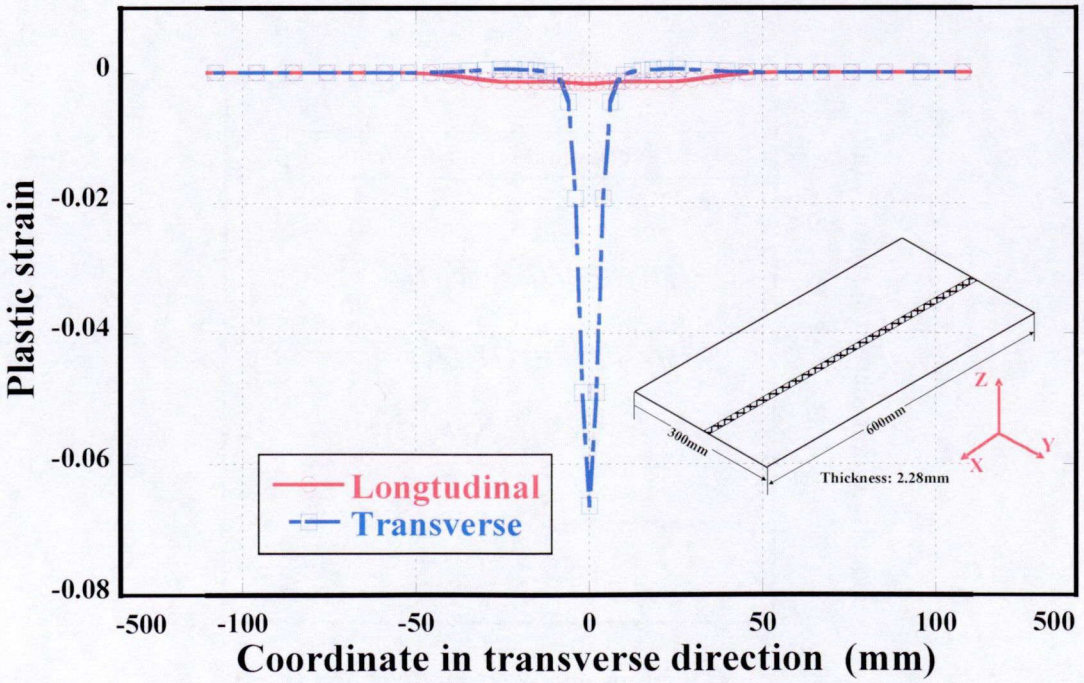

Fig. 3.5 Distribution of plastic strain on neutral plane in a middle transverse cross section.

3.2.2.1 Integration of Inherent Strain

As discussed in **Chapter 2**, in carbon steel, the plastic strain is the dominant component of the inherent strain. Plastic strain can be obtained by thermal elastic plastic FE analysis [80]. Considering the welded joint shown in **Fig. 3.3** as an example, **Figure 3.5** shows a typical distribution of plastic strain in the longitudinal direction (welding direction) and the transverse direction (normal to welding line) on the neutral plane in a mid transverse cross section.

The longitudinal inherent shrinkage δ_L^* may then be evaluated as in the following **Eq. (3-6)** using the longitudinal inhere strain ε_L^* on a transverse cross section in the middle of the joint.

$$\delta_L^* = \frac{1}{h}\iint \varepsilon_L^* dydz \tag{3-6}$$

If the same integrating process is carried out for each transverse cross section, the distribution of the longitudinal inherent shrinkage along the welding line can be obtained as shown in **Fig. 3.6**. As may be seen from this figure, the distribution of the longitudinal inherent shrinkage in the middle region of the welding line is almost constant.

For the special case of a very thin plate, the distribution of longitudinal inherent strain is nearly uniform through the thickness. **Eq. (3-6)** can be simplified as follows:

$$\delta_L^* = \int \varepsilon_L^* dy \tag{3-7}$$

Where ε_L^* is the longitudinal inherent strain, considered to be uniform in Z direction.

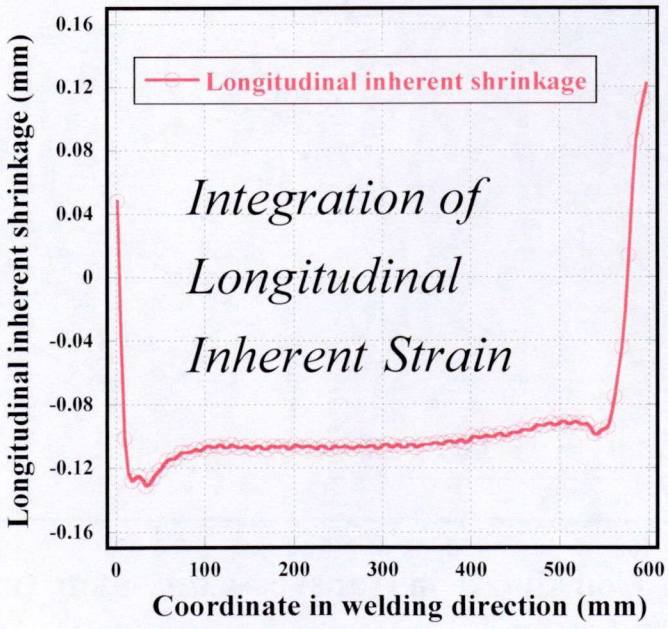

Fig. 3.6 Distribution of longitudinal inherent shrinkage along the welding line (integrating longitudinal inherent strain).

3.2.2.2 Integration of Residual Stress

If the longitudinal residual stress σ_{rL} is known, the tendon force or the longitudinal inherent shrinkage can be evaluated through its integration. **Figure 3.7** shows a typical distribution of longitudinal residual stress on the neutral plane in a middle cross section normal to the welding line.

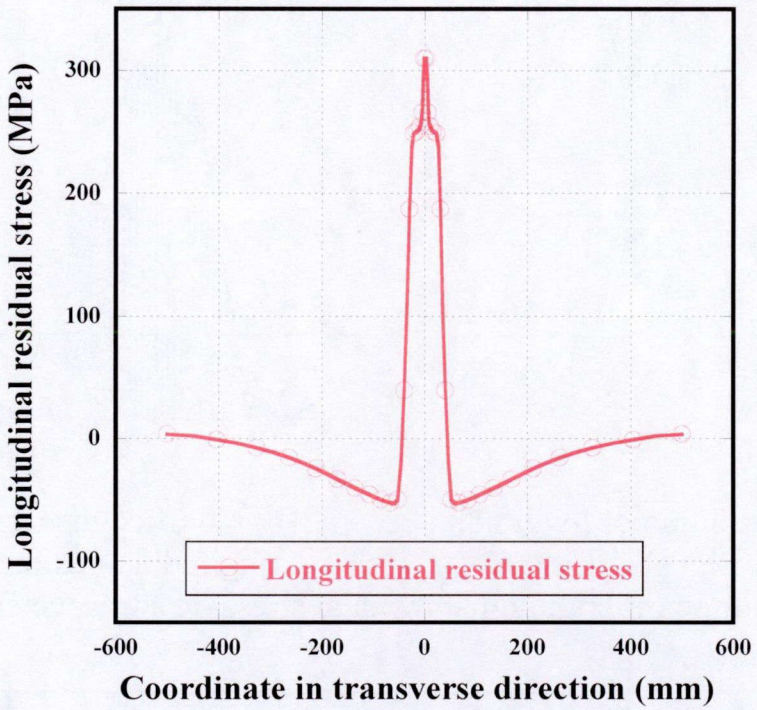

Fig. 3.7 Distribution of longitudinal residual stress on the neutral plain in a middle transverse cross section of the considered plate.

After welding, the region close to the welding line has tensile residual stress because of the shrinkage of the welding region, and corresponding compressive residual stress is produced in the region away from the weld to balance the tensile residual stress as shown in **Fig. 3.8(a)**. Since the longitudinal inherent strain is distributed between points A and B in **Fig. 3.8(b)**, the longitudinal inherent deformation can be predicted from the integration of the stress distributed between points A and B i.e.

$$\delta_L^* = \int \varepsilon_L^* dy = \int \frac{(\sigma + \sigma_c)}{E} dy = \frac{F_{tendon}}{Eh} \tag{3-8}$$

Where, σ_c is the compressive residual stress at points A and B.

Figure 3.9 shows the distribution of longitudinal inherent shrinkage along the welding line as evaluated by integrating the longitudinal residual stress. Uniform distribution of longitudinal inherent shrinkage is observed in the middle region, and its magnitude has a good agreement with that obtained by integrating the longitudinal inherent strain.

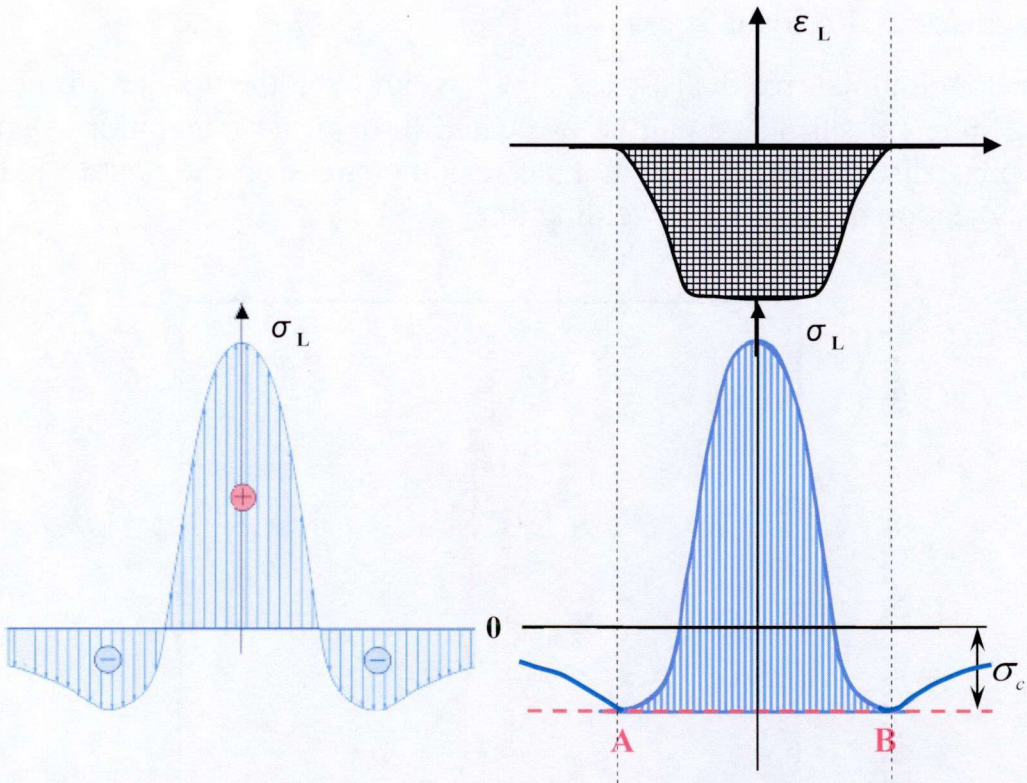

(a) Distribution of longitudinal residual stress

(b) modified distribution of longitudinal residual stress

Fig. 3.8 Distribution of longitudinal residual stress on a transverse cross section.

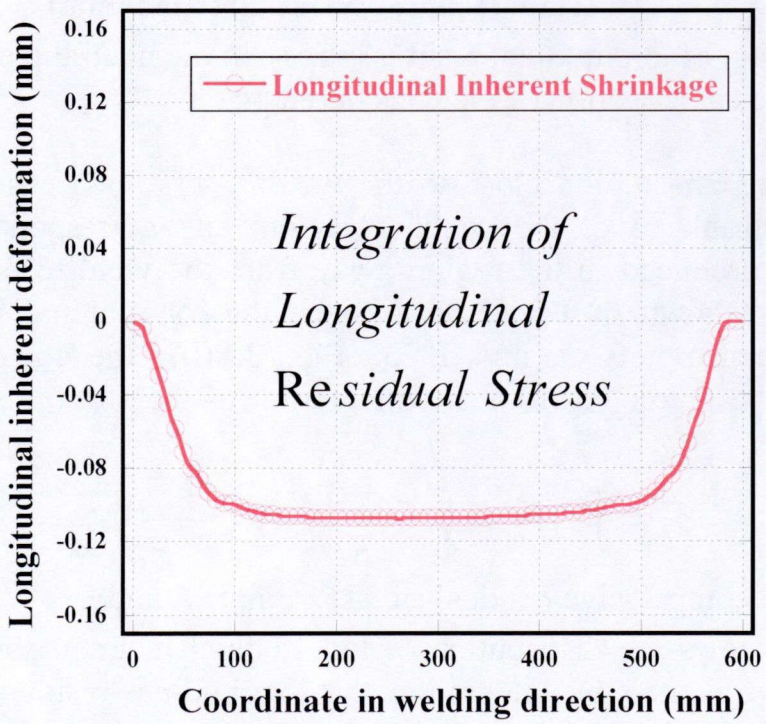

Fig. 3.9 Distribution of longitudinal inherent shrinkage along the welding line (integrating longitudinal residual stress).

Table 3.1 Comparison of estimated longitudinal inherent shrinkages.

Formula Method		Calculation using Longitudinal Displacement	Integration Method	
Empirical Formula	Theoretical Solution		Integrating Inherent Strain	Integrating Residual Stress
0.0961 mm	0.1129 mm	0.1024 mm	0.1036mm	0.1052mm

As a conclusion of this section, the longitudinal inherent shrinkages evaluated by five different methods are compared in **Table 3.1**. As may be seen from this table, the longitudinal inherent shrinkage predicted from the result of FE analysis using three different methods based on the concept of inherent deformation agree well with those predicted using empirical and theoretical formulae.

3.3 Factors Affecting the Distribution and Magnitude of Longitudinal Inherent Shrinkage

Although elastic analysis using the inherent deformation method is a practical and effective computational approach, in order to get accurate results, it is necessary to accurately evaluate the inherent deformation.

Using the empirical formula given by **Eq. (3-1)** or theoretical formula given by **Eq. (3-2)**, the longitudinal inherent shrinkage can be easily obtained. However, the theoretical formula is obtained assuming an infinite welded plate considering one dimensional heat conduction normal to the weld line. In an actual welding process of a joint with a finite size, factors that affect the inherent deformation and are not considered in theoretical formula are summarized as follows:

(1) Size of welded plate;
(2) Distribution of heat input (size and shape of molten pool);
(3) Three dimensional heat conduction;
(4) Heat lost by convection and radiation;
(5) Temperature dependent material properties;
(6) Speed of moving heat source.

Using the longitudinal inherent strain and residual stress computed by the thermal elastic plastic FE analysis considering the above mentioned influential factors, the longitudinal inherent shrinkage can be accurately evaluated.

Investigation of inherent deformation in line heating [82, 83] shows that the inherent deformation mostly depends on material properties, plate thickness and heat input. The effect of factors influential to the longitudinal inherent shrinkage in welding can be examined using thermal elastic plastic FE analysis.

First, welded joints with extreme dimensions, such as very narrow or very short welded joints, are examined to clarify the size effect. Then, the influence of heat input on the longitudinal inherent shrinkage is investigated keeping the size of the plate fixed.

3.3.1 Influence of Plate Size

A series of computations of bead on plate using thermal elastic plastic FE analysis is carried out with different plate lengths and widths as shown in **Table 3.2**. The thickness of the plate is fixed in all computations and equals to 2.28 mm. For case 1, plate width is fixed to 300mm and plate length is changed. In case 2, plate length is fixed to 600mm and plate width is changed.

Table 3.2 Dimensions of plates examined.

	Length (mm)	Width (mm)
Case 1	1200/900/600/300/100/60	300
Case 2	600	1000/600/400/300/200/100/60

(Thickness of welded plate: 2.28mm)

Figure 3.10 shows the solid element model of a typical bead on plate for thermal elastic plastic FE analysis. The boundary conditions shown in **Fig. 3.10** are applied to prevent the rigid body motion. MIG welding is assumed and the corresponding welding condition is shown in **Table 3.3**. Due to the small plate thickness, the temperature gradient in thickness direction is negligibly small because the welding heat quickly penetrates the whole thickness of such a thin plate.

Before presenting the results of FE analysis, it is noted here that, using the theoretical formula **Eq. (3-2)**, the longitudinal inherent shrinkage can be evaluated from the heat input as follows:

Table 3.3 Welding condition for bead on plate welding.

Current (A)	Voltage (V)	Velocity (mm/s)	Efficiency
120	15	6.25	0.8

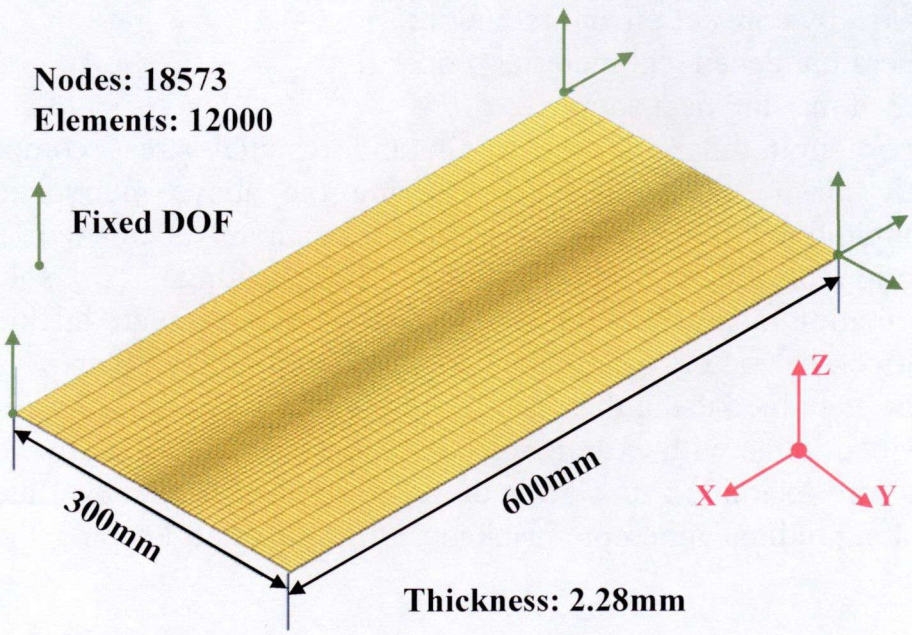

Fig. 3.10 Solid element model for TEP FE analysis.

$$\delta_L^* = \frac{F_{tendon}}{Eh} = \frac{0.235Q_{net}}{Eh} = \frac{0.235\times 0.8\times 120\times 15/6.25}{210000Mpa\times 2.28mm} = 0.113mm \quad (3\text{-}9)$$

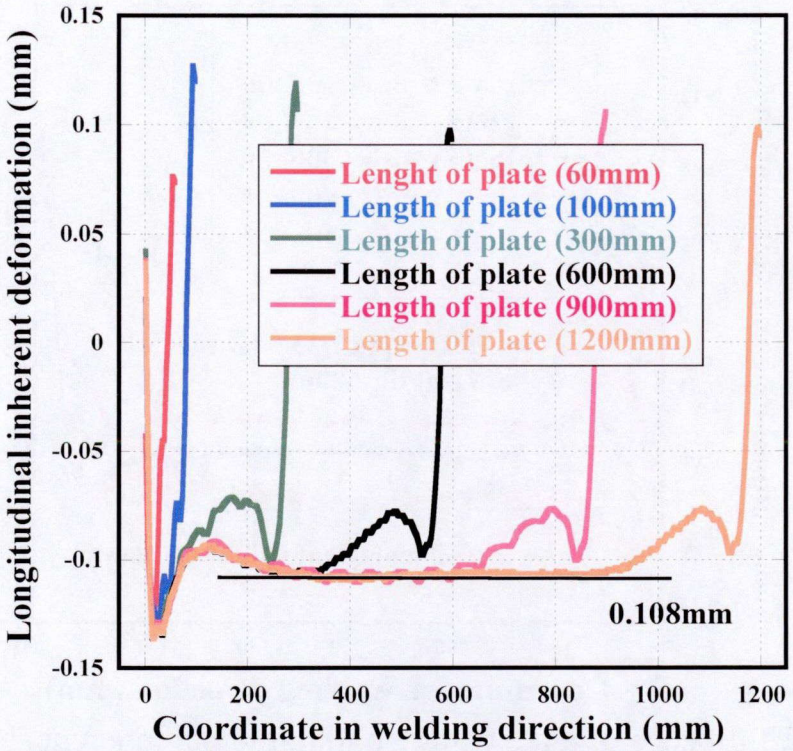

Fig. 3.11 Influence of plate length on longitudinal inherent shrinkage.

3.3.1.1 Effect of Plate Length on Longitudinal Inherent Shrinkage

The distribution of evaluated longitudinal inherent shrinkage along the welding line of the plates of case 1of **Table 3.2** is shown in **Fig. 3.11**. As may be seen from the figure, the longitudinal inherent shrinkages in the middle regions of the plates are nearly the same and the distribution is nearly constant (0.108mm) when the length of the plate is larger than 600 mm. However, when the length of the plate is small, such as the cases of 60, 100 and 300 mm, plate length is too short to have such a middle region due to the edge effect.

3.3.1.2 Effect of Plate Width on Inherent Longitudinal Shrinkage

The influence of plate width on longitudinal inherent shrinkage is examined by changing the plate width according to case 2 in **Table 3.2** while fixing plate length to 600mm. **Figure 3.12** shows the distribution of longitudinal inherent shrinkage along the welding line for different plate widths. The magnitude of longitudinal inherent shrinkage increases with the plate width until about 300 mm, and then it stays nearly constant (0.106mm). However, it is smaller than the theoretical value given by **Eq. (3-8)**.

Since longitudinal inherent shrinkage is evaluated by integrating the longitudinal inherent strain on transverse cross sections, it is necessary to consider the distribution

of longitudinal inherent strain on the middle transverse cross section. **Figure 3.13** shows that longitudinal inherent strain becomes larger, but the width of its distribution becomes smaller as plate width becomes narrower.

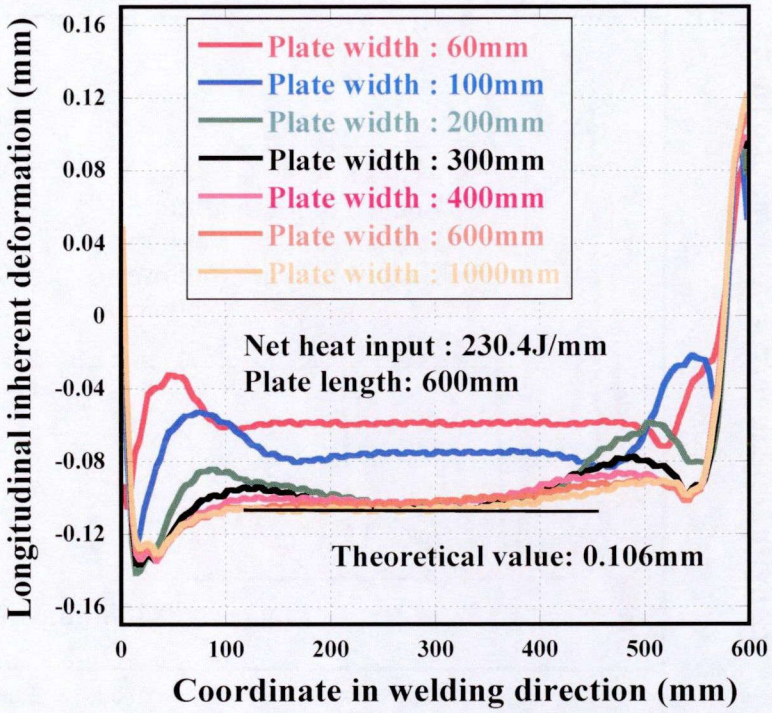

Fig. 3.12 Influence of plate width on longitudinal inherent shrinkage.

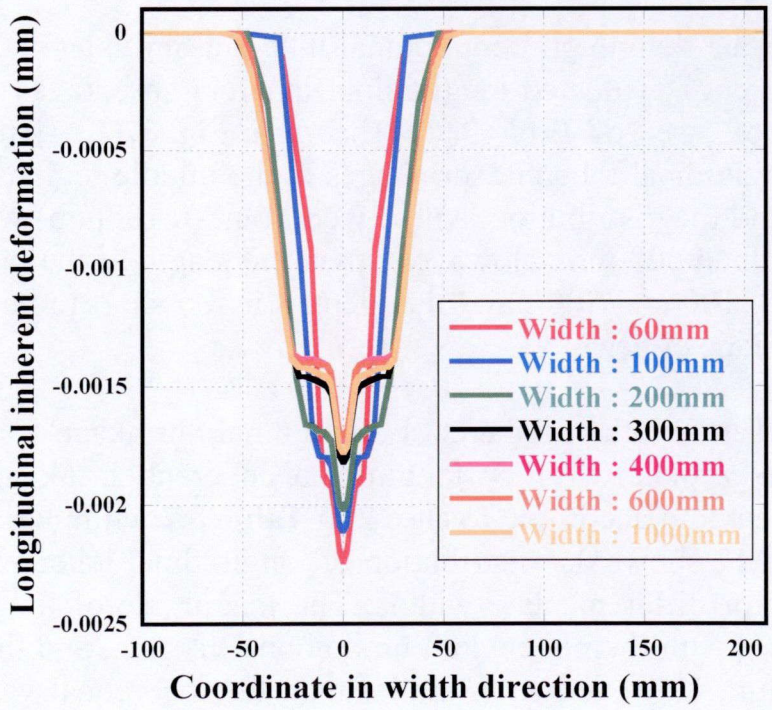

Fig. 3.13 Distribution of longitudinal inherent strain on neutral plane in a middle transverse cross section.

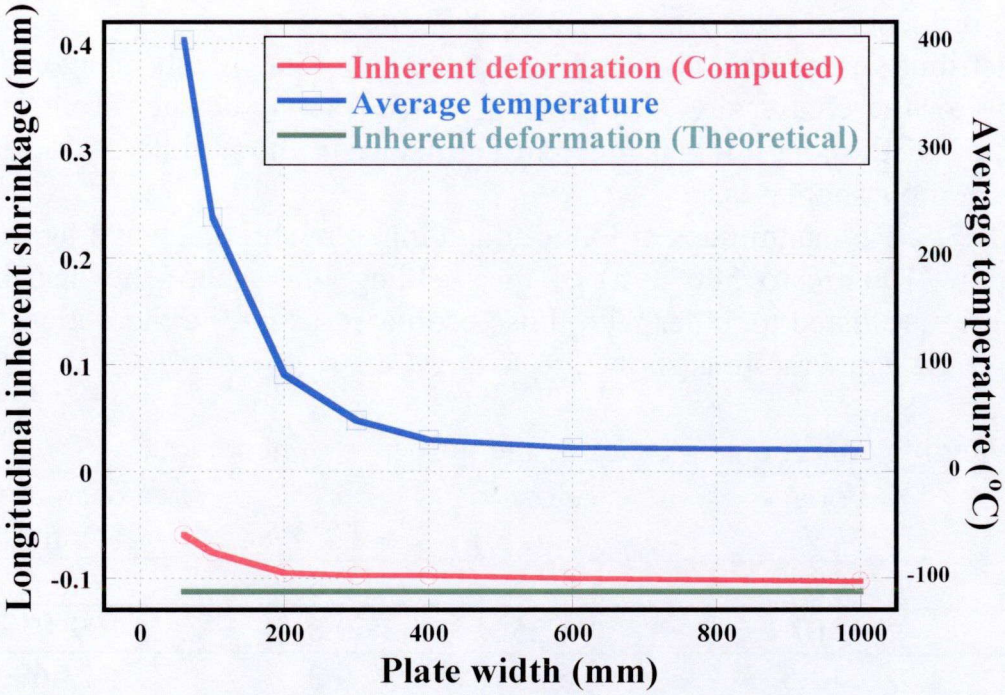

Fig. 3.14 Influence of plate width on estimated longitudinal inherent shrinkage and average temperature.

According to the understanding in welding mechanics, the inherent strain is determined by the maximum temperature reached during the thermal cycle and the constraint provided by the surrounding base metal [37], the difference in the distribution of longitudinal inherent strain shown in **Fig. 3.14** can be explained as follows:

(1) Although the temperature distribution near the welding line is almost the same the mechanical constraint is different when the plate width is different. In case of narrow plate in which the restraint is small, however, the longitudinal inherent deformation becomes small and it becomes close to the theoretical value if the plate is wide and restraint is large.

(2) The plastic strain or the inherent strain is produced by the thermal stress caused by temperature gradient. If the plate width is small, the average temperature when the temperature distribution becomes nearly uniform is high. When the average temperature is high, the temperature gradient becomes small. Thus, the longitudinal inherent deformation becomes small when the plate width is small as shown in **Fig. 3.14.** The effect of the plate width becomes small when the plate width is larger than 300 mm or the average temperature is less than 50 °C.

3.3.2 Influence of Heat Input

Equation (3-2) suggests that longitudinal inherent shrinkage is proportional to the net heat input. Thermal elastic plastic FE analysis is also employed to investigate the influence of heat input on the longitudinal inherent shrinkage. The same FE model shown in **Fig. 3.10** is used and the cases with different heat input shown in

Table 3.4 are examined. The welding condition shown shaded in the table is that used to study the influence of plate size presented in **Table 3.3**.

The distributions of the computed longitudinal inherent shrinkage along the welding line for these cases are shown in **Fig. 3.15**. As may be seen from the figure, the magnitude of the longitudinal inherent shrinkage in the middle region increases when the heat input increases.

In **Table 3.5,** the magnitudes of longitudinal inherent shrinkage averaged over the middle region (100mm to 500 mm) of the welding line where the distribution is nearly uniform are listed together with those estimated using the theoretical formula. Also the average temperature is shown.

Table 3.4 Welding conditions to examine the influence of heat input.

Current (A)	Voltage (V)	Velocity (mm/sec)	η	Area of molten pool (mm^2)
75	6	6.25	0.8	4.56
90	10	6.25	0.8	9.12
100	13.5	6.25	0.8	13.68
120	15	6.25	0.8	18.24
130	17.3	6.25	0.8	22.8

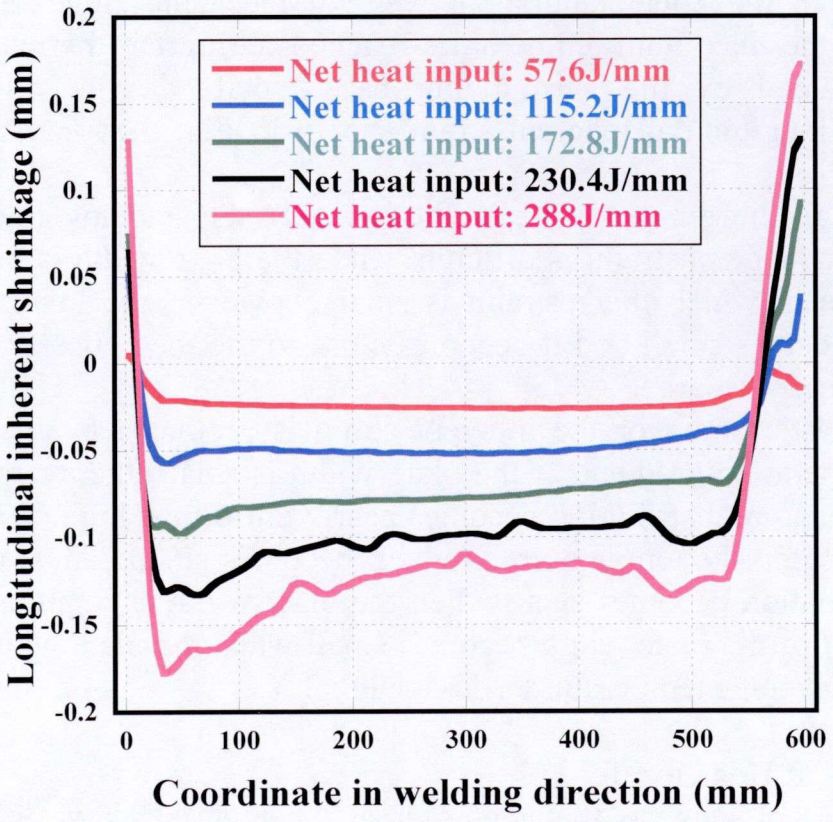

Fig. 3.15 Influence of heat input on the distribution of longitudinal inherent shrinkage along the welding line.

Figure 3.16 shows the relation between the heat input parameter (Q_{net}/h^2) and the longitudinal inherent shrinkage predicted using FE analysis and the theoretical formula. As may be seen from the figure, the longitudinal inherent deformation computed by FE analysis increases linearly as predicted by the theory. This linearity comes from the fact that, in all cases, the average temperature is smaller than 85 °C, which means that the plate is fairly wide. Quantitatively, the theoretical prediction gives larger value compared to the value computed by FE analysis.

Table 3.5 Estimated longitudinal inherent shrinkage for different heat input.

Heat Input Q_{net} (J/mm)	Heat Parameter (Q_{net}/h^2)	Average Temperature (°C)	Longitudinal Inherent Shrinkage① (mm)	Longitudinal Inherent Shrinkage② (mm)
57.6	11.08	40	0.02532	0.028271
115.2	22.16	56	0.05007	0.056541
172.8	33.24	67	0.07617	0.084812
230.4	44.32	81	0.10002	0.113083
288	55.40	85	0.12400	0.141353

Where, ① and ② indicate numerically calculated longitudinal inherent shrinkage, and that calculated using the theoretical formula shown in **Eq. (3-2)**, respectively.

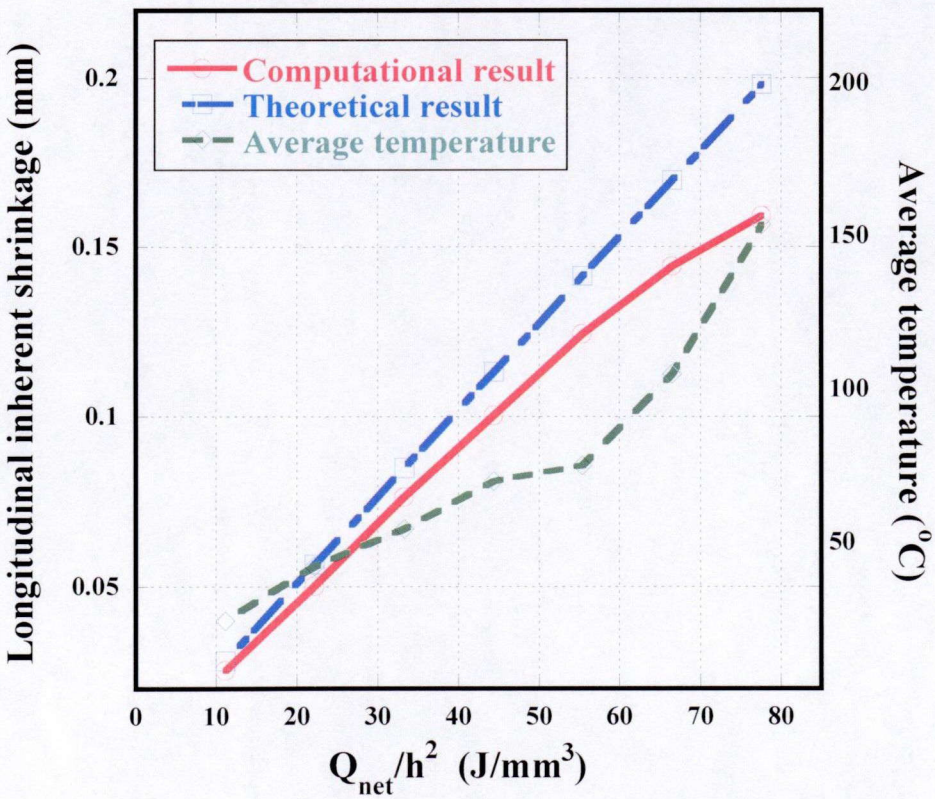

Fig. 3.16 Relation between the heat input parameter and the longitudinal inherent shrinkage.

3.4 Conclusions

For prediction of welding distortion, the inherent deformation used in the elastic FE analysis must be obtained beforehand. Basically, the inherent deformation can be obtained by integrating the inherent strain if it is known. Due to the importance of longitudinal inherent shrinkage to welding induced buckling, three practical methods to evaluate the longitudinal inherent shrinkage, namely empirical or theoretical formulae, calculation using longitudinal displacement and integration of inherent strain or residual stress are presented. Also the influences of plate size and heat input on the predicted longitudinal inherent shrinkage are examined and it is shown that a value consistent with the theoretical formula can be obtained by the thermal elastic plastic FE analysis if the plate is large enough so that the average temperature is low.

Chapter 4 Overview of Buckling Behavior during Welding

As discussed in **Chapter 1**, welding induced buckling occurs when the structure is assembled by thin plates. Welding induced buckling is considered to be the most critical mode of welding distortion compared with other modes of welding distortion because of its instability and difficulty of straightening. When thin plates with high tensile strength are used to assemble welded structures, not only residual buckling after cooling but also transient buckling during heating may be produced.

Transient buckling during welding is a local buckling that occurs around the welding torch. It can inversely influence the welding process and damage the welding equipment. First, in this chapter, transient buckling and residual buckling are reproduced by thermal elastic plastic FE analysis for a thin plate with bead on plate welding. Influential factors affecting transient buckling is investigated using thermal elastic plastic FE analysis. The causes of occurrence of transient buckling and different modes of transient/residual buckling are clarified using theoretical explanation and computed longitudinal stresses.

Since transient buckling is likely to appear only in thin plate welded structures using high tensile strength steel, the residual buckling is usually considered to be the dominant issue of welding induced buckling.

4.1 Investigation of Buckling Behavior by Thermal Elastic Plastic FE Analysis

Thermal elastic plastic FE analysis is carried out to investigate the buckling behavior of a thin plate welded joint made of high tensile strength steel (yield stress: 950MPa).

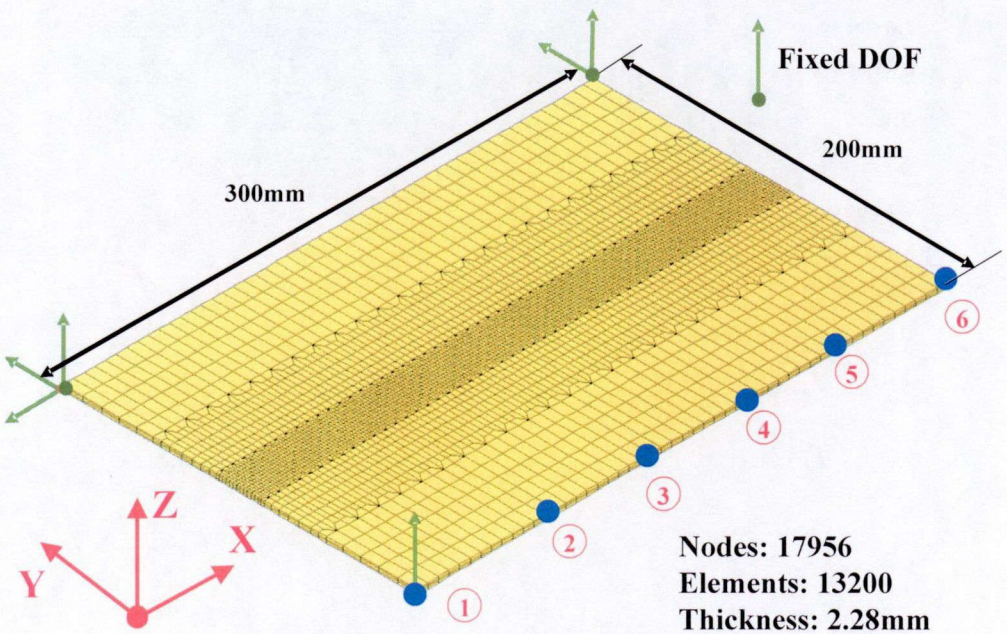

Fig. 4.1 FEM Model of Thin Plate.

Table 4.1 Welding condition (TIG).

Current	Voltage	Velocity	Efficiency
175-185(A)	14-16(V)	3.6mm/sec	0.7-0.8

Figure 4.1 shows the FE model of the plate. FE model has 17956 nodes and 13200 elements. Boundary conditions to prevent rigid body motion are adopted as shown in the figure. In order to investigate transient buckling and residual buckling, the six points shown in **Fig. 4.1** are selected to monitor the time history of out-of-plane welding distortion. Welding condition of a bead on plate is assumed as given in **Table 4.1.** Welding heat is assumed to uniformly penetrate the full thickness of the plate and the influence of inherent bending due to temperature gradient is ignored.

4.1.1 Buckling Distortion of the Examined Plate in the Entire Welding Process

In **Fig. 4.2**, the distributions of out-of-plane welding distortion at different times during the welding process are presented. As may be seen from the figure, the plate deforms in a dish form during welding and in a saddle form after cooling. This difference in deformation modes can be explained as the response to the different distributions of compressive stress during welding and after cooling as discussed in the following sections.

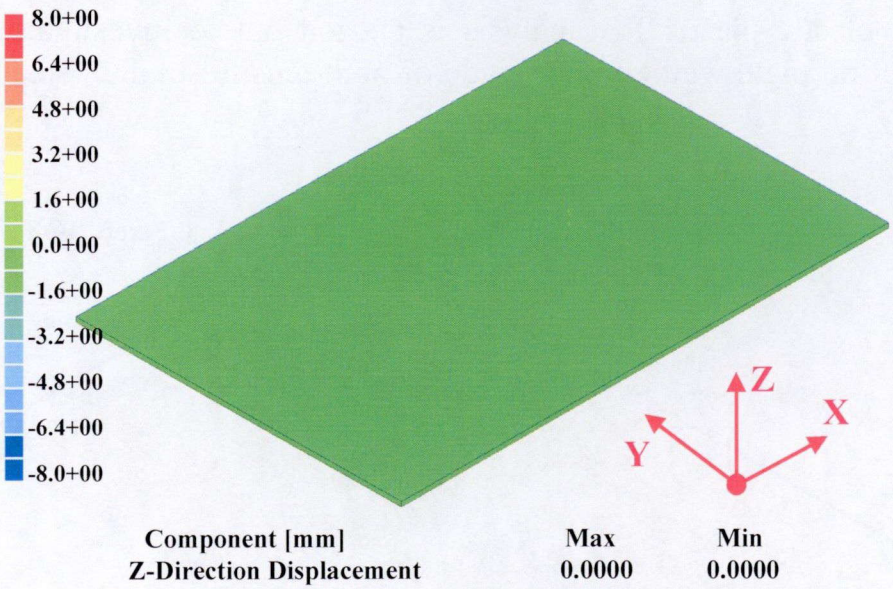

(a) Out-of-plane displacement before welding

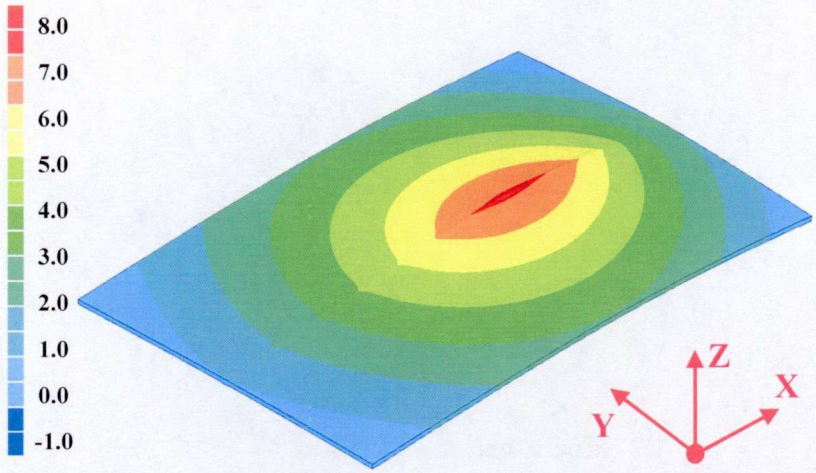

Component [mm]	Max	Min
Z-Direction Displacement	7.400	0.004

(b) Transient buckling during welding

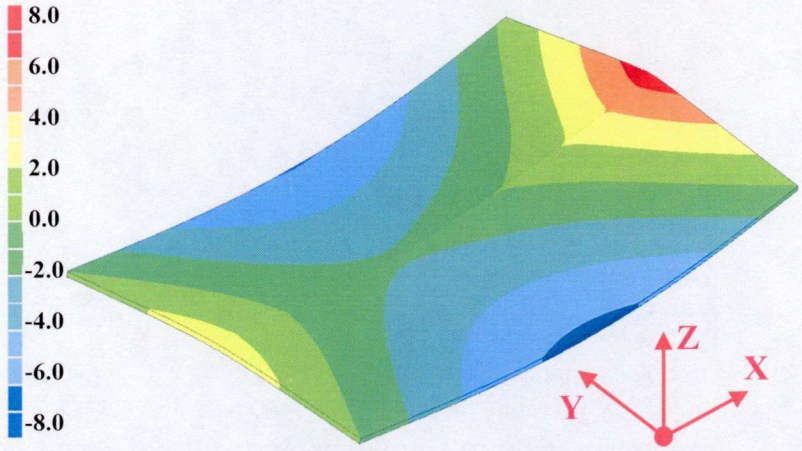

Component [mm]	Max	Min
Z-Direction Displacement	7.186	-6.36

(c) Residual buckling after cooling

Fig. 4.2 Out-of-plane welding distortion during whole welding process.

4.1.2 Transient Buckling during Welding

To understand the behavior at the time when transient buckling occurs during welding, temperature distribution, and longitudinal compressive stress distribution are presented in **Fig. 4.3**. As may be seen from **Fig. 4.3(b)**, compressive thermal stresses in the longitudinal and transverse directions are produced around the weld with the high yield stress of high tensile strength steel, longitudinal compressive stress will become large and if it exceeds the buckling stress, transient buckling occurs.

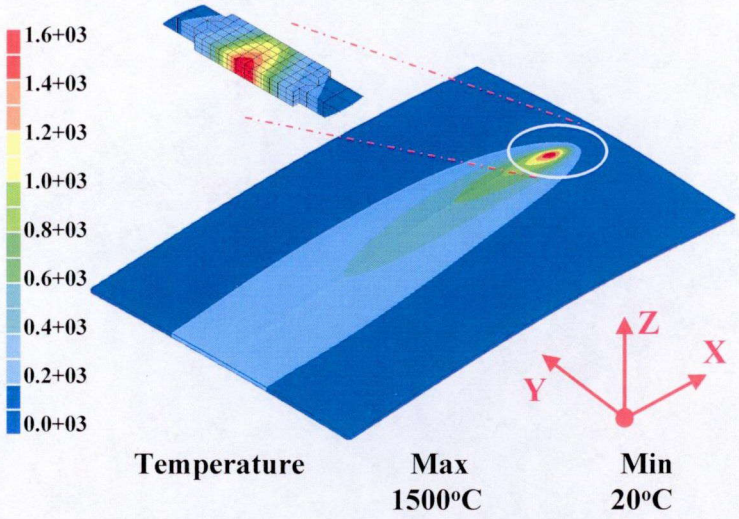

(a) Transient temperature distribution

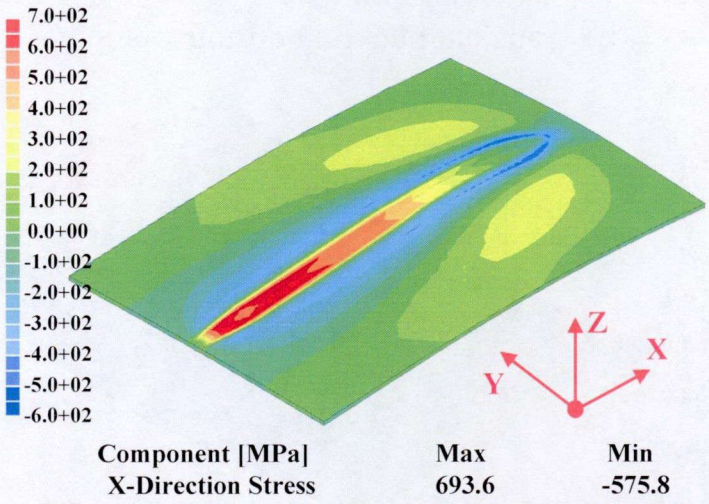

(b) Distribution of transient longitudinal stress

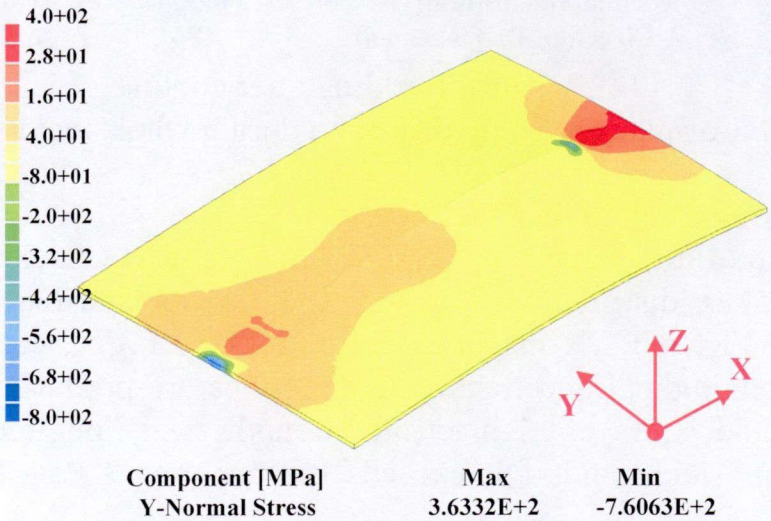

(c) Distribution of transient transverse stress

Fig. 4.3 Computed results of thermal/mechanical analysis when transient buckling occurs.

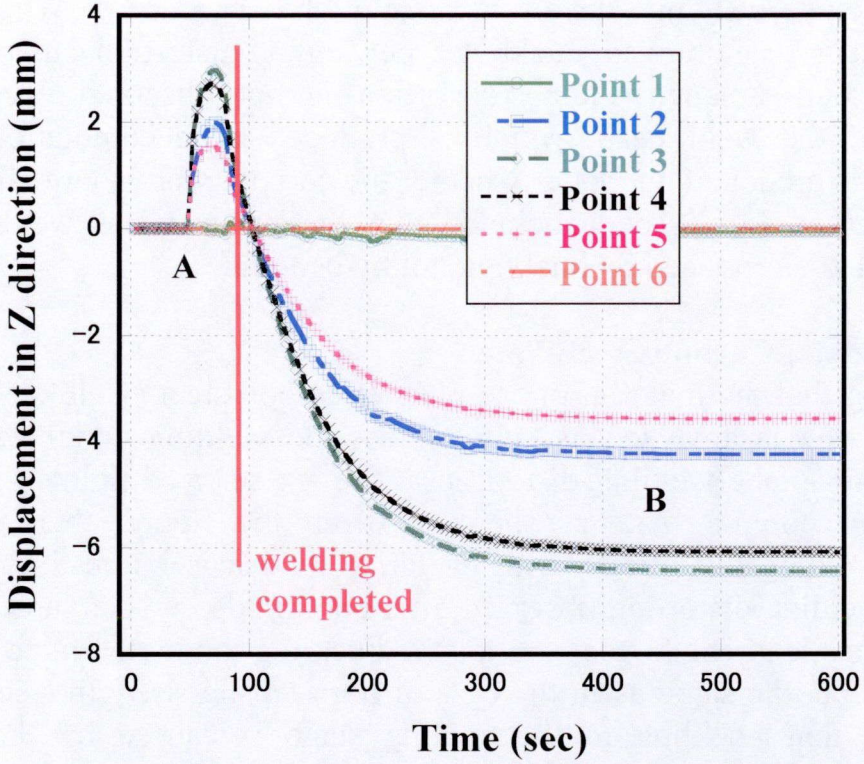

Fig. 4.4 Time history of displacement in Z direction during welding (high tensile strength steel).

4.1.3 History of Out-of-plane Welding Distortion during Welding

To closely examine the deformation of the plate during welding, out-of-plane displacements at the six selected points shown in **Fig. 4.1** are plotted in **Fig. 4.4** from the start of welding to the completion of cooling down. As maybe see from the figure, the magnitude of deflection increases during heating, and increases in the opposite direction during cooling down. Noting that no bending deformation can be produced by the resulting temperature gradient as shown in **Fig. 4.3(a)**, it may be concluded that the observed deflection is produced by buckling.

4.2 Discussion on Factors Influential of Transient Buckling

Through thermal elastic plastic FE analysis, it has been shown that, when the material of the plate is high tensile strength steel, buckling may happen both during welding and after completion of cooling down. To confirm buckling and the influence of yield stress of the plate, computations assuming small deformation and assuming carbon steel are carried out and presented in this section.

4.2.1 Out-of-plane Welding Distortion under Small Deformation

In order to confirm transient buckling during welding, the small deformation theory is employed to analyze the same problem and the computed out-of-plane welding distortion is shown in **Fig. 4.5**.

Because the heat is assumed to penetrate uniformly through the investigated thin plate during welding, there is almost no temperature gradient in thickness direction,

therefore welding bending distortion cannot be produced. When the small deformation theory is employed, buckling type welding distortion cannot be predicted. As expected, out-of-plane welding distortion is not observed except the local deformation of the weld bead, which is produced by accumulation of in-plane shrinkage that is predicted no matter whether the computation is large deformation or small deformation. It can be concluded that the out-of-plane welding distortion shown in **Fig 4.2** is produced by buckling not by bending.

4.2.2 Buckling of a Carbon Steel Plate

Assuming that the material of the plate is carbon steel (yield stress: 345MPa), welding distortion is analyzed assuming the same welding condition. **Figure 4.6** shows the out-of-plane welding distortion at the six selected points during welding and subsequent cooling. As may be seen from the figure, there is almost no out-of-plane welding distortion during welding. And it is interesting to notice that out-of-plane welding distortion observed after cooling down is as large as that in the case of high tensile strength steel. As for the buckling mode, the plate has deformed in a saddle shape, the same as in the case of high tensile strength steel. This comes from the fact that buckling in the cooling stage is caused by the longitudinal compressive stress, which is produced in the region away from the welding line to balance the tendon force. Noting that the tendon force is mostly dependent on the heat input and less sensitive to the yield stress of the material, it may be seen that the longitudinal compressive stress in carbon steel plate and high tensile strength steel plate are nearly equal.

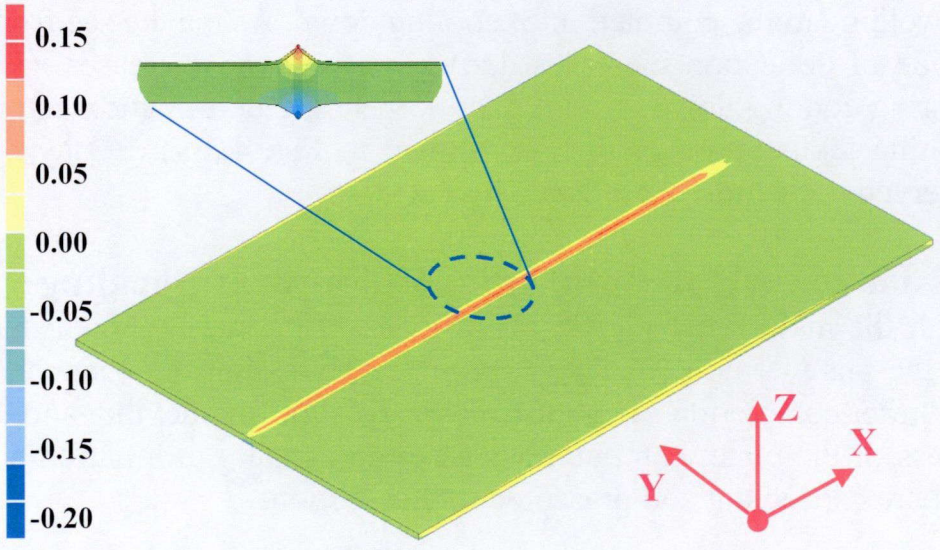

Fig. 4.5 Out-of-plane welding distortion after welding considering small deformation.

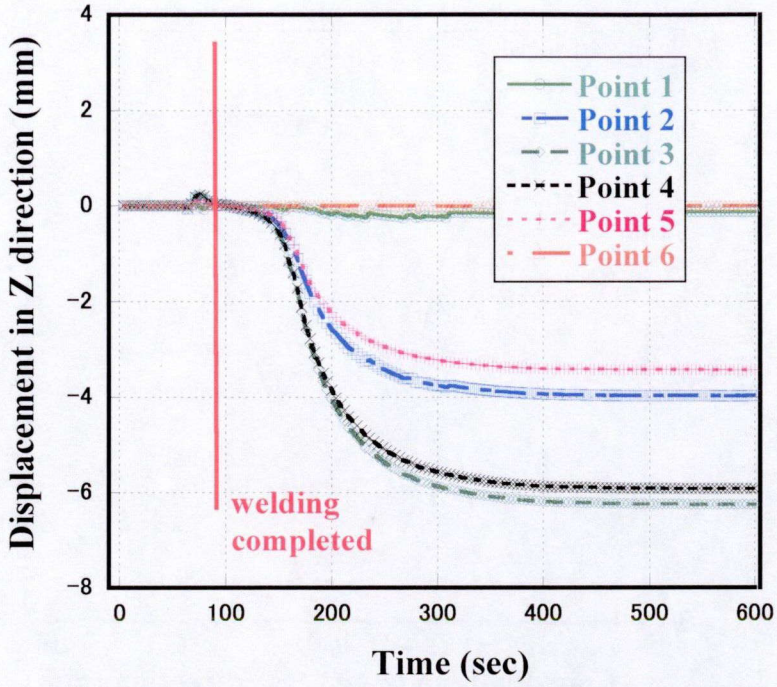

Fig. 4.6 Time history of displacement in Z direction during welding (carbon steel).

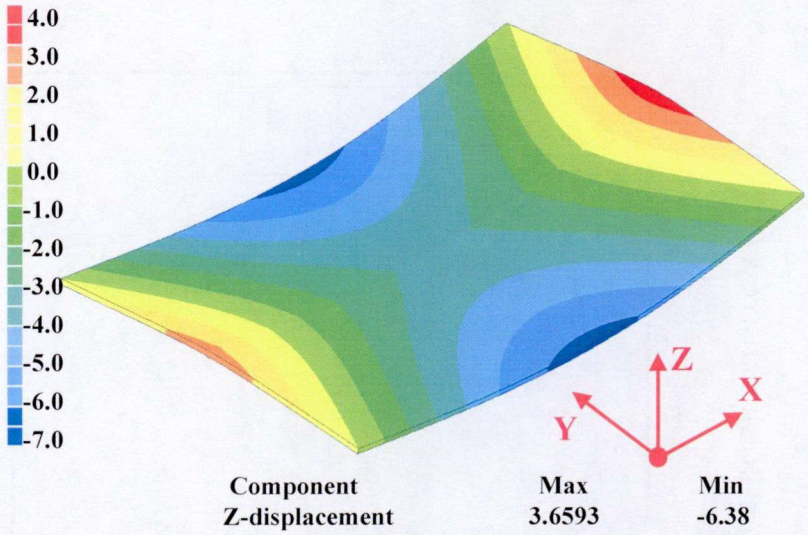

Fig. 4.7 Buckling distortion of plate after welding (carbon steel).

4.3 Clarifying the Mechanism of Welding Induced Buckling

To closely examine the stress distribution just before buckling starts to develop, the stress distributions of the carbon steel plate and the high tensile strength steel plate are compared at time *A* in **Fig. 4.4,** when the heat source is passing the middle of the plate. **Figure 4.8** shows the distribution of the longitudinal stress on the middle cross section (at the heat source). As may be seen from the figure, in the case of high tensile steel, compressive stress observed in the area adjacent to the welding line is larger that in the case of carbon steel. This explains why transient buckling during is likely to occur when the yield stress of the material is high.

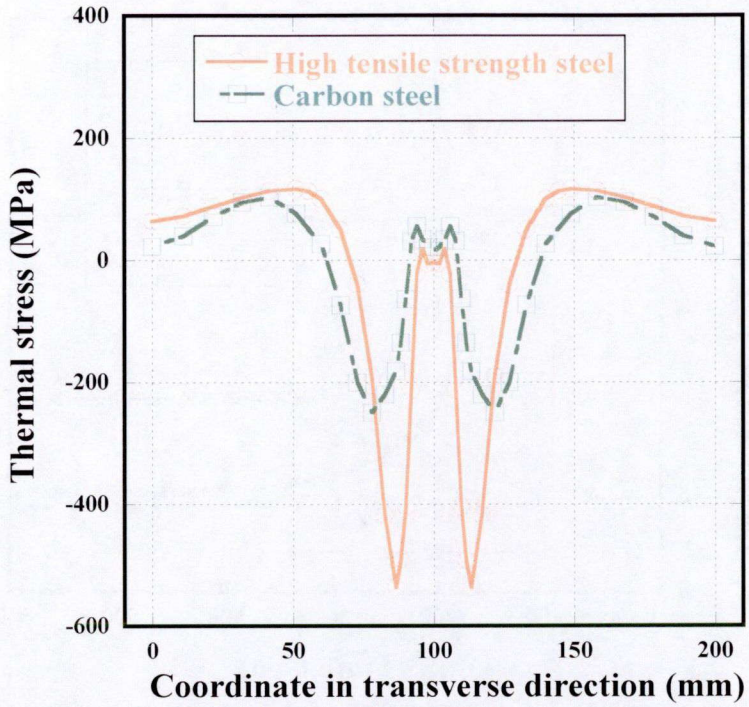

Fig. 4.8 Comparison of transient longitudinal stresses in the cases of high tensile strength steel and carbon steel.

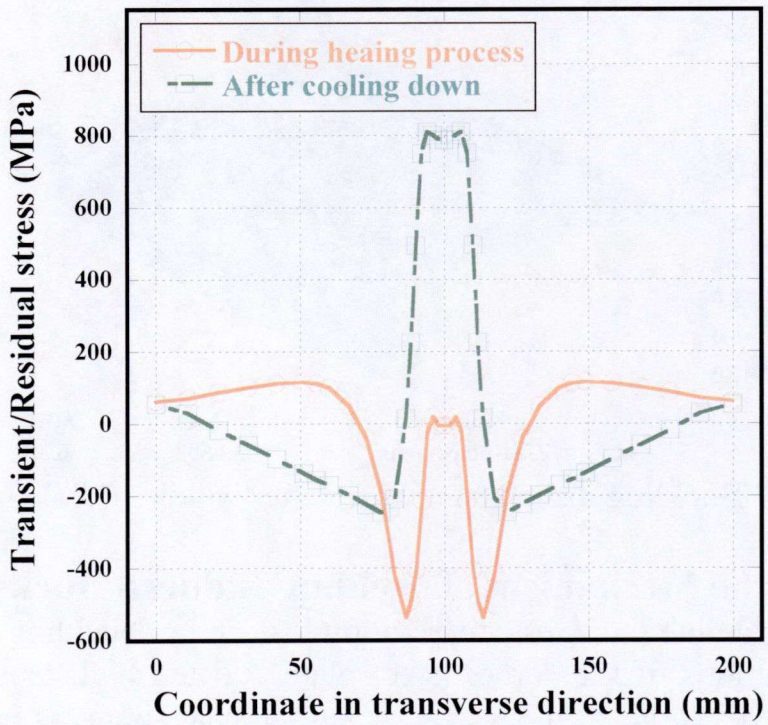

Fig. 4.9 Comparison of transient thermal longitudinal stress and residual longitudinal stress under welding.

Figure 4.9 shows the distributions of longitudinal stress in the case of high tensile strength steel at times A and B in **Fig. 4.4** when transient buckling is about to happen and after cooling. After cooling, the typical residual stress distribution with a

strong narrow tension band at the welding line and compressive stress away from the welding line is observed. Because of these different stress distributions, dish type buckling is promoted during heating and saddle type buckling is promoted after cooling.

4.4 Conclusions

Using thermal elastic plastic FE analysis, buckling behavior in bead on plate welding of a thin plate is investigated. It is found that the plate may buckle both during and after welding. The mode of buckling during the heating process in welding is a dish type mode. This is transient buckling and is likely to occur when the material has a high tensile strength. The mode of residual buckling after the end of welding and cooling is a saddle type mode. Both types of buckling are produced by the compressive stress associated with the transient thermal stress or the residual stress respectively.

Since the material considered in the following chapters is carbon steel, only residual buckling after complete cooling is discussed.

Chapter 5 Buckling of Rectangular Plate under Welding

Bead on plate is often selected to examine welding problems and to clarify the mechanism of welding induced physical behavior in thin plates' butt welded joints. In this chapter, a test specimen with bead on plate is examined to investigate welding induced buckling of rectangular plates. For this purpose, computational approach is employed to investigate and clarify the mechanism of welding induced buckling.

Firstly a bead on plate test with TIG welding is carried out. Initial deflection and out-of-plane welding distortion are measured using a digital photometric measuring method. A computational approach incorporating a 3D thermal elastic plastic FE analysis, a shell element eigenvalue analysis and large deformation elastic analysis using the inherent deformation theory is employed to investigate welding induced buckling. Thermal elastic plastic FE analysis is used to evaluate plastic strain. Then the magnitude of inherent deformation is evaluated by integrating these plastic strains. Using a shell element model, eigenvalue analysis is conducted to predict critical buckling inherent deformation and buckling mode. Also, elastic analysis using a shell element model is carried out to predict out-of-plane welding distortion considering initial deflection.

5.1 Experimental Procedure and Results

A thin rectangular plate is selected as a test specimen. Specimen size is 300×200×2.28 (mm) and its material is carbon steel, whose material properties are presented in **Section 2.2**. Bead on plate is performed using MIG welding. Welding condition is shown in **Table 5.1**.

The test specimen is shown in **Fig. 5.1** and is marked with 60 grid lines in length and 40 grid lines in width directions. This test specimen is simply placed on a work bench without restraint. Before welding, a digital photometric measuring method is used to obtain the initial deflection of this test specimen at grid nodes. The distribution of initial deflection is shown in **Fig. 5.2**. Because this test specimen is only 2.28 mm thick, welding heat almost uniformly penetrates the whole plate thickness. **Figure 5.3** shows the out-of-plane welding distortion of the plate. A saddle type buckling distortion is observed. The out-of-plane welding distortions at the grid nodes are also measured and depicted in **Fig. 5.4**. This experiment and measurement are carried out by the group of Associate Prof. Xianqing Yin in Xi'an Jiaotong University, China.

Table 5.1 Welding condition of bead on plate welding.

Current	Voltage	Velocity
100(A)	13.5(V)	6.25(mm/s)

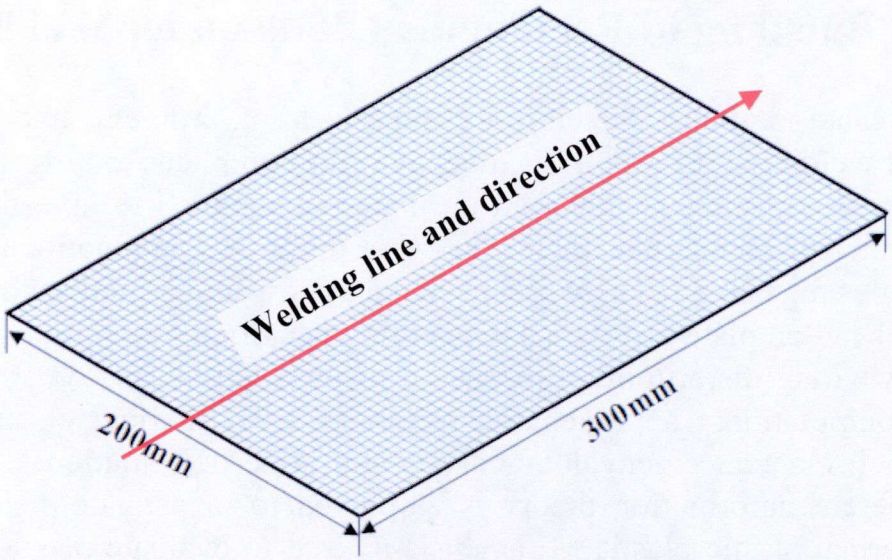

Fig. 5.1 Test specimen and marked grid for measuring deflection.

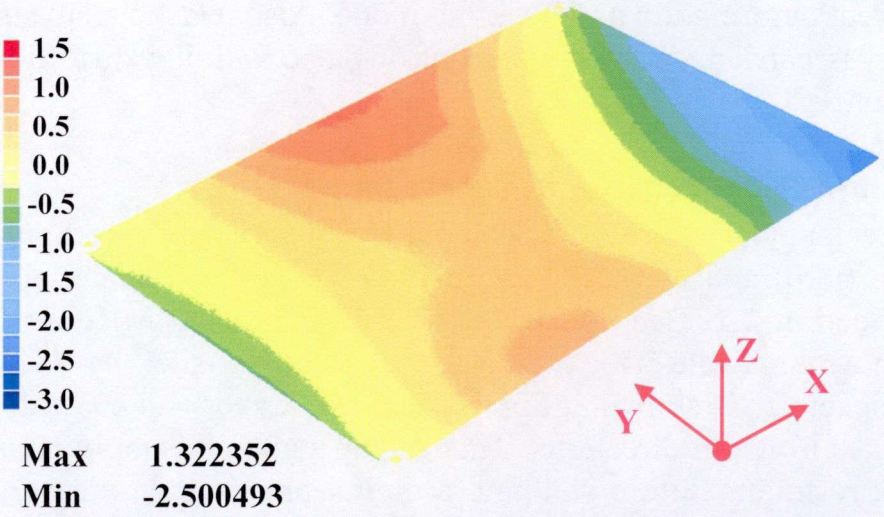

Fig. 5.2 Distribution of initial deflection in test specimen.

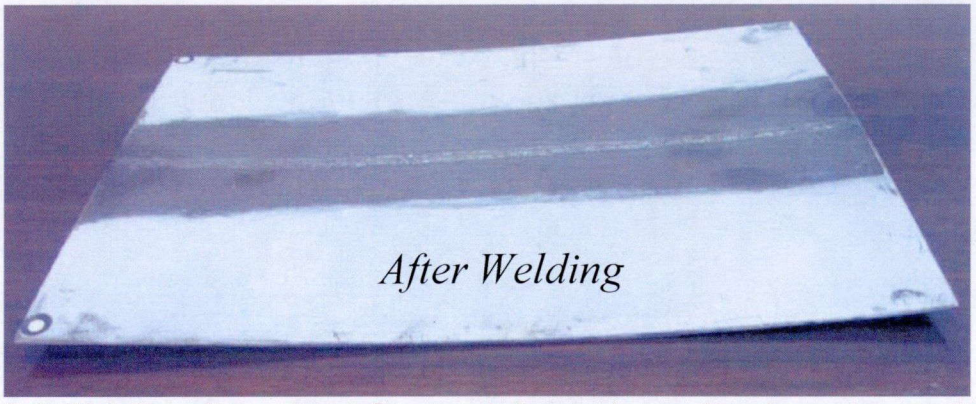

Fig. 5.3 Welding distortion of test specimen due to bead on plate welding.

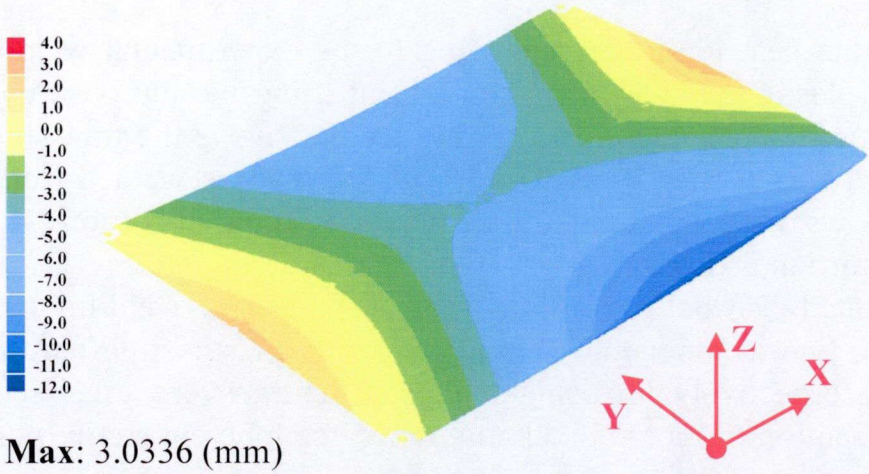

Max: 3.0336 (mm)
Min: -11.2079 (mm)

Fig. 5.4 Measured out-of-plane welding distortion due to bead on plate welding.

5.2 Numerical Analysis of Welding Induced Buckling

Using the in-house code JWRIAN mentioned in **Chapter 2**, the three approaches discussed in the beginning of the same chapter are carried out to predict the out-of-plane welding distortion, and to investigate the critical force/inherent deformation and the corresponding buckling mode when buckling occurs.

5.2.1 Evaluation of Inherent Deformation

A 3D solid element model of test specimen for thermal elastic plastic FE analysis is shown in **Fig. 5.5**. The model consists of 17675 nodes and 13600 elements. Only rigid body motion is prevented as shown in **Fig. 5.5**. Initial deflection is not considered in this case. The welding condition given in **Table 5.1** is used and the welding direction is along the positive direction of the X axis at the center of the plate.

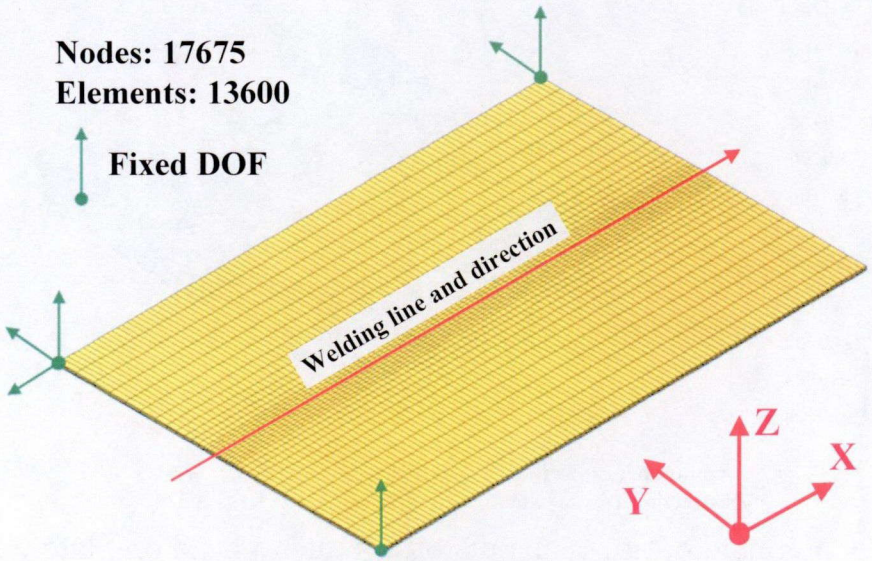

Fig. 5.5 Solid element model of test specimen.

Applying the heat input corresponding to the experimental welding condition, thermal elastic plastic FE analysis is carried out using the in-house code JWRIAN. Large deformation theory is considered. **Figure 5.6** shows the transient temperature distribution at the 240th step when the 3/4 of the plate is welded (total 320 steps). **Figure 5.7** shows the computed out-of-plane welding distortion. A symmetrical saddle type distortion is observed.

The computed distributions of longitudinal (parallel to weld line) and transverse (normal to weld line) components of inherent strain (plastic strain) are shown in **Fig. 5.8 (a)** and **(b)**, respectively. Focusing on the middle transverse cross section, **Fig. 5.9** shows the distribution of longitudinal and transverse inherent strain (plastic strain) at the neutral plane along the transverse direction.

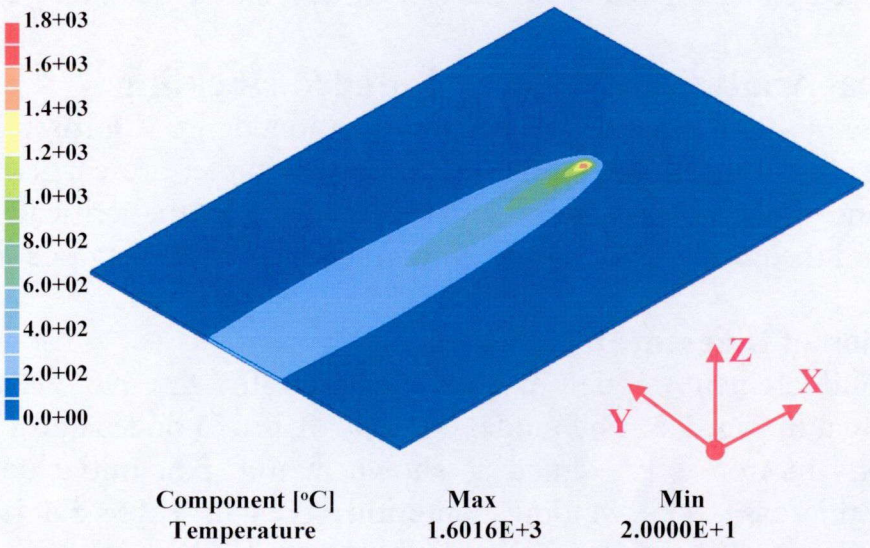

Fig. 5.6 Transient temperature distribution during bead on plate welding.

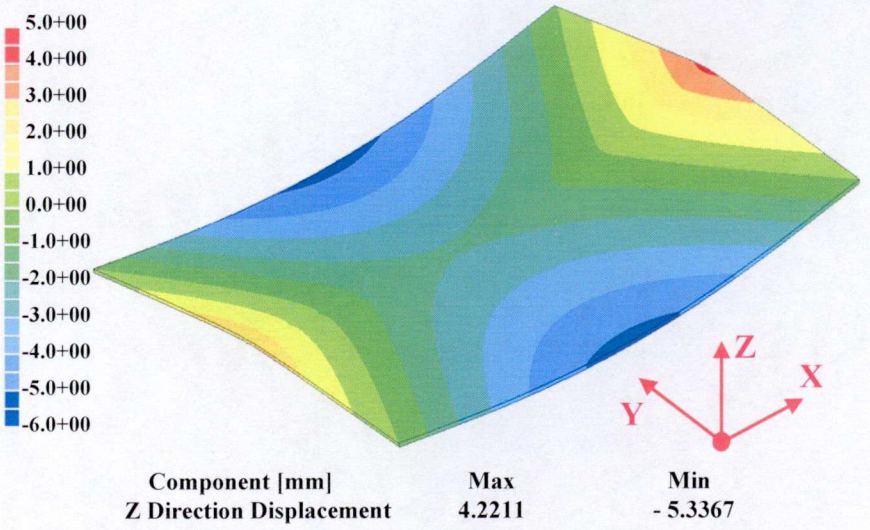

Fig. 5.7 Computed out-of-plane distortion due to bead on plate welding.

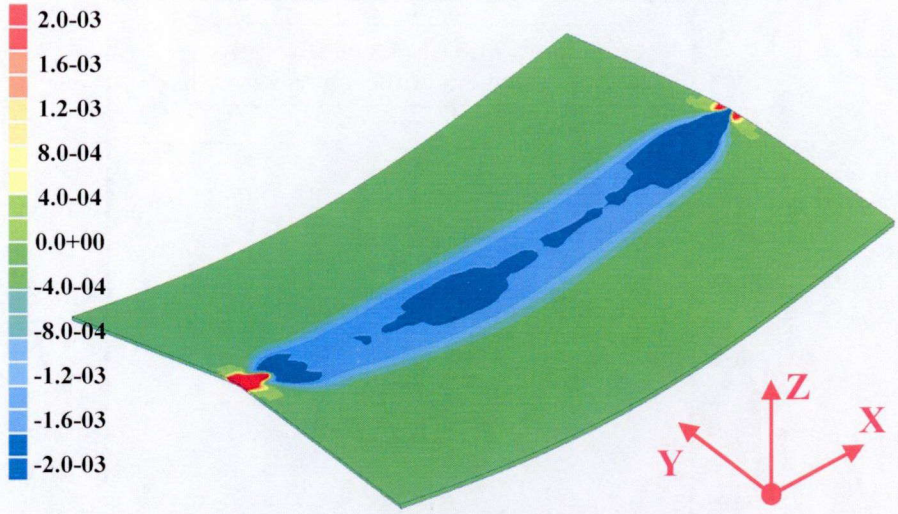

(a) Distribution of longitudinal inherent strain

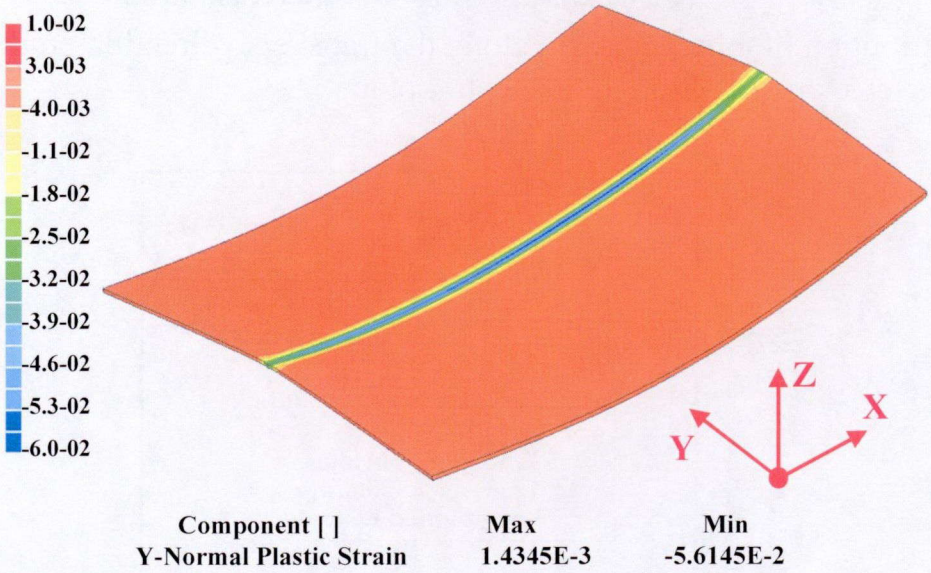

(b) Distribution of transverse inherent strain

Fig. 5.8 Distribution of inherent strain in welded joint.

Integrating the inherent strain, the inherent deformations are evaluated on each transverse cross section and the distributions of all components of inherent deformation along the welding line are shown in **Fig. 5.10**. To avoid difficulty when applying the computed distributions of inherent deformation components to shell element models in elastic analysis, constant magnitudes of inherent deformation components are used assuming that the welding line is long enough to neglect the edge effect. The inherent deformations of this bead on plate, evaluated by averaging the inherent deformation along the middle region (50 mm to 250 mm) of the welding line where the inherent deformation is approximately constant, are given in **Table 5.2**.

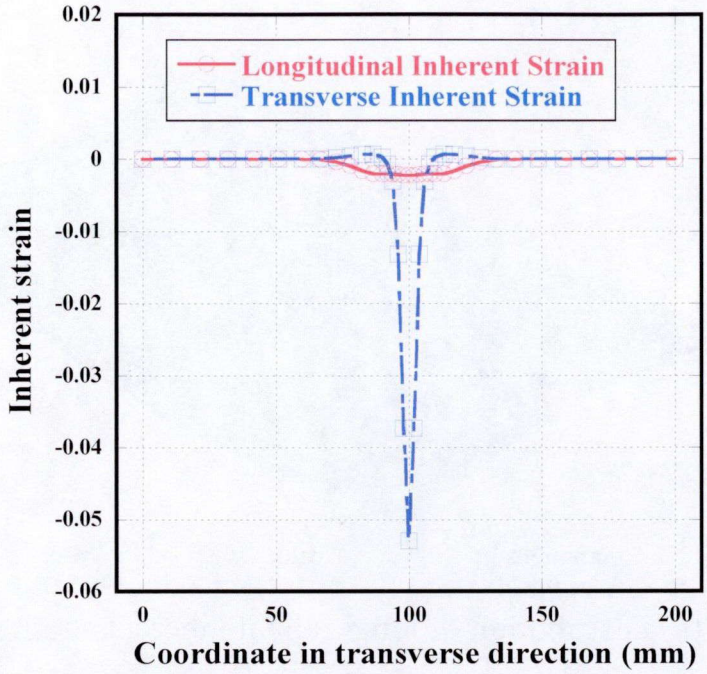

Fig. 5.9 Distribution of inherent strain along the transverse direction on the middle transverse cross section at the neutral plane.

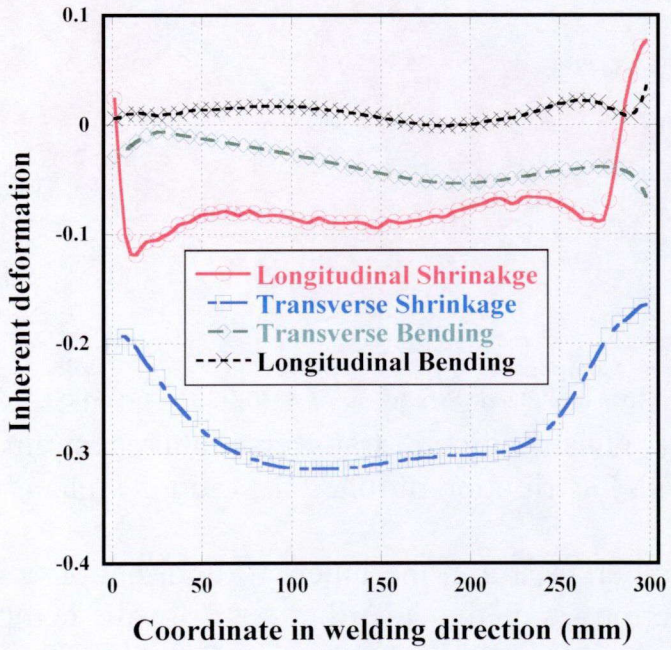

Fig. 5.10 Distributions of inherent deformation components along the welding line.

Table 5.2 Magnitudes of inherent deformation components caused by bead on plate welding.

Longitudinal Shrinkage (mm)	Transverse Shrinkage (mm)	Transverse Bending (rad)	Longitudinal Bending (rad)
-0.07507	-0.27451	-0.03521	0.01094

5.2.2 Investigation of Welding Induced Buckling Using Eigenvalue Analysis

In the following, eigenvalue analysis is employed to examine the condition for welding induced buckling. **Figure 5.11** shows a shell element model of the test specimen. The model has 2562 elements (2501 shell elements and 61 interface elements) and 2400 nodes. As in **5.2.1,** only rigid body motion is fixed as shown in **Fig. 5.11**.

The longitudinal component of the inherent deformation is considered to be the dominant cause of welding induced buckling [89]. Therefore, and for ease of interpreting the results, other components of inherent deformation are not considered in this analysis. Applying the computed magnitude of longitudinal inherent shrinkage shown in **Table 5.2**, the eigenvalue analysis is carried out to investigate the buckling behavior of test specimen. This applied longitudinal inherent shrinkage δ_L^* can be converted to an applied tendon force $F_{applied}$ using the following relation.

$$F_{applied} = E \times h \times \delta_L^*(computed)$$
$$= 210000MPa \times 2.28mm \times 0.07507mm = 35.94KN \qquad (5\text{-}1)$$

According to the definition of the eigenvalue presented in **Section 2.4**,

$$eigenvalue(N^{th}) = \frac{\delta^*_{critical}(N^{th})}{\delta^*_{applied}} = \frac{F^{critical}_{tendon}(N^{th})}{F^{applied}_{tendon}} \qquad (5\text{-}2)$$

Where, $F_{critical}(N^{th})$ is the critical force of N^{th} buckling mode and $eigenvalue(N^{th})$ is the corresponding eigenvalue. The computed buckling modes and corresponding critical (buckling) forces/inherent deformations are shown in **Fig. 5. 12**.

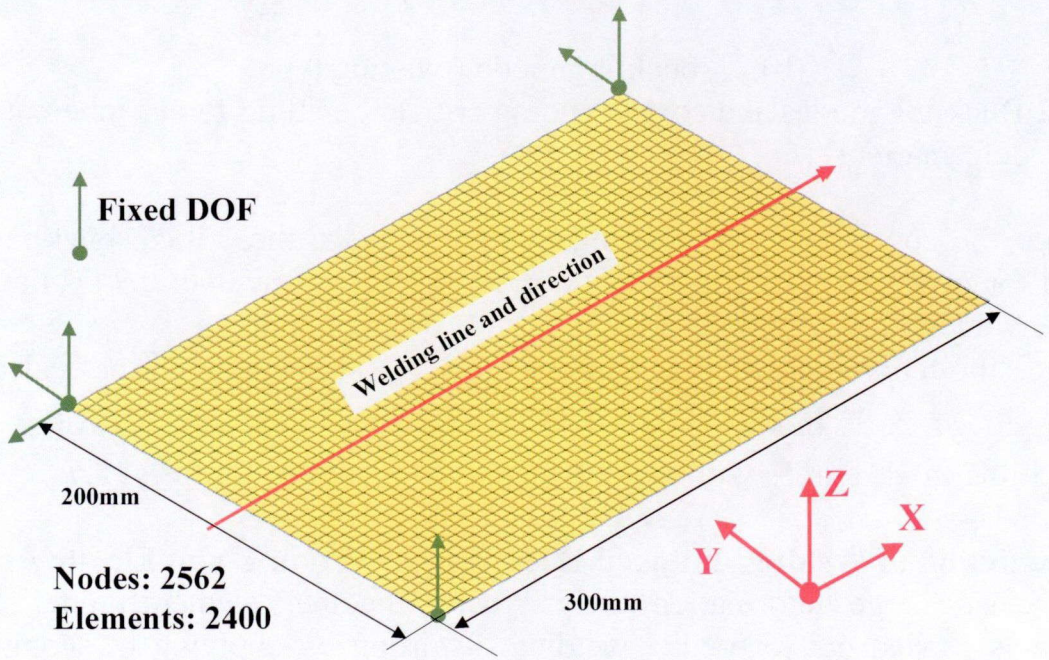

Fig. 5.11 Elastic analysis FE model and boundary condition.

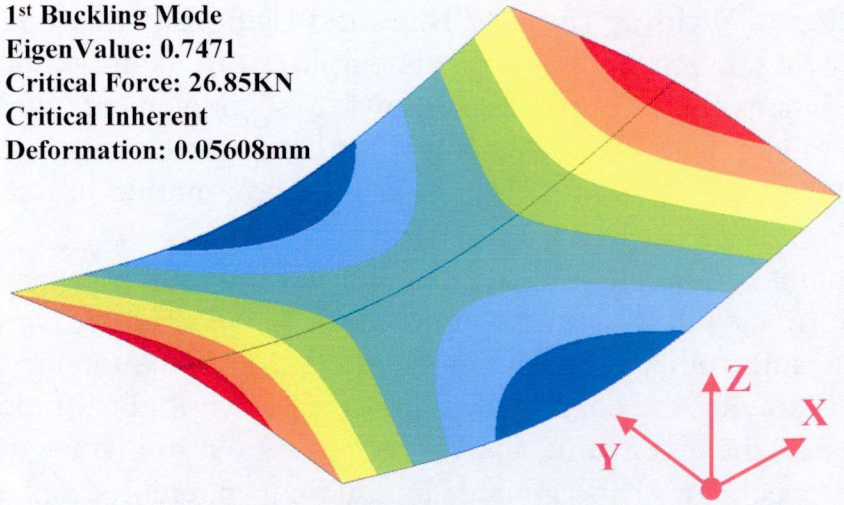

(a) 1st buckling mode (saddle type)

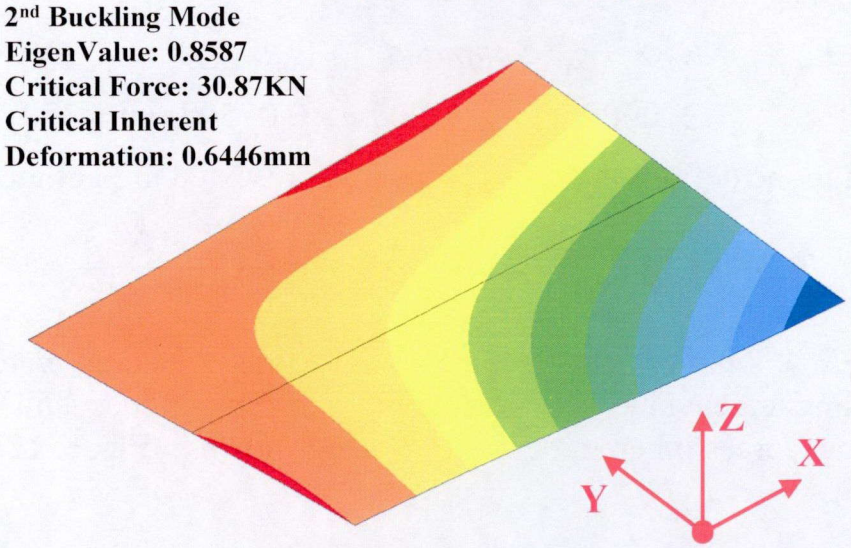

(b) 2nd buckling mode (twisting type)

Fig. 5.12 Buckling modes and corresponding critical buckling forces/inherent deformations.

From the computed results of eigenvalue analysis, the critical buckling forces for the 1st and the 2nd buckling modes are 26.85 kN (eigenvalue: 0.7471) and 30.87 kN (eigenvalue: 0.8587), respectively.

Since the tendon force caused by welding $F_{applied}$ exceeds the critical buckling force $F_{critical}$ of the 1st mode, buckling occurs in the first mode shown in **Fig. 5.12 (a)**. This buckling mode agrees with the deformed shape presented in **Fig. 5.7**.

5.2.3 Prediction of Welding Induced Buckling Distortion Using Elastic Analysis

An elastic large deformation analysis using the shell element model shown in **Fig. 5.11** is carried out to predict welding distortion by applying the computed all inherent deformation shown in **Table 5.2** to the welding line. Initial deflection is not considered.

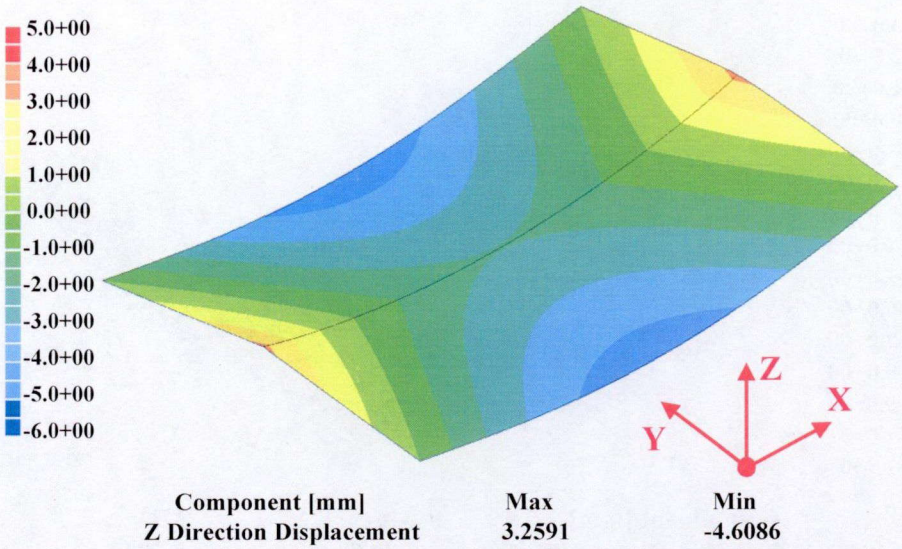

Fig. 5.13 Out-of-plane welding distortion using elastic FE analysis and constant inherent deformation.

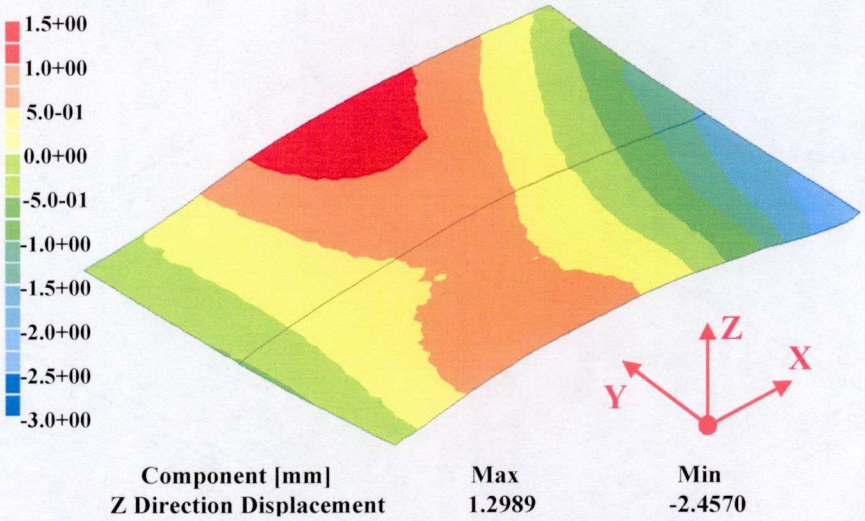

Fig. 5.14 Initial deflection introduced in elastic FE analysis model.

Out-of-plane welding distortion is obtained as shown in **Fig. 5.13**which shows a symmetrical saddle type buckling mode. Comparing with the computed out-of-plane welding distortion using thermal elastic plastic FE analysis shown in **Fig. 5.7**, it may be seen that elastic analysis using constant inherent deformation can predict welding distortion with good accuracy consuming a short computation time. However, a large difference is observed between computed out-of-plane welding distortions using both elastic and thermal elastic plastic analyses and the measured one shown in **Fig. 5.4**.

Since this difference may come from the initial deflection of the specimen, the measured initial deflection is introduced to the shell element model in elastic analysis as shown in **Fig. 5.14**. **Figure 5.15** shows the computed out-of-plane welding distortion considering this initial deflection. A saddle type buckling mode is observed. However the deformed shape is unsymmetrical.

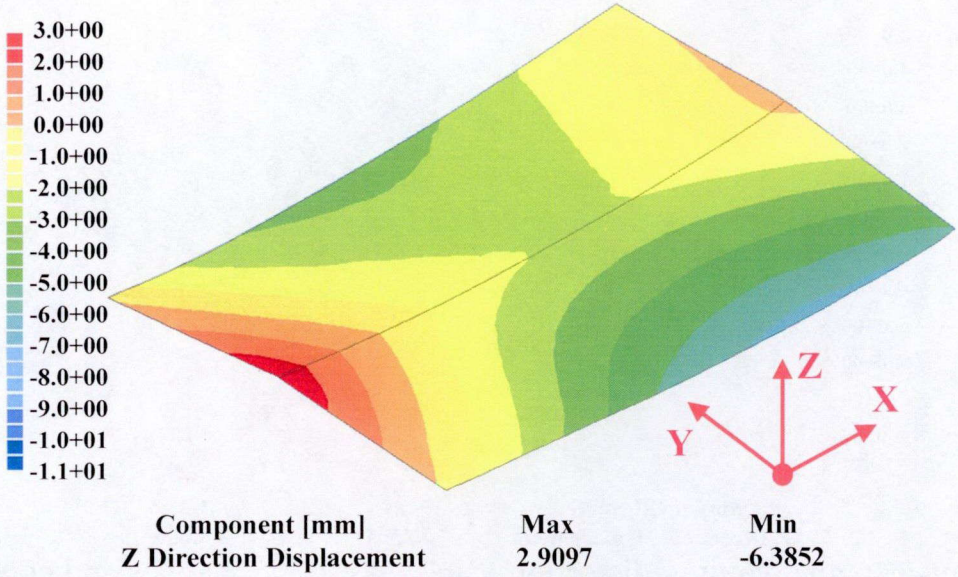

Fig. 5.15 Out-of-plane welding distortion considering initial deflection.

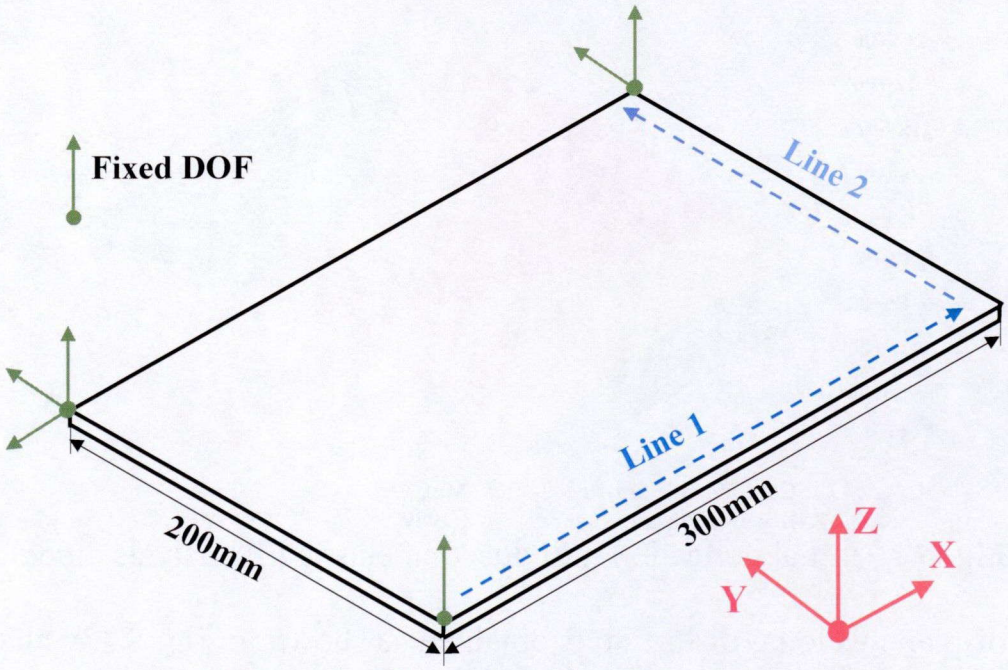

Fig. 5.16 Position of line 1 and line 2 in test specimen.

Points on line 1 and line 2 shown in **Fig. 5.16** are selected to compare the computed and measured out-of-plane welding distortion. The computed out-of-plane welding distortion has the same tendency as the measured one as shown in **Fig. 5.17**.

5.3 Influential Factors Affecting Welding Induced Buckling

Buckling behavior is difficult to investigate because of its instability. In particular, welding induced buckling is influenced by many factors and is difficult to accurately predict. In this section, influential factors are investigated using thermal elastic plastic and elastic FE analysises.

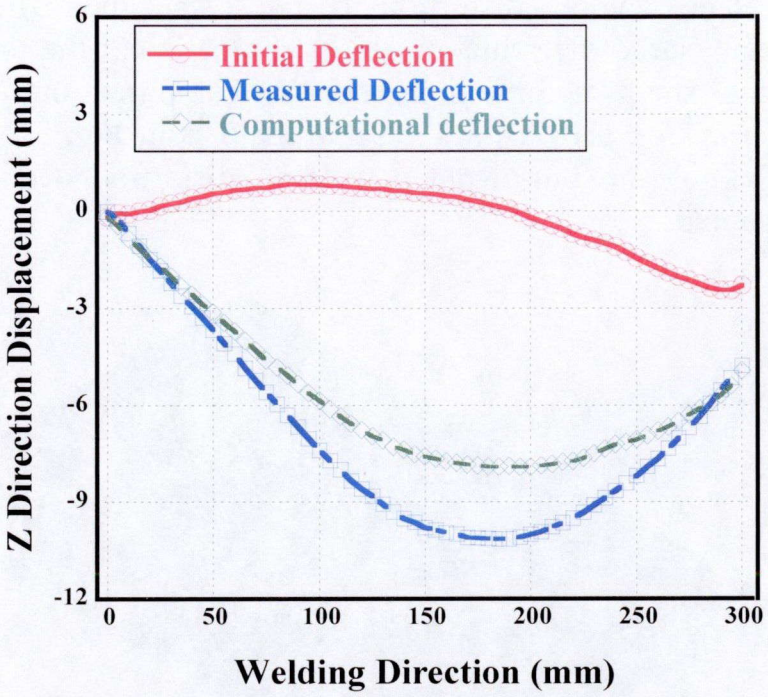

(1) Out-of-plane welding distortion along line 1

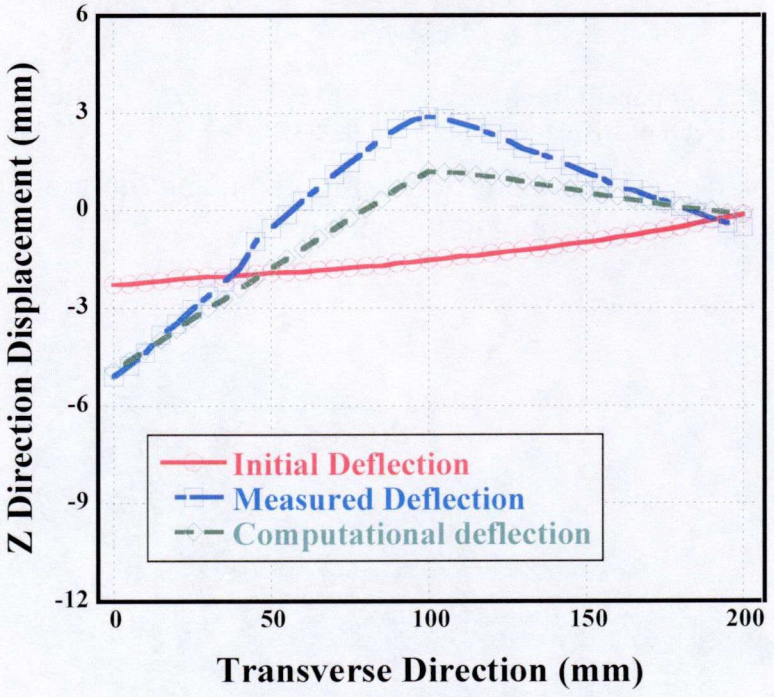

(2) Out-of-plane welding distortion along line 2

Fig. 5.17 Comparisons of welding distortion between computation and measurement.

5.3.1 Comparison between the Results Using Small and Large Deformation Theories

In order to investigate buckling behavior of structures, the large deformation theory should be considered. To distinguish welding induced buckling from bending type distortion, thermal elastic plastic FE analyses using small and large deformation

theories are carried out. Initial deflection is not considered. **Figure 5.7** shows the computed out-of-plane welding distortion of a test specimen after bead on plate welding considering large deformation. For comparison, the same problem is computed assuming small deformation and the computed out-of-plane welding distortion is shown in **Fig. 5.18** using the same scale as in **Fig. 5.7**. As may be seen from the figure, almost no out-of-plane welding distortion occurred when small deformation is assumed.

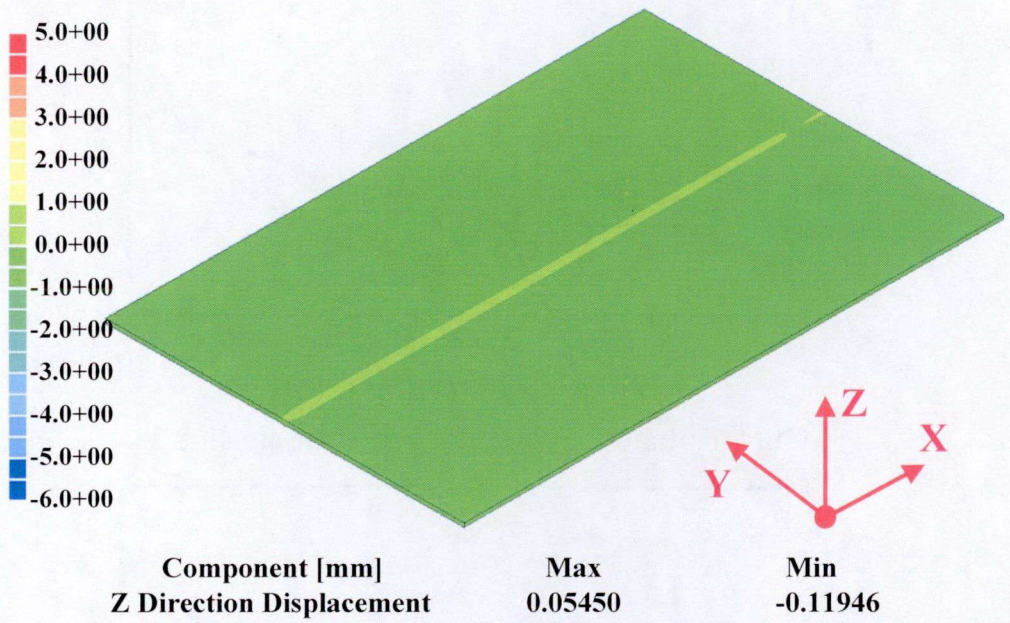

Fig. 5.18 Out-of-plane welding distortion computed using thermal elastic plastic FE analysis considering small deformation theory.

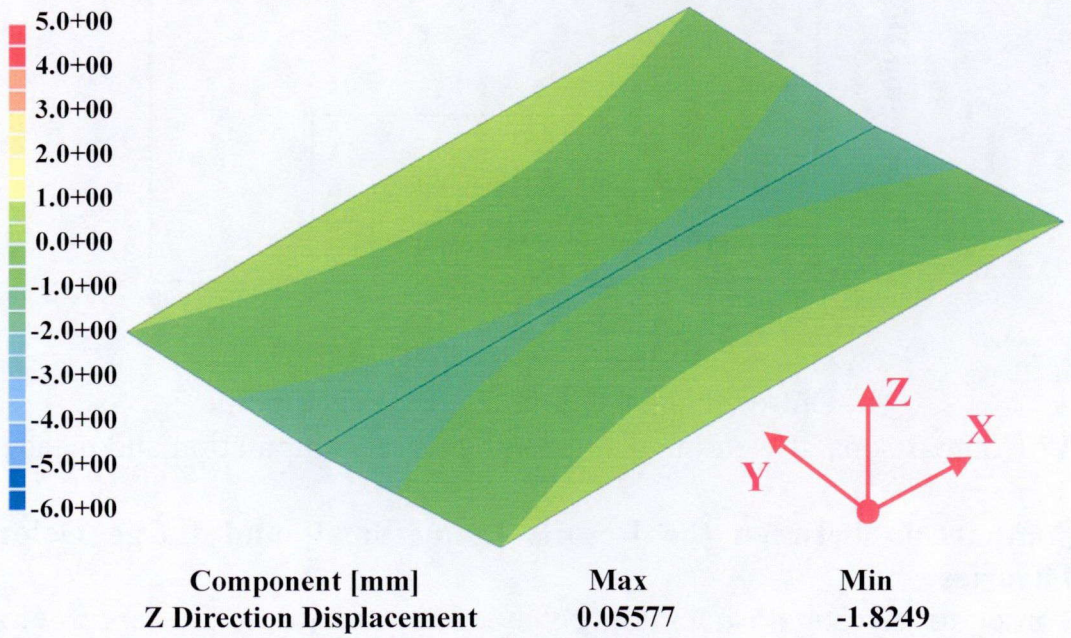

Fig. 5.19 Out-of-plane welding distortion computed using elastic FE analysis assuming small deformation.

Similarly, elastic FE analysis using the shell element model shown in **Fig. 5.11** is carried out assuming small deformation and applying all inherent deformation components given in **Table 5.2**. **Figure 5.19** shows the computed out-of-plane welding distortion. As seen from this figure, the magnitude of deflection is about 2 mm and buckling type distortion is not observed.

5.3.2 Influence of Disturbance to Welding Induced Buckling

As mentioned before, longitudinal residual stress or the tendon force (longitudinal shrinkage force) is considered to be the dominant reason of welding induced buckling in a thin plate welded joint [89]. Buckling occurs when the stress (tendon force) in the plate exceeds the critical stress (critical tendon force) as discussed in **5.2.2** above.

When only a tendon force (longitudinal inherent shrinkage) which exceeds the critical value is considered in large deformation elastic analysis with no disturbance adopted, the model shown in **Fig.5.11** is used and only the longitudinal inherent shrinkage shown in **Table 5.2** is employed, no out-of-plane welding distortion is produced as shown in **Fig. 5.20**.

The reason can be understood from the theory of eigenvalue analysis. Eigenvalue analysis predicts when the solution has a bifurcation. At and beyond the bifurcation point, more than one solution becomes possible. One is the trivial solution $\{u\} = 0$. This is a simple compression without lateral deflection. The other solution is a lateral deflection in an eigenmode. In FE analysis if a perfectly flat plate is incrementally compressed in its plane, the plate follows the first (trivial) solution and remains flat even when the critical load is exceeded. In order that the plate follows the second solution and exhibits lateral deflection, some kind of disturbance, which serves as a trigger of buckling, is necessary.

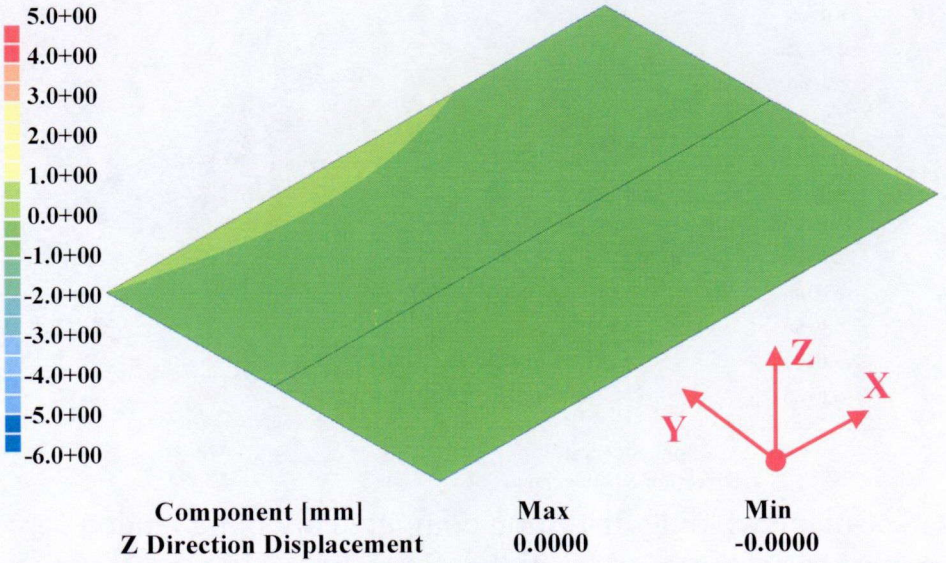

Fig. 5.20 Out-of-plane welding distortion applying tendon force (longitudinal inherent shrinkage) only.

Figure 5.21 illustrates the influence of initial deflection on buckling. In the figure δ is the deflection. When the plate has no initial deflection and the applied in-plane compressive force F exceeds the critical force F_{cr}, there are two possible solutions. One is increased load without lateral deflection, and the other is the deformation in the buckling mode. The point where $F/F_{cr}=1$ is the bifurcation point corresponding to the ideal buckling force. If there is no initial deflection, the plate remains flat in incremental FE analysis even when the applied compressive force exceeds the critical force. Only when the plate has disturbance, buckling type distortion can be obtained. In other words, disturbance is necessary to trigger buckling in incremental FE analysis. In actual structures, disturbance such as initial deflection always exist.

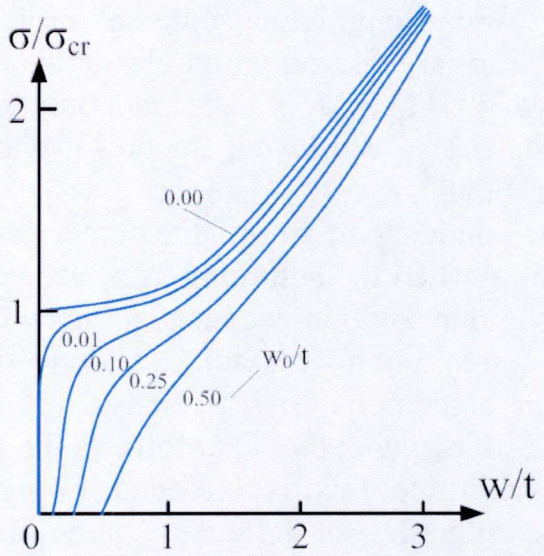

Fig. 5.21 Influence of initial deflection to buckling behavior.

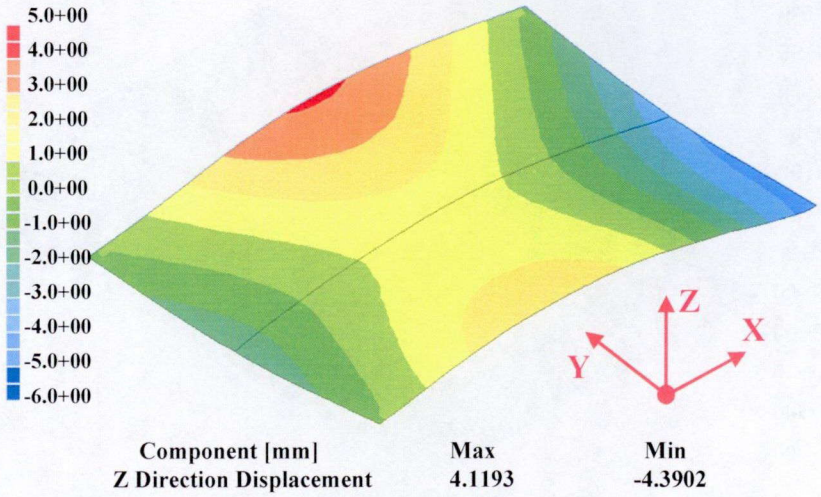

Fig. 5.22 Out-of-plane welding distortion computed applying tendon force and considering the measured initial deflection.

Therefore, in FE analysis of flat plates, and when buckling is expected, disturbance, usually in the form of initial deflection or a small lateral load, should be introduced to trigger buckling. Initial deflection and welding inherent bending are considered as two kinds of disturbance. Their influence on buckling is examined in the following section using large deformation elastic analysis.

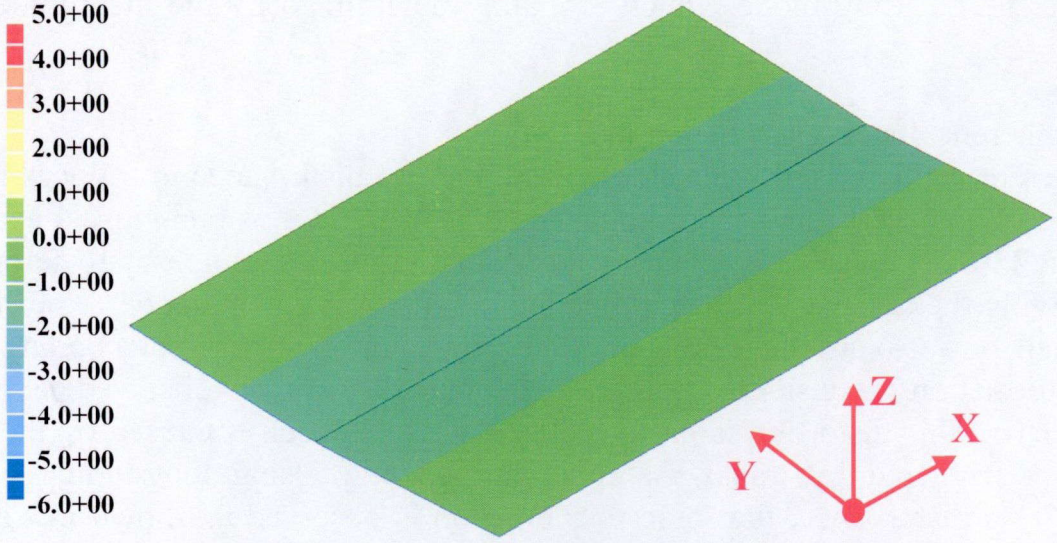

(a) out-of-plane welding distortion caused by transverse inherent bending (small deformation theory)

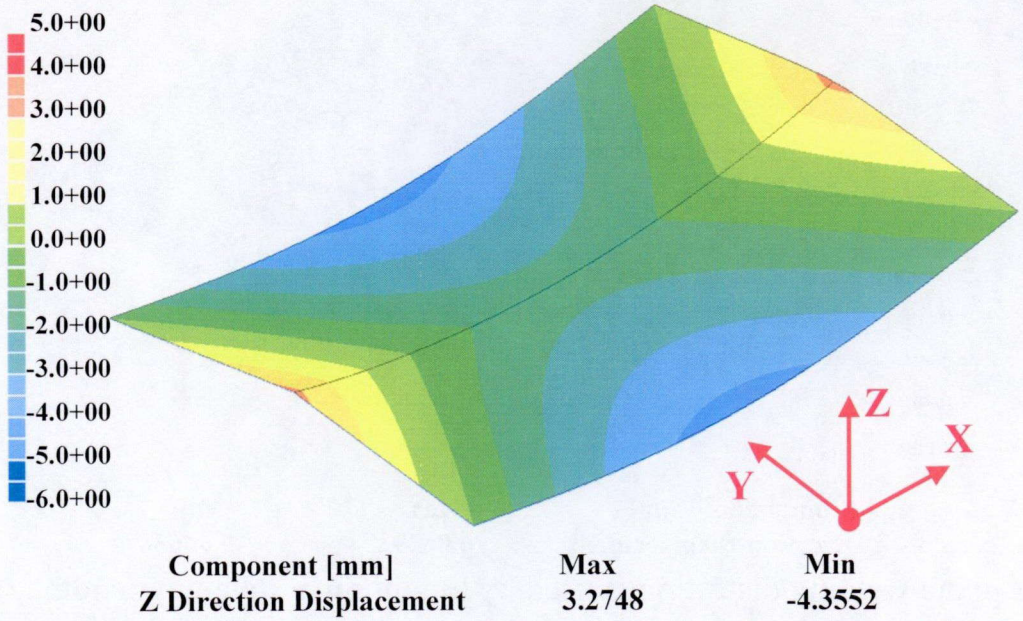

(b) out-of-plane welding distortion caused by transverse inherent bending and tendon force (large deformation theory)

Fig. 5.23 Computed out-of-plane welding distortion considering transverse inherent bending as disturbance.

5.3.2.1 Initial Deflection as Disturbance

As shown by **Fig. 5.20,** in large deformation elastic FE analysis considering longitudinal inherent shrinkage only and no initial deflection is introduced, buckling is not obtained. As shown in **Fig. 5.22,** buckling type distortion is obtained when initial deflection exists. Small initial deflection is considered as only a disturbance. It influences the magnitude of out-of-plane welding distortion. However, it may not influence the buckling mode, which is mainly determined by the magnitude of the tendon force.

5.3.2.2 Inherent Bending as Disturbance

Inherent bending is also considered as a kind of disturbance to trigger buckling. Influence of transverse and longitudinal inherent bending on buckling is examined. **Figure 5.23(a)** shows out-of-plane welding distortion assuming small deformation and applying the transverse inherent bending in addition to the tendon force. There is only small out-of-plane distortion produced by transverse inherent bending. When large deformation is considered, large out-of-plane distortion is observed as shown in **Fig. 5.23(b)**. This distortion is produced by buckling which is caused by the tendon force, but triggered by transverse inherent bending. Using longitudinal inherent bending as a disturbance, the same phenomenon is observed as shown in **Fig. 5.24**. **Fig. 5.24** also shows that inherent bending triggers buckling when the tendon force exceeds the critical force.

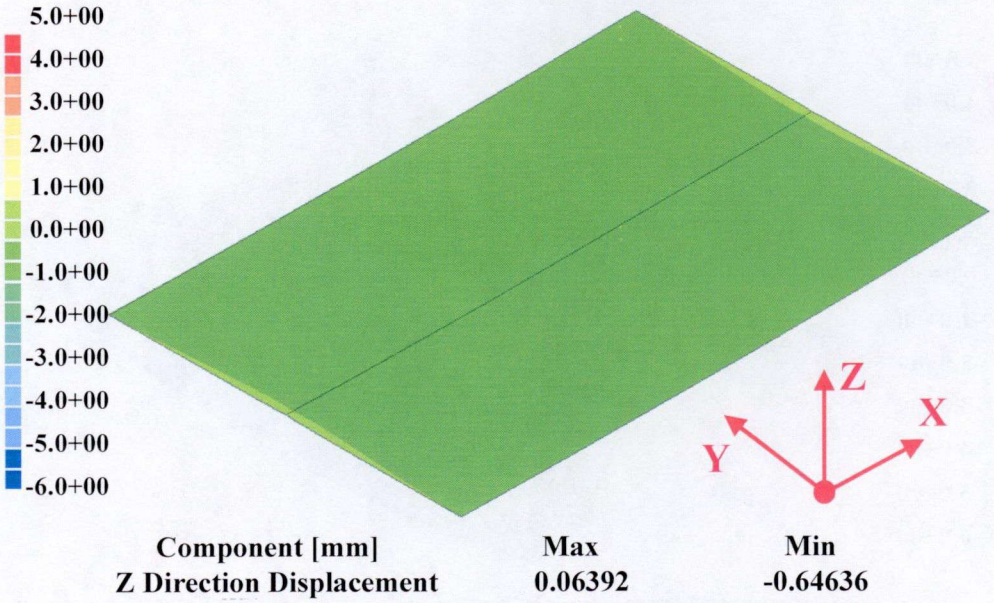

(a) out-of-plane welding distortion caused by longitudinal inherent bending (small deformation theory)

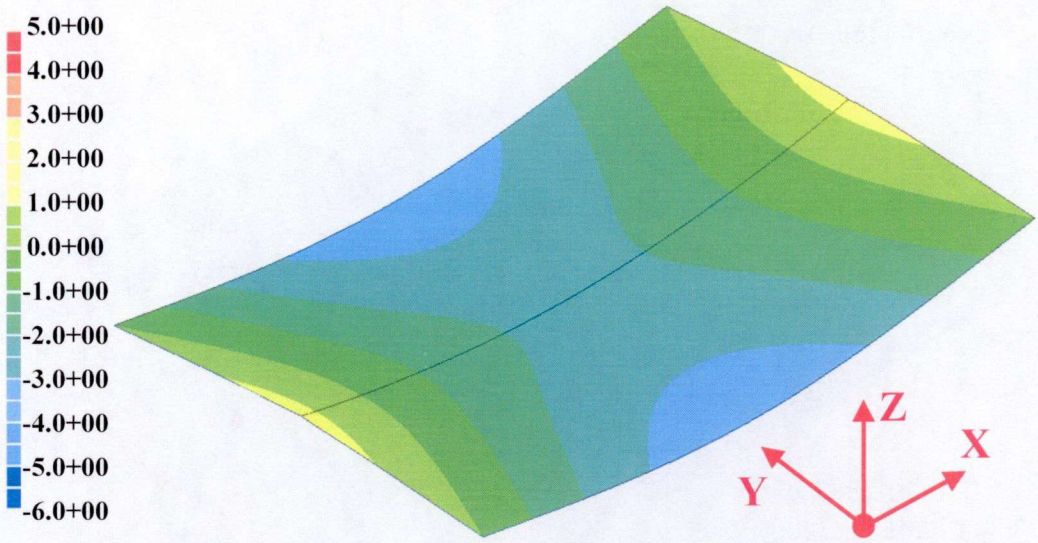

Component [mm]	Max	Min
Z Direction Displacement	1.3991	-3.7490

(b) out-of-plane welding distortion caused by longitudinal inherent bending and tendon force (large deformation theory)

Fig. 5.24 Computed out-of-plane welding distortion considering longitudinal inherent bending as disturbance.

The above discussion confirms that although eigenvalue analysis shows that a welded structure buckles when the welding tendon force exceeds the critical force, buckling does not occur if there is no disturbance which trigger buckling. Eigenvalue analysis only predicts the critical buckling force/inherent deformation at which buckling can happen. Actual buckling depends on not only the critical compressive force but also the triggering disturbance such as initial deflection.

The whole magnitude of out-of-plane welding distortion is contributed by initial deflection, inherent bending distortion, deflection magnification by in-plane loads and buckling. Therefore, in the analysis presented in the rest of this chapter, initial deflection and all components of inherent deformation are considered to accurately predict out-of-plane welding distortion.

5.3.3 Distribution of Inherent Deformation

According to the inherent deformation theory, the edge effect can be ignored and a constant inherent deformation can be employed in elastic analysis when the welding line is long enough. To consider the influence of distributed inherent deformation to out-of-plane welding distortion and obtain more accurate out-of-plane welding distortion compared with experimental results, the shell element model shown in **Fig. 5.25** is used. In this model, the plate is divided into three regions, namely welding start region, middle region and welding end region.

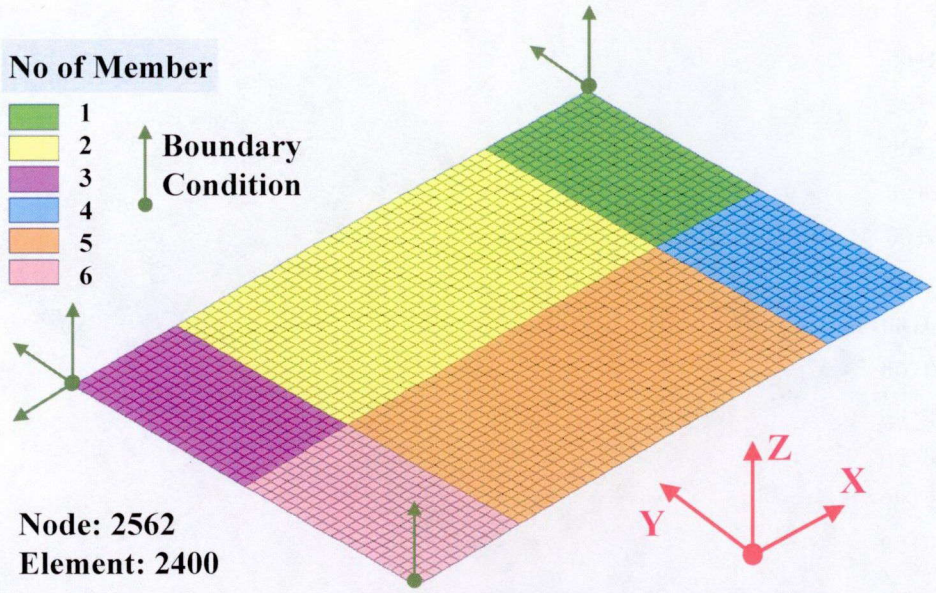

Fig. 5.25 Shell element model for utilizing distributed inherent deformation.

Inherent deformation is also divided into three sets, a set for each region. Inherent deformation computed using thermal elastic plastic FE analysis and distributed along the welding line is averaged in each region as shown by **Table 5.3**.

Table 5.3 Estimated inherent deformation due to welding.

	Longitudinal Shrinkage (mm)	Transverse Shrinkage (mm)	Transverse Bending (rad)	Longitudinal Bending (rad)
Start region	-0.08876	-0.23998	-0.01329	0.01070
Middle region	-0.08222	-0.30503	-0.03972	0.00868
End region	-0.03992	-0.21748	-0.04363	0.01793

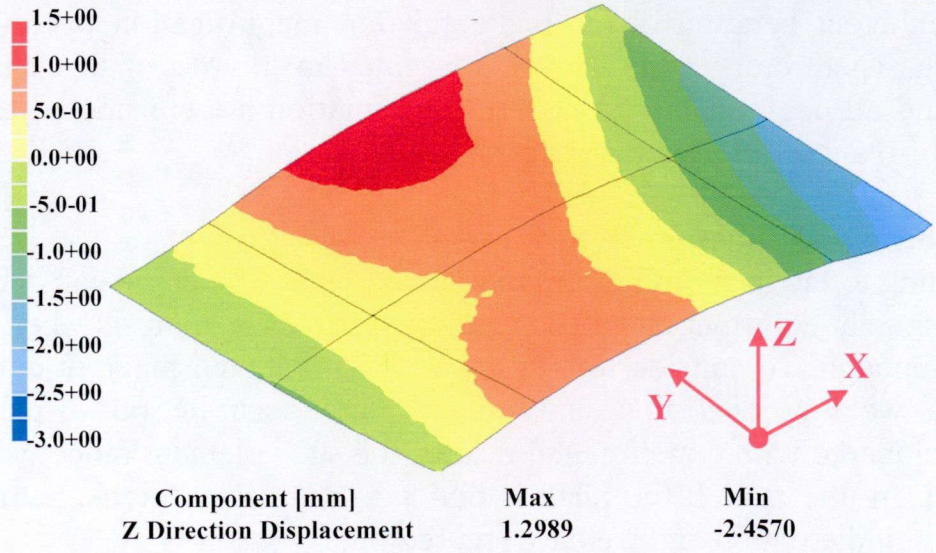

Fig. 5.26 Initial deflection assumed in shell element model used to apply the tabulated inherent deformation.

Figure 5.26 shows the distribution of the initial deflection in the shell element model. Out-of-plane welding distortion is computed considering large deformation and applying the inherent deformation tabulated in **Table 5.3**. Computed out-of-plane welding distortion is shown in **Fig. 5.27**. As shown in the figure, saddle type buckling distortion is obtained. Comparison with measured results is shown in **Fig. 5.28.** Out-of-plane welding distortion along line 1 and line 2 defined in **Fig. 5.16** are plotted. Out-of-plane welding distortion computed using constant inherent deformation is also shown. Although the computed out-of-plane welding distortion using constant inherent deformation show the same tendency as that computed using the tabulated inherent deformation, the latter gives better accuracy in a welded plate with relatively a short length.

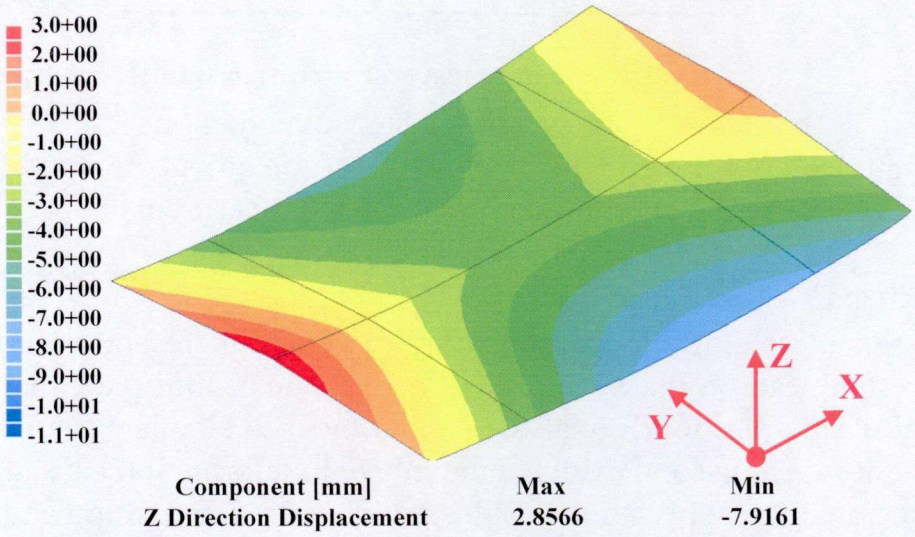

Fig. 5.27 Out-of-plane welding distortion computed using the tabulated inherent deformation.

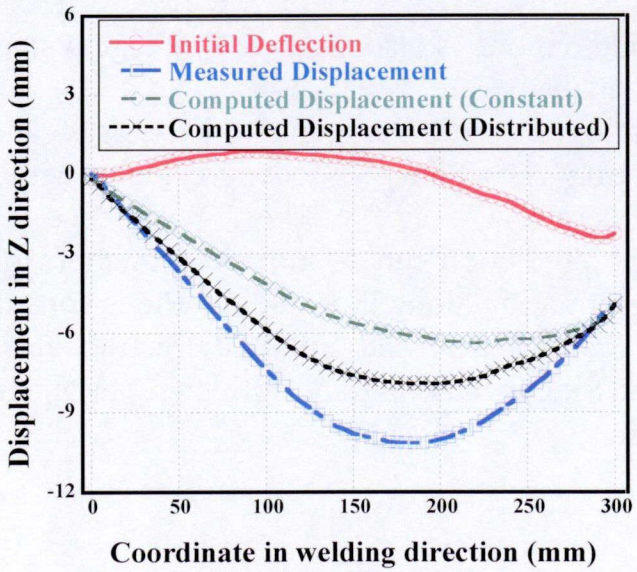

(a) Out-of-plane welding distortion along line 1

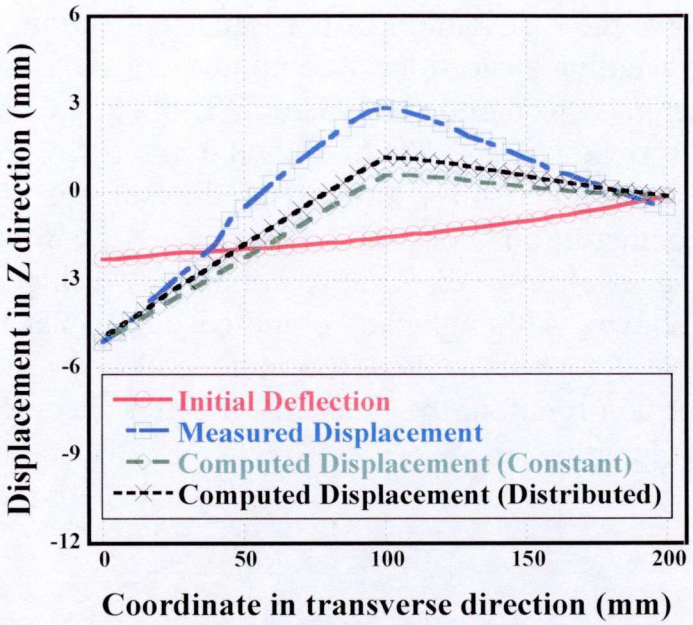

(b) Out-of-plane welding distortion along line 2

Fig. 5.28 Comparison of out-of-plane welding distortion among computations applying different inherent deformation and measurement.

5.4 Conclusions

To investigate welding induced buckling, an experiment and computations are carried out for the bead on plate welding of a rectangular thin plate made of carbon steel. Thermal elastic plastic FE analysis is employed to simulate the whole process of welding and it is also used to evaluate the inherent deformation caused by welding. Then the elastic analysis applying the evaluated inherent deformation and considering the initial deflection is carried out. Also eigenvalue analysis is carried out.

From these investigations, the following conclusions are drawn.

(1) The experiment shows that buckling with saddle type deformation is produced by welding.

(2) The buckling in saddle mode is also predicted by eigenvalue analysis and thermal elastic plastic FE analysis.

(3) Out-of-plane welding distortion computed by elastic analysis using constant inherent deformation show fairly good agreement with experiment if initial deflection is considered.

(4) The accuracy of the prediction can be improved in short joints if the distribution of the inherent deformation along the welding line is considered.

(5) Inherent bending deformation and initial deflection are considered to act as imperfections that trigger buckling and influence the magnitude of out-of-plane welding distortion.

Chapter 6 Investigation of Twisting Buckling Distortion in Stiffened Welded Structures under Welding

Investigations of welding induced buckling in thin plate structures reviewed in **chapter 1** and considered in **chapter 5** focus on bending type buckling, where buckling distortion appears as half-wave mode at several positions of the welded structure. However, there are cases in which a thin plate stiffened structure under welding buckles torsionally or in twisting mode, and the plate panels surrounded by stiffeners remain straight.

In this chapter, a thin plate stiffened structure is examined. First, welding induced twisting type buckling distortion of this structure is experimentally examined (experiment is carried out by Hitachi Research Laboratory, Hitachi Ltd.). Then, large deformation thermal elastic plastic FE analysis of the whole structure is carried out. Also a combined FE analysis, in which welding induced inherent deformation is evaluated using thermal elastic plastic FE analysis of a small scale welded joint and an elastic FE analysis with relatively coarse shell element mesh of the whole welded structure is employed to predict the final welding distortion applying the evaluated inherent deformation. Further, eigenvalue analysis with elastic shell element model is performed to predict the critical buckling inherent deformation and the corresponding buckling mode during the assembly process. Finally, the computed results obtained from two computational approaches are compared with the experiments.

6.1 Experimental Procedure and Results

To study the twisting type buckling behavior, a thin plate stiffened structure is selected as a test specimen. The structure consists of one rectangular skin plate: 1200mm×600mm×6mm, two longitudinal and three transverse I shape stiffeners with 6mm thickness. The detail size and the relative position of the members are shown in **Fig. 6.1**. This thin plate stiffened structure is pre-assembled by tack welding fixing the stiffeners together. **Figure 6.1** also shows the positions of tack welding. During the welding process, welding was performed using the following sequence, first the longitudinal stiffeners are welded to the skin plate and then the transverse stiffeners are welded to the skin plates as shown in **Fig. 6.1**. The stiffeners are jointed together only by the tack welding performed in the pre-assembly stage. The material of this structure is carbon steel.

In this experiment, MIG welding is used to assemble the structure, and the welding condition is shown in **Table 6.1**. The deformations are measured at 22 locations shown **Fig. 6.2**.

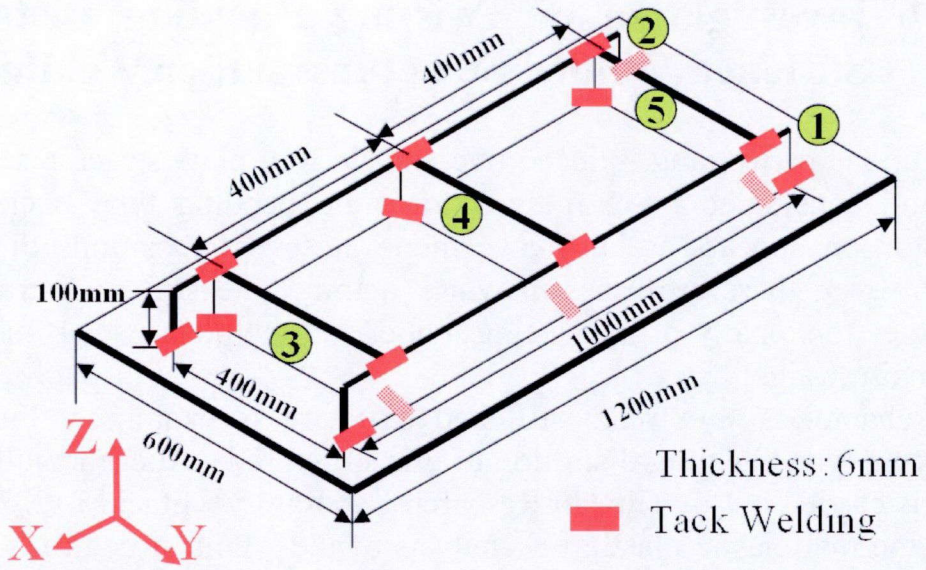

Fig. 6.1 Dimension and welding sequence of the considered thin plate stiffened structure.

Table 6.1 Welding condition of thin plate stiffened structure.

Current(A)	Voltage(V)	Velocity(mm/s)
170-180	24-26	4.3

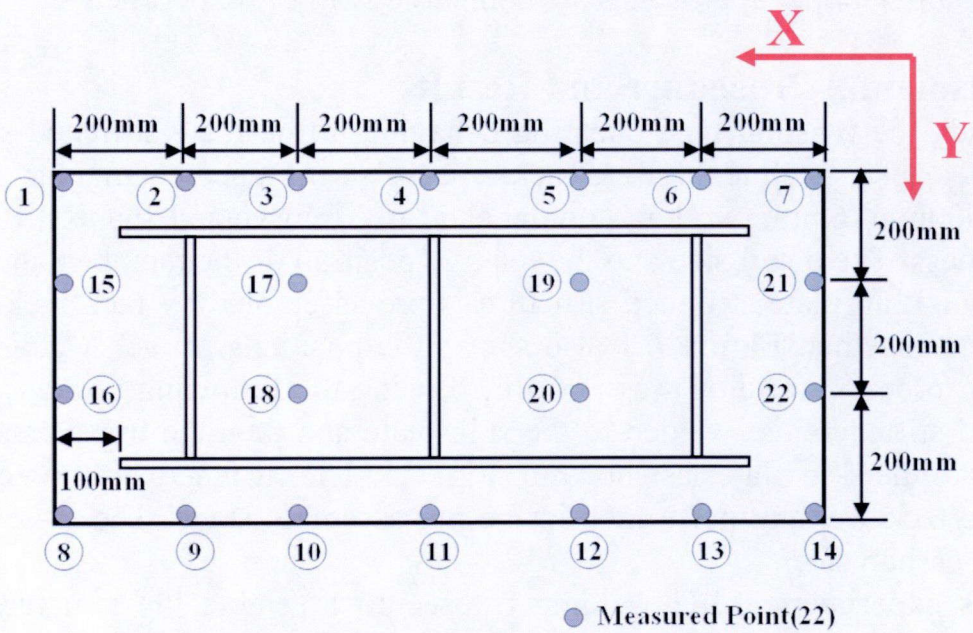

Fig. 6.2 Position of measuring points (top view).

Figure 6.3 shows that the maximum out-of-plane welding distortion measured after welding is 105mm. From the magnitude of the welding distortion and the deformed shape of the welded structure, twisting type buckling distortion is clearly observed in this specimen.

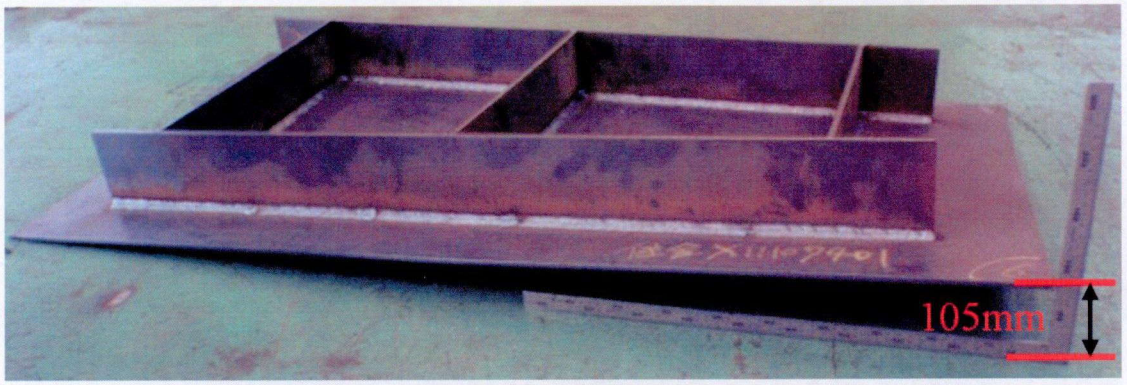

Fig. 6.3 Deformed shape of welded structure after welding.

When the plates that compose the welded structure are thin, buckling may occur under the compressive residual stress produced by the tendon force (longitudinal inherent shrinkage) acting along the welding line. The buckling modes can be separated into two types, one is local buckling of each panel surrounded by stiffeners and the other is overall buckling of the structure or part of it. In the case of the tested structure, buckling mode is the overall twisting mode. This happened because the buckling load in twisting mode is lower than the buckling load of the individual panels.

6.2 Prediction of Twisting Buckling using Thermal Elastic Plastic FE Analysis

A 3D thermal elastic plastic FE analysis is employed to investigate twisting buckling. In this analysis, temperature dependent material properties shown in **Fig. 2.2** are used.

Figure 6.4 shows the FE model of the whole structure. The model consists of 30250 nodes and 45072 elements. A close view of the weld joint is also shown. The adopted boundary conditions only prevent rigid body motion as shown in **Fig. 6.4**. Welding distortion is computed assuming the same welding condition and welding sequence as in the experiment. Computations considering small deformation and large deformation theories are carried out. The final distribution of out-of-plane welding distortion in the whole structure is presented in **Fig. 6.5** (small deformation theory) and **Fig. 6.6** (large deformation theory). Note that the deformation scale is different in these figures. When the small deformation theory is considered in which only the linear terms in the strain-displacement relationship is used, the out-of-plane welding distortion shown in **Fig. 6.5** becomes symmetric and its magnitude is very small compared with experimental result. When the large deformation theory is considered, overall out-of-plane welding distortion occurs in a twisting mode as shown in **Fig. 6.6** and the magnitude of the deflection 109.25 mm shows a good agreement with the 105mm measured in the experiment.

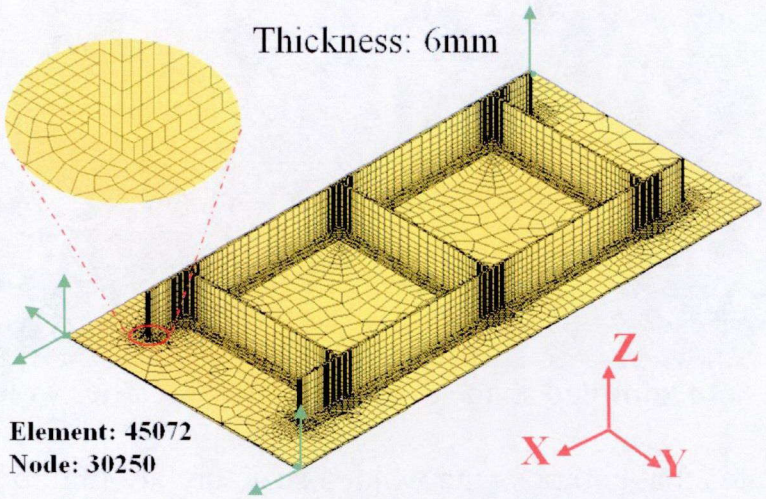

Fig. 6.4 Thermal elastic plastic FE model of the considered structure.

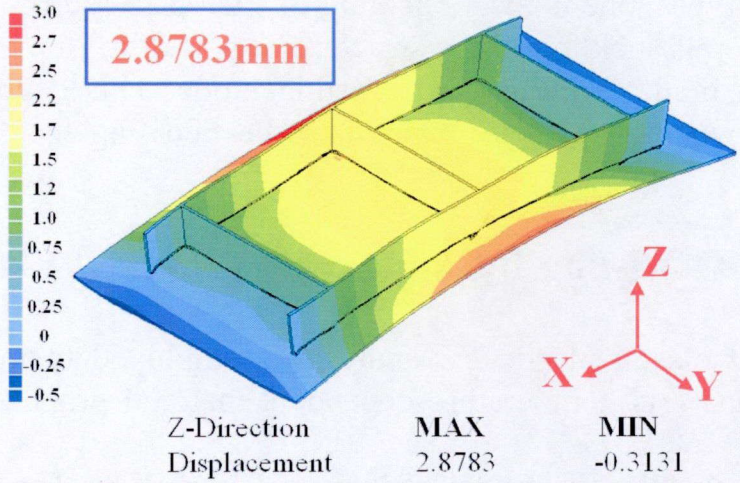

Fig. 6.5 Out-of-plane symmetric welding distortion (small deformation theory).

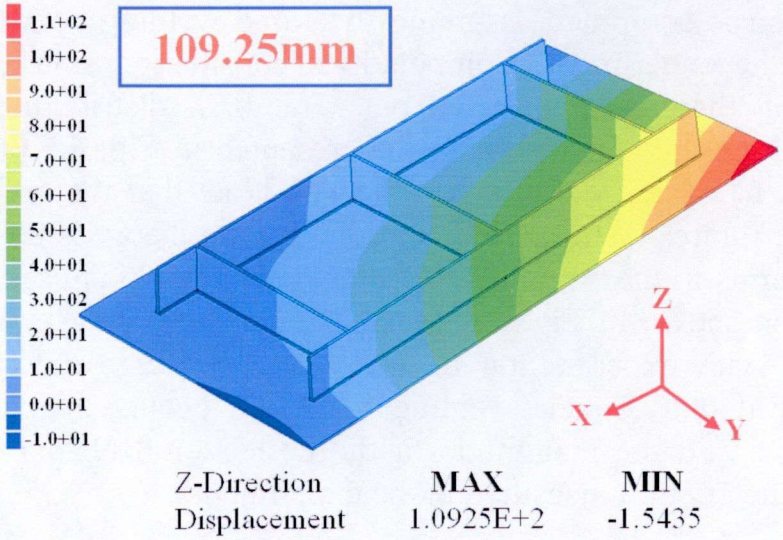

Fig. 6.6 Out-of-plane twisting buckling distortion (large deformation theory).

6.3 Investigation of Twisting Buckling Using Elastic Analysis Based on Inherent Deformation Theory

To carry out an elastic analysis of welding distortion, it is first necessary to evaluate the inherent deformation. There are two ways to evaluate the inherent deformation, one is based on experimental measurements and the other is based on a thermal elastic plastic FE analysis of small scale welded joints. The later is used for the evaluation of inherent deformation in this study. However, comparison of experimental and FE results are carried out to confirm the validity of the FE analysis.

6.3.1 Experiment of Small Scale Welded Joint

First, a small scale fillet welded joint similar to the joints in the structure under investigation is examined to confirm the validity of FE analysis. **Figure 6.7(a)** shows this fillet welded joint, which consist of a flange (300mm×200mm×6mm) and a web (300mm×100mm×6mm). The directions of the two welding lines are also shown. In order to obtain the angular distortion, out-of-plane welding distortion at the six points along one side of the flange as shown in **Fig. 6.7(a)** is measured. A cross section is shown in **Fig. 6.7(b)** showing the clamping applied along the other side of the flange.

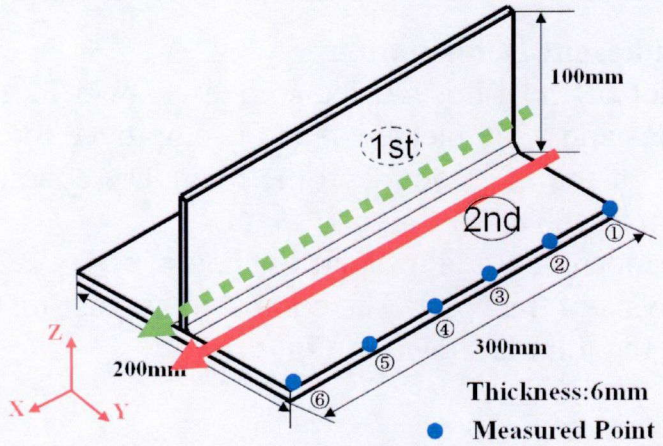

(a) Experimental Fillet welded joint

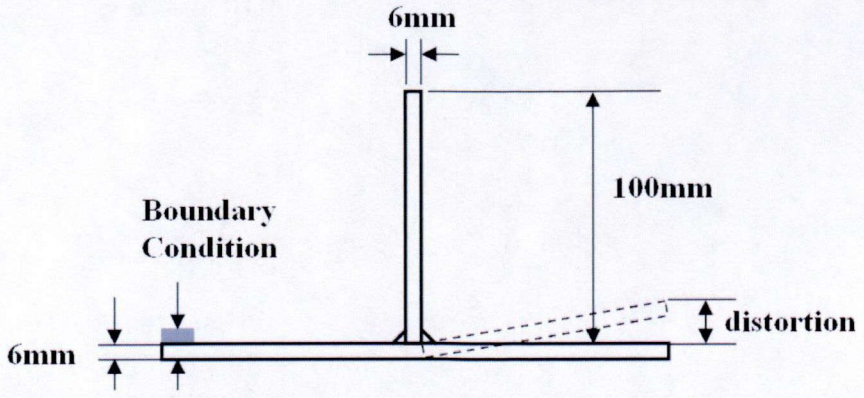

(b) Cross section of fillet welded joint

Fig. 6.7 Dimensions and boundary condition of the fillet welded joint used in the experiment.

Table 6.2 Measured value of angular distortion (out-of-plane welding distortion).

Measuring Position	No.1	No.2	No.3	No.4	No.5	No.6
Angular Distortion (mm)	2.59	2.79	2.93	3.23	3.18	3.12

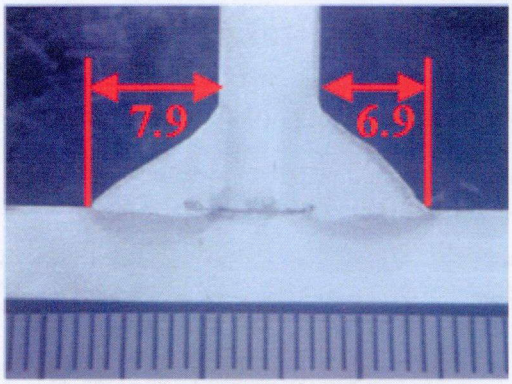

Fig. 6.8 Cross section in the weld zone of the fillet welded joint showing fillet size.

A middle cross section in the weld zone of this joint after welding is shown in **Fig. 6.8**. Angular distortion of the six measuring points is shown in **Table 6.2**.

6.3.2 Evaluation of Inherent Deformation

A solid FE model of the fillet welded joint is shown in **Fig. 6.9**. The model consists of 10478 nodes and 8220 elements, and is employed to evaluate the inherent deformation. The size of the FE model and the boundary condition are the same as those in the experiment as shown in **Fig. 6.7**.

Temperature dependent material properties shown in **Fig. 2.2** are used in thermal elastic plastic FE analysis of this joint. The computed angular distortion (out-of-plane welding distortion) of the joint is shown in **Fig. 6.10**.

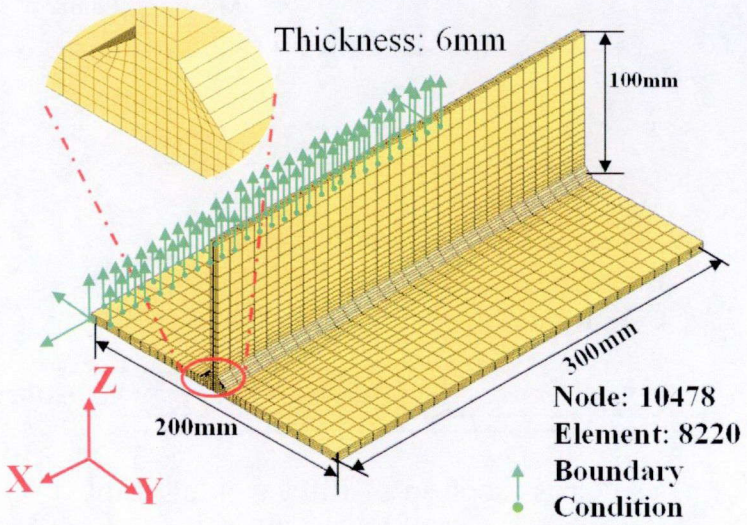

Fig. 6.9 FE model and boundary conditions of the considered fillet welded joint.

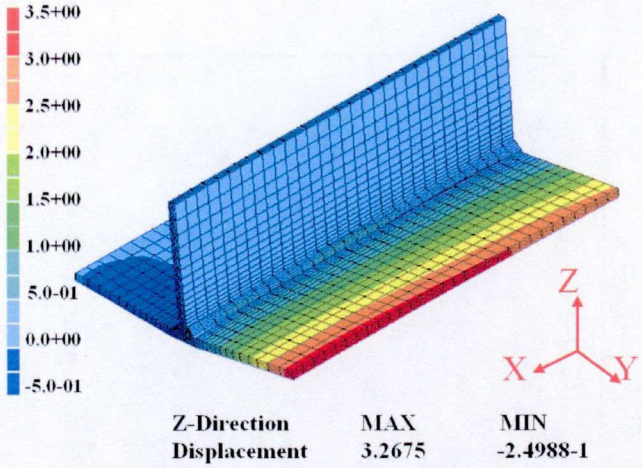

Fig. 6.10 Computed angular distortion (out-of-plane welding distortion of the joint).

As shown in **Fig. 6.11,** good agreement is observed between the computed and the measured angular distortion. From this thermal elastic plastic FE analysis, the distribution and magnitude of longitudinal and transverse plastic strain are obtained. **Figure 6.12 (a) and (b)** show the distribution of longitudinal and the transverse plastic strain on the middle cross section on the neutral plane of the plate after the 1st and the 2nd welding lines, respectively. The region in which the longitudinal plastic strain exists is wider than that of the transverse plastic strain. However, the magnitude of longitudinal plastic strain is much smaller than that of the transverse plastic strain. This difference of distribution and magnitude are mainly caused by the difference of constraint in the longitudinal and the transverse directions [81]. **Figure 6.12 (b)** clearly shows two separate transverse plastic strain zones and a larger longitudinal plastic strain zone formed by overlapping of the two longitudinal plastic strain zones.

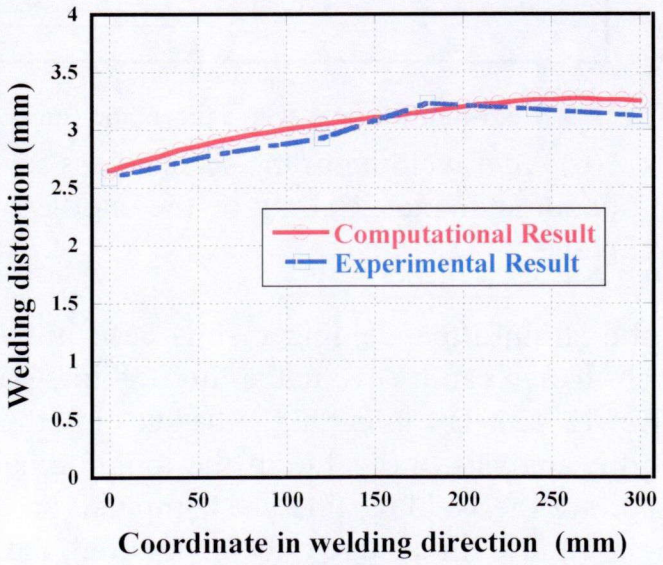

Fig. 6.11 Comparison between computed and measured results of angular distortion (out-of-plane welding distortion).

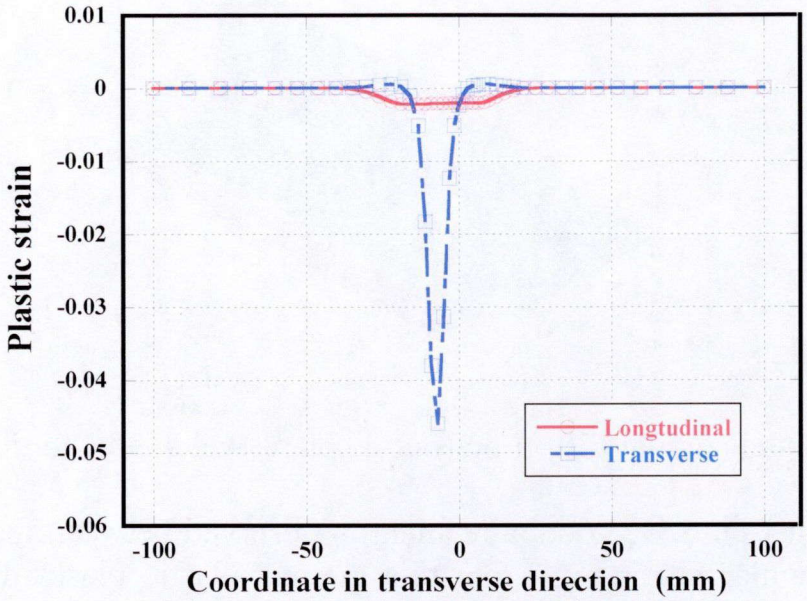

(a) After welding of the first pass

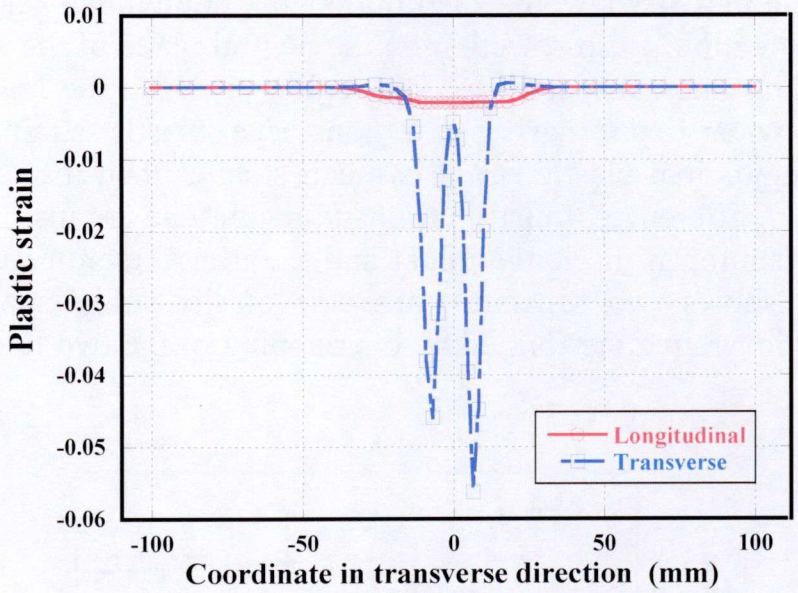

(b) After welding of the second pass

Fig. 6.12 Distribution of computed plastic strain on the middle cross section on the flange neutral plane.

Because the plastic strain after welding in this case is the inherent strain, the longitudinal inherent shrinkage can be evaluated through integration according to the definition given by **Eq. (2-13).** By integrating the plastic strain obtained from the thermal elastic plastic FE analysis, the value of the longitudinal inherent shrinkages on each cross section along the welding line are computed and plotted in **Fig. 6.13**. As may be seen from the figure, if the edge effect is ignored, the longitudinal inherent shrinkage has almost a uniform distribution along the welding line.

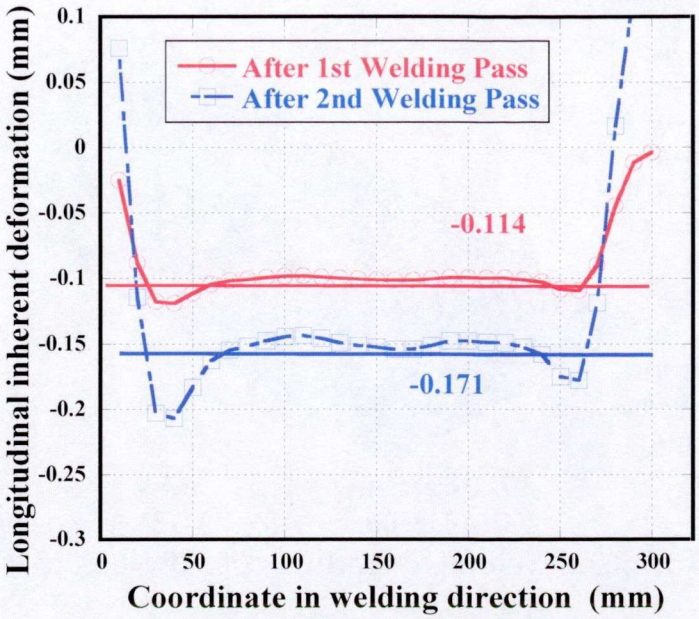

Fig. 6.13 Distributions of longitudinal inherent shrinkage along the welding line and the corresponding average value.

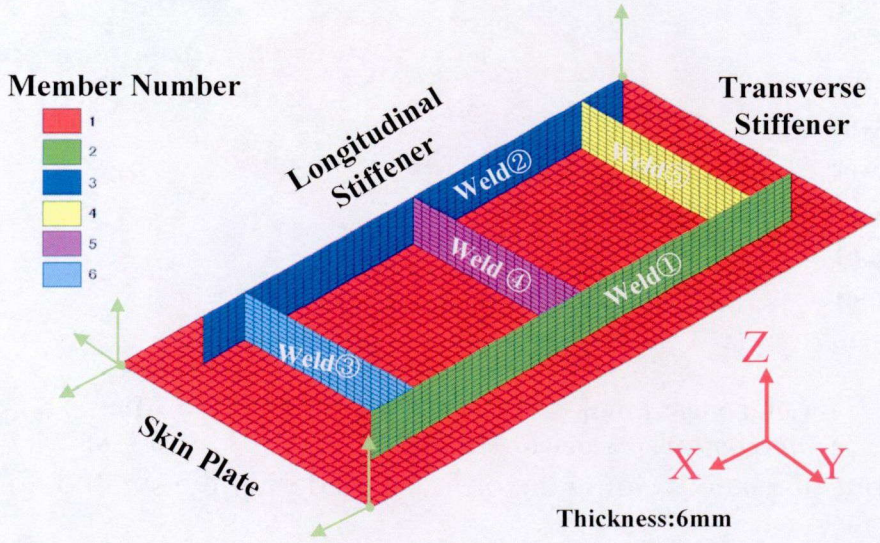

Fig. 6.14 Elastic FE model of thin plate stiffened structure.

Since the restraint in the transverse direction is small, the transverse inherent shrinkage and the transverse inherent bending can be evaluated by directly measuring the displacements. The values of inherent deformation evaluated from this small fillet welded joint are summarized in **Table 6.3**.

Table 6.3 Evaluated inherent deformation of fillet welded joint under welding.

Longitudinal Shrinkage	Transverse Shrinkage	Longitudinal Bending	Transverse Bending
-0.171(mm)	-0.535(mm)	0.00012(rad)	-0.030(rad)

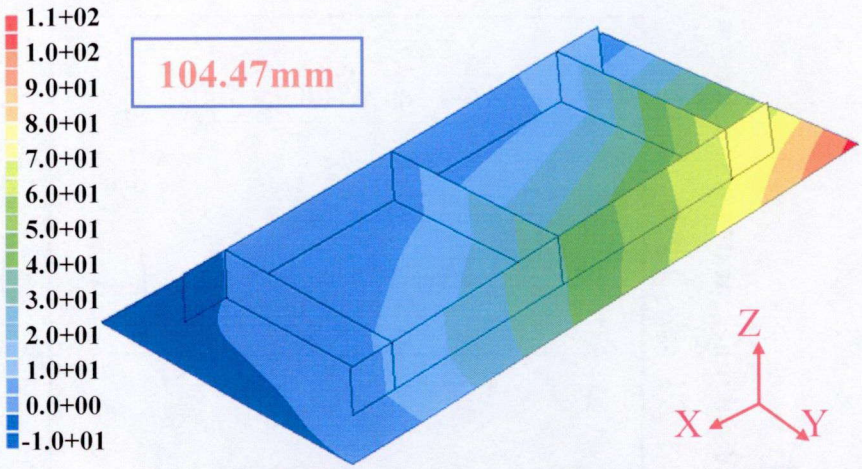

Z-Direction Displacement	MAX	MIN
	1.0413E+2	-6.3302

(a) Computed out-of-plane welding distortion considering the large deformation theory

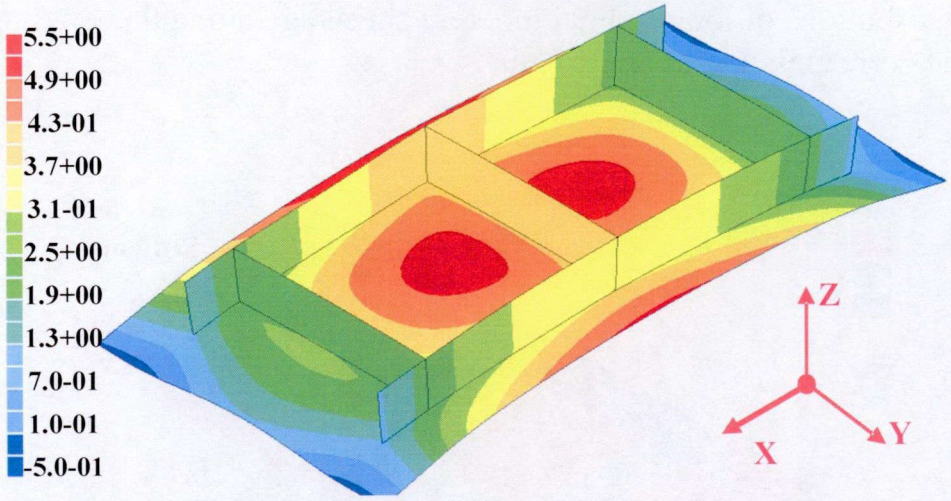

Component [mm] Z Direction Displacement	Max	Min
	5.4734	-0.1565

(b) Computed out-of-plane welding distortion considering the small deformation theory

Fig. 6.15 Out-of-plane welding distortion of the considered thin plate stiffened structure using elastic FE analysis based on the inherent deformation.

6.3.3 Prediction of Welding Distortion based on The Inherent Deformation Theory

Figure 6.14 shows the elastic FE model of the thin plate stiffened structure under investigation. Rigid body motion is prevented as shown in **Fig. 6.14.** Considering the large deformation theory and following the actual welding sequence, analysis is carried out using elastic FE method and applying the inherent deformation at welding lines. The computed out-of-plane welding distortion is presented in **Fig. 6.15(a)**. As may be seen from the figure, the twisting type buckling distortion occures, and the magnitude of out-of-plane welding distortion is in good agreement with both

the experiment shown in **Fig. 6.3** and results of thermal elastic plastic FE analysis shown in **Fig. 6.6**. As shown in **Fig. 6.15(b)**, when the small deformation theory is considered, a symmetric deformed shape with small magnitude of out-of-plane welding distortion is obtained. This confirms that, the large deformation theory is essential to consider welding induced buckling.

6.4 Eigenvalue Analysis of Thin Plate Stiffened Structure under Welding

Eigenvalue analysis using a shell element model can be employed to investigate the buckling behavior of the considered thin plate stiffened structure. Critical buckling condition and corresponding buckling mode can be computed. The elastic FE model and the boundary condition shown in **Fig. 6.14** are employed.

6.4.1 Only Considering Longitudinal Inherent Shrinkage

According to the common understanding, welding induced buckling is produced by the residual compressive stress acting in the panel. Such compressive stress is introduced by the welding shrinkage of the welding lines and the resulting tendon force (longitudinal inherent shrinkage). **Chapter 4** shows that the longitudinal inherent shrinkage is the dominant reason of welding induced buckling of thin plates. Therefore, only the longitudinal inherent shrinkage of the fillet weld joint is considered in this eigenvalue analysis. The eigenvalue analysis is carried out using the computed longitudinal inherent shrinkage (0.171mm). The resulting tendon force $F_{tendon}^{applied}$ serves as a reference to convert the eigenvalue to the critical tendon force $F_{tendon}^{critical}$. **Figure 6.16** shows the first 4 buckling modes of the welded structure under investigation and the corresponding eigenvalues. The magnitude of the critical tendon force can be calculated as follows:

$$F_{tendon}^{critical} = (Eigenvalue) \times F_{tendon}^{applied} \tag{6-1}$$

Where the tendon force $F_{tendon}^{applied}$ produced by the applied welding longitudinal inherent shrinkage can be calculated as follows:

$$F_{tendon}^{applied} = Eh\delta_L^* = 210000MPa \times 6mm \times (-0.171mm) = -215.46KN \tag{6-2}$$

Table 6.4 summarizes the results of eigenvalue analysis, which shows the eigenvalue and the required tendon force of each buckling mode.

Table 6.4 Computed results of eigenvalue and critical buckling force.

	Eigenvalue	Critical Tendon Force
1st mode	1.5923	343.08KN
2nd mode	1.9419	418.40KN
3rd mode	2.8398	611.86KN
4th mode	3.3404	719.72KN

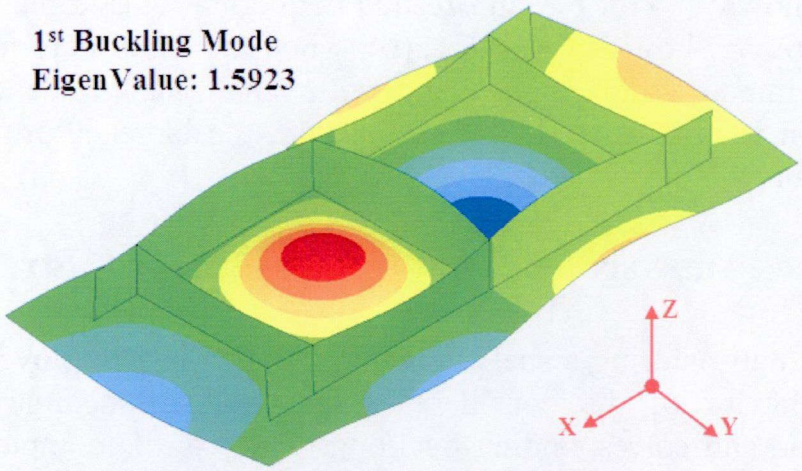

(a) 1st buckling mode and corresponding eigenvalue

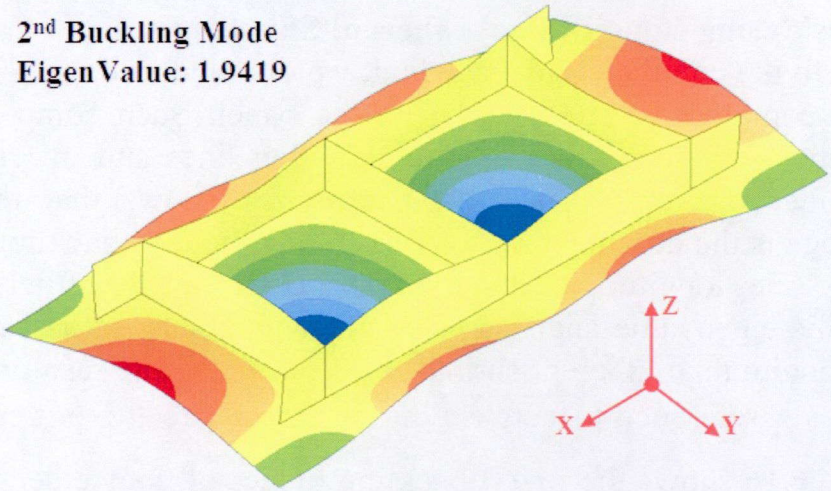

(b) 2nd buckling mode and corresponding eigenvalue

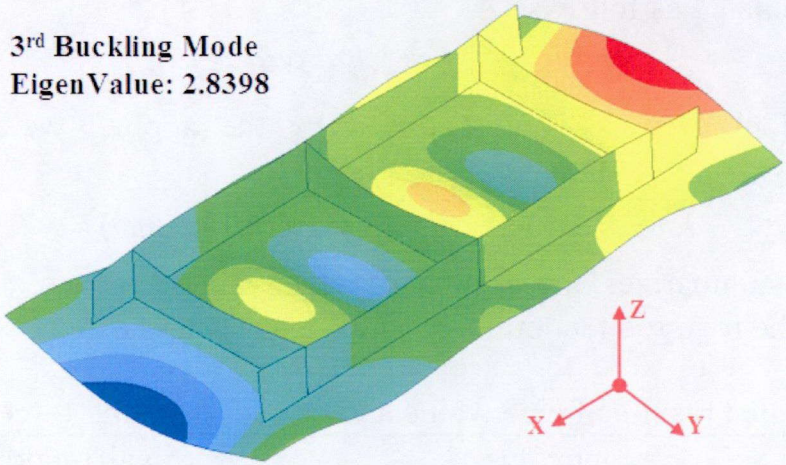

(c) 3rd buckling mode and corresponding eigenvalue

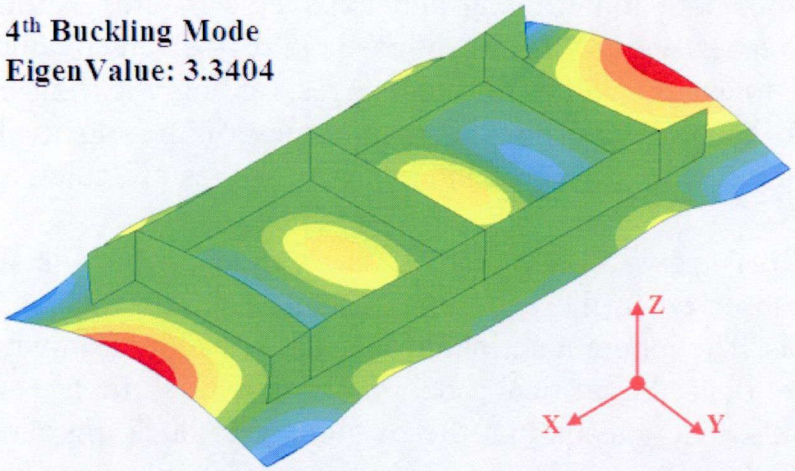

(d) 4th buckling mode and corresponding eigenvalue

Fig. 6.16 Buckling modes and corresponding eigenvalues predicted by eigenvalue analysis.

Comparing the magnitude of the applied tendon force $F_{tendon}^{applied}$ caused by welding with the force required for buckling as given in **Table 6.4**, it is readily seen that the magnitude of the tendon force $F_{tendon}^{applied}$ is not large enough to produce buckling, and the twisting mode is not found among the lowest four modes shown in **Fig. 6.16.** These differences between the experiment and the eigenvalue analysis come from the fact that only the longitudinal inherent shrinkage is considered and other components are ignored. As shown in **Chapter 5** for buckling distortion of a rectangular plate, all components of the inherent deformation are necessary to correctly reproduce the welding distortion. The influence of other components of inherent deformation, especially the transverse inherent shrinkage, is examined in the following Section.

6.4.2 Twisting Buckling of the Considered Stiffened Structure by Eigenvalue Analysis

As discussed in the above Section, the results of eigenvalue analysis shown in **Fig. 6.16** tell that twisting type buckling distortion can not be produced when only the tendon force (longitudinal inherent shrinkage) is considered.

Table 6.5 Computed eigenvalues and critical buckling inherent deformations.

	Eigenvalue	Critical Buckling Inherent Deformation (Longitudinal /Transverse)
1st mode	0.6312	-0.1079mm/-0.3377mm
2nd mode	1.1020	-0.1884mm/-0.5896mm
3rd mode	1.1096	-0.1897mm/-0.5936mm
4th mode	1.4666	-0.2508mm/-0.7846mm

In this section, both longitudinal and transverse inherent shrinkage (0.171mm and 0.535mm, respectively) are introduced into the eigenvalue analysis. The computed lowest four eigenvalues and the corresponding buckling modes are shown in **Table 6.5** and **Fig. 6.17.** From the magnitudes of the eigenvalues, the critical buckling longitudinal and transverse inherent shrinkages are calculated and given in **Table 6.5**.

Figure 6.17(a) shows the lowest buckling mode, which is the twisting type buckling mode, observed in the experiment, thermal elastic plastic FE analysis and elastic FE analysis. The inherent shrinkage caused by welding shown in **Table 6.3** has larger magnitude than the critical buckling inherent shrinkage obtained by the eigenvalue analysis. This means that the twisting type buckling can be produced by the combination of the longitudinal and the transverse inherent shrinkage. Inherent bending is considered to be a disturbance to trigger buckling, but does not influence the buckling mode.

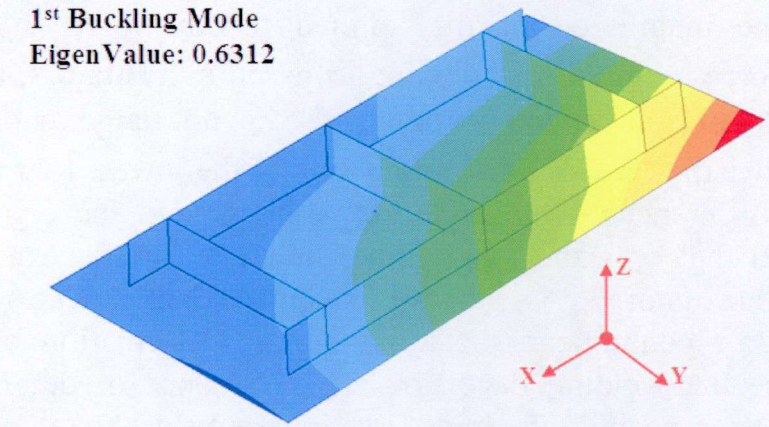

(a) 1st buckling mode and corresponding eigenvalue

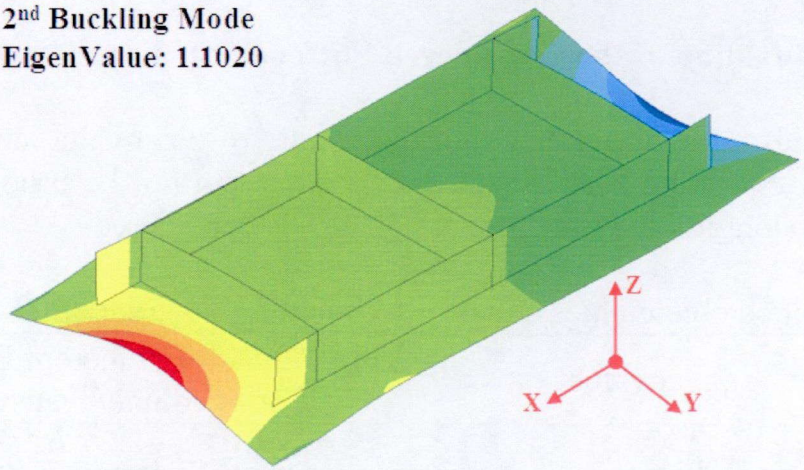

(b) 2nd buckling mode and corresponding eigenvalue

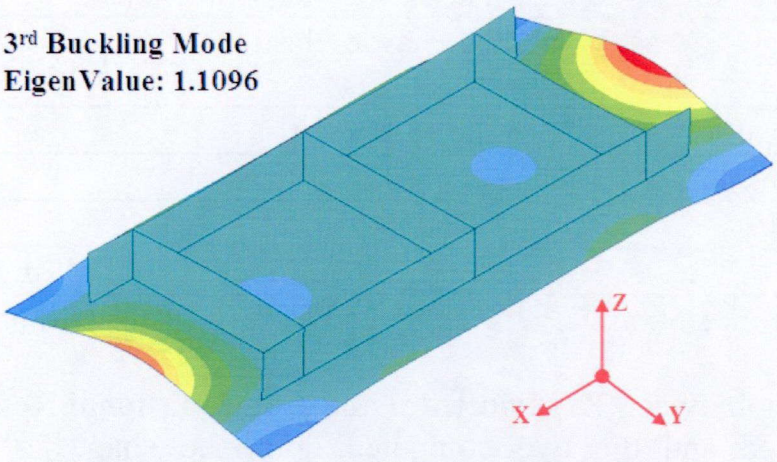

(c) 3rd buckling mode and corresponding eigenvalue

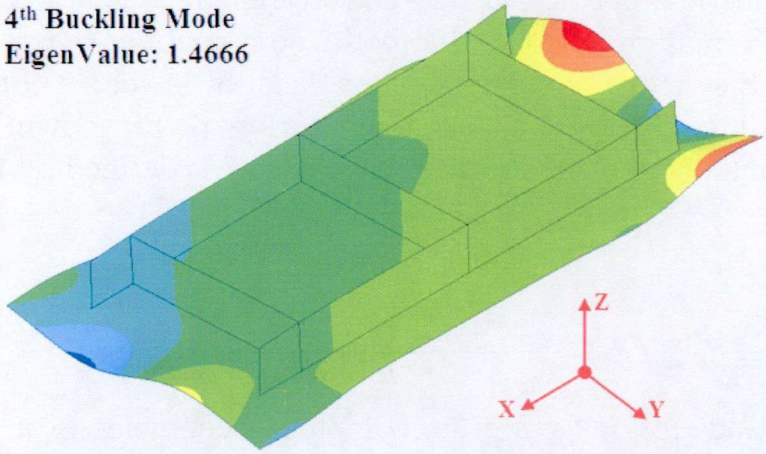

(d) 4th buckling mode and corresponding eigenvalue

Fig. 6.17 Buckling modes and corresponding eigenvalues predicted by eigenvalue analysis considering the inherent longitudinal and transverse shrinkage.

6.5 Results and Discussion

6.5.1 Comparison between Computational Approaches

Two different computational approaches are employed, i.e. thermal elastic plastic FE analysis and elastic FE analysis based on the inherent deformation theory. Although both computed results have good agreement with experimental measurements, the required computer effort (memory and storage requirements and CPU time) for the two computational approaches area significantly different. The comparison between these two computational approaches is presented in **Table 6.6**.

The computational time required for elastic FE analysis is roughly 1/1000 that required for the thermal elastic plastic FE analysis. When the inherent deformation is evaluated by experiment or thermal elastic plastic FE analysis of small scale welded joint, the elastic FE analysis applying the evaluated inherent deformation is an ideal computational approach for large-scale and complex welded structure to predict the welding distortion.

Table 6.6 Comparison between thermal elastic plastic and elastic FE analyses.

	Thermal Elastic Plastic Analysis	Elastic FE Analysis
Element Type	Solid (8-nodes)	Shell (4-nodes)
Node No	45072	3481
Element No	30250	3400
CPU Time *	97 (hour) 19 (min) 29 (sec)	4 (min) 22 (sec)

*Using a Linux work station (CPU: Xeon Quad Core 3.33GHZ; Memory: 8G×12)

6.5.2 Comparison between Experimental and Computational Results

The measured and the two computed deformed shapes of the considered structure after welding are presented in **Fig. 6.3**, **6.6** and **6.15(a).** Computations are performed using thermal elastic plastic FE analysis and elastic FE analysis applying the inherent deformation theory. In both computations large deformation is considered, and the actual welding sequence is followed. **Table 6.7** shows the out-of-plane welding distortion at each measuring point shown in **Fig. 6.2**. The accuracy of computational results shown in **Table 6.7** is defined by **Eq. (6-3)**.

$$P_{TEP}(P_n) = 1 - \frac{|M(P_n) - TEP(P_n)|}{M_{\max}(P)}\% \qquad (6\text{-}3)$$

$$P_{Elastic}(P_n) = 1 - \frac{|M(P_n) - Elastic(P_n)|}{M_{\max}(P)}\%$$

Where, $P_{TEP}(P_n)$ and $P_{Elastic}(P_n)$ are the computed accuracies of nth point in thermal elastic plastic and elastic FE analyses, respectively. $M(P_n)$, $TEP(P_n)$ and $Elastic(P_n)$ are the out-of-plane welding distortion of nth point by measurement, thermal elastic plastic and elastic FE analyses, respectively. $M_{\max}(P)$ is the maximum magnitude of out-of-plane welding distortion among all measuring points.

Table 6.7 Magnitude of out-of-plane welding distortion at measuring points.

Measured Point**	Experiment Result (mm)	Computational Result			
		Thermal Elastic Plastic Analysis (mm) /accuracy (%)		Elastic FE Analysis (mm) /accuracy (%)	
1	0.000238	0.005156	100.00%	0	100.00%
2	5.985198	3.68015	97.81%	-4.23442	90.27%
3	8.870159	3.89563	95.26%	-5.53895	86.28%
4	1.285119	3.4375	97.95%	-6.33026	92.75%
5	0.250079	2.47388	97.88%	-5.98012	94.07%
6	-1.96496	0.722314	97.44%	-5.38999	96.74%
7	-0.7	0.084707	99.25%	0	99.33%
8	0.46	0.016877	99.58%	0	99.56%

9	18.68496	17.838	99.19%	12.5126	94.12%
10	37.05992	36.7426	99.70%	29.3779	92.69%
11	53.13488	56.9384	96.38%	46.3891	93.58%
12	72.75984	76.7287	96.22%	64.4954	92.13%
13	90.2248	93.3998	96.98%	83.1816	93.29%
14	105.0298	109.257	95.98%	104.135	99.15%
15	-2.30987	0.98438	96.86%	-2.43012	99.89%
16	-5.52994	-1.1543	95.83%	-2.58807	97.20%
17	10.52006	13.8787	96.80%	5.76376	95.47%
18	27.78	23.5234	95.95%	17.4027	90.12%
19	9.3	26.1549	83.95%	17.2107	92.47%
20	65.72994	51.5927	86.54%	40.6899	76.16%
21	27.96994	35.9113	92.44%	31.3653	96.77%
22	69.44987	73.0721	96.55%	66.9936	97.66%

** The location of each measured point can be seen in **Fig. 6.2**

6.5.2.1 Comparison of Out-of-plane Welding Distortion with 3D Column Graph

According to the coordinates of measuring points shown in **Fig. 6.2**, the 3D column graphs shown in **Fig. 6.18**, **Fig. 6.19** and **Fig. 6.20** show the magnitude of out-of-plane welding distortion at each measuring point for the experimental results, results of thermal elastic plastic FE analysis and those of elastic FE analysis applying the inherent deformation, respectively.

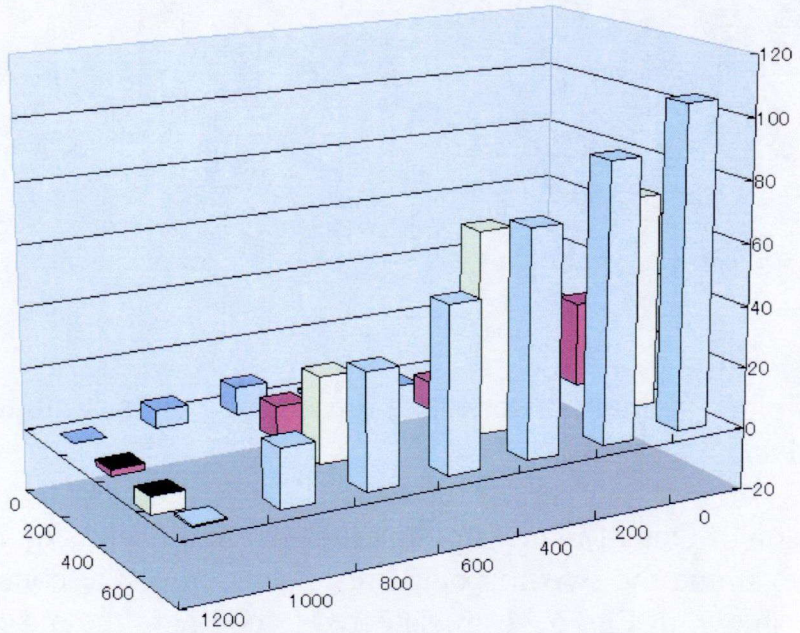

Fig. 6.18 Measured out-of-plane welding distortion at measuring points.

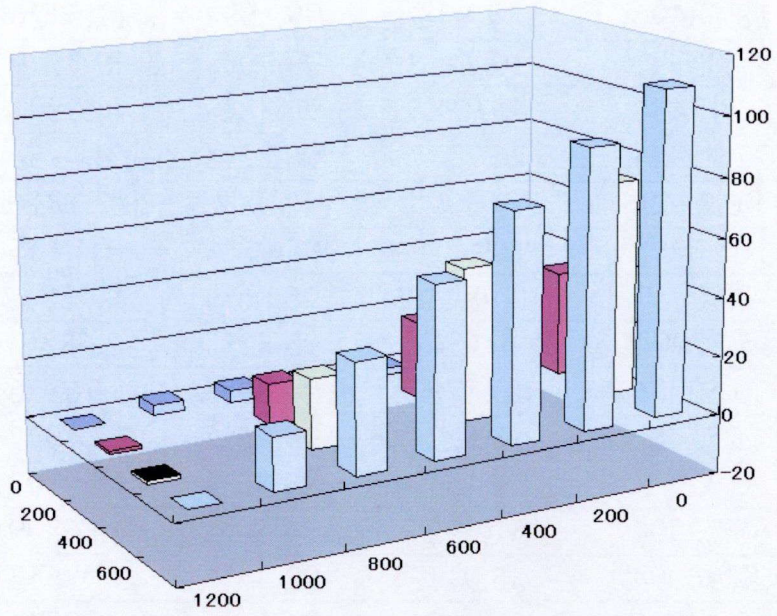

Fig. 6.19 Out-of-plane welding distortion at measuring points computed using thermal elastic plastic FE analysis.

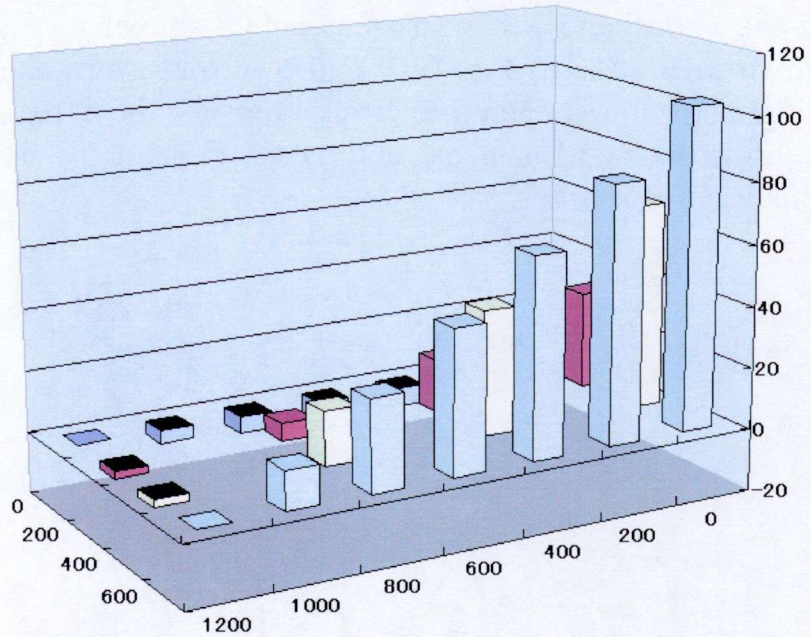

Fig. 6.20 Out-of-plane welding distortion at measuring points computed using elastic FE analysis.

6.5.2.2 Comparison of Out-of-plane Welding Distortion of Points on Edges

To closely examine the twisting buckling distortion of the considered structure, line 1 and line 2 shown in **Fig. 6.21** are selected to compare the out-of-plane welding distortion obtained by measurement, thermal elastic plastic FE analysis and elastic FE analysis. **Figure 6.22(a)** shows the out-of-plane welding distortion along line 1 obtained by the three different methods. Out-of-plane welding distortion along line 2

is shown in **Fig. 6.22(b)**. As shown in **Fig. 6.22**, good agreement is observed among out-of-plane welding distortions obtained by experiment and two types of FE analyses.

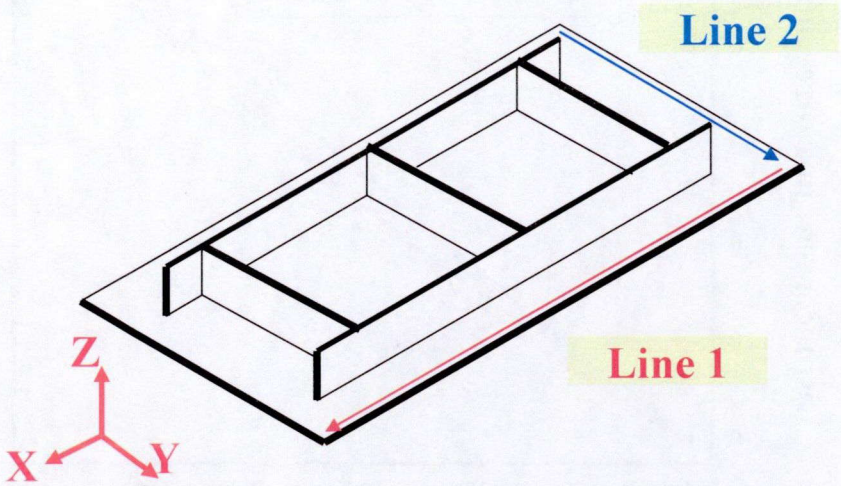

Fig. 6.21 Lines to compare out-of-plane welding distortion.

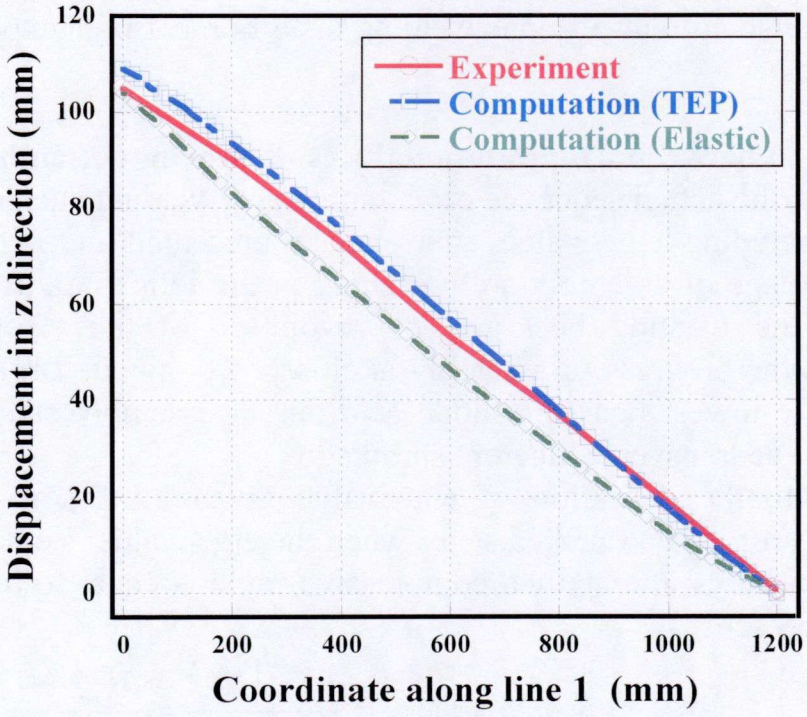

(a) Out-of-plane welding distortion along line 1

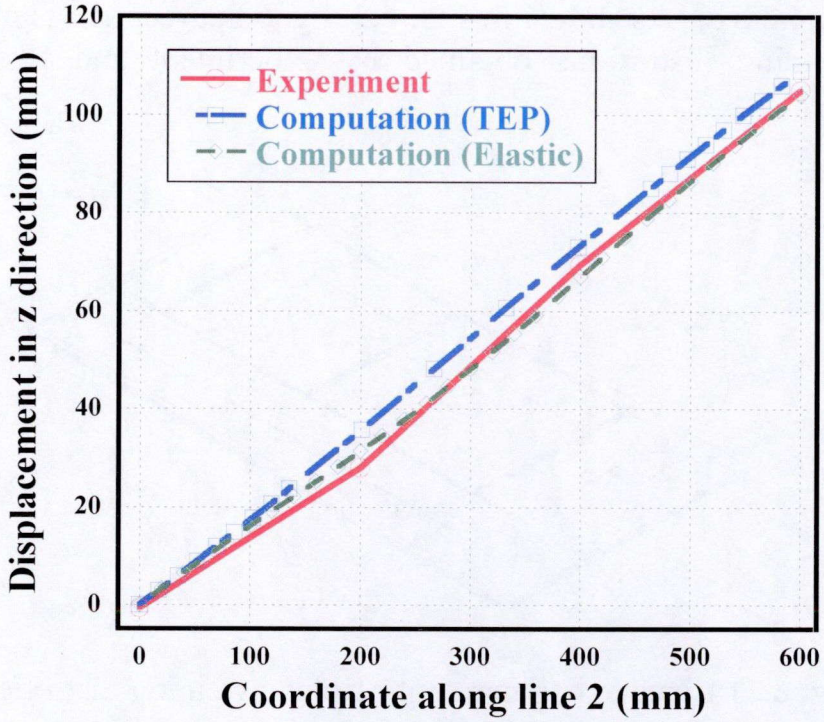

(b) Out-of-plane welding distortion along line 2

Fig. 6.22 Comparison of out-of-plane welding distortion between experiment and FE analyses.

6.5.3 Comparison between Computational Results during Assembly Process

Considering the actual sequence of assembly and welding shown in **Fig. 6.1**, all computations including eigenvalue analysis are presented in preceding sections. Results at each stage of assembly are presented in the following. To understand the mechanism of the twisting buckling, the evolution of the eigenvalue and the eigenmode with the progress of assembly is closely examined. **Table 6.8** shows the eigenvalue of the lowest buckling mode at different assembly stages applying the longitudinal and the transverse inherent shrinkage.

According to the definition of eigenvalue given by **Eq. (5-2),** the welded structure buckles (or is in a buckled state) when the eigenvalue is equal to (or smaller than) 1. In other words, the applied compressive force is equal to or larger than the critical buckling force.

$$eigenvalue(N^{th}) = \frac{\delta^*_{critical}(N^{th})}{\delta^*_{applied}} = \frac{F^{critical}_{tendon}(N^{th})}{F^{applied}_{tendon}} \qquad (5\text{-}2)$$

Table 6.8 Computed eigenvalues for lowest buckling mode at different assembly stages.

After Stage	①	①②	①②③	①②③④	①②③④⑤
Eigenvalue	2.5251	2.1932	1.1273	0.8800	0.6312

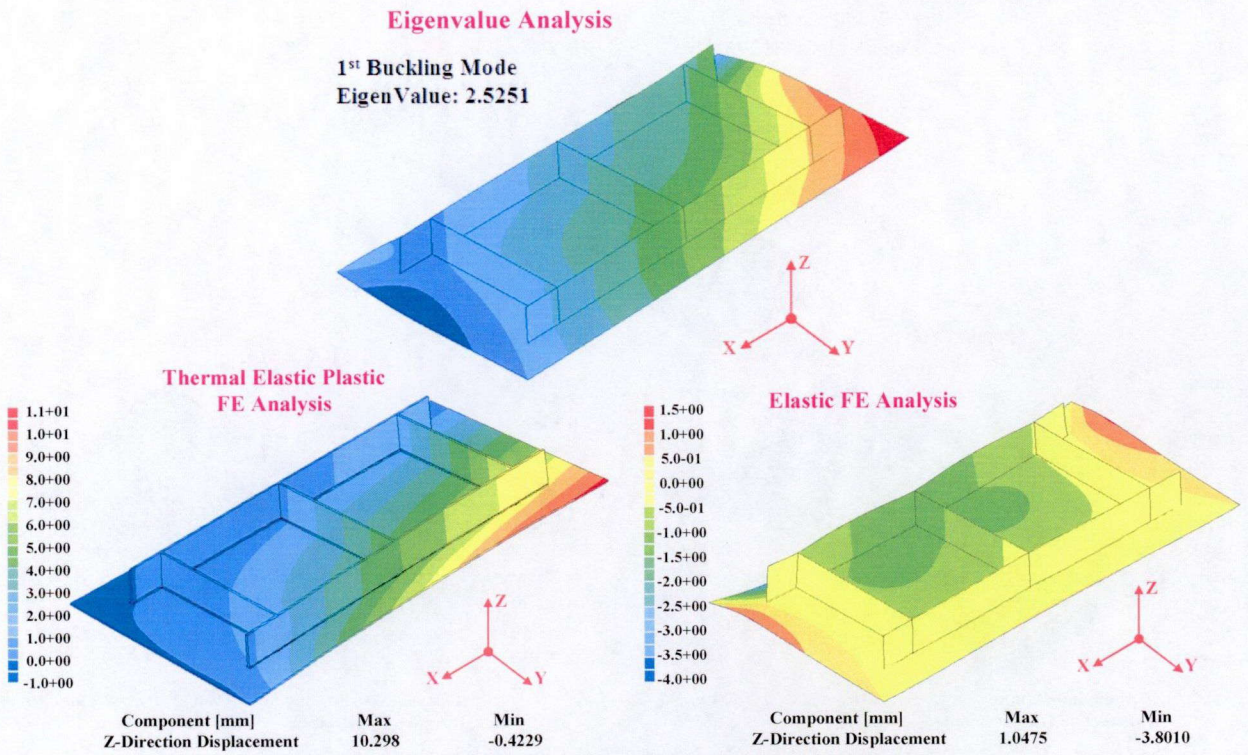

(a) After the 1st step of assembly process

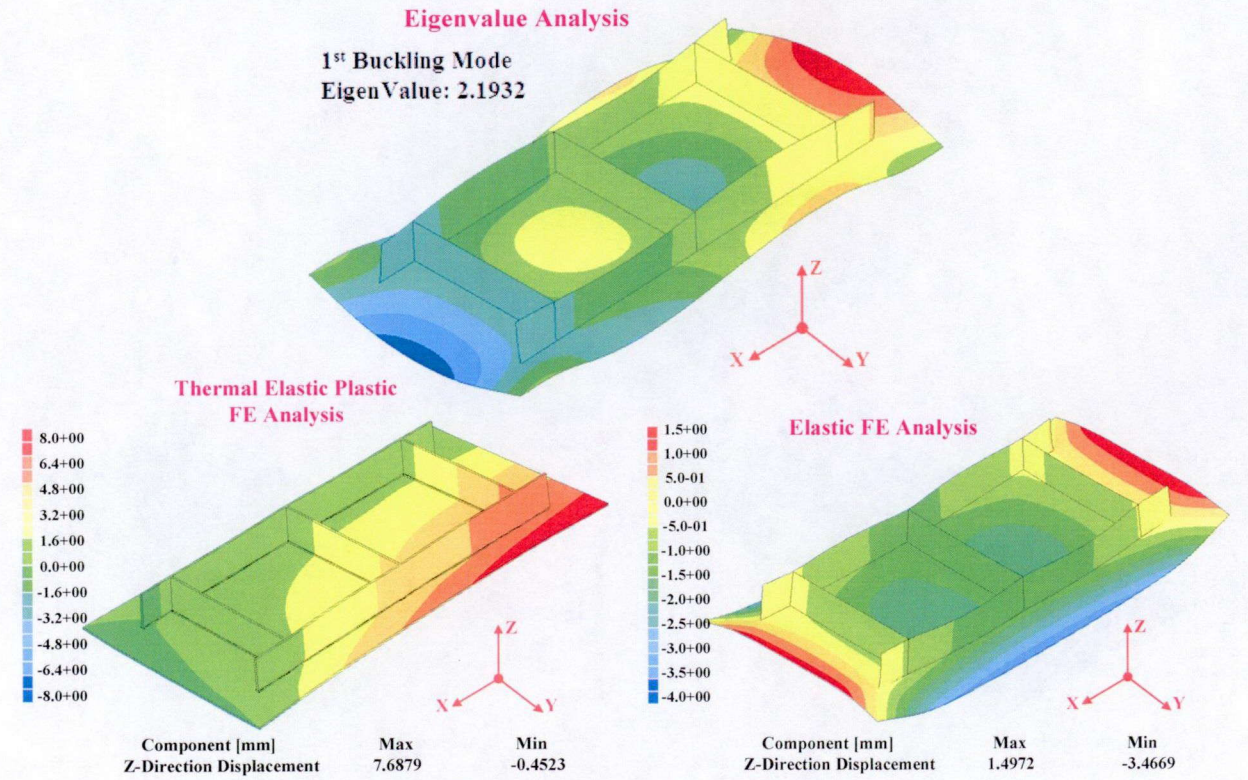

(b) After the 2nd step of assembly process

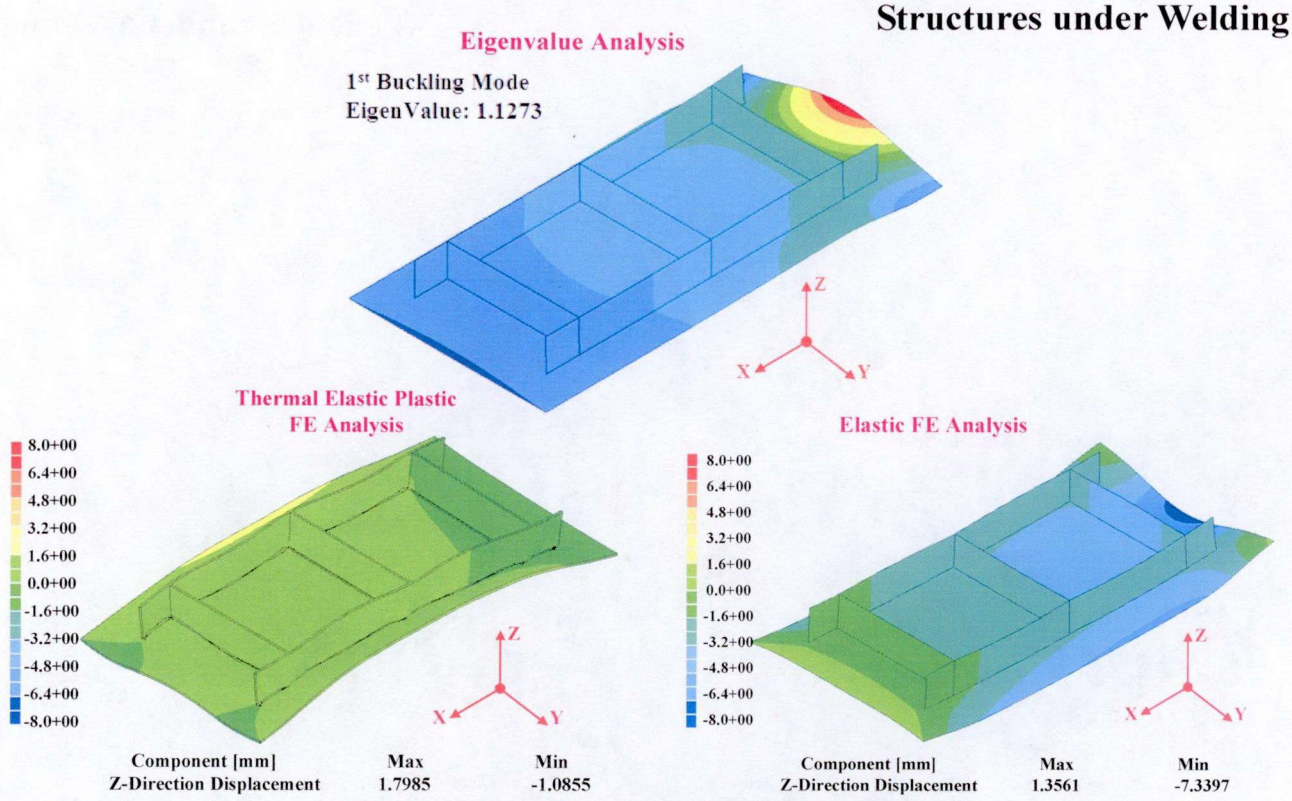

(c) After the 3rd step of assembly process

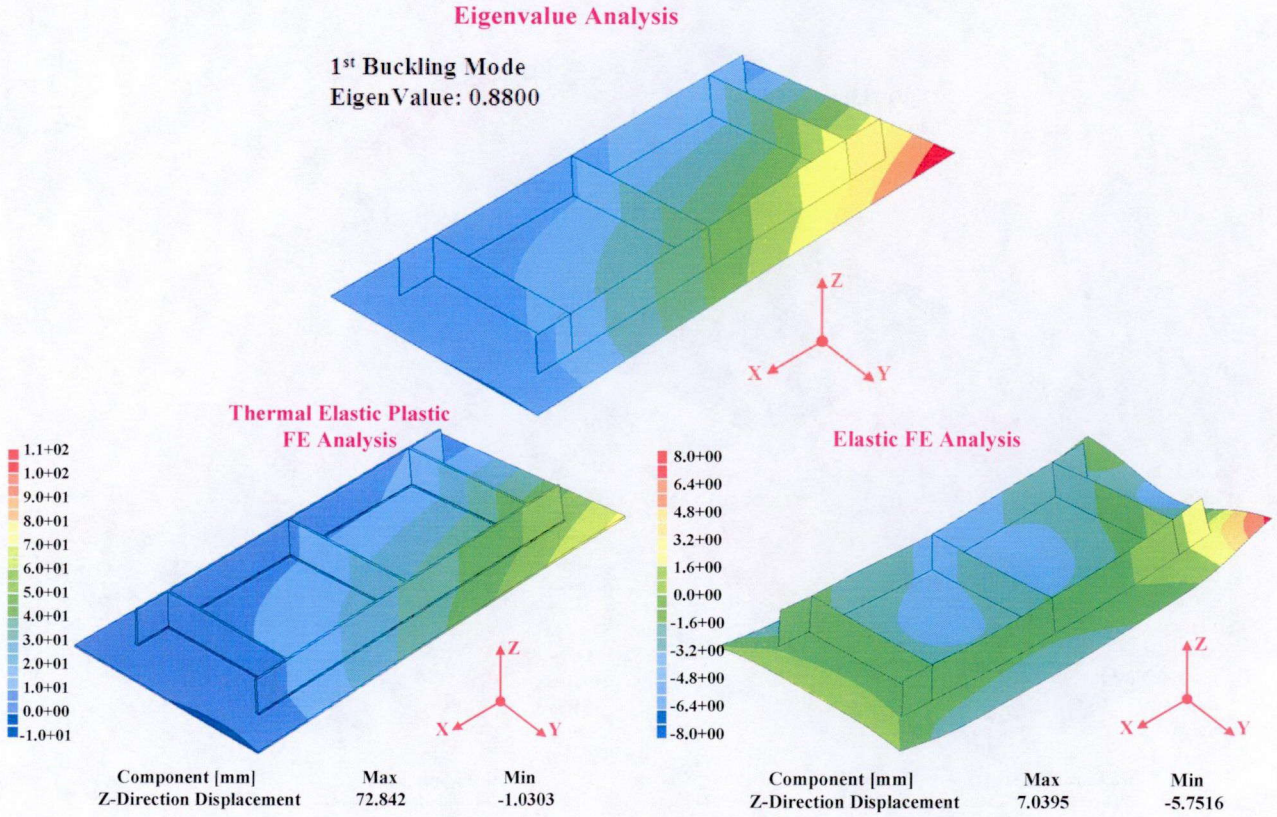

(d) After the 4th step of assembly process

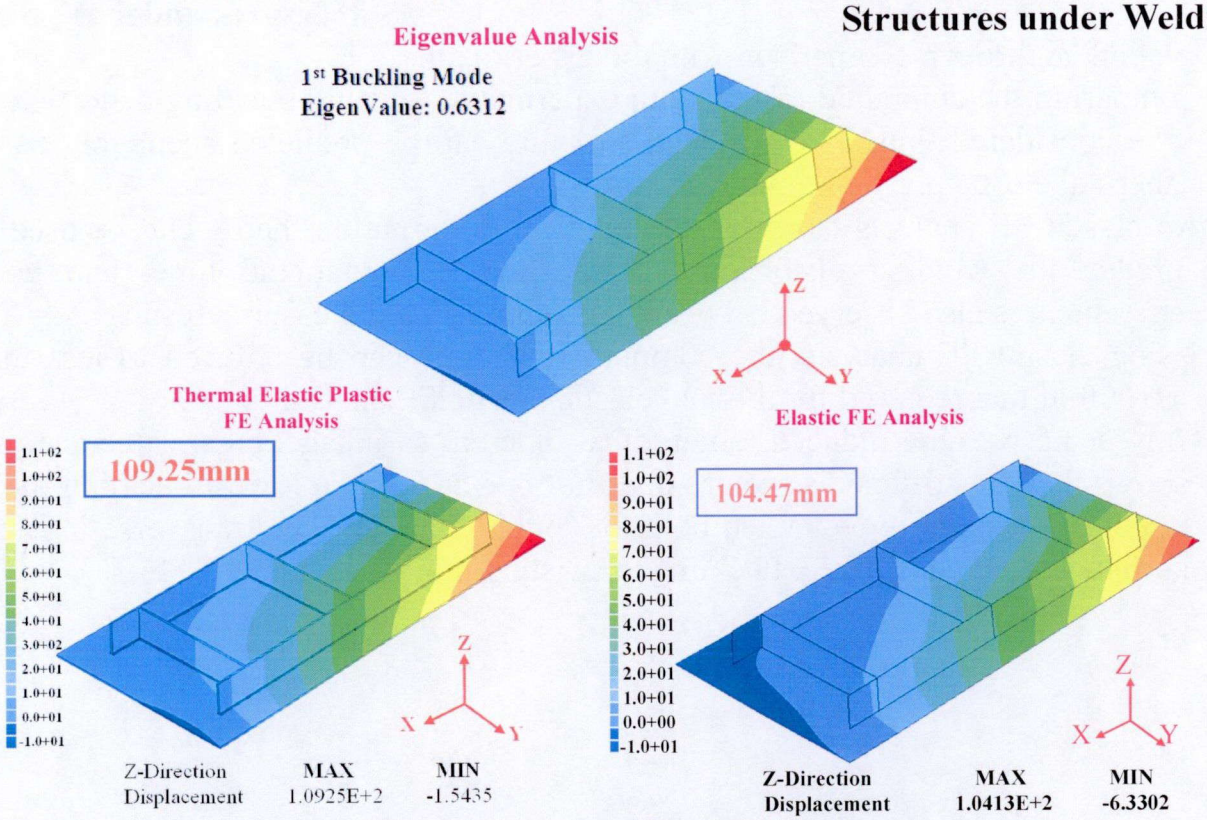

(e) After the 5th step of assembly process

Fig. 6.23 Comparison of buckling behavior among computed results by three different computational approaches.

The buckling distortions computed by 3D thermal elastic plastic FE analysis and elastic FE analysis are compared with the buckling mode predicted by eigenvalue analysis in **Fig. 6.23**. **Figure 6.23(e)** shows the lowest buckling mode and corresponding eigenvalue after the whole assembly process. As may be seen from these results, twisting buckling mode appears at the 4th stage and the corresponding eigenvalue is less than one. In this stage, the middle transverse stiffener is welded. In the 5th stage, the predicted buckling mode is also the twisting mode and the eigenvalue becomes smaller. This suggests that the twisting buckling mode is produced by the transverse inherent shrinkage associated with welding transverse stiffeners.

6.6 Conclusions

In this chapter, twisting type buckling distortion of a thin plate stiffened structure after welding is investigated through an experiment and computations. For computations, large deformation thermal elastic plastic FE analysis, large deformation elastic FE analysis based on the inherent deformation theory and Eigen value analysis are employed.

From the above investigations, the following conclusions can be drawn:

(1) The inherent deformation is evaluated according to its definition using the computed plastic strain obtained by thermal elastic plastic FE analysis and it is

validated through comparison with the experiment.

(2) Comparing the computed results with experiment, twisting buckling distortion of the considered thin plate stiffened structure can be predicted accurately using thermal elastic plastic FE analysis.

(3) An elastic FE analysis based on the inherent deformation theory can be used to predict the welding distortion with a short computational time, and good agreement is also observed between the computed and measured results.

(4) Using elastic FE analysis, the computational time can be reduced to less than 1/1000 of that required for thermal elastic plastic FE analysis.

(5) Only using welding induced longitudinal inherent shrinkage, eigenvalue analysis shows that the stiffened structure does not buckle and the lowest buckling mode is not the twisting type. When both the longitudinal and the transverse inherent shrinkages are considered, buckling in twisting mode occurs.

Chapter 7 Prediction and Straightening of Buckling Distortion for Ship Panel Structure

In the preceding chapters, the effectiveness of the elastic analysis using the inherent deformation to predict welding induced buckling distortion is demonstrated for a rectangular plate and a small size thin plate stiffened welded structure. As a practical application of prediction of buckling distortion using the inherent deformation theory, a stiffened panel structure of a pure car carrier ship is selected as a structure to be studied in this chapter.

To use elastic analysis, the inherent deformations of welded joints contained in the structure are evaluated beforehand using thermal elastic plastic FE analysis applying the welding conditions corresponding to actual practice. To understand welding distortion during actual welding assembly process, elastic FE analysis considering large deformation, welding sequence and gravity are carried out. Due to the complexity of the phenomena associated with the contact problem under gravity, ideal boundary condition is employed to extract the essential feature of welding induced buckling. Further, eigenvalue analysis is carried out to correlate welding distortion predicted by large deformation elastic FE analysis and eigen buckling modes. After clarifying the mechanism which produces the buckling distortion, strategy for straightening welding distortion is discussed.

7.1 Description of Ship Panel Structure and Assembly Process

Typical examples of ship panel structures are shown in **Fig. 7.1**. Details of the car deck panel structure considered in this chapter are shown in **Fig. 7.2**, upside down. The panel is 13.12m×13.12m. **Figure 7.2** shows that the structure is divided into 4 plates, each is stiffened by 3 longitudinal stiffeners. An I section stiffener is fitted between each two adjacent unit panels for ease of assembly. Four transverse stiffeners and one transverse edge angle section are welded across the four unit panels. The number of members fitted in this car deck panel structure is listed in **Table 7.1**.

Table 7.1 Parts information of ship panel structure.

	Plate	Longitudinal Stiffener	I Section Stiffener	Transverse Stiffener	Edge Angle Section
Number of Parts	4	12	3	4	1

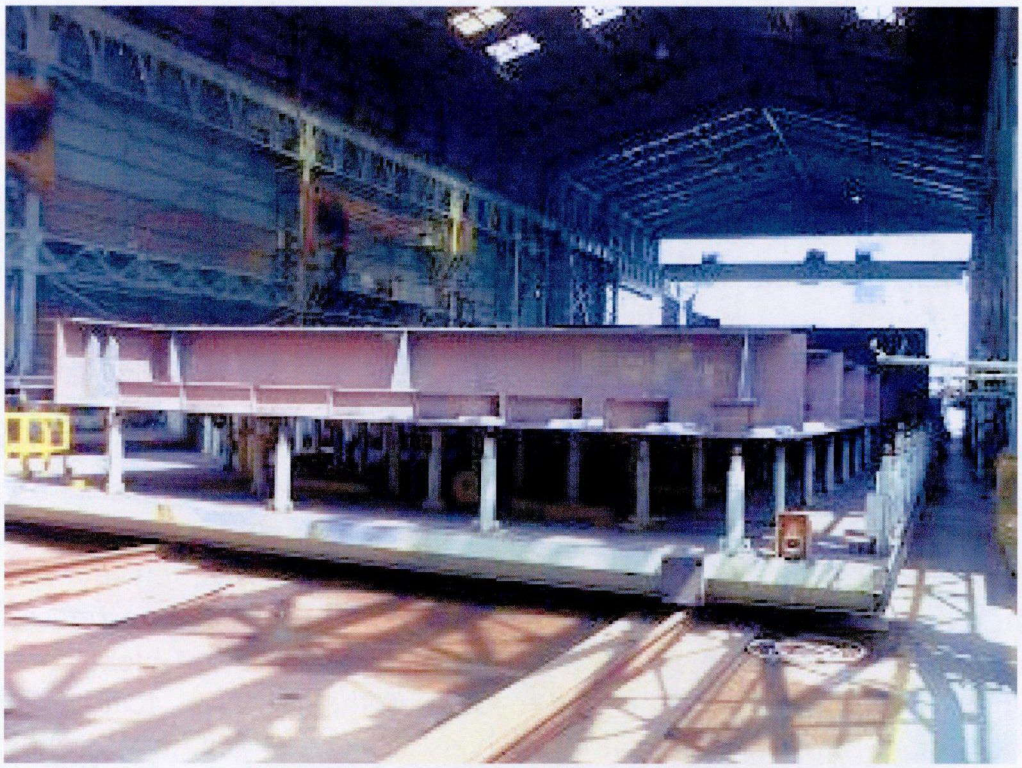

(a) Overview of a ship panel structure on support pins

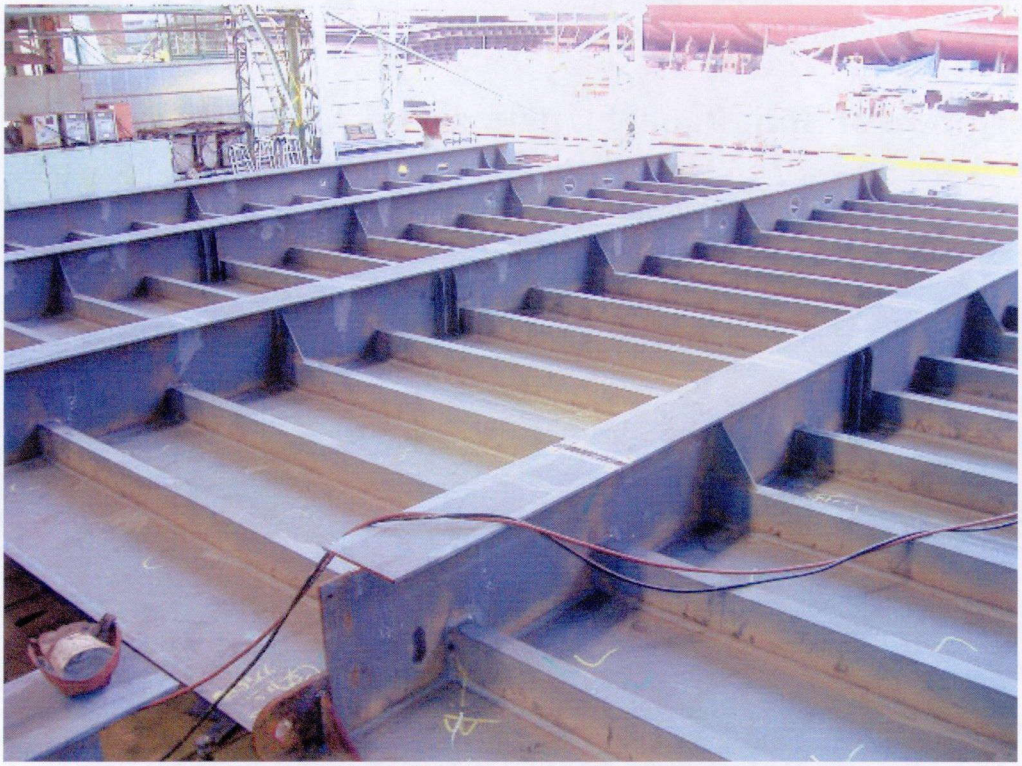

(b) Plates and stiffeners of a ship panel structure

Fig. 7.1 Photos of typical ship panel structures in shipyards.

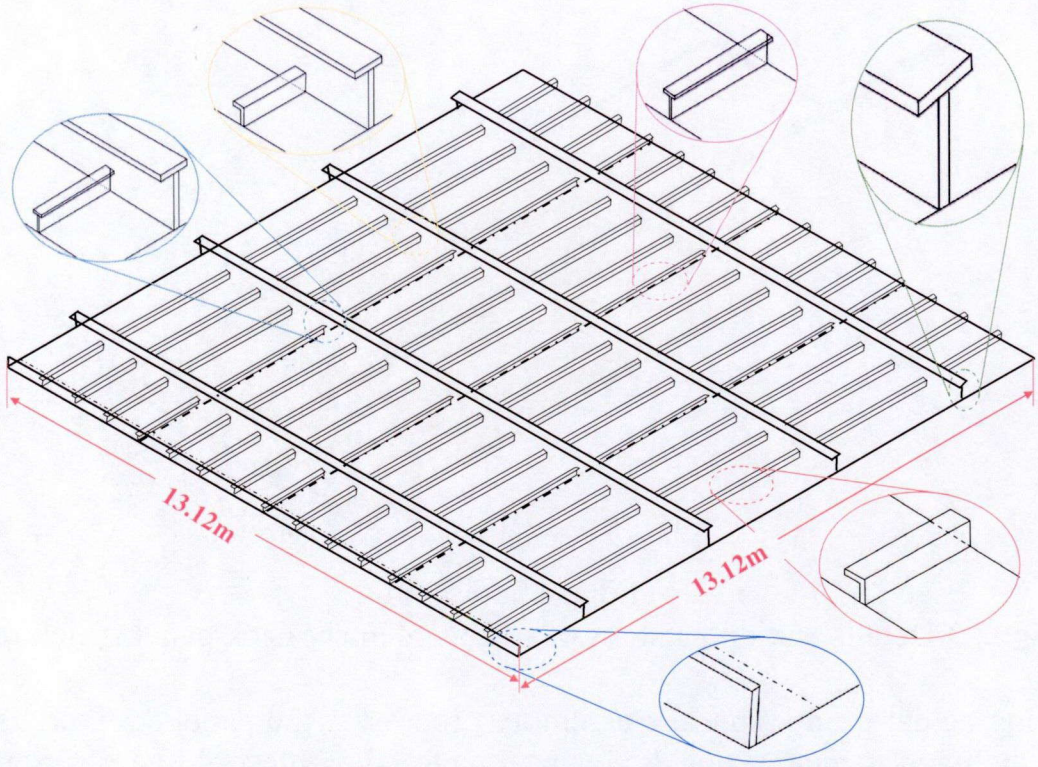

Fig. 7.2 Considered car deck panel structure.

Details and dimensions of each stiffener are illustrated in **Fig. 7.3**. These are used to create FE models for evaluating welding inherent deformation.

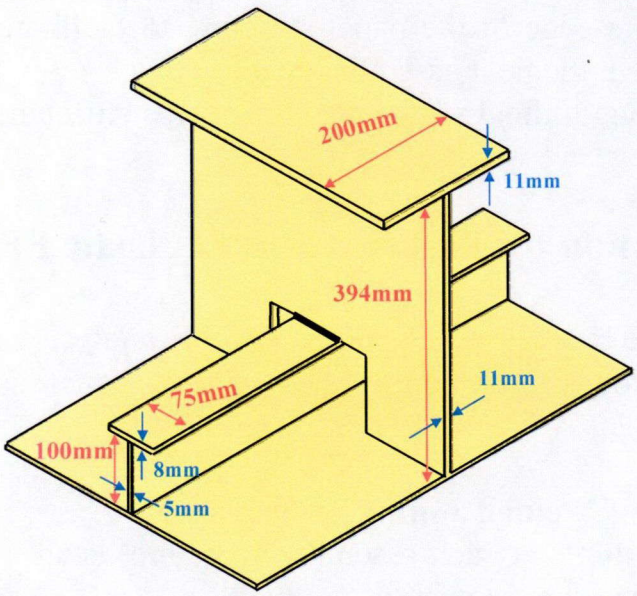

(a) I and transverse stiffeners

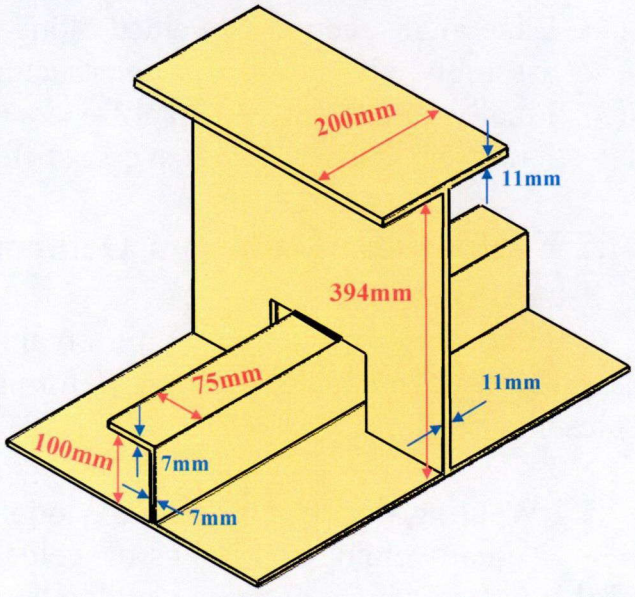

(b) Longitudinal and transverse stiffeners

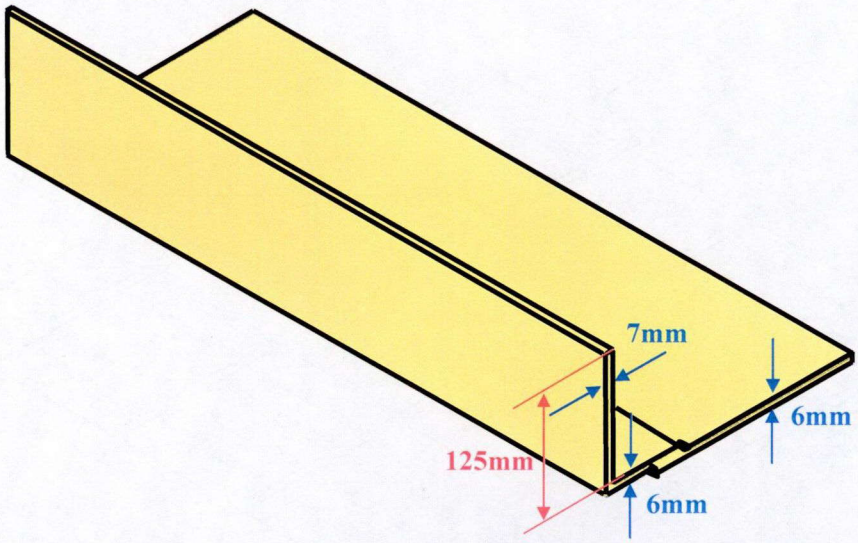

(c) Edge angle section

Fig. 7.3 Details and dimensions of stiffeners in car deck panel structure.

During actual production, the assembly process of the panel structure is carried out with the panel structure upside down to have favorable welding positions and is roughly divided into 5 stages as follows:

(1) All longitudinal stiffeners are welded to the four plates using automatic, both sides, simultaneous fillet welding; to create four unit panels
(2) Then each I section stiffener is used to assemble each two adjacent unit panels;
(3) Transverse stiffeners are then welded across the already joined four unit panels;
(4) Edge angle section is welded along one edge of the panel structure to facilitate assembly with adjacent panel structure in the next assembly stage;
(5) Finally, joints between all stiffeners (longitudinal stiffener to transverse stiffener; I section stiffeners to transverse stiffener) are welded.

7.2 Evaluation of Inherent Deformation by Thermal Elastic Plastic FE Analysis

Integration of inherent strain obtained by thermal elastic plastic FE analysis is employed to evaluate inherent deformation of the joints used in this panel as presented below.

7.2.1 Welding Condition and FE Models of Welded Joints

Actual welding conditions of welded joints at each assembly stage are listed in **Table 7.2**, in which the same welding heat input efficiency is assumed.

Six small welded joints are investigated to evaluate inherent deformation. **Figure 7.4** shows solid element models of these joints for thermal elastic plastic FE analysis. In all joints, only rigid body motion is prevented. Dimensions of each joint and geometries of welding beads are also shown in **Fig. 7.4**.

Table 7.2 Welding conditions of different welded joints contained in the considered car deck panel structure.

Welded joint	Current (A)	Voltage (V)	Velocity (mm/sec)	Heat Efficiency
Longitudinal Stiffener to Plates	325	32	13.3	0.8
I Section to Unit Panels	330	32	10	0.8
	330	32	10	0.8
Transverse Stiffener to Plate	330	32	10	0.8
Angle Section to Plate	220	28	6.7	0.8
Longitudinal Stiffener to Transverse Stiffener	220	28	6.7	0.8
I Section to Transverse Stiffener	220	28	6.7	0.8

Using the in-house code JWRIAN to perform thermal elastic plastic FE analysis, thermal analysis is carried out first to obtain the history of the transient temperature field, which is applied as a thermal load in a subsequent mechanical analysis. The inherent strain (plastic strain in this case) of each welded joint is computed and its distributions on each cross section normal to the welding line are obtained.

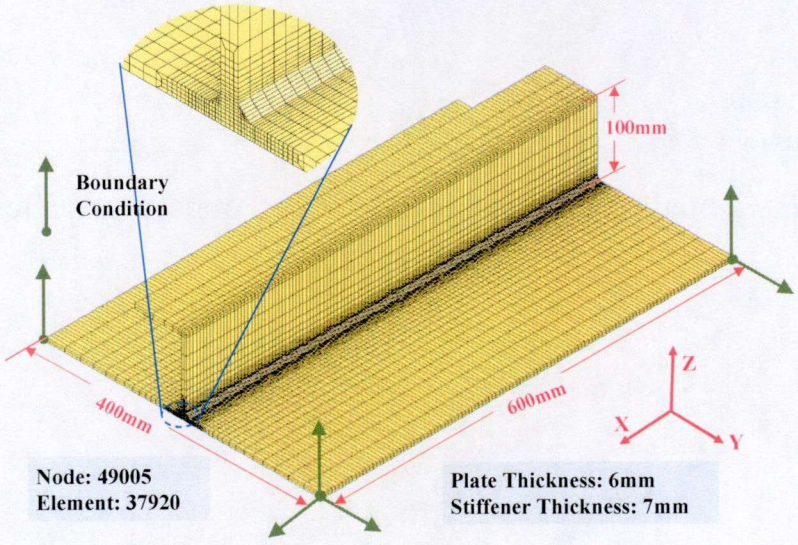

(a) Solid element model of welded joint between longitudinal stiffener and plate

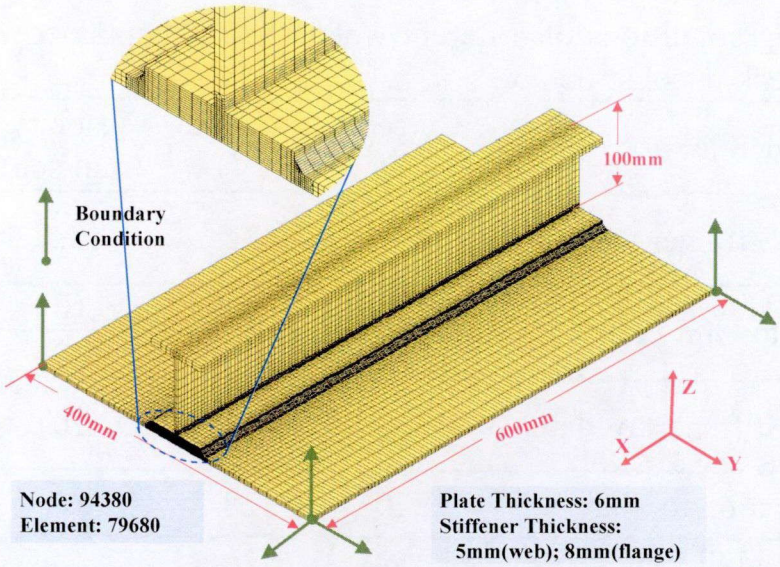

(b) Solid element model of welded joint between I section stiffener and plate

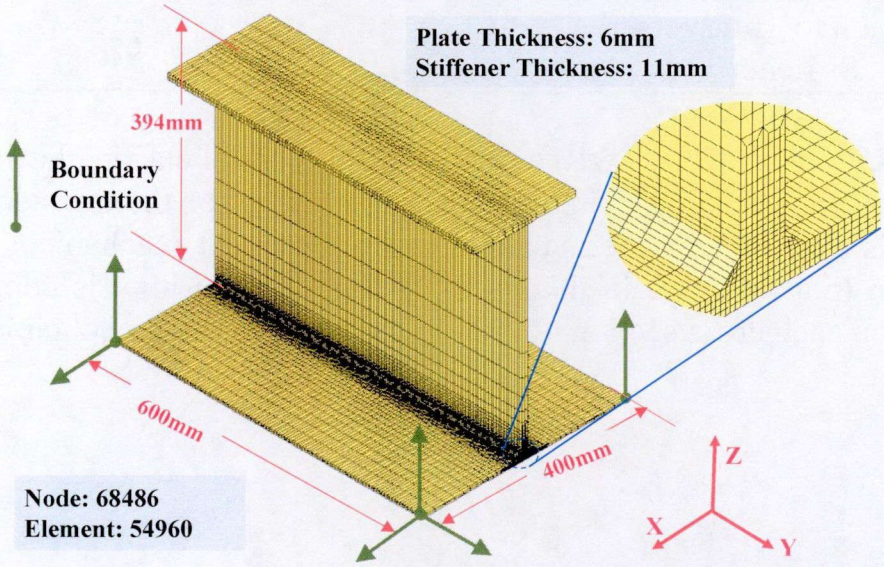

(c) Solid element model of welded joint between transverse stiffener and plate

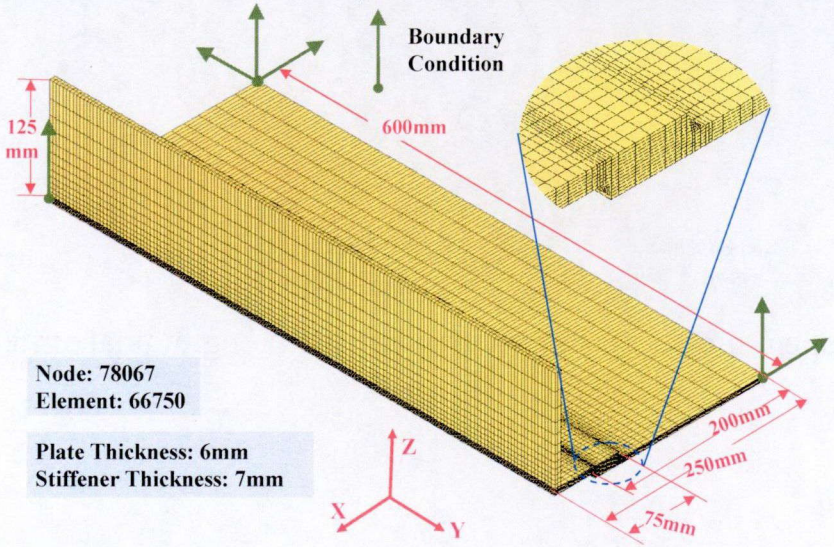

(d) Solid element model of welded joint between edge angle section and plate

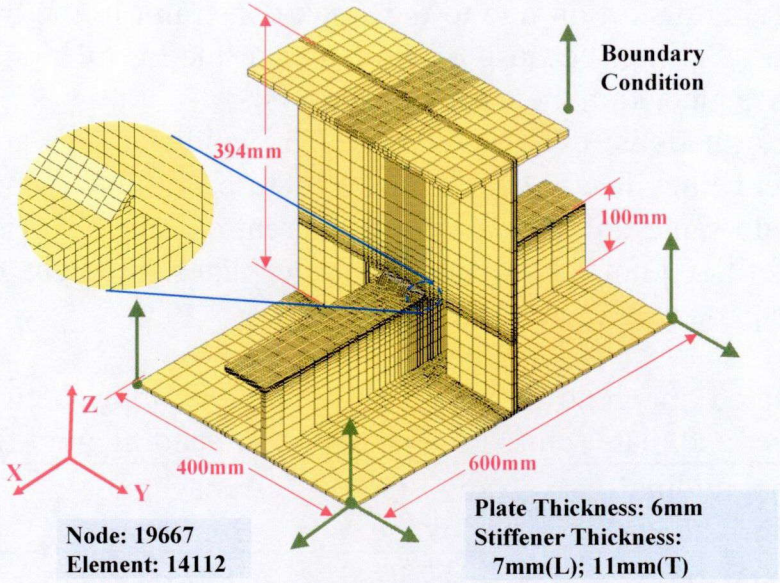

(e) Solid element model of welded joint between longitudinal stiffener and transverse stiffener

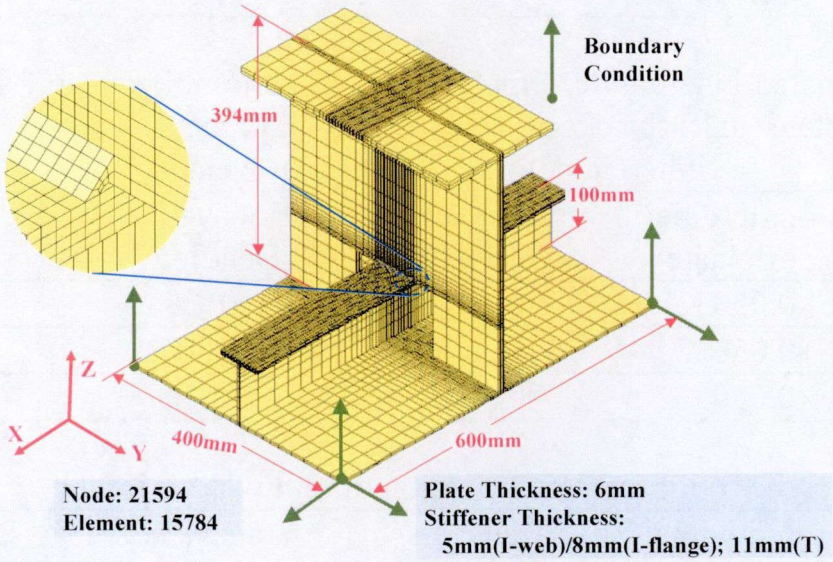

(f) Solid element model of welded joint between I section stiffener and transverse stiffener

Fig. 7.4 Solid element models of welded joints in car deck panel structure.

7.2.2 Evaluation of Inherent Deformation

Based on computed plastic strain of each welded joint using thermal elastic plastic FE analysis as stated in the preceding section, corresponding inherent deformation can be evaluated.

According to the definition of the inherent deformation, longitudinal inherent shrinkage can be evaluated by integration of the longitudinal inherent strain obtained over cross sections normal to welding line. It is then averaged over the full length of the welding line to get the longitudinal inherent shrinkage used in the elastic FE analysis.

Transverse inherent shrinkage and inherent bending are approximately evaluated

directly from welding distortion due to the weak constraint in the transverse and out of plane directions. Further, because of the small influence of longitudinal bending, this component is neglected in the elastic FE analysis.

Inherent deformations evaluated for each welded joint are introduced to corresponding weld lines in car deck panel structure. In case of butt welded joints between plates with same thickness, half of inherent deformations is applied to each plate. In case of fillet joints consisting of three plates, inherent deformations are divided into three parts as shown in **Tables 7.3-7.8**.

Table 7.3 Estimated inherent deformation of welded joint between longitudinal stiffener and plate (unit: shrinkage in mm, bending in rad).

	Longitudinal Shrinkage	Transverse Shrinkage	Transverse Bending	Longitudinal Bending
Flange	-0.04055	-0.15720	-0.02192	0
Flange	-0.04055	-0.15720	-0.02229	0
Web	-0.04055	-0.00153	-0.00220	0

Table 7.4 Estimated inherent deformation of welded joint between I section stiffener and plate (unit: shrinkage in mm, bending in rad).

(a) Inherent deformation of fillet welded joint

	Longitudinal Shrinkage	Transverse Shrinkage	Transverse Bending	Longitudinal Bending
Flange	-0.05032	-0.12462	+0.01283	0
Flange	-0.05032	-0.12462	+0.01283	0
Web	-0.05032	-0.50805	0.00323	0

(b) Inherent deformation of butt welded joint

	Longitudinal Shrinkage	Transverse Shrinkage	Transverse Bending	Longitudinal Bending
Flange	-0.07548	-0.12462	0	0
Flange	-0.07548	-0.12462	0	0
Web	0	0	0	0

Table 7.5 Estimated inherent deformation of welded joint between transverse stiffener and plate (unit: shrinkage in mm, bending in rad).

	Longitudinal Shrinkage	Transverse Shrinkage	Transverse Bending	Longitudinal Bending
Flange	-0.05908	-0.32215	-0.00520	0
Flange	-0.05908	-0.32215	-0.00531	0
Web	-0.05908	-0.01020	-0.00181	0

Table 7.6 Estimated inherent deformation of welded joint between edge angle section and plate (unit: shrinkage in mm, bending in rad).

	Longitudinal Shrinkage	Transverse Shrinkage	Transverse Bending	Longitudinal Bending
Flange	-0.11731	-0.255141	-0.00592	0
Flange	-0.11731	-0.255141	-0.00690	0
Web	0	0	0	0

Table 7.7 Estimated inherent deformation of welded joint between longitudinal and transverse stiffeners (unit: shrinkage in mm, bending in rad).

	Longitudinal Shrinkage	Transverse Shrinkage	Transverse Bending	Longitudinal Bending
Flange	-0.04618	-0.04326	-0.00247	0
Flange	-0.04618	-0.04326	-0.00236	0
Web	-0.04618	-0.04106	-0.00772	0

Table 7.8 Estimated inherent deformation of welded joint between I section and transverse stiffener (unit: shrinkage in mm, bending in rad).

	Longitudinal Shrinkage	Transverse Shrinkage	Transverse Bending	Longitudinal Bending
Flange	-0.03760	-0.03091	-0.00227	0
Flange	-0.03760	-0.03091	-0.00188	0
Web	-0.03760	-0.03930	-0.00750	0

7.3 Representation of Actual Situation of Car Deck Panel Structure by Elastic FE Analysis

In the assembly of car deck panel structure, parts are assembled one by one following the assembly procedure mentioned in the preceding section. Assembly is carried out on supporting pins. **Figure 7.5** shows shell element model of the considered car deck panel structure. Supporting columns are modeled by supporting piece elements as shown in the bottom view in **Fig. 7.5(b)** and the supporting problem is treated as a contact problem.

To consider the boundary condition of car deck panel structure in elastic FE analysis, all lower sides of supporting elements are fixed (translations and rotations) as shown in **Fig. 7.6**.

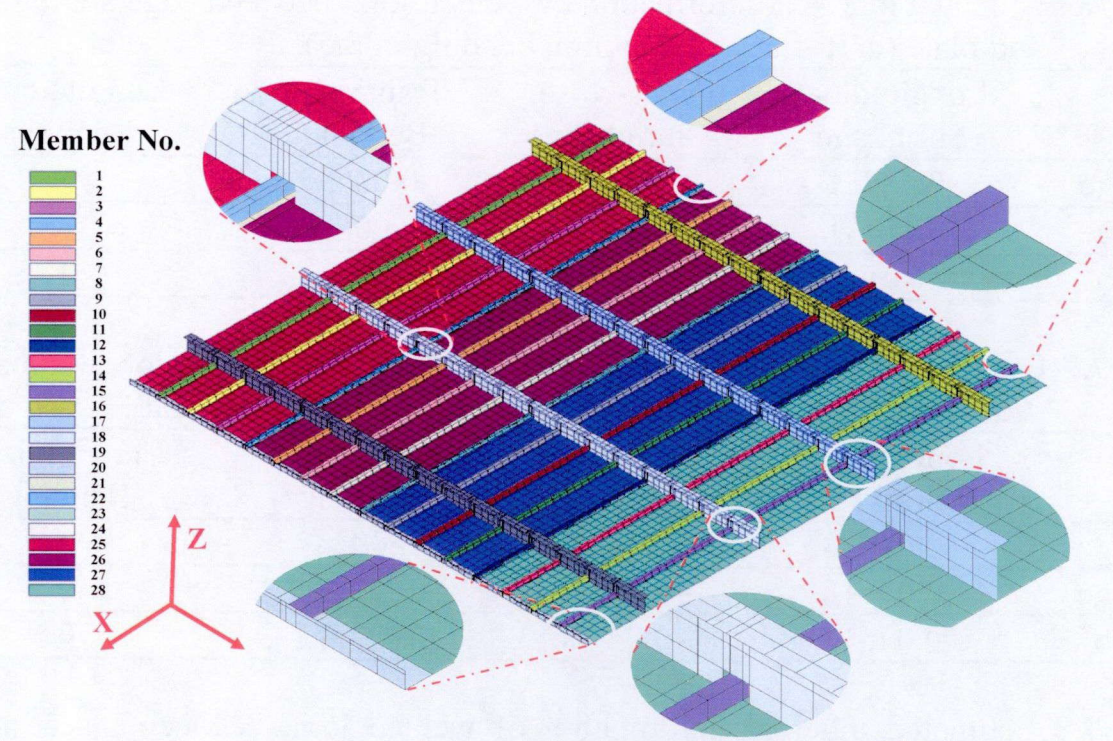

(a) Top view of car deck panel structure model, upside down

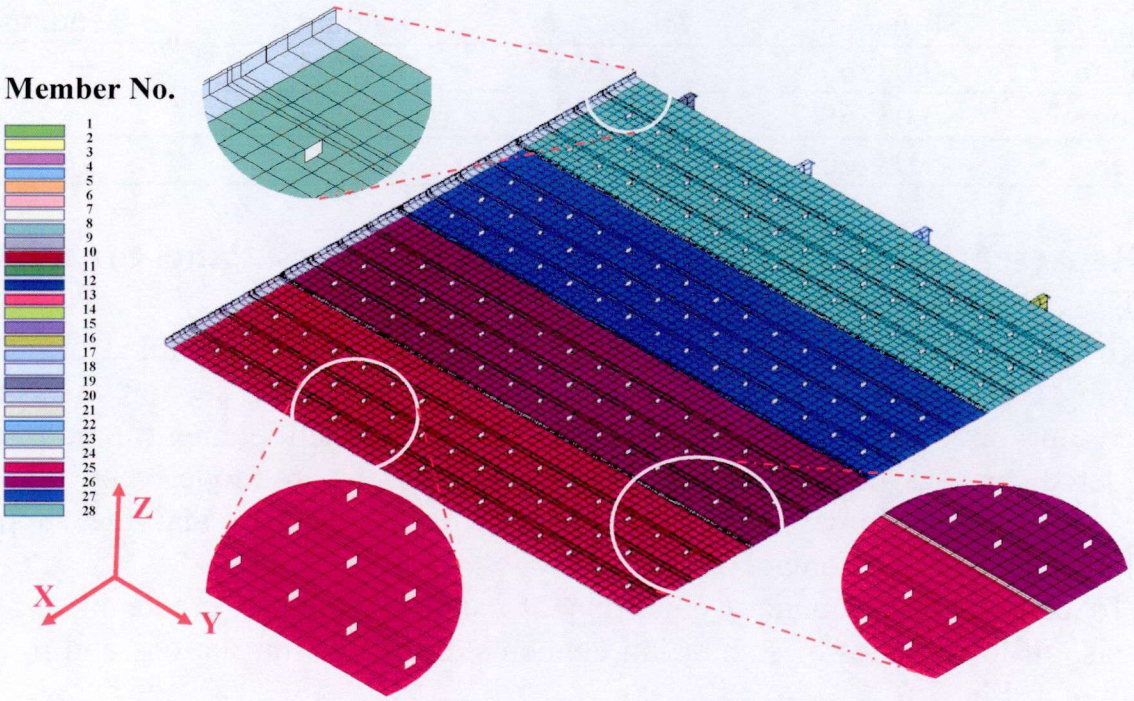

(b) Bottom view of car deck panel structure model, upside down

Fig. 7.5 Shell element model of car deck panel structure.

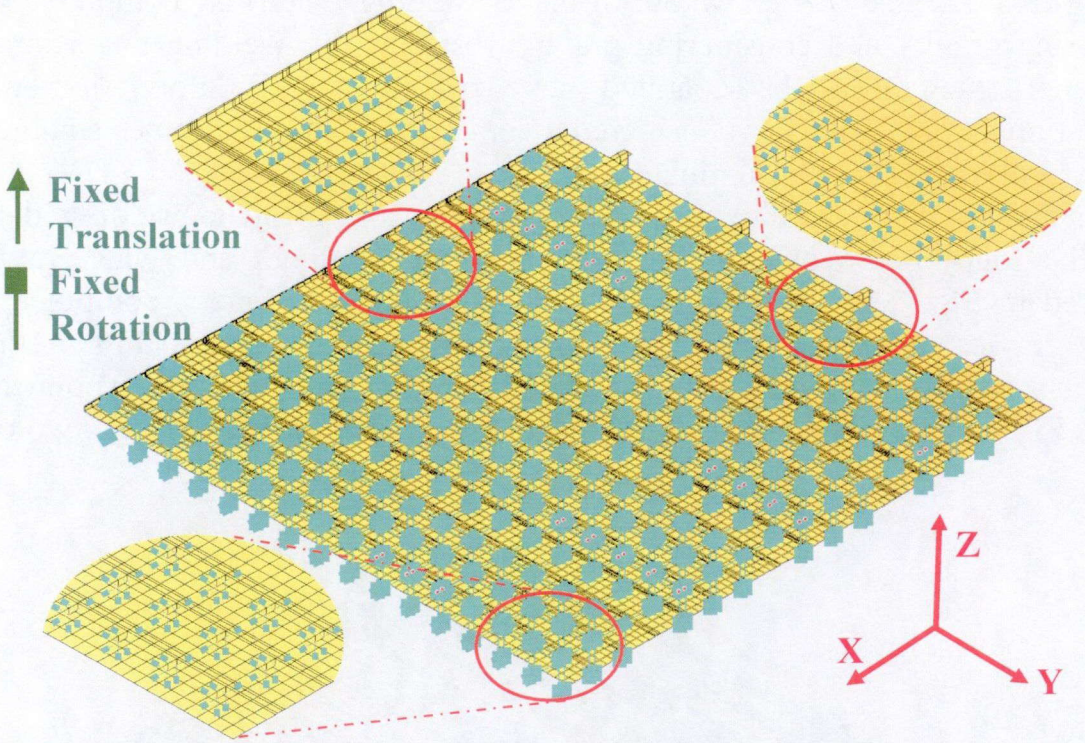

Fig. 7.6 Boundary condition fixing the lower sides of supporting elements.

Using the elastic FE analysis code in JWRIAN, out-of-plane welding distortion is predicted by applying inherent deformation to welding lines. Since the considered structure is thin, the large deformation theory is necessary to investigate non-linear and unstable responses, such as buckling.

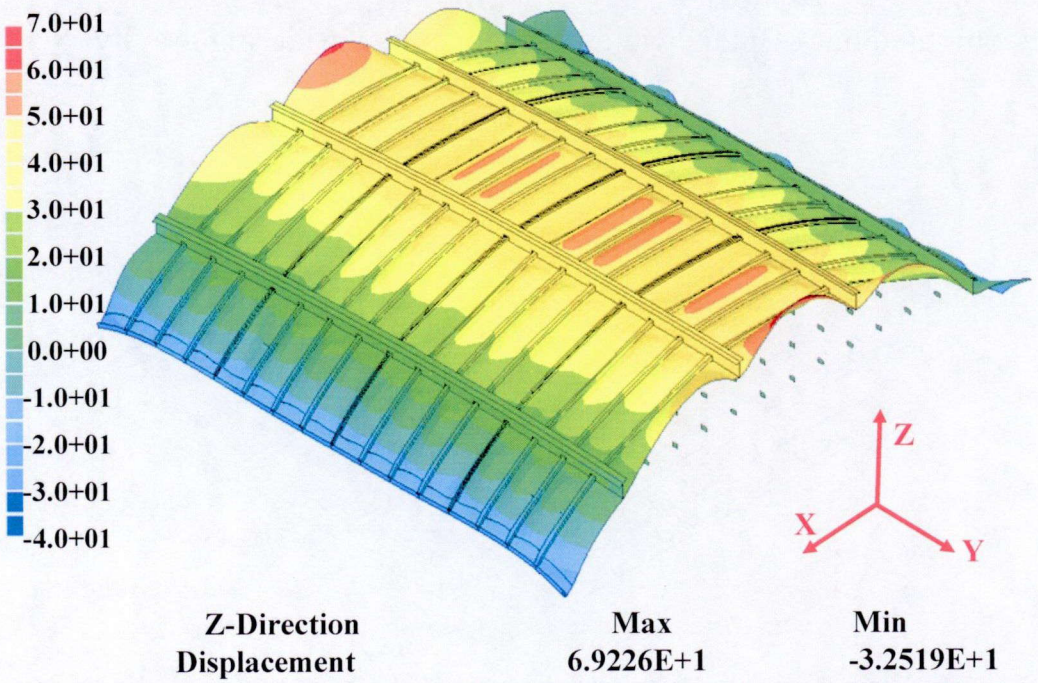

Fig. 7.7 Computed out-of-plane welding distortion without gravity (Scale: 40:1).

Figures 7.7 and **7.8** show out-of-plane welding distortion computed without considering gravity and considering gravity, respectively. Welding distortion of car deck panel structure may be separated into two parts, overall deformation and local deformation. When gravity is considered, overall deformation becomes small and the local deformation becomes dominant.

To closely examine the influence of gravity, out-of-plane welding distortion along the four lines shown in **Fig. 7.9,** computed without and with gravity, are compared in **Fig. 7.10.** In the direction of longitudinal stiffeners, computed results without gravity and with gravity has a large difference as shown in **Fig. 7.10(a)** and **(b)**. This difference comes from the overall deformation which is suppressed by gravity. **Figures 7.10(c)** and **(d)** also show a large difference between the two cases.

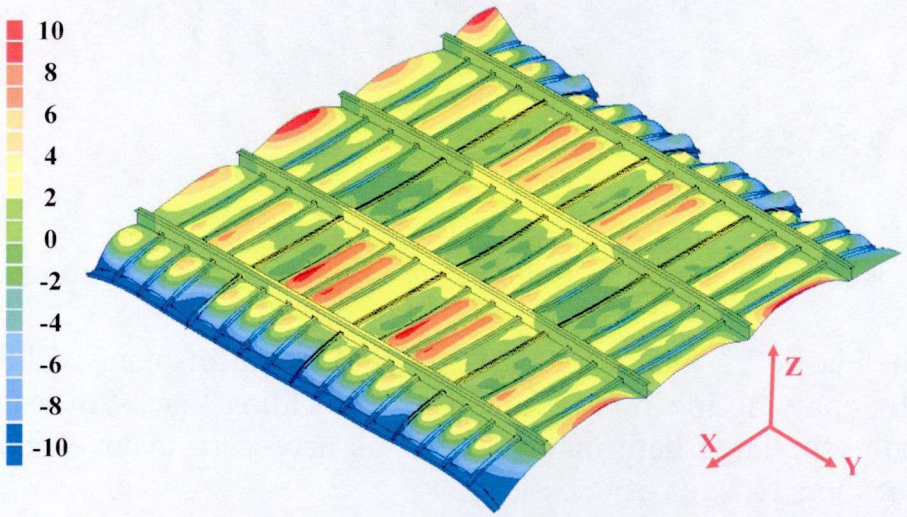

Fig. 7.8 Computed out-of-plane welding distortion considering gravity (Scale: 40:1).

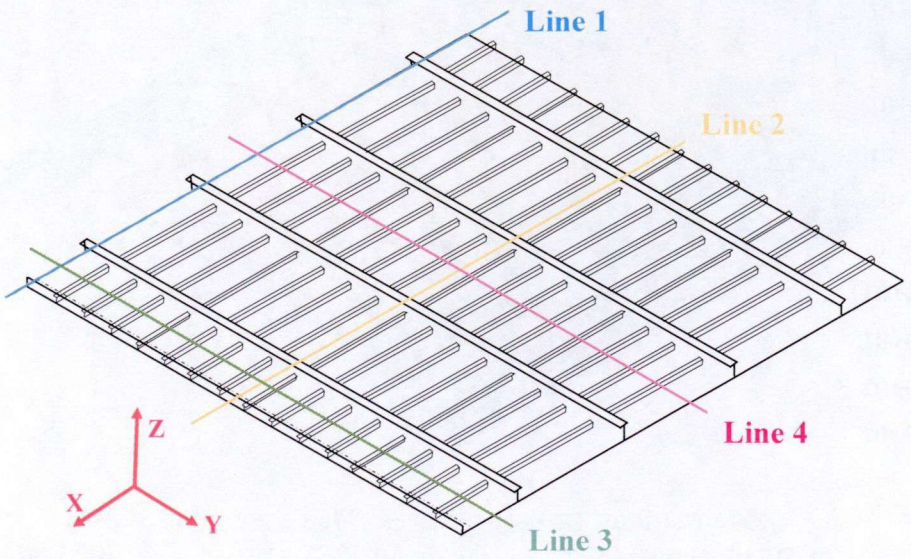

Fig. 7.9 Selected 4 lines to compare out-of-plane welding distortion.

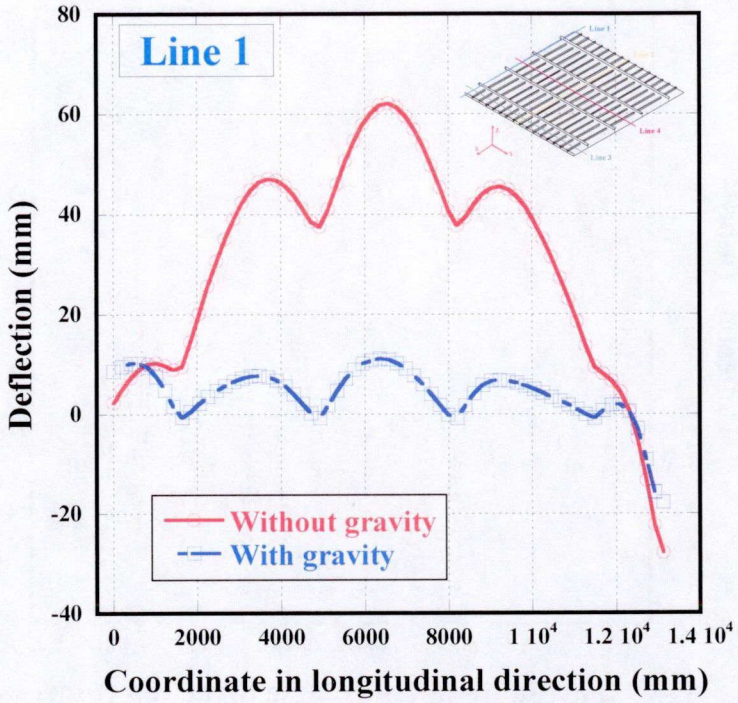

(a) Comparison of out-of-plane welding distortion along line 1

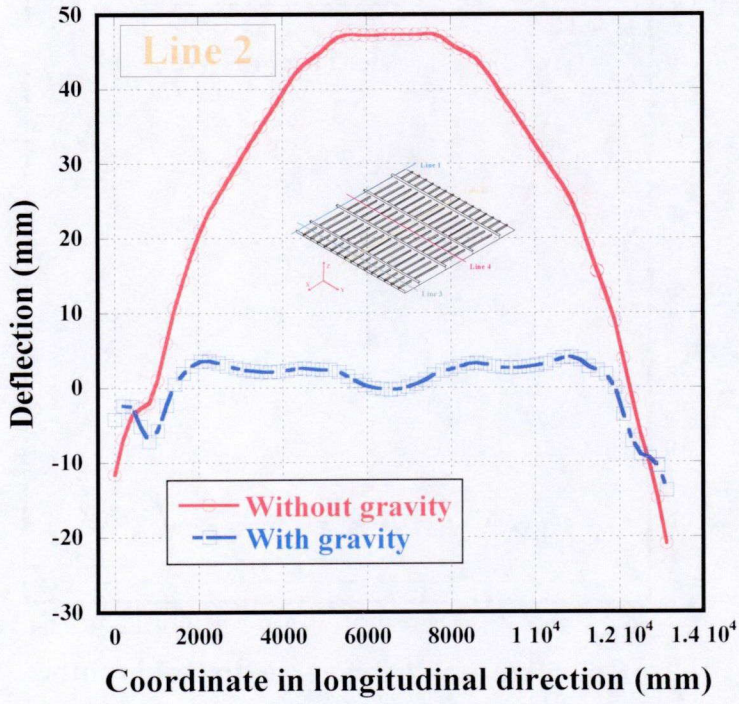

(b) Comparison of out-of-plane welding distortion along line 2

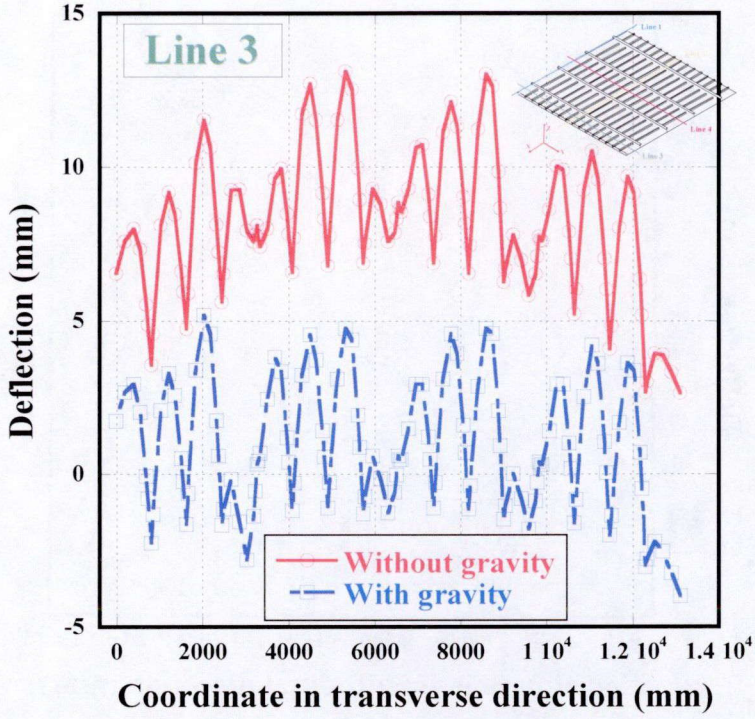

(c) Comparison of out-of-plane welding distortion along line 3

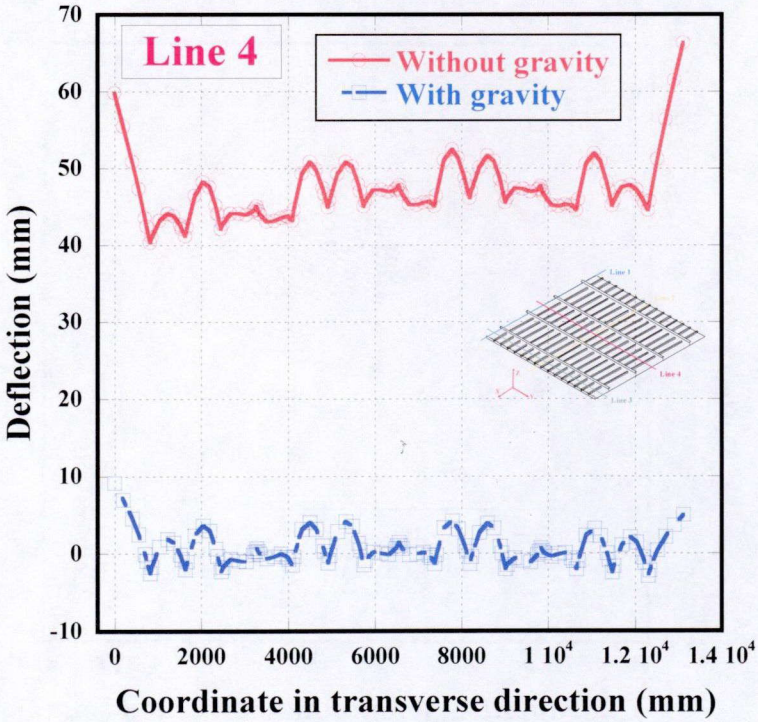

(d) Comparison of out-of-plane welding distortion along line 4

Fig. 7.10 Comparisons of out-of-plane welding distortion with and without gravity (considering large deformation).

Since contact problem is a highly nonlinear problem, combined with buckling, conversion of the analysis may be difficult. Also, since overall deformation is not significant when the gravity is considered, an ideal boundary condition is employed

to replace gravity and supporting elements, thus avoiding the complexity associated with the contact problem. Local deformation is then closely examined.

7.4 Prediction of Welding Induced Buckling Using Ideal Boundary Condition

To closely examine local deformation caused by welding of car deck panel structure, ideal boundary condition as shown in **Fig. 7.11** is employed in the following investigations.

In this section, factors influential to welding induced buckling are investigated. Since large deformation theory is essential to investigate buckling, differences between computations using small and large deformation theories is utilized to recognize buckling. In-plane inherent shrinkages, which are considered to be dominant cause of buckling, are employed to reproduce buckling behavior.

As for other components of inherent deformation, inherent bending may influence buckling behavior by promoting or retarding it. Transverse shrinkage can generate in-plane stress in plates and it may influence buckling. Initial deflection may also be a factor influential to buckling when its magnitude is sufficiently large.

7.4.1 Investigation on Influence of Large Deformation Theory

First, out-of-plane welding distortion is computed considering small deformation theory and the computed out-of-plane welding distortion is shown in **Fig. 7.12**. The maximum and minimum deflections are both observed at the edge of the panel structure. **Figure 7.13** shows the computed out-of-plane welding distortion when large deformation theory is considered. The maximum and minimum deflections also occur at the edge. The magnitude of the out-of-plane welding distortion considering large deformation is larger than that shown in **Fig. 7.12** assuming small deformation. From the comparison between **Figs. 7.12** and **7.13**, it may be seen that welding distortion is larger in **Fig. 7.13**. However, it is difficult to judge whether the panel structure has bucked due to welding or not.

To closely examine the influence of large deformation on out-of-plane welding distortion, out-of-plane welding distortion computed using small and large deformation theories along the four lines shown in **Fig. 7.9** are compared. . **Figure 7.14 (a)** and **(b)** shows a comparison of out-of-plane welding distortion along line 1 and line2, which are at the edge and the center of the panel structure in the direction of longitudinal stiffeners. In **Fig. 7.14 (c)** and **(d)**, comparisons of out-of-plane welding distortion along line 3 and line 4, which are at the edge and the center in the transverse direction, are shown. Significant difference is observed in the magnitudes of out-of-plane welding distortion between small and large deformation theories in **Fig. 7.14(a)** and **(c)** which shows the distortion along the edge. **Fig. 7.14(b)** and **(d)** show almost the same magnitudes of out-of-plane welding distortion along lines in the central region.

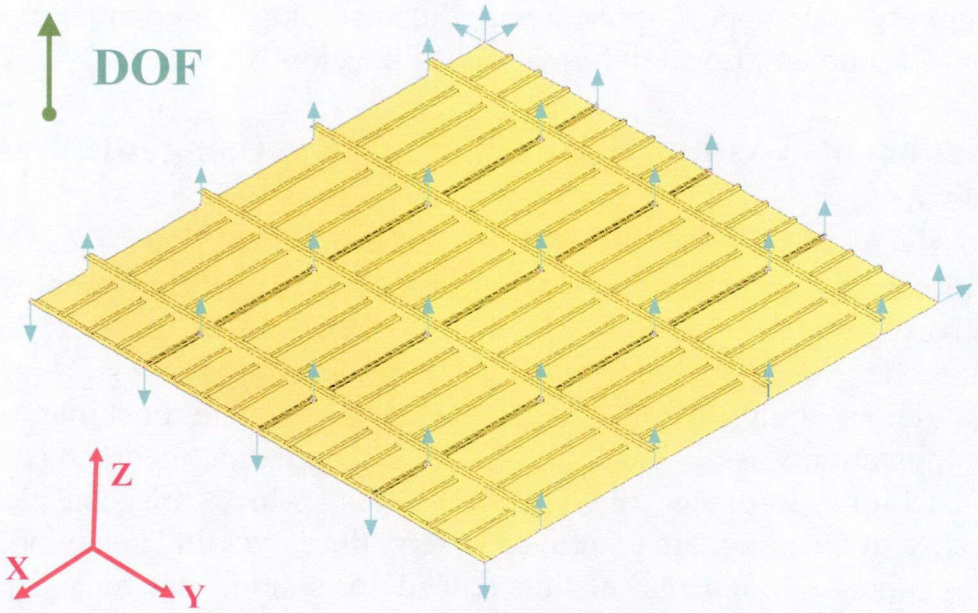

Fig. 7.11 Ideal boundary condition of of car deck panel structure for elastic FE analysis.

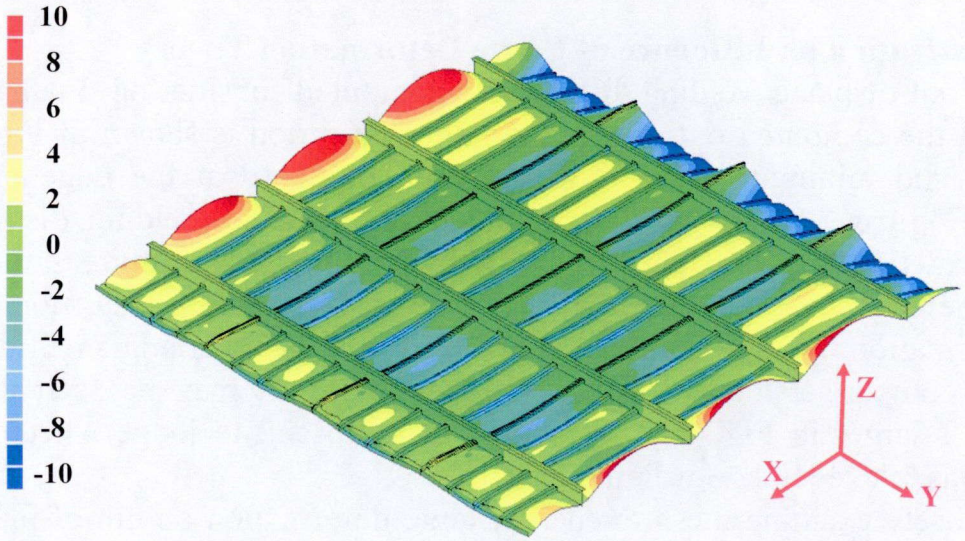

Fig. 7.12 Computed out-of-plane welding distortion using small deformation theory (Scale: 40:1).

From these comparisons, it can be seen that the deformations in the center part of the panel structure computed by small and large deformation FE analysis are almost the same in both magnitude and deformation mode. Only in the panels along the edge, difference between out-of-plane welding distortions computed using the two theories is observed.

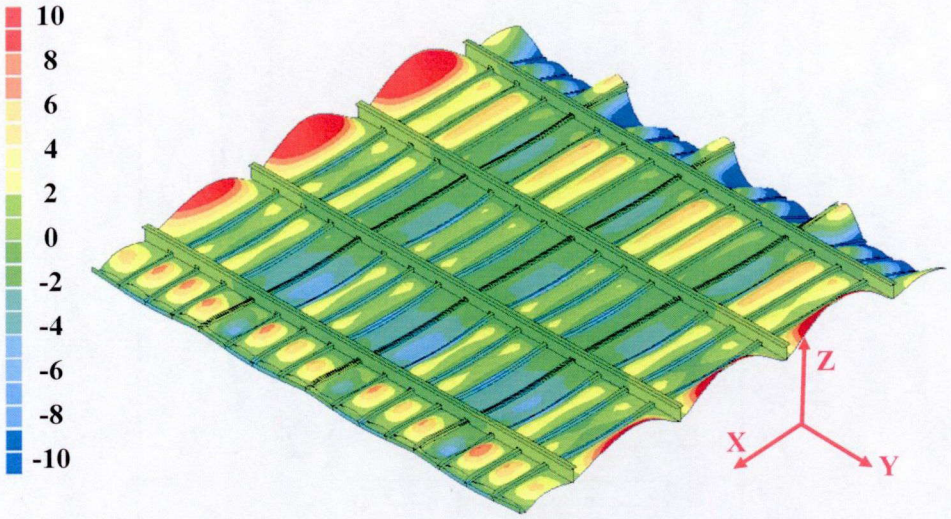

Fig. 7.13 Computed out-of-plane welding distortion using large deformation theory (Scale: 40:1).

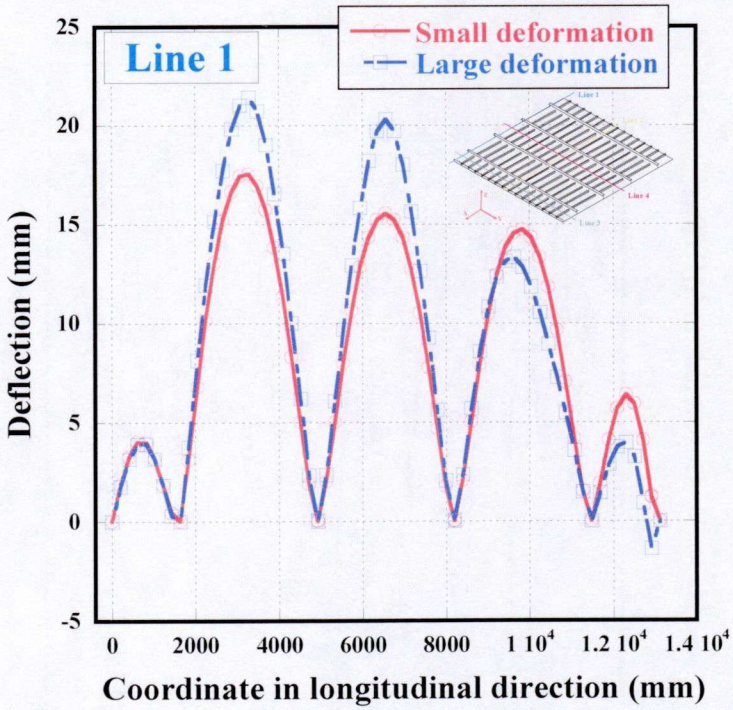

(a) Comparison of out-of-plane welding distortion along line 1

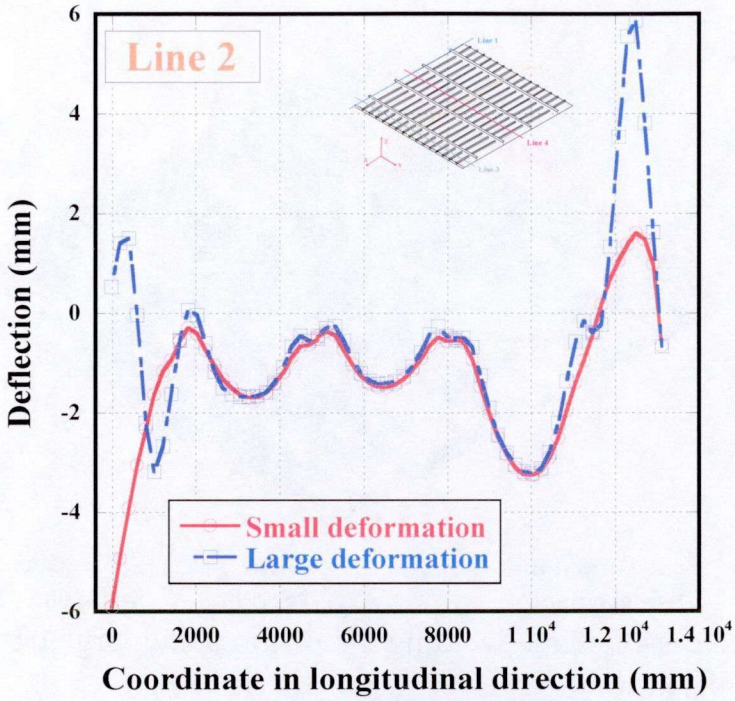

(b) Comparison of out-of-plane welding distortion along line 2

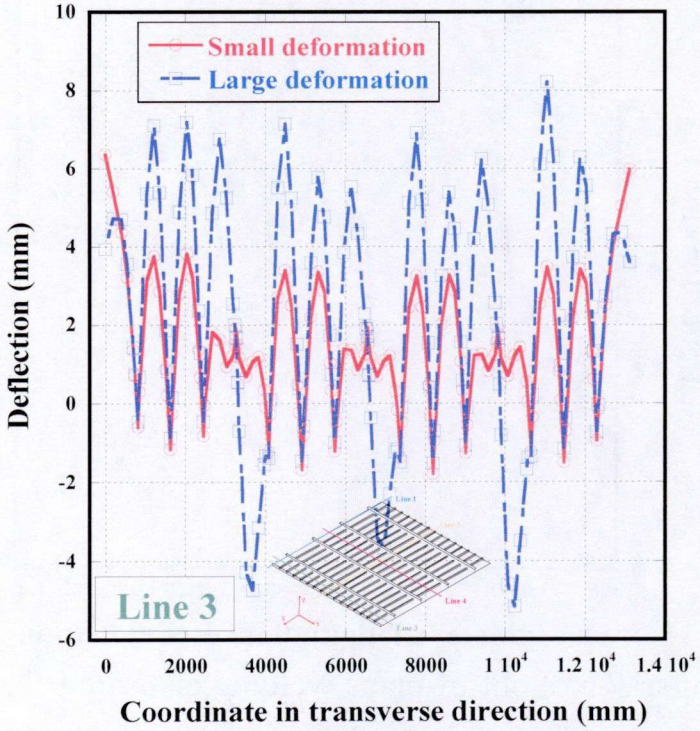

(c) Comparison of out-of-plane welding distortion along line 3

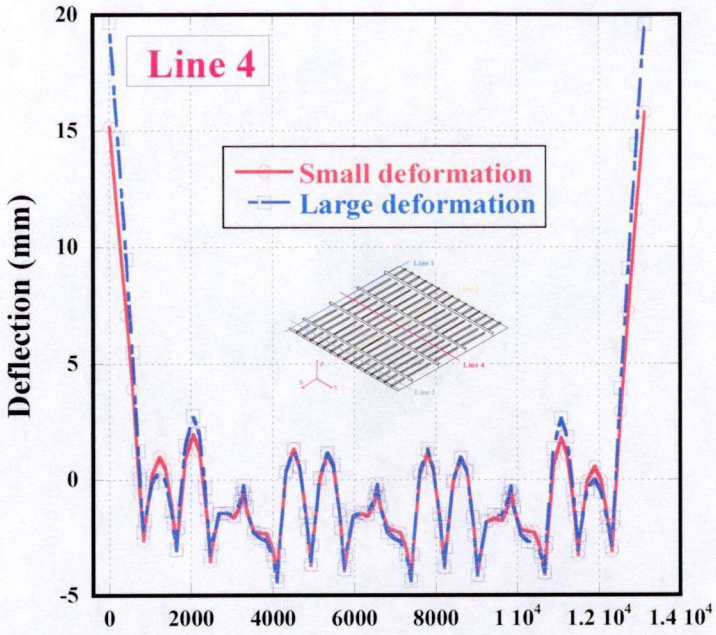

(d) Comparison of out-of-plane welding distortion along line 4

Fig. 7.14 Comparisons of out-of-plane welding distortion computed using small and large deformation theories (applying all components of inherent deformation).

From the above discussion, it is difficult to judge whether the panel structure is already buckled in the internal region due to the applied inherent deformation produced by welding, or it will buckle and is closed to the buckling.

As mentioned earlier, inherent bending is considered as a disturbance to trigger buckling. It may not determine buckling mode but influences the magnitude of out-of-plane welding distortion. Relatively large bending deformation produced by inherent bending deformation may obscure the occurrence of buckling. Therefore, an investigation considering only in-plane inherent shrinkages and ignoring inherent bending is presented in the following section.

7.4.2 Investigation on Buckling Behavior without Inherent Bending

Sine in-plane inherent shrinkages (both longitudinal and transverse) are the dominant reason of welding induced buckling , elastic FE analysis considering only in-plane shrinkages is employed to study buckling in the considered panel structure. This is a simplified buckling problem based on unrealistic assumption. However it is useful in understanding buckling.

When only in-plane inherent shrinkages are considered, significant difference is observed between the computed out-of-plane distortion considering small and large deformation theories as shown in **Figs. 7.15** and **7.16**. Comparison of out-of-plane welding distortion shown in these figures concluded that not only the magnitude but also the mode of welding distortion is different especially near the edge of the panel structure.

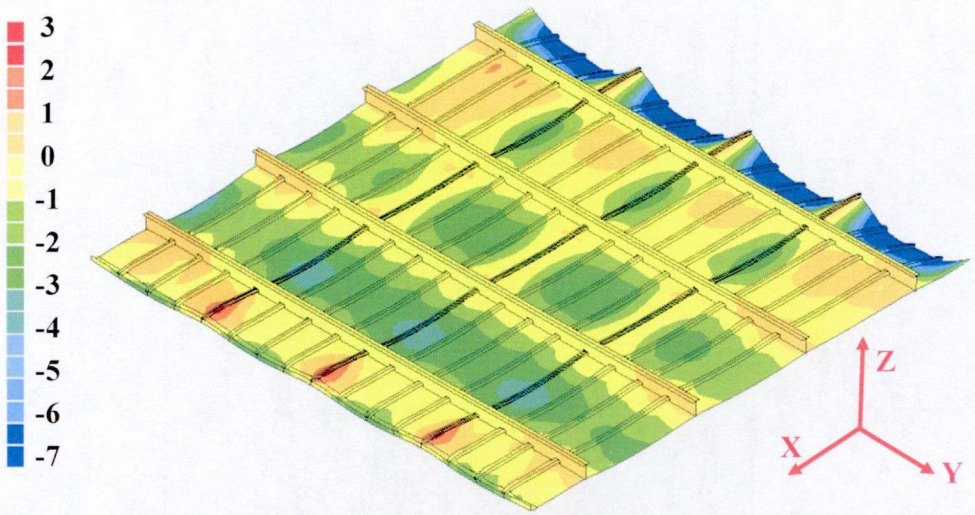

Fig. 7.15 Computed out-of-plane welding distortion considering small deformation theory and applying only in-plane inherent shrinkages (Scale: 40:1).

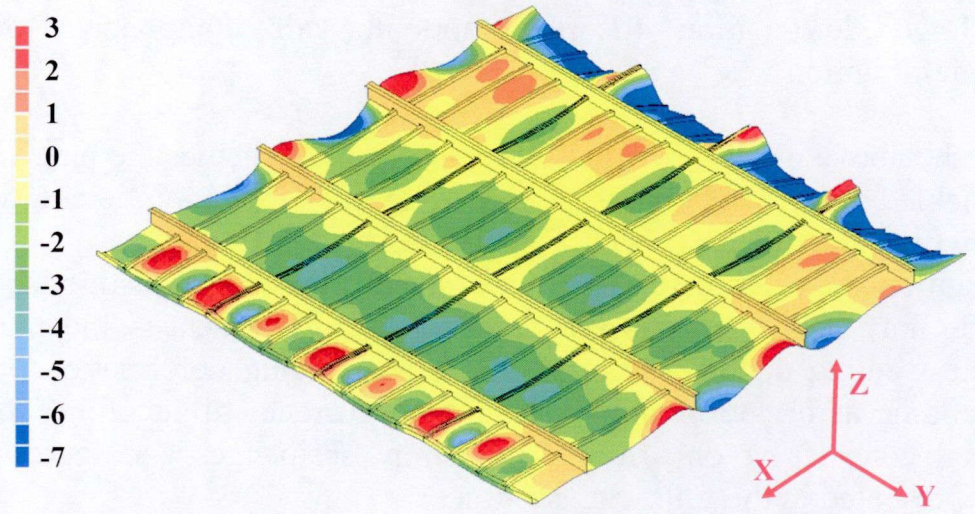

Fig. 7.16 Computed out-of-plane welding distortion considering large deformation theory and applying only in-plane inherent shrinkages (Scale: 40:1).

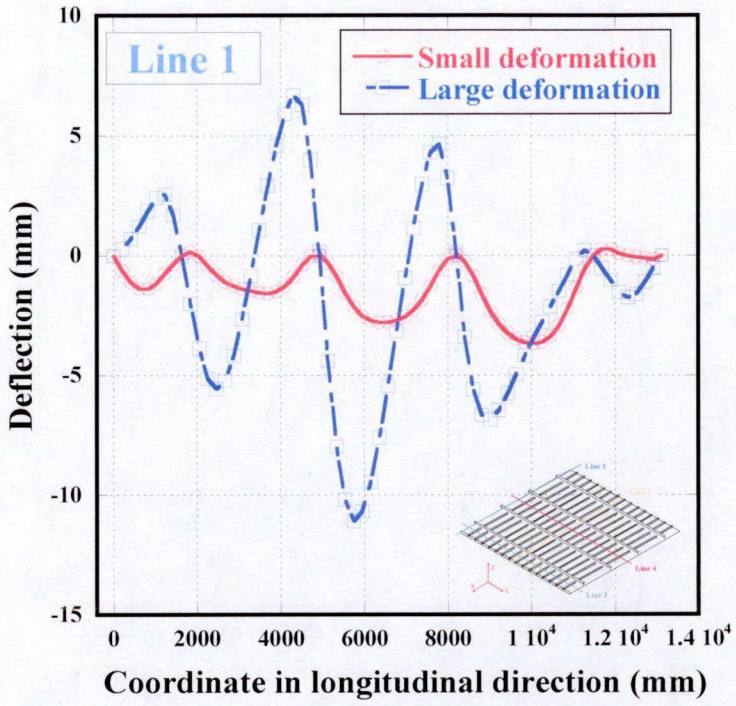

(a) Comparison of out-of-plane welding distortion along line 1

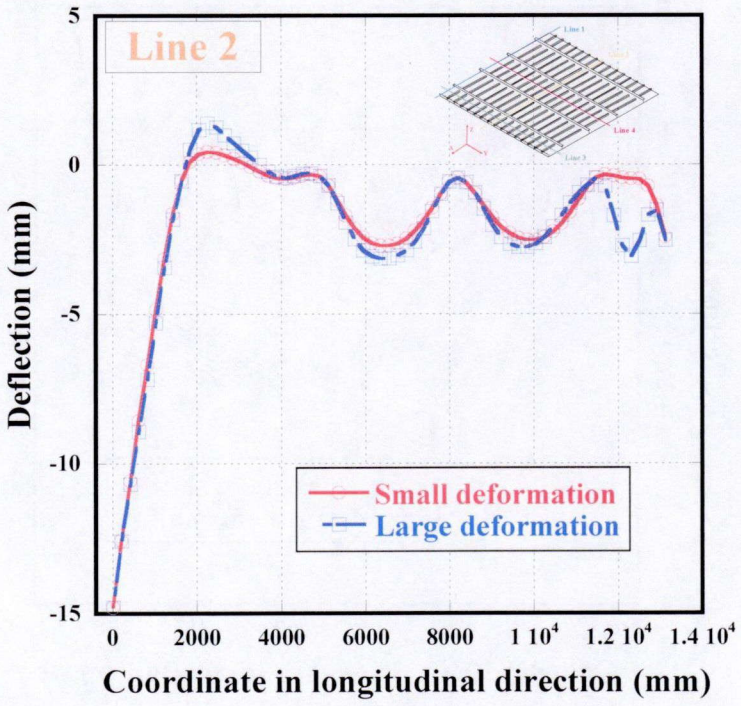

(b) Comparison of out-of-plane welding distortion along line 2

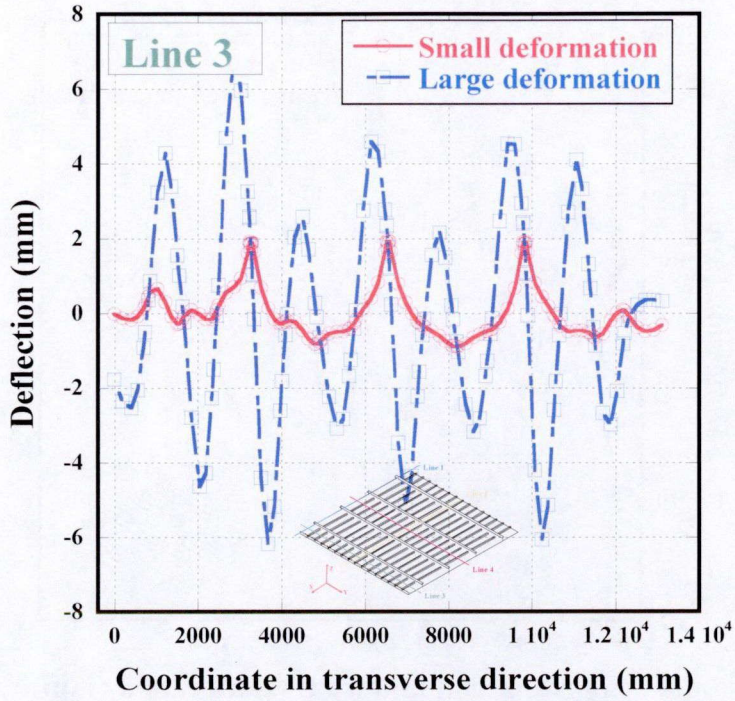

(c) Comparison of out-of-plane welding distortion along line 3

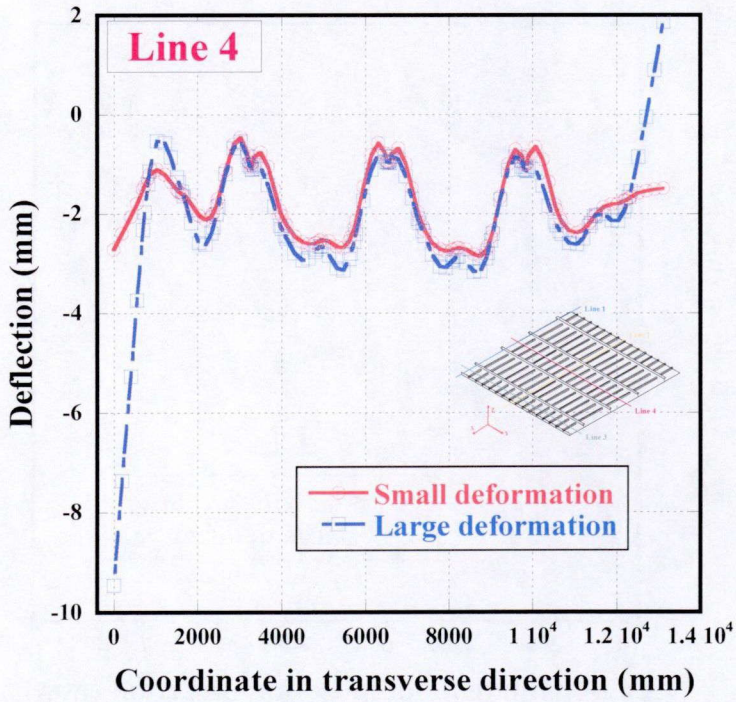

(d) Comparison of out-of-plane welding distortion along line 4

Fig. 7.17 Comparisons of out-of-plane welding distortion computed considering small and large deformation theories (only applying in-plane inherent shrinkages).

Now, it can be concluded that inherent deformation produced by welding causes the panel structure to buckle near the edge. Out-of-plane welding distortion when

only in-plane inherent shrinkages are applied is compared along the four lines shown in **Fig. 7.9**. The computed distortion considering large deformation theory clearly shows significant feature of buckling. As may be seen from **Fig. 7.17 (a)** and **(c)**, buckling distortion, in which the direction of deflection is reversed across stiffeners, occurs when considering large deformation theory, while hungry horse type welding distortion is dominant when considering small deformation theory. However, as shown in **Fig. 7.17 (b)** and **(d)**, deflection along line 2 and line 4 at the center of the panel structure show almost the same magnitude and mode when considering small or large deformation theories.

The hungry horse type welding distortion is usually produced by transverse inherent bending (angular distortion) existing along filet joints, which is not considered in these computations. The reason why the hungry horse type welding distortion is observed in **Figs. 7.17** (a) and (c), showing results using small deformation theory needs to be explained. This phenomenon can be understood if welding distortion of longitudinal stiffeners is closely examined with progress of assembly. Taking the longitudinal stiffener marked with red color in **Fig. 7.18** as an example, **Fig. 7.19** shows out-of-plane welding distortion along the welding line (blue line shown in **Fig. 7.18**) during assembly process. As may be seen from the figure, when only longitudinal members that is longitudinal stiffeners and I sections are welded to plate, the considered longitudinal stiffener deflects upwards due to the longitudinal inherent shrinkage. When transverse members, that are transverse stiffeners and edge angle section, are welded, the considered longitudinal stiffener deflects downward. This is attributed to bending of the considered longitudinal stiffener at crossings with transverse stiffeners. When transverse stiffeners are welded to the plate, the plate shrinks in the longitudinal direction, at the lowest part of the longitudinal stiffener, due to transverse inherent shrinkage associated with welding transverse stiffeners to the plate. Plate shrinkage at the lowest part of the longitudinal stiffener exerts a down ward bending moment on the stiffener. This moment is the reason of the hungry horse type welding distortion, even when considering small deformation and applying only in-plane inherent shrinkage.

For welding induced buckling, transverse shrinkage of car deck panel structure during sequential assembly is also important. **Figure 7.20** shows transverse shrinkage of the panel structure after completing welding assembly. As may be seen from the figure, transverse stiffeners are longer than the plate width. This difference comes from the sequence of assembly. In the present case, longitudinal members are welded to the plate first. At this stage, the plate shrinks freely in the transverse direction. Then, transverse stiffeners are fitted and welded.

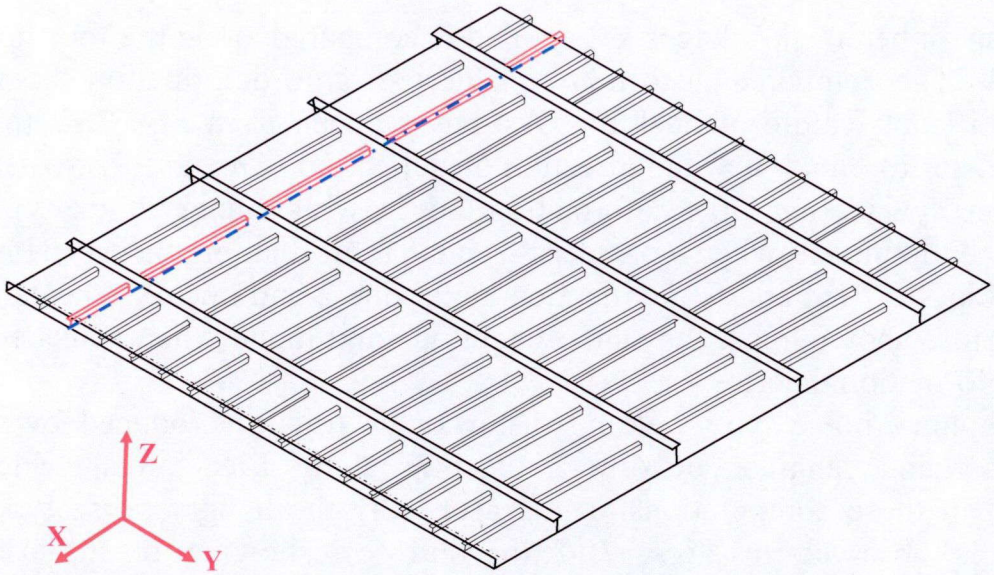

Fig. 7.18 Considered longitudinal stiffener in ship panel structure.

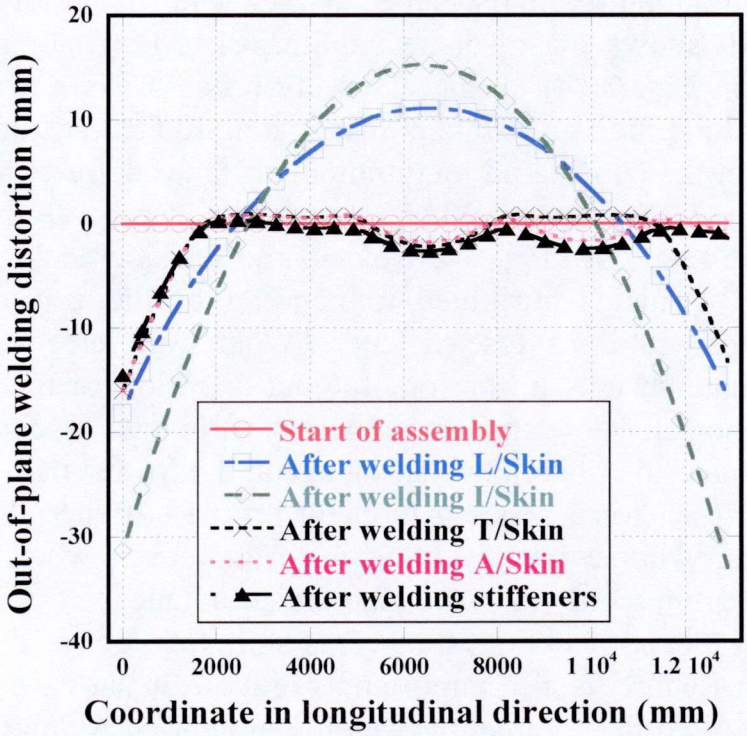

Fig. 7.19 Out-of-plane welding distortion of lower part of considered longitudinal stiffener during assembly process.

If the all members are fitted and tack welded in the beginning of assembly, this type of mismatching does not occur. Comparing to this, in the case of sequential welding the plate is compressed more, and a larger compressive stress is introduced in the plate. Thus, from the view of preventing the plate buckling, sequential assembly is not preferable. However due attention should be paid to excessive compressive stress that may arise in the stiffeners.

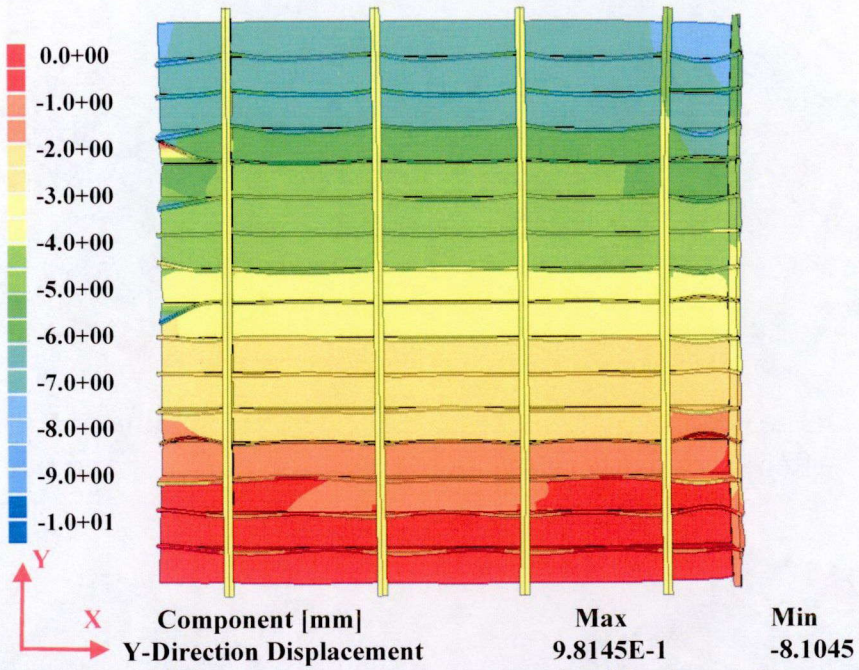

Fig. 7.20 Transverse shrinkage of panel compared with that of transverse stiffeners (Scale: 40:1).

7.5 Investigation of Buckling Behavior of Car Deck Panel Structure by Eigenvalue Analysis

Following the assembly process of the considered car deck panel structure introduced in **Section 7.1**, eigenvalue analyses are carried out. Predicted lowest eigenvalue and the corresponding buckling mode at each assembly stage are shown in **Fig. 7.21** together with the out-of-plane welding distortion computed by large deformation elastic FE analysis. As may be seen from **Fig. 7.21 (1)**, the plate buckles when it is welded to longitudinal stiffeners. From **Fig. 7.21 (2),** showing out-of-plane distortion after the four unit panels are welded together, overall buckling of unit panels occurs. After transverse stiffeners are welded, deformations promoted by buckling of plate along the edge of the panel structure become dominant as shown in **Fig. 7.21 (3)**, **(4)** and **(5)**.

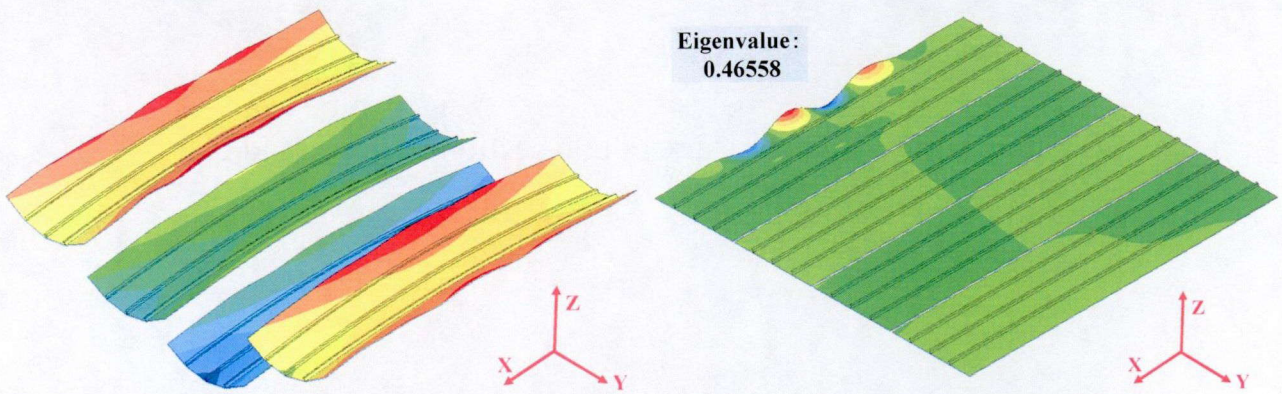

(a) large deformation analysis (b) eigenvalue analysis

(1) After first assembly stage (longitudinal stiffener and plate)

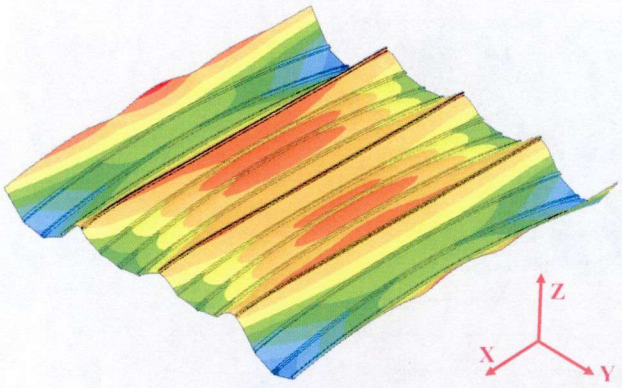

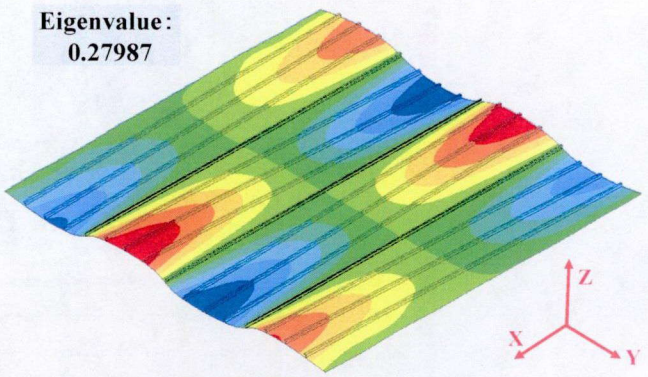

(a) large deformation analysis (b) eigenvalue analysis

(2) After second assembly stage (I section stiffener and plate)

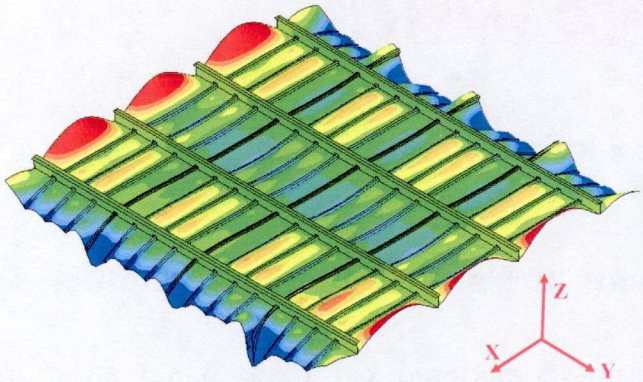

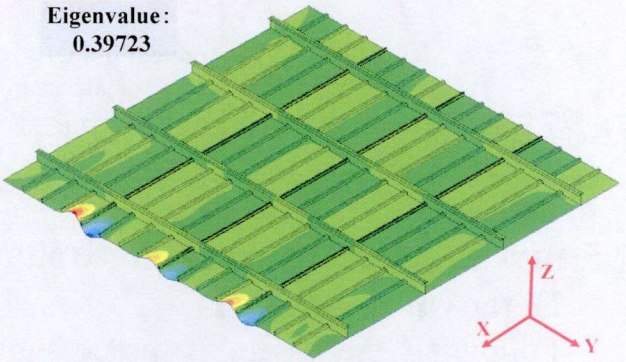

(a) large deformation analysis (b) eigenvalue analysis

(3) After third assembly stage (transverse stiffener and plate)

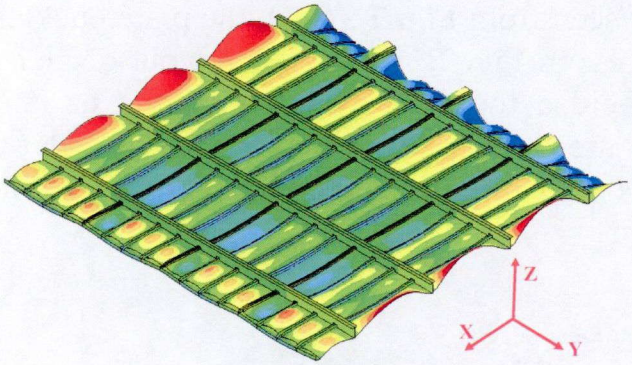

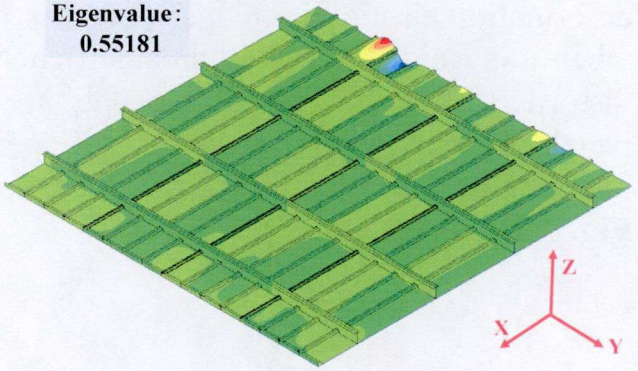

(a) large deformation analysis (b) eigenvalue analysis

(4) After fourth assembly stage (angle section stiffener and plate)

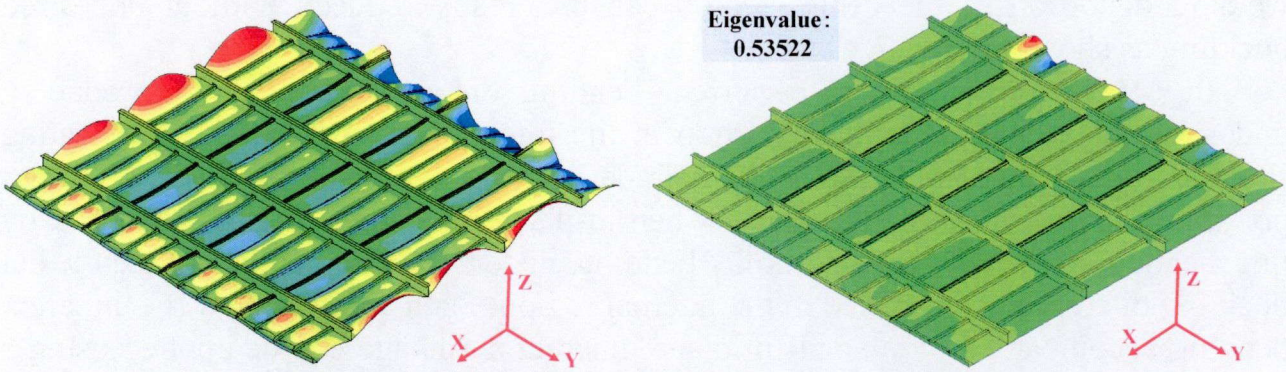

(a) large deformation analysis (b) eigenvalue analysis

(5) After fifth assembly stage (between stiffeners)

Fig. 7.21 Predicted deformed shape and buckling mode during the assembly process.

7.6 Straightening of Welding Distortion by Line Heating

From the above discussion, dominant out-of-plane welding distortion of the considered car deck panel structure can be roughly divided into two types: bending distortion in the internal region and buckling distortion near the edge. Straightening process to correct welding distortion is carried out using line heating. First, line heating is applied on the opposite side of the stiffeners in the internal region to correct bending distortion by introducing almost the same magnitude of bending distortion with reversed sign and the corresponding in-plane shrinkage as inherent deformation. Then, only in-plane shrinkage produced by line heating is applied to the region at the edge for correction of buckling distortion.

7.6.1 Straightening of Bending Distortion in Center Region

When line heating is used on the opposite side of welded joint, out-of-plane welding distortion may be corrected.

Though it is possible only in computational simulation, transverse inherent bending with the same magnitude as that produced by welding but in the opposite direction is assumed to be generated in the straightening process. Noting that longitudinal and the transverse shrinkage accompany transverse bending regardless of the direction of bending, longitudinal and transverse inherent shrinkage with the same magnitude as that produced by welding are also applied in straightening. **Figure 7.22** shows computed out-of-plane welding distortion after straightening bending distortion in the internal region. It is clearly seen that the internal region buckles as a consequence of this straightening process. Also, significant difference may be observed in the buckling mode of panels at the edge before and after straightening. This suggests that the influence of transverse and the longitudinal components of inherent deformation applied in straightening cannot be ignored.

Since the magnitude of the in-plane components of inherent deformation can be controlled to a certain extent by properly selecting the heating condition, in-plane components of inherent deformation are reduced to one half of the previous magnitude while keeping inherent bending the same. In this case, out-of-plane

welding distortion of the center region can be greatly reduced without undesired buckling as shown in **Fig. 7.23**.

In conclusion, in order to correct bending distortion and avoid producing undesired additional buckling distortion in the internal region, applied line heating should produce almost the same magnitude of inherent bending and as small as possible in-plane inherent shrinkage. When in-plane inherent shrinkage produced by line heating exceeds a critical limit, bending distortion can not be corrected but buckling distortion is produced in the internal region. Such a large transverse inherent bending accompanied by a small in-plane inherent shrinkage can be applied using a fast moving heating torch.

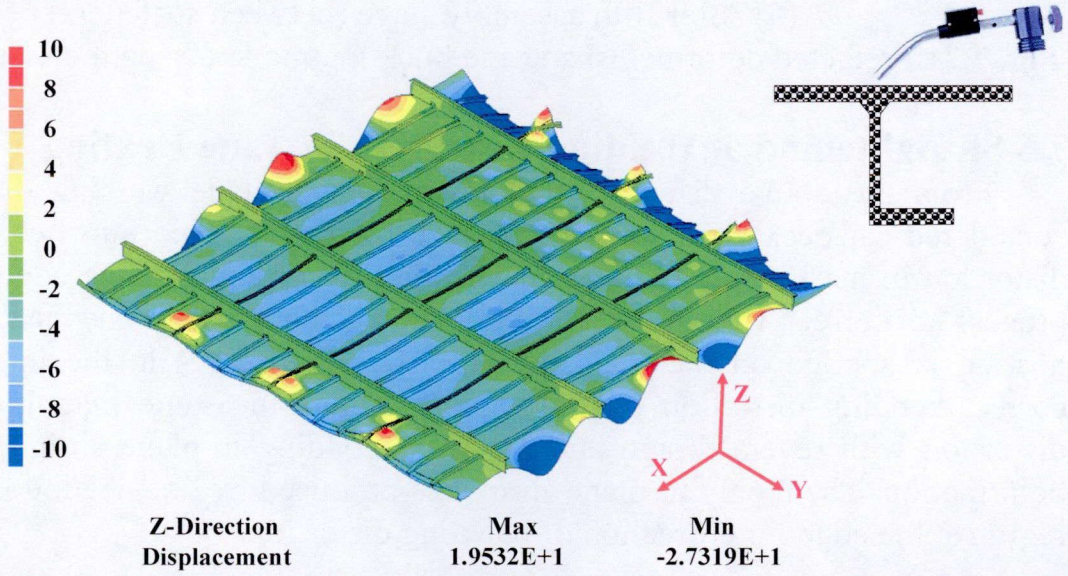

Fig. 7.22 Straightening of bending distortion while applying large in-plane inherent shrinkage.

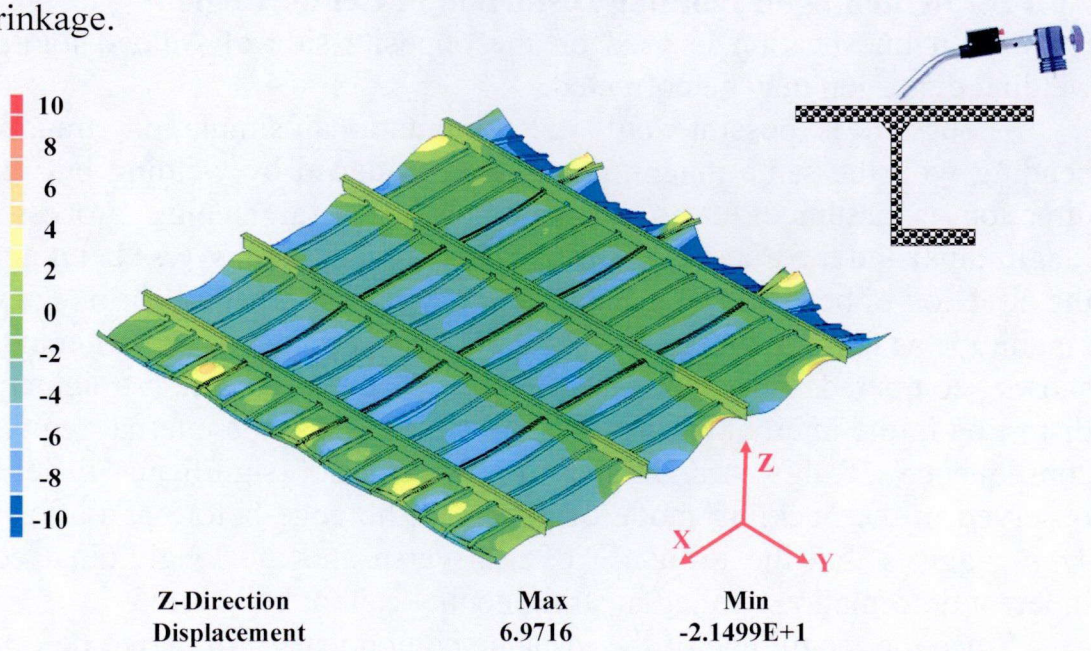

Fig. 7.23 Straightening of bending distortion while applying small in-plane inherent shrinkage.

7.6.2 Straightening of Buckling Distortion at Edge

Straightening of buckling distortion is always difficult in shipbuilding. According to common practice in shipyards, a buckled plate field is shrunk by applying line heating with appropriate heating condition to the plate field away from stiffeners.

To simulate this in the considered panel, uniformly distributed inherent strain is applied to panels along the edge. To examine the optimum amount of shrinkage, three cases with different amount of in-plane inherent strain, namely 0.0002, 0.0003 and 0.0004 are analyzed using elastic FE analysis.

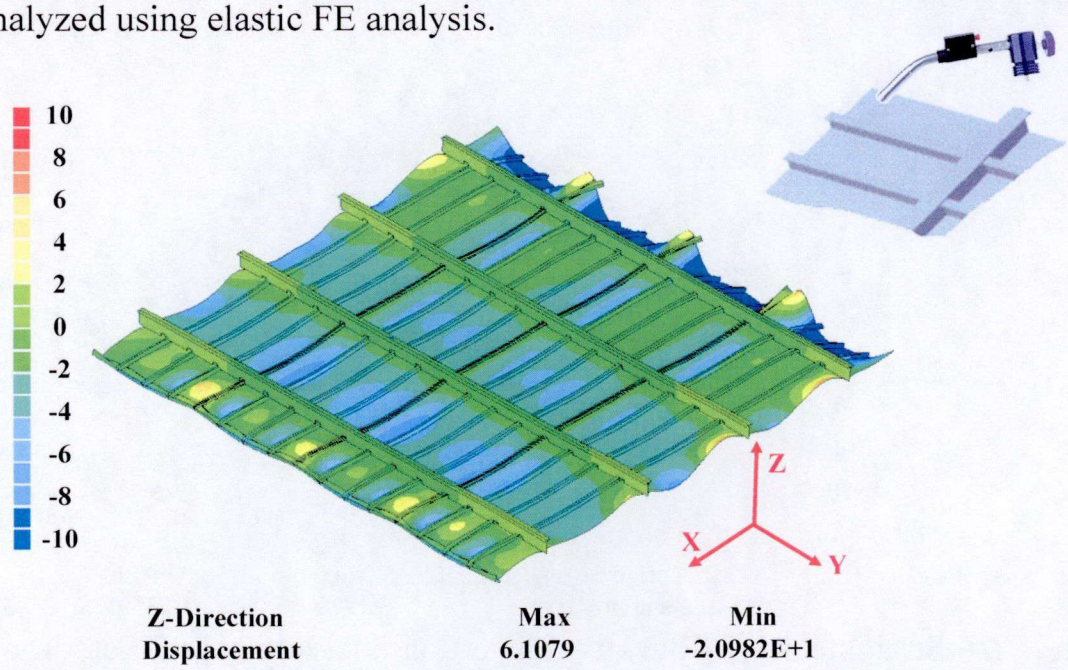

Fig. 7.24 Straightening of buckling distortion applying small in-plane inherent strain (0.0002).

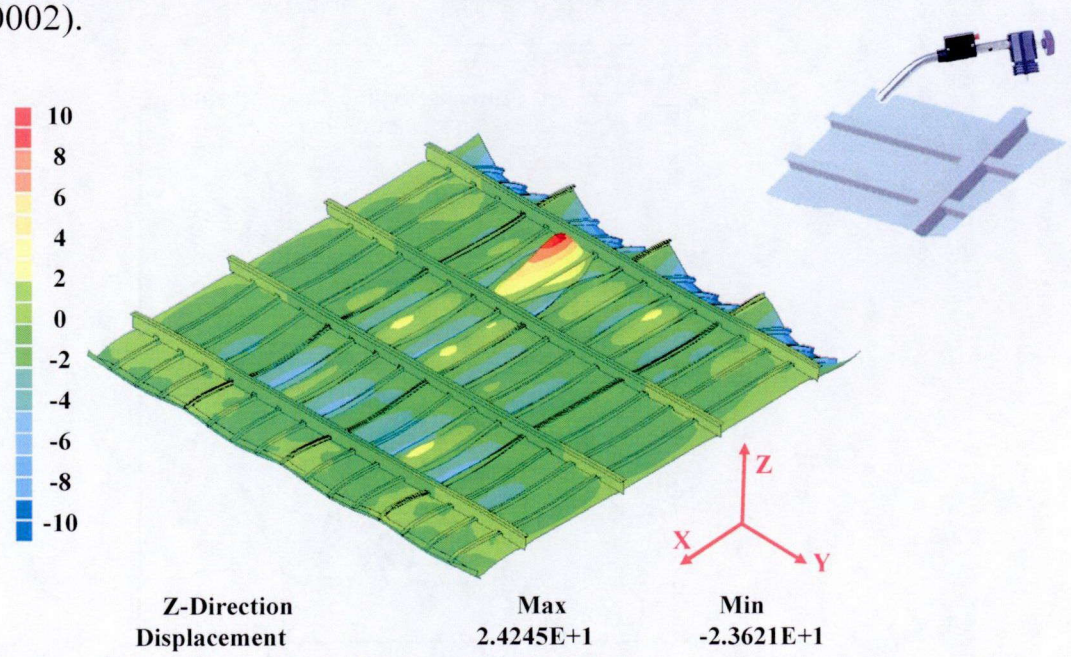

Fig. 7.25 Straightening of buckling distortion applying large in-plane inherent strain (0.0004).

Figures 7.24, 7.25 and 7.26 show the out-of-plane distortion after straightening applying inherent strain with three different magnitudes. When the inherent strain is small (0.0002), significant difference is not observed after the straightening. When the inherent strain is large (0.0004), deflection at the edge is reduced. However, the plate field next to the plate field at edge buckles as shown in **Fig. 7.25**. **Figure 7.26** shows the out-of-plane distortion when an appropriate amount of in-plane inherent strain (0.0003) is applied. As may be seen from this figure, out-of-plane distortion at the edge can be minimized without undesired buckling of other plate fields.

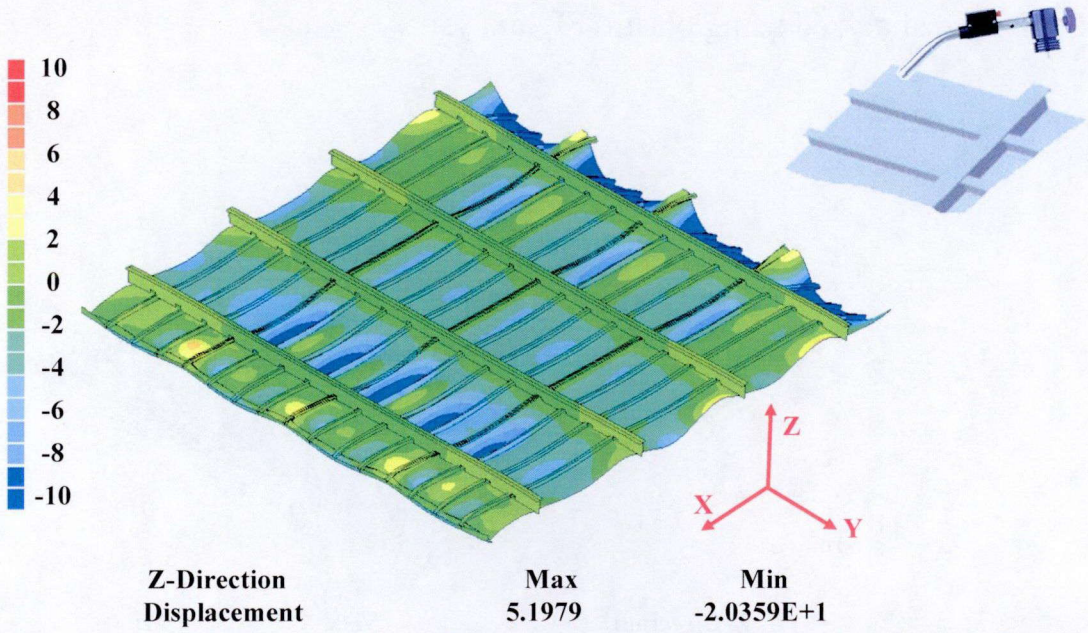

Fig. 7.26 Straightening of buckling distortion applying appropriate in-plane inherent strain (0.0003).

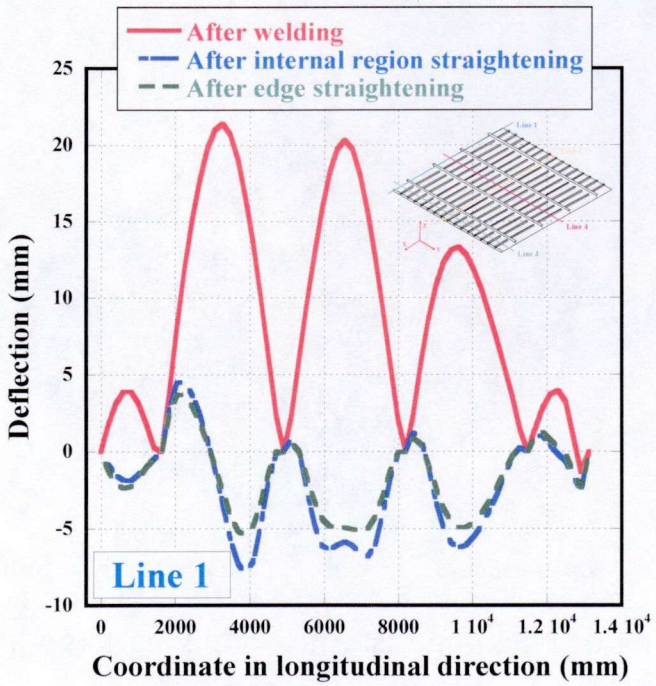

(a) Comparison of out-of-plane welding distortion along line 1

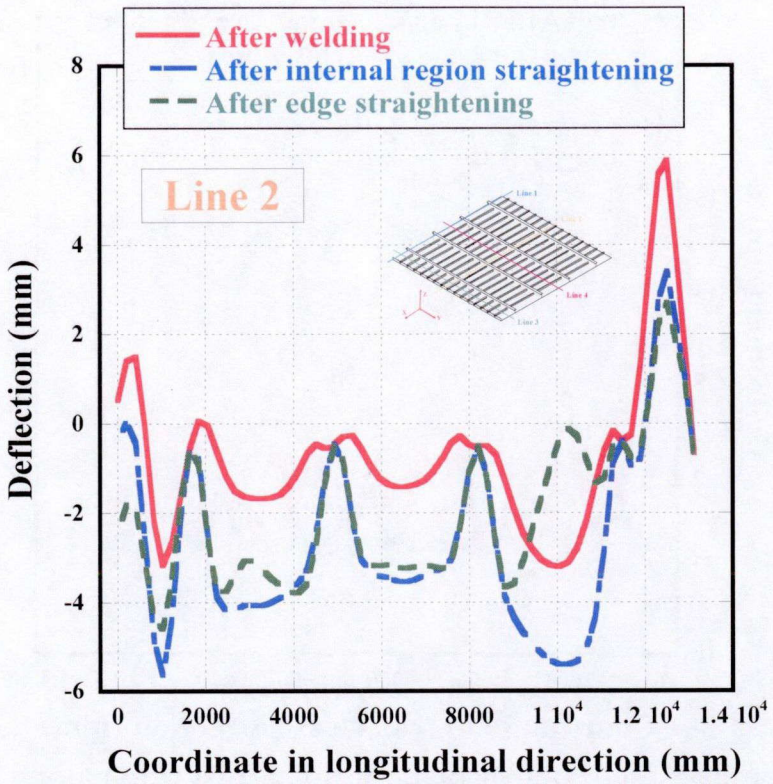

(b) Comparison of out-of-plane welding distortion along line 2

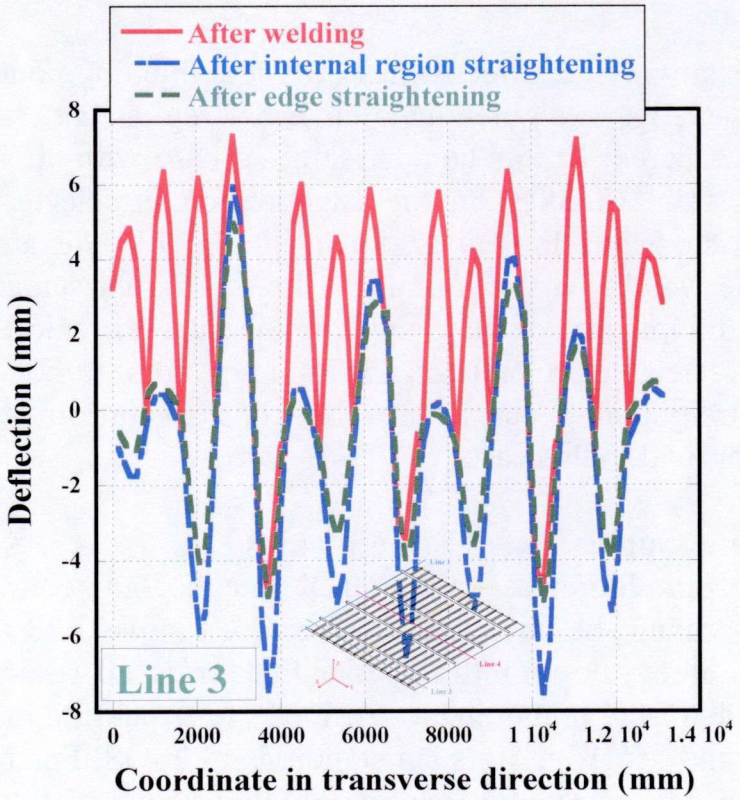

(c) Comparison of out-of-plane welding distortion along line 3

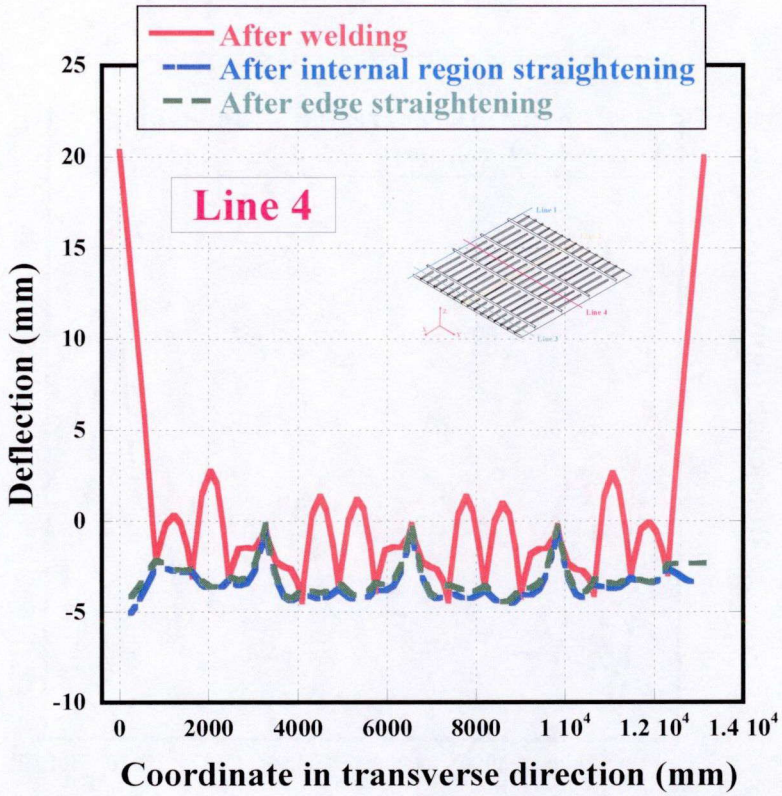

(d) Comparison of out-of-plane welding distortion along line 4

Fig. 7.27 Comparisons of out-of-plane welding distortion during welding and straightening.

To closely examine the effectiveness of straightening, out-of-plane welding distortions after welding, straightening of internal region and straightening of the edge region are compared. In this comparison, the case with appropriate amount of in-plane inherent strain (0.0003) in the edge region is selected and out-of-plane welding distortion along the four lines shown in **Fig. 7.9** is examined. **Figure 7.27** shows out-of-plane welding distortion at the three different stages. As may be seen from this figure, straightening of plate fields in the internal region to remove angular distortion is very effective in reducing the hungry horse type welding distortion. Shrinkage type straightening can reduce buckling distortion at the edge but its effectiveness is marginal in this case.

7.6.3 Discussion and Suggestion of Straightening

As shown in simulation assuming ideal line heating condition, out-of-plane welding distortion cannot be completely corrected. **Figure 7.28** shows out-of-plane welding distortion along the monitoring four lines after all straightening processes. Since the magnitude of the remaining distortion is less than 5 mm, it is acceptable to regulatory bodies and according to such standards as JSQS. For further reduction of distortion, it is necessary to remove bending of longitudinal stiffeners caused by plate shrinkage introduced by welding of transverse stiffeners.

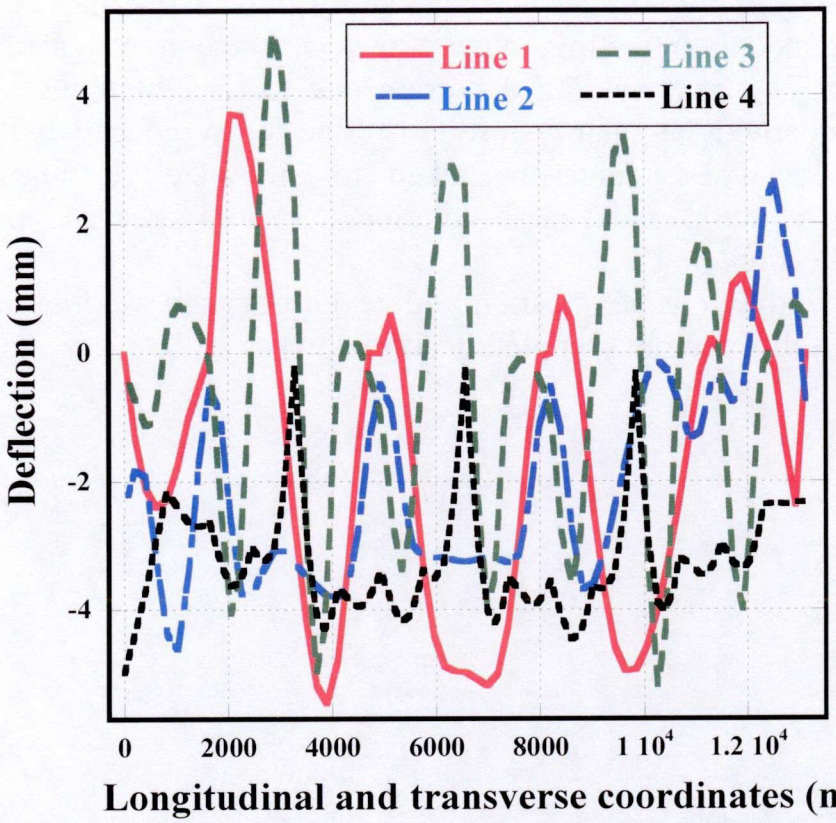

Fig. 7.28 Out-of-plane welding distortion after all straightening processes.

7.7 Conclusions

As a practical application of the prediction of buckling distortion using the inherent deformation theory, a stiffened panel structure, which is a part of a car deck of a PCC, is selected to be studied in this chapter.

To use elastic FE analysis, the inherent deformations of the welded joints contained in the structure are evaluated using thermal elastic plastic FE analysis. Then buckling distortion of the panel structure is investigated using large and small deformation elastic FE analyses and eigenvalue analysis. After clarifying the mechanism which produces buckling distortion, the process of straightening is also studied using the same methods.

From the above discussions, the following conclusions can be drawn:

(1) Large deformation elastic FE analysis considering gravitational force shows that overall bending of the panel is suppressed by gravity and contact with supporting pins. Considering this, idealized boundary conditions, fixing the overall bending deformation are employed.

(2) When all components of inherent deformation are considered in elastic FE analyses, it is difficult to conclude that the panel buckles due to welding. This is because bending can obscure buckling and significant difference is not observed between results computed employing small and large deformation theories.

(3) If only in-plane inherent shrinkages are considered in large deformation elastic FE analysis, buckling behavior is clearly observed.

(4) Eigenvalue analysis for each welding assembly stage show that welding induced buckling occurs only in the region near the edge of the investigated panel.

(5) Computed out-of-plane welding distortion due to straightening shows that line heating for removing angular distortion is effective to reduce welding distortion. However, special care must be taken to minimize the in-plane inherent deformation to avoid undesirable additional tendon force and thus additional buckling distortion.

(6) Straightening with line heating can minimize out-of-plane welding distortion to an accepted level but can not completely correct it.

Chapter 8 Summary and Conclusion

In this research, welding induced buckling is investigated using the inherent deformation theory. Bead on plate welding of a rectangular thin plate, thin plate stiffened structure and a thin plate ship stiffened panel are examined. In the following, a summary of the research and the reached conclusions are presented.

(1) Investigations of welding distortion and especially welding induced buckling are thoroughly reviewed.

(2) Theories and methods incorporated in the in-house code JWRIAN, which is used to carry out all the computational analysis through out the whole investigation, are introduced. **JWRIAN** consists of a solid element thermal elastic plastic FE analysis, a shell element elastic analysis and eigenvalue analysis based on the inherent deformation theory.

- In the thermal elastic plastic FE analysis, the computational process incorporates a transient thermal analysis and a subsequent transient mechanical analysis using the computed history of temperature distribution.
- In the elastic analysis, the inherent deformation is evaluated using thermal elastic plastic FE analysis of typical welded joints, and then it is applied to the welding lines between the parts to be welded. The interface element is used to consider the actual state of the connection between the parts to be welded during the assembly process.
- Eigenvalue analysis is employed to compute the theoretical buckling mode and corresponding critical inherent deformation.
- Buckling will not be numerically predicted using the small deformation theory. To predict buckling, the large deformation theory is necessary.

(3) To understand the concept of, and accurately evaluate the longitudinal inherent shrinkage and the tendon force, three methods are proposed as follows:

- Empirical and theoretical formula;
- Calculation from computed longitudinal displacements;
- Integration of computed plastic strain; or computed longitudinal residual stress.

The average temperature (the temperature at which the whole welded joint has a uniform temperature distribution, and starts to cool uniformly) is used to explain the influence of width of a welded joint and the heat input used in welding on the magnitude of inherent deformation. Calculations show that if the plate is large enough so that the average temperature is low, computed longitudinal inherent shrinkage using thermal elastic plastic FE analysis has a good agreement with that obtained using the theoretical formula.

(4) When high tensile strength steel thin plates are welded, not only residual buckling

after cooling, but also transient buckling during welding may occur.

- In case of a high tensile strength steel plate 300×200×2.28 mm in length, width and thickness, and yield stress equals to 950 MPa, transient buckling occurs during welding. On cooling down, residual buckling occurs.
- During heating, Because of the high yield stress, compared with carbon steel, larger compressive thermal stress is produced near the welding line. Therefore thin plate structures made of high tensile strength steel may buckle due to thermal expansion during welding.
- During cooling, the compressive thermal stress in the region close to the welding line disappears, and therefore, transient buckling also disappears. Meanwhile, tensile residual stress is produced in and around the welding line due to contraction. Compressive residual stress is then produced away from the welding line to balance the tensile stress in and around the welding line. This compressive residual stress, when it exceeds the critical buckling condition, will change the deformed shape to a saddle buckling type.
- For the thicknesses considered in this research, transient buckling does not occur in carbon steel thin plate welded structures, only residual buckling may occur.

(5) An experiment and several computations of bead on plate welding on a plate made of carbon steel are carried out to investigate welding induced buckling. Saddle type buckling is observed.

- First, a thermal elastic plastic FE analysis is employed to evaluate the inherent deformation caused by welding.
- Then an elastic analysis applying the evaluated inherent deformation and considering the initial deflection is carried out. The computed out-of-plane welding distortion has a good agreement with experimental measurements.
- Also, eigenvalue analysis shows that longitudinal inherent shrinkage caused by welding is the dominant cause of buckling in bead on plate welding. Inherent bending and initial deflection are considered to act as imperfections that trigger buckling and influence the magnitude of out-of-plane welding distortion.

(6) A thin plate stiffened welded structure is examined to investigate the twisting type buckling.

- A comparison of computed results with experimental measurements shows that the twisting type buckling of thin plate stiffened structures can be predicted accurately using either thermal elastic plastic FE analysis, or elastic FE analysis employing the inherent deformation theory. However, thermal elastic plastic FE analysis requires large computational resources. The large deformation theory is considered in both computational analysises.
- Further, for this thin plate stiffened welded structure, eigenvalue analysis shows that the longitudinal and transverse inherent shrinkage together determine the buckling mode. The computed lowest buckling mode in this case is twisting

type in agreement with experiment and other computations.

- Using elastic FE analysis, the computational time can be reduced to less than 1/1000 of that required for thermal elastic plastic FE analysis.

(7) A PCC car deck panel is considered. Elastic FE analysis is employed to predict welding induced buckling using the inherent deformation theory.

- The inherent deformations for different welded joints in the panel are first evaluated using thermal elastic plastic FE analysis.
- Applying idealized boundary conditions to focus on local deformation, elastic FE analysis and eigenvalue analysis show that the considered panel buckles near the edge and only bending distortion is produced in the internal region.
- Straightening of out-of-plane welding distortion using line heating is also considered. In the internal region, inherent bending with the same magnitude as welding induced inherent bending is applied on the opposite side of welded joint assuming a fast moving torch.
- Only the in-plane inherent strain produced by line heating assuming a slow moving torch is introduced to plate fields in the edge region to mitigate buckling. It is shown that out-of-plane welding distortion of the considered car deck panel can be reduced to an accepted level after the welding and straightening.

In this research, an approach is established to investigate welding distortion in particular welding induced buckling. Not only residual buckling but also transient buckling could be predicted by this approach. Especially, elastic FE analysis using inherent deformation is proved to be accurate in comparison with experiments and thermal elastic plastic FE analysis.

Mechanism of welding induced buckling in thin plates and stiffened panels is clarified using this approach. It is shown that longitudinal inherent shrinkage is the dominant cause of welding induced buckling in flat plates, however, transverse inherent shrinkage plays an important role in buckling of stiffened panels in twisting mode. In large stiffened panels, inherent transverse shrinkage influences the welding distortion depending on the sequence of welding. After clarifying the mechanism which produces buckling distortion, the effectiveness of the straightening process is also clarified using the same approach.

Through these investigations, the mechanism of welding induced buckling is clarified using the concept of inherent deformation. The effectiveness of elastic FE analysis using inherent deformation in prediction of buckling distortion caused by welding of large scale thin plate structures and the subsequent straightening is demonstrated.

As the future research, the following issues need to be investigated.

- Efficient and accurate methods to evaluate welding and straightening inherent deformation is highly desirable.
- Further validation of the proposed approach through comparison with

measurements of distortion of large scale structure should be carried out.

- Improving dimensional accuracy of large structures by optimization of welding and assembly processes can contribute to shipbuilding technology in Japan and world wide.
- Efficient methods of straightening of welding induced buckling need to be proposed.
- With development of advanced high strength materials, transient buckling becomes an important issue that needs more investigation.

Reference

[1] K. Satoh, Y. Ueda and J. Fujimoto (1979). Welding distortion and residual stresses. *Sanpo Publications*, Tokyo, 1979.
[2] D. Radaj (1992). Heat effects of welding: temperature field, residual stress and distortion. *Springer Verlag Publishing*, Berlin Heidelberg, 1992.
[3] G. Verhaeghe (1999). Predictive formulae for weld distortion – a critical review. *Abington Publishing*, England Cambridge, 1999.
[4] D.A. Deng (2002). Theoretical prediction of welding distortion in thin curved structure during assembly considering gap and misalignment. *Doctoral Dissertation*, Osaka University, 2002.
[5] C. L. Tsai, S. C. Park and W. T. Cheng (1999). Welding distortion of a thin-plate panel structure: the effect of welding sequence on panel distortion is evaluated. *Welding Journal*, 78(5), pp: 156-165.
[6] J.W. Anderson and R.E. Holt (1974). Prestressing for warpage control of welded steel sheet. *Welding Journal*, 53(7), pp: 430-437.
[7] A.P. Chakravarti and L.M. Malik (1990). Distortion control in simulated one-pass panel bead welds. *Marine Structure*, 3(1), pp: 3-24.
[8] C. Conrardy and R. Dull (1997). Control of distortion in thin ship panels. *Journal of Ship Production*, 13(2), pp: 83-92.
[9] P. Michaleris, J. Dantzig and D. Tortorelli (1999). Minimization of welding residual stress and distortion in large structures. *Welding Journal*, 78(11), pp: 361-366.
[10] J.U. Park, H.W. Lee and H.S. Bang (2002). Effects of mechanical constraints on angular distortion of welded joints. *Science and Technology of Welding and Joining*, 7(4), pp: 232-239.
[11] M. Adak and N.R. Mandal (2010). Numerical and experimental study of mitigation of welding distortion. *Applied Mathematic Modeling*, 34(1), pp: 146-158.
[12] A.K. Dhingra and C.L. Murphy (2005). Numerical simulation of welding-induced distortion in thin-walled structures. *Science and Technology of Welding and Joining*, 10(5), 528-536.
[13] K. Satoh and T. Terasaki (1976). Effect of welding condition on welding deformation in welded structural materials. *Journal of Japan Welding Society*, 45(4), pp: 302-308.
[14] K. Masubuchi (1980). Analysis of welded structures: residual stresses, distortion and their consequences. *Pergamon Press*, England Oxford, 1980.
[15] Y. Ueda and T. Yamakawa (1971). Analysis of thermal elastic plastic stress and strain during welding by finite element method. *Transactions of Japan Welding Society*, 2(2), pp: 90-100.
[16] H.D. Hibbitt and P.V. Marcal (1973). A numerical thermo-mechanical model for the welding and subsequent loading of a fabricated structure. *Computers and*

Structures, 3(5), pp: 1145-1174.
[17] E. Friedman (1975). Thermo mechanical analysis of the welding process using the finite element method. *Journal of Pressure Vessel Technology*, 97(3), pp: 206-213.
[18] L.E. Lindgren and L. Karlsson (1988). Deformations and stresses in welding of shell structures. *International Journal for Numerical Methods in Engineering*, 25(2), pp: 635-655.
[19] J.A. Goldak (1989). Modeling thermal stresses and distortions in welds. *Proceeding of the 2nd International Conference on Trends in Welding Research*, USA Gatlinburg, pp: 71-82.
[20] J.A. Goldak, A. Chakravarti and M. Bibby (1984). A new finite element model for welding heat sources. *Metallurgical Transactions B*, 15(2), pp: 299-305.
[21] Y. Ueda and H. Murakawa (1985). Applications of computer and numerical analysis techniques in welding research. *Materials and Design*, 6(3), pp: 103-111.
[22]S.M Gu, M. Ishiyama, H, Murakawa, Y Okumoto and Y Ueda (1997). Simulation of out-of-plane deformation in butt welding of large size steel plate. *Mathematical Modeling of Weld Phenomena 3*, pp: 689-712.
[23] Y. Ueda, H. Murakawa, K. Nakacho and N. X. Ma (1995). Establishment of computational welding mechanics. *Transactions of JWRI*, 24(2), pp: 73-86.
[24] Y. Ueda, H. Murakawa, S.M. Gu, Y. Okumoto and R Kamichika (1992). Simulation of welding deformation for precision ship assembling (report 1): in-plane deformation of butt welded plate. *Transactions of JWRI*, 21(2), pp: 265-275.
[25] Y. Ueda, H. Murakawa, S.M. Gu, Y. Okumoto and M. Nakamura (1993). Simulation of welding deformation for accurate ship assembling (report 2): influence of initial geometrical imperfection on butt welded plate. *Transactions of JWRI*, 22(1), pp: 135-144.
[26] S.M. Gu, H. Murakawa, Y. Ueda, Y. Okumoto and M. Ishiyama (1996). Simulation of welding deformation for accurate ship assembling (report 3): influence of initial geometrical imperfection on butt welded plate. *Transactions of JWRI*, 25(1), pp: 69-79.
[27] L.E. Lindgren (2001). Finite element modeling and simulation of welding (part 1): increased complexity. *Journal of Thermal Stresses*, 24(2), pp: 141-192.
[28] L.E. Lindgren (2001). Finite element modeling and simulation of welding (part 2): improved material modeling. *Journal of Thermal Stresses*, 24(3), pp: 195-231.
[29] L.E. Lindgren (2001). Finite element modeling and simulation of welding (part 3): efficiency and integration. *Journal of Thermal Stresses*, 24(4), pp: 305-334.
[30] L.E. Lindgren (2006). Numerical modeling of welding. *Computer Methods in Applied Mechanics and Engineering*, 195(48-49), pp: 6710-6736.
[31] J.A. Goldak and M. Akhlaghi (2005). Computational welding mechanics. *Springer Science & Business Media*, U.S.A New York, 2005.
[32] Y. Ueda (1999). Computational welding mechanics (selected from papers published in English). *Joining and Welding Research Institute, Osaka University*, Japan Osaka, 1999.
[33] L.E. Lindgren (2007). Computational welding mechanics: thermomechanical

and microstructural simulations. *Woodhead Publishing Limited*, England Cambridge, 2007.
[34] S.B. Brown and H. Song (1992). Implications of three-dimensional numerical simulations of welding of large structures. *Welding Journal*, 71(2), pp: 55-62.
[35] J.H. Wang, Y. Ueda, H. Murakawa, M.G. Yuan and H.Q. Yang (1996). Improvement in numerical accuracy and stability of 3D FEM analysis in welding. *Welding Journal*, 75(2), pp: 129-134.
[36] J.H. Wang and H. Luo (2000). Prediction of welding deformation by FEM based on inherent strains. *Journal of Shanghai Jiaotong University (English Editorial Board)*, 5(2), pp: 83-87.
[37] Y. Luo, H. Murakawa and Y. Ueda (1997). Prediction of welding deformation and residual stress by elastic FEM based on inherent strain (first report): mechanism of inherent strain production. *Transactions of JWRI*, 26(2), pp: 49-57.
[38] H. Murakawa, Y. Luo and Y. Ueda (1998). Inherent Strain as an interface between computational welding mechanics and its industrial application. *Mathematical Modeling of Weld Phenomena 4*, pp: 597-619.
[39] Y. Luo, M. Ishiyama and H. Murakawa (1999). Welding deformation of plates with longitudinal curvature. *Transactions of JWRI*, 28(2), pp: 57-65.
[40] Y. Luo, D. Deng, L. Xie and H. Murakawa (2004). Prediction of deformation for large welded structures based on inherent strain. *Transactions of JWRI*, 33(1), 65-70.
[41] D. Deng, H. Murakawa and W. Liang (2007). Numerical simulation of welding distortion in large structures. *Computer Methods in Applied Mechanics Engineering*, 196(45-48), pp: 4613-4627.
[42] R. Wang, J.X. Zhang, H. Serizawa and H. Murakawa (2009). Study of welding inherent deformation s in thin plates based on finite element analysis using interactive substructure method. *Materials and Design*, 30(9), pp: 3474-3481.
[43] J.C. Wang, X. Ma, H. Murakawa, B.G. Teng and S.J. Yuan (2011). Prediction and measurement of welding distortion of a spherical structure assembled form multi thin plates. *Materials and Design*, 32(10), pp: 4728-4737.
[44] P. Michaleris and A. Debiccari (1997). Prediction of welding distortion. *Welding Journal*, 76(4), pp: 172-181.
[45] A. Bachorski, M.J. Painter A.J. Smailes and M.A. Wahab (1999). Finite element prediction of distortion during gas metal arc welding using the shrinkage volume approach. *Journal of Materials Processing Technology*, 92-93, pp: 405-409.
[46] G.H. Jung and C.L. Tsai (2004). Plasticity-based distortion analysis for fillet welded thin-plate T-joints. *Welding Journal*, 83(6), pp: 177-187.
[47] D. Camilleri, T. Comlekci and T.G.F. Gray (2005). Computational prediction of out-of-plane welding distortion and experimental investigation. *Journal of Strain Analysis*, 40(2), pp: 161-176
[48] W.T. Cheng (2005). In-plane Shrinkage strain and their effects on welding distortion in thin-wall structure. *Doctoral Dissertation*, Ohio State University, 2005.
[49] L. Zhang, P. Michaleris and P. Marugabandhu (2007). Evaluation of applied plastic strain methods for welding distortion prediction. *Journal of Manufacturing*

Science and Engineering, 129(6), pp: 1000-1010.
[50] G.H. Jung (2007). A shell-element-based elastic analysis predicting welding induced distortion for ship panels. *Journal of Ship Research*, 51(2), pp: 128-136.
[51] Y.P. Yang, H. Castner and N. Kapustka (2011). Developmeng of Distortion Modeling Methods for Large Welded Structures. *Journal of Ship Production and Design*, 27(1), pp: 26-34.
[52] H. Nishikawa, H. Serizawa and H. Murakawa (2007). Actual application of FEM to analysis of large scale mechanical problems in welding. *Science and Technology of Welding and Joining*, 12(2), pp: 147-152.
[53] H. Nishikawa (2006). Development of FEM for analysis of large scale mechanical problems in welding and its application to practical problems. *Doctoral Dissertation*, Osaka University, 2006.
[54] K. Ikushima, M. Shibahara, S. Itoh and N. Ma (2012). Ultra large scale FE computation using idealized explicit FEM accelerated by GPU. *Transactions of JWRI*, Special Issue on WSE2011, pp: 91-92.
[55] H. Runnemalm and S. Hyun (2000). Three dimensional welding analysis using an adaptive mesh scheme. *Computer Methods in Applied Mechanics and Engineering*, 189(2), pp: 515-523.
[56] J. Kim, S. Im and H.G. Kim (2005). Finite element analysis of arc welding process by parallel computation. *Transactions of Japan Welding Society*, 23(2), pp: 203-208.
[57] Y. Tian, C. Wang, D. Zhu and Y. Zhou (2008). Finite element modeling of electron beam welding of a large complex Al alloy structure by parallel computations. *Journal of Materials Processing Technology*, 199, pp: 41-48.
[58] H. Murakawa, H. Serizawa and J.C. Wang (2011). Prediction of buckling type welding deformation produced in thin plate structures using inherent deformation method. *Preprints of the National Meeting of Japan Welding Society*, 88, pp: 180-181.
[59] K. Masubuchi (1953). Buckling type deformation of thin plate due to welding. *Proceedings of the 3rd Japan National Congress for Applied Mechanics*, Japan, pp: 107-111.
[60] M. Watanabe and K. Satoh (1957). On the type of distortion in various welded joints: shrinkage distortion in welded joint (Report 5). *Journal of Japan Welding Society*, 26(6), pp: 399-405.
[61] M. Watanabe and K. Satoh (1958). Fundamental study on buckling of thin steel plate due to bead-welding. *Journal of Japan Welding Society* 27(6), pp: 313-320.
[62] M.P. Frank (1975). Buckling distortion of thin aluminum plates during welding. *Master Thesis*, Massachusetts Institute of Technology, 1975.
[63] T. Terasaki, K. Maeda, H. Murakawa and T. Nomoto (1998). Critical conditions of plate buckling generated by welding. *Transactions of the Japan Society of Mechanical Engineers (A)*, 64(625), pp: 2239-2244.
[64] N. Toshiharu, T. Terasaki and K. Maeda (1997). Study of parameters controlling weld buckling. *Transactions of the Japan Society of Mechanical Engineers (A)*,

63(609), pp: 1063-1068.
[65] X.M. Zhong, H, Murakawa and Y. Ueda (1995). Buckling behavior of plates under idealized inherent strain. *Transactions of JWRI*, 24(2), pp: 87-91.
[66] M. Zaeem, M.R. Nami and M.H. Kadivar (2007). Prediction of welding buckling distortion in a thin wall aluminum T joint. *Computational Materials Science*, 38, pp: 588-594.
[67] P. Mollicone, D. Camilleri and T. Gray (2008). Procedural influences on non-linear distortions in welded thin-plate fabrication. *Thin-walled Structures*, 46, pp: 1021-1034.
[68] C.L. Tsai, M.S. Han and G.H. Jung (2006). Investigating the bifurcation phenomenon in plate welding. *Welding Journal*, 85(7), pp: 151-162.
[69] P. Michaleris and A. Debiccari (1996). A predictive technique for buckling analysis of thin section panels due to welding. *Journal of Ship Production*, 12(4), pp: 269-275.
[70] P. Michaleris (2011). Minimization of welding distortion and buckling: modelling and implementation. *Woodhead Publishing limited*, England Cambridge, 2011.
[71] O.A. Vanli and P. Michaleris (2001). Distortion analysis of welded stiffeners. *Journal of Ship Production*, 17(4), pp: 226-240.
[72] M.V. Deo, P. Michaleris and J. Sun (2003). Prediction of buckling distortion of welded structures. *Science and Technology of Welding and Joining*, 8(1), pp: 55-61.
[73] P. Michaleris, L. Zhang, S.R. Bhide and P. Marugabandhu (2007). Evaluation of 2D, 3D and applied plastic strain methods for predicting buckling welding distortion and residual stress. *Science and Technology of Welding and Joining*, 11(6), pp: 707-716.
[74] S.R. Bhide, P. Michaleris, M. Posada and J. Deloach (2006). Comparison of buckling distortion propensity for SAW, GMAW and FSW. *Welding Journal*, 85(9), pp: 189-195.
[75] T.D. Huang, P. Dong, L. Decan, D. Harwig and R. Kumar (2004). Fabrication and engineering technology for lightweight ship structures, part 1: distortions and residual stresses in panel fabrication. *Journal of Ship Production*, 20(1), pp: 43-59.
[76] T.D. Huang, C. Conrardy, P. Dong, P. Keene, L. Kvidahl and L. Decan (2007). Engineering and production technology for lightweight ship structures, part 2: distortion mitigation technique and implements. *Journal of Ship Production*, 23(2), pp: 89-93.
[77] Y.P. Yang and P. Dong (2012). Buckling distortion and mitigation techniques for thin-section structures. *Journal of Materials Engineering and Performance*, 21(2), pp: 153-160.
[78] Y. Tajiama, S. Rashed, Y. Okumoto, Y. Katayama and H. Murakawa (2007). Prediction of welding distortion and panel buckling of car carrier decks using database generated by FEA. *Transactions of JWRI*, 36(1), pp: 65-71.
[79] D. Deng and H. Murakawa (2008). FEM prediction of buckling distortion induced by welding in thin plate panel structures. *Computational Materials Science*,

43, 591-607.
[80] J.C. Wang, S. Rashed, H. Murakawa and M. Shibahara (2011). Investigation of buckling deformation of thin plate welded structures. *Proceeding of 21st International Society of Ocean and Polar Engineering*, USA Hawaii, pp: 125-131.
[81] Y. Ueda, H. Murakawa and N. Ma (2007). Computational approach to welding deformation and residual stress. *Sanpo Publication*, Japan Tokyo, 2007.
[82] Y. Ueda and M.G. Yuan (1991). The characteristics of the source of welding residual stress (inherent strain) and its application to measurement and prediction. *Transactions of JWRI*, 20(2), pp: 119-127.
[83] A. Vega, S. Rashed, S. Serizawa and H. Murakawa (2007). Influential factors affecting inherent deformation during plate forming by line heating (report 1): the effect of plate size and edge effect. *Transactions of JWRI*, 36(2), pp: 57-64.
[84] A. Vega (2009). Development of inherent deformation database for automatic forming of thick steel plates by line heating considering complex heating patterns. *Doctoral Dissertation*, Osaka University, 2009.
[85] W. Liang, D. Deng, S. Sone and H. Murakawa (2005). Prediction of welding distortion by elastic finite element analysis using inherent deformation estimated through inverse analysis. *Welding in the Word*, 49(11-12), 30-39.
[86] W. Liang (2005). Prediction of welding distortion of large structure using inherent deformation estimated by inverse analysis. *Doctoral Dissertation*, Osaka University, 2005.
[87] H. Murakawa, D. Deng and N. Ma (2010). Concept of inherent strain, inherent stress, inherent deformation and inherent force for prediction of welding distortion and residual stress. *Proceeding of the 1st International Symposium on Visualization in Joining and Welding Science*, Japan Osaka, pp: 115-116.
[88] H. Murakawa, D. Deng, S. Rashed and S. Sato (2009). Prediction of distortion produced on welded structures during assembly using inherent deformation and interface element. *Transactions of JWRI*, 38(2), pp: 63-69.
[89] D. Dean, N. Ma and H. Murakawa (2011). Finite element analysis of welding distortion in a large thin-plate panel structure. *Transactions of JWRI*, 40(1), pp: 89-100.
[90] J.C. Wang, X.Q. Yin, N. Ma and H. Murakawa (2012). Study tendon force for buckling welding distortion. *Preprints of the National Meeting of Japan Welding Society*, 90, pp: 140-141.
[91] J.D. White, R.H. Leggatt and J.B. Dwight (1980). Weld shrinkage prediction. *Welding and Metal Fabrication*, 1980 (11), 587-596.
[92] T. Terasaki, M. Nakatani and T. Ishimura (2000). Study of tendon force generating in welded joint. *Journal of Japan Welding Society*, 18(3), pp: 479-486.
[93] Y. Luo, H.Y. Lu, L. Xie and Z.F. Zhu (2004). Concept and evaluated method of tendon force. *Marine Technology*, 2004(4), pp: 35-37.
[94] J.C. Wang, Y. Matsuo and H. Murakawa (2012). Numerical study on longitudinal inherent deformation and inherent force produced in bead on plate welding. *Preprints of the National Meeting of Japan Welding Society*, 91, pp:.

[95] W. Liang, S. Sone, M. Tajima, H. Serizawa and H. Murakawa (2004). Measurement of inherent deformation in typical weld joint using inverse analysis (part 1): inherent deformation of bead on welding. *Transactions of JWRI*, 33(1), pp: 45-51.

Acknowledgement

First, I wish to express my deepest and sincerest appreciation and gratitude to my supervisor, Professor Hidekazu Murakawa for his encouragement, expert advice and guidance throughout the whole doctoral duration of research. His enthusiastic and patient guidance always encourage me and give me infinite confidence of investigation. Fortunately as his student, this experience of comprehend understanding and scientist training will provide the greatest far-reaching effect for my future academic life. Also, I really appreciate his effort for reading and correcting of my manuscript.

I also wish to express my most grateful appreciation to Professor Sherif Rashed for his logical guidance, patient discussion, valuable suggestions and correcting of my manuscript.

I would like to thank Prof. Keiji Nakacho, Prof. Hisashi Serizawa, Prof. Naoki Osawa, and Prof. Masahiko Fujikubo for serving as dissertation committee members and providing evaluation contributions.

I am very grateful to Prof. Ninshu Ma (JSOL), Prof. Yu Luo (Shanghai Jiaotong University), Prof. Dean Deng (Chongqing University), Prof. Yasuhisa Okumoto (Kinki University), Prof. Masakazu Shibahara (Osaka Prefecture University), and Prof. Adan Vega Saenz (Technological University of Panama). Thanks are also extended to Prof. Haiyan Zhao (Tsinghua University, China), Dr Jian Lin (Beijing University of Technology) for their assistance.

I appreciate the effort and cooperation for carrying out the experiments by Prof. Xianqing Yin (Xi'an Jiaotong University), Dr. Xudong Zhang (Hitachi, Ltd) and Mr. Y Katayama, Mr. Masanori Sano (Nankai Shipbuilding). Also Thanks to the relevant staffs whom contribute fruitful measurement database and valuable discussions during my investigation.

I would also like to express my thanks to all my fellow lab mates and them who already graduated from this laboratory for their all help to me during research and life in Japan. Many thanks are extends to Miss. Noriko Fujimoto, the staffs of Joining and Welding Research Institute and Department of Naval Architecture and Ocean Engineering (Osaka University) for their responsible and warm help.

Also, I would like to acknowledge the financial support provided by the CSC (China Scholarship Council, China) for me to finish my doctoral course in Japan. I would like to extend my sincere appreciation for the staffs of consulate and education room in Osaka.

Finally, and most importantly, I would like acknowledge the encouragement of my family and friends without whom this thesis would never have been completed.

Publications related to this thesis

[1] Jiangchao Wang, Yu Luo, Hidekazu Murakawa and Kunming Ma (2009). Prediction of Welding Distortion of Stainless Steel Independent Liquid Tank of LNG Carrier. *International Conference on Welding Science and Engineering*, Shanghai China, pp: 204-205.

[2] Jiangchao Wang, Ninshu Ma and Hidekazu Murakawa (2010). Prediction and Measurement of Welding Distortion of Thin Shell Structure. *Proceeding of 1st International Symposium on Visualization in Joining & Welding Science,* Osaka Japan, pp: 105-106.

[3] Jiangchao Wang, Ninshu Ma and Hidekazu Murakawa (2010). Prediction and Measurement of Welding Distortion of Thin Shell Structure. *Transactions of JWRI*, 39(2), pp: 88-90.

[4] Hidekazu Murakawa, Hisashi Serizawa, Jiangchao Wang, Dean Deng and Ninshu Ma (2011). Application of Inherent Deformation and Interface Element to Prediction of Welding Distortion during Assembly Process from Cutting through Straightening. *International Workshop on Thermal Forming and Welding Distortion*, Bremen German, pp: 25-33.

[5] Hidekazu Murakawa, Hisashi Serizawa and Jiangchao Wang (2011). Prediction of Buckling Type Welding Deformation Produced in Thin Plate Structure Using Inherent Deformation Method. *Preprints of the National Meeting of Japan Welding Society,* 88, pp: 180-181.

[6] Jiangchao Wang, Ninshu Ma, Hidekazu Murakawa, Bugang Teng and Shijian Yuan (2011). Prediction and Measurement of Welding Distortion of a Spherical Structure Assembled from Multi Thin Plates. *Materials and Design*, 32(10), pp: 4728-4737.

[7] Jiangchao Wang, Sherif Rashed, Hidekazu Murakawa and Masakazu Shibahara (2011). Investigation of Buckling Deformation of Thin Plate Welded Structures. *Proceedings of International Society of Ocean and Polar Engineering*, Maui U.S.A, pp: 125-131.

[8] Hidekazu Murakawa, Dean Deng, Ninshu Ma and Jiangchao Wang (2011). Application of Inherent Strain and Interface Element to Simulation of Welding Deformation in Thin Plate Structures. *Computational Materials Science*, 51, pp: 43-52.

[9] Jiangchao Wang, Hidekazu Murakawa, Masakazu Shibahara and Xudong Zhang (2011). Twisting Deformation of Thin Plate Stiffened Structure Under Welding. *Preprints of the National Meeting of Japan Welding Society*, 89, pp: 162-163.

[10] Jiangchao Wang, Masakazu Shibahara, Xudong Zhang and Hidekazu Murakawa (2011). Analysis of Twisting Distortion of Thin Plate Stiffened Structure Caused by Welding. *Proceedings of Symposium of Welded Structures*, Osaka Japan, pp: 29-36.

[11] Jiangchao Wang and Hidekazu Murakawa (2011). Study on Transient Buckling Behavior of Thin Plate Structures During Welding Process. *International Conference on Welding Science and Engineering*, Osaka Japan, pp: 51-54.
[12] Jiangchao Wang and Hidekazu Murakawa (2011). Study on Transient Buckling Behavior of Thin Plate Structures During Welding Process. *Transactions of JWRI*, Special Issue, pp: 87-90.
[13] Hidekazu Murakawa, Juan Blandon and Jiangchao wang (2012). Theoretical Prediction of Buckling in Thermal Manufacturing Process. *Preprints of the National Meeting of Japan Welding Society*, 90, pp: 138-139.
[14] Jiangchao Wang, Xianqing Yin, Ninshu Ma and Hidekazu Murakawa (2012). Study of Tendon Force for Buckling Welding Distortion. *Preprints of the National Meeting of Japan Welding Society*, 90, pp: 140-141.
[15] Jiangchao Wang, Masakazu Shibahara, Xudong Zhang and Hidekazu Murakawa (2012). Investigation on Twisting Distortion of Thin Plate Stiffened Structure under Welding. *Journal of Materials Processing Technology*, 212, pp: 1705-1715.
[16] Jiangchao Wang and Hidekazu Murakawa (2012). Fundamental Study of Buckling Behavior in Thin Plate Butt Welding by the Inherent Deformation Method. *Proceeding of 9th International Conference on Trends in Welding Research*, U.S.A Chicago,
[17] Jiangchao Wang, Masanori Sano, Sherif Rashed and Hidekazu Murakawa (2012). Reduction of Hatch Coaming Top Surface Deflection during Assembly to Ship Deck. *Proceeding of the 26th Asia-Pacific Technical Exchange and Advisory Meeting on Marine Structure*, Fukuoka Japan,
[18] Hidekazu Murakawa, Masanori Sano and Jiangchao Wang (2012). Influence of Root Gap and Tack Weld on Transverse Shrinkage during Welding. *Transactions of JWRI*, 41(1), pp: 65-70.
[19] Jiangchao Wang, Yuki Matsuo and Hidekazu Murakawa (2012). Numerical Study on Longitudinal Inherent Deformation and Inherent Force Produced in Bead on Plate Welding. *Preprints of the National Meeting of Japan Welding Society*, 91
[20] Jiangchao Wang, Xianqing Yin, Sherif Rashed and Hidekazu Murakawa (2012). Theoretical Analysis on Buckling of Thin Plate Structures Due to Welding. *Proceeding of 2nd International Symposium on Visualization in Joining & Welding Science*, Osaka Japan,